

The potential of direct mineral extraction from geothermal fluids

Zur Erlangung des akademischen Grades eines

Doktors der Naturwissenschaften

von der KIT-Fakultät für
Bauingenieur-, Geo- und Umweltwissenschaften
des Karlsruher Instituts für Technologie (KIT)

genehmigte

DISSERTATION

Tesis para optar al grado de doctor en ciencias, mención geología

Departamento de geología
Facultad de ciencias físicas y matemáticas
Universidad de Chile (UCHILE)

M.Sc. Valentin Magnus Goldberg

Referent KIT:

Prof. Dr. Thomas Kohl

Profesor Guía UCHILE:

Prof. Dr. Diego Morata

Karlsruhe 2024
Santiago de Chile 2024

Acknowledgments

When this work started in 2019 I could not even imagine where it would lead me. The realization of this work spreading over two continents during a global pandemic crisis was influenced by many unexpected turns, restrictions, and required over the years several realignments. The fact that it has now come to a good end is due to the support of my family, friends, colleagues, and colleagues who have become friends over the years. The list of all the people would go beyond the scope of this passage, so please excuse me if someone is not mentioned here.

First, I want to thank Thomas Kohl. I am grateful for your trust in me and for giving me the opportunity to pursue my ideas, even though you were often afraid at the beginning that I would overreach myself. Thank you for all the guidance in the past years and for entrusting me with the BrineMine project, which has opened up so many doors for me.

I would also like to thank Diego Morata for his supervision from the Chilean site and for hosting me at the Universidad de Chile and especially at CEGA. Many thanks for the numerous discussions in the past years and the support in the preparation of the fieldwork as well as the help in not losing track of all the administrative hurdles.

Thank you to Jochen Kolb. I have always greatly appreciated the lively exchange over the last few years and your honest and direct advice.

I would also like to thank Linda Daniele for agreeing to act as co-supervisor and for always being on hand with help and advice in case of questions or problems.

The last few years would not have been so enjoyable without the great working atmosphere of our geothermal working group. The sometimes more or less scientific discussions during lunch, coffee breaks, or Thursday evenings helped a lot not to lose motivation and to find advice and made furthermore everyday life easier and better.

In particular, I would like to thank Fabian for the countless meetings and advice he has given me over the years, which have been indispensable to this work.

I would also like to thank Silke for all her support with the administrative hurdles at KIT. One day, I will manage to fill out a travel expense form without any mistakes.

I am also very grateful to my colleagues at the Chair of Geochemistry & Economic Geology enabling me access to the laboratories and all their support regarding sampling. Special thanks to Eli Eiche for her advice on sample analysis, preparation and interpretation of results. Furthermore, I would like to thank Tobias Kluge for the discussions and the support during the preparation of the Li study. In addition, I want to thank Klemens, Rebekka, and Michèle for the close exchange throughout the years.

Many thanks also to Kirsten Drüppel for the support during the preparation and evaluation of my solid samples. Thank you very much for your numerous pieces of advice and for always being attentive and ready with competent guidance.

Por supuesto, también quiero dar las gracias a mis colegas del CEGA! Verónica Rodríguez I want to thank for her guidance in the lab and together with Diego Aravena and Mauricio for the support during the preparation of my sampling campaigns. Pato I want to thank you for our countless language tandem coffee breaks and Karin, Nicolás and Esteban for bringing me into the infamous desierto florido. I would also like to thank Martin Reich for his availability as an additional reviewer and for his constructive criticism during the preparation of this thesis.

My deepest gratitude also goes to my friends Mafi, Vale, Diego, Javiera, Alejo, Gabs, Lucho, and Tomas from the postgraduate room of the geological department. Thank you for welcoming me so warmly into your midst. Thank you for the lunch breaks, the Cueca dance lessons, the evenings at Mephisto, and the introduction to all the modistos chilenos – Lo pasamos chancho!

From the faculties of Universidad de Chile and KIT I want to thank Maritza Acuña, Ms. Engelmann and Ms. Büyüksahin for their patience in going through all the necessary steps with me to make this binational dissertation possible.

Furthermore, I would like to thank the colleagues from the BrineMine project, especially Joachim Koschikowski and Daniel Winter from Fraunhofer ISE for the excellent exchange about the project and beyond, and for the collegial collaboration. Additionally, I would like to thank Carolina Wechsler from Transmark Chile and Peter Seibt, Ingmar Budach and Julian Heboldt from GTN for their great cooperation.

I would like to thank Ignacio Perez for the time during our campaign in northern Chile and for the 1000 phone calls and conversations that allowed us to reach the most remote springs in the Andes.

I would especially like to thank Alberto Espinoza for the unique experience during our Tolhuaca campaign, the support when I had to leave the country abruptly in 2020 due to the pandemic, and for the friendship that has grown out of it all.

Talking about friendship, I'd like to express my gratitude to my friends right here in Karlsruhe. Especially to Jonas and Qasid for their input on my work. Furthermore, many thanks to Nadja, Alex, Thorben, Jan, and Constantin from the quiz team. Wednesday evenings were the highlight of every week, even though I cursed them on the odd Thursday morning.

My deepest gratitude goes to my family. First and foremost, I would like to thank my parents, who have always supported me and given me the necessary backing in every situation, as well as my siblings Janina, Niklas, and Vincent. Without you, none of this would have been possible.

Finally, I would like to express my deepest and most heartfelt thanks to my fiancée, Aura. Thank you for your loving support and for always being by my side, and accompanying me on this journey from the very beginning.

Abstract

The human-caused climate change and the resulting necessity for transitions in energy and mobility are creating enormous challenges and will continue to do so for upcoming generations. Fossil CO₂-emitting energy carriers are replaced by renewable alternatives. In particular, base load-capable energy sources such as coal and gas will leave a large gap in the energy landscape – a gap that needs to be filled with climate-neutral, more sustainable, and base load-capable energies. Furthermore, newly emerging technologies create a large and very diverse demand for high-tech materials. The electrification of the mobility sector in particular presents a significant challenge for global supply chains of critical raw materials.

On a global scale, geothermal energy demonstrates the potential for the ecological, economical provision of baseload heat and energy with an installed capacity that is continuously growing. The large fluid volume streams constantly circulating in geothermal power plants in combination with the enrichment of specific elements moreover entail significant potential in raw materials. Among the various elements occurring in geothermal fluids worldwide, there are a number defined as critical elements by the EU, such as lithium (Li), cesium (Cs), magnesium (Mg), strontium (Sr), boron (B), silicon (Si), antimony (Sb) or fluorine (F).

A new concept of advanced multi-use of hydrothermal systems producing electricity, heat, and raw materials could bring several national and international benefits. In mining countries such as Chile, the new approach could help transiting the local mining sector towards more sustainability. Due to the water's inherent energy, external energy consumption would be minimized. By using Direct Lithium Extraction (DLE), water losses occurring in conventional evaporation ponds for Li extraction could be avoided, thus eliminating a typical topic of conflict in mining. Moreover, the newly tapped resources could open up larger global market shares for Chile's lithium sector. For a country like Germany, which currently imports all of its primary Li, this minimal-invasive mining approach opens up the perspective for a renaissance of the local mining sector.

The studies presented demonstrate the diverse resource potential of hydrothermal systems in Germany and Chile. For Germany, the potential of the existing geothermal power plants for Li extraction is analyzed and possible coverage of the local Li demand is quantified. For Chile, the general raw material potential of the country's abundant geothermal systems is described.

For determining the challenges potentially arising from DLE from geothermal fluids, different extraction technologies are compared and quantified. Frequently discussed technologies such as liquid-liquid extraction, selective extraction by inorganic sorbents, electrochemical methods, and membrane technologies are evaluated on their specific influence on the physiochemical properties of the water (pH, Eh, T, p, etc.) and further classified based on their technological readiness level (TRL). Key parameters for the process design are the usable volume fraction of the geothermal fluid and the extraction efficiency.

Based on the technology comparison, different extraction scenarios for the geothermal sector in Germany are developed and set into the context of the future local demand for the upcoming battery industry. Depending on the extraction efficiency and the market development, the already existing geothermal power plants in Germany could cover up to 12 % of the future Li demand. In Chile, with its already significant lithium production, the amount of lithium circulated in the only geothermal power plant could increase the country's lithium production by up to 3%.

For analyzing the potential during continuous production, a first full-scale model, based on the geology of the Upper Rhine Graben in Germany, was developed, simulating a 30-year operational period for Li extraction. The simulation revealed a depletion of Li by 30 – 50 % during the observation period, while the heat production remains constant. Nonetheless, the model also demonstrates a mean Li production of 231 t per year, which could significantly enhance the economic prospects of a geothermal power plant and, if applied to multiple plants, reduce Germany's dependence on global Li imports.

The remaining challenges for implementing DLE in geothermal cycles are among others uncontrolled mineral precipitations, like Si scaling, and especially in Chile the overall low mineralization of volcanic geothermal fluids. To approach these challenges, a pre-treatment setup for geothermal fluids was developed. The system includes a chemical pre-treatment based on lime/caustic precipitation for reducing initially the Si concentration in the brine. Depending on the geothermal setting, a post- and a pre-concentration step is implemented for increasing the concentration of the target elements and enabling, fresh water production for instance in Chile. The combination of chemical pretreatment with reverse osmosis and membrane distillation was implemented in a demonstrator system that was tested in continuous operation in a geothermal power plant in Germany as well as at a thermal spring in Chile. In Germany, a successful Si reduction of 98 % was demonstrated as well as a concentration of the dissolved minerals by a factor of three, reaching a Li concentration of ~500 mg/L. In Chile, the Si was removed by 50% during flow-through testing. The test phase achieved furthermore concentration rates up to a factor of 20 during continuous operation and demonstrated the possibility of operating this process with geothermal heat.

Kurzfassung

Der vom Menschen verursachte Klimawandel und die daraus resultierende Notwendigkeit einer Energie- und Mobilitätswende stellen uns vor enorme Herausforderungen und werden dies auch für kommende Generationen tun. Fossile CO₂-emittierende Energieträger werden durch erneuerbare Alternativen ersetzt. Insbesondere grundlastfähige Energieträger wie Kohle und Gas werden eine große Lücke in der Energielandschaft hinterlassen - eine Lücke, die mit klimaneutralen, nachhaltigeren und grundlastfähigen Energien gefüllt werden muss. Darüber hinaus schaffen neu entstehende Technologien eine große und sehr vielfältige Nachfrage nach Hightech-Materialien. Insbesondere die Elektrifizierung des Mobilitätssektors stellt eine große Herausforderung für die globalen Lieferketten kritischer Rohstoffe dar.

Die Geothermie zeigt im globalen Maßstab das Potenzial für eine ökologische und ökonomische Bereitstellung von Grundlastwärme und -energie mit einer stetig wachsenden installierten Leistung. Die in Geothermiekraftwerken permanent zirkulierenden großen Fluid-Volumenströme in Kombination mit der hohen Konzentrationen spezifischer Elemente bergen darüber hinaus ein erhebliches Rohstoffpotenzial. Unter den verschiedenen Elementen, die weltweit in geothermischen Fluiden vorkommen, gibt es eine Reihe von Elementen, die von der EU als kritische Elemente definiert wurden, wie Lithium (Li), Cäsium (Cs), Magnesium (Mg), Strontium (Sr), Bor (B), Silizium (Si), Antimon (Sb) oder Fluor (F).

Ein neues Konzept einer erweiterten Mehrfachnutzung hydrothermalen Systeme zur Erzeugung von Strom, Wärme und Rohstoffen könnte auf nationaler und internationaler Ebene mehrere Vorteile bringen. In Bergbauländern wie Chile könnte das neue Konzept dazu beitragen, den lokalen Bergbausektor nachhaltiger zu gestalten. Aufgrund der Wasser inhärenten Energie würde der externe Energieverbrauch minimiert werden. Durch den Einsatz von Direkter Lithiumextraktion (DLE) könnten die Wasserverluste, die in herkömmlichen Verdunstungsbecken für die Li-Extraktion auftreten, vermieden werden, wodurch ein typisches Konfliktthema im Bergbau beseitigt würde. Darüber hinaus könnten die neu erschlossenen Ressourcen dem chilenischen Lithiumsektor größere globale Marktanteile erschließen. Für ein Land wie Deutschland, das derzeit sein gesamtes primäres Li importiert, eröffnet dieser minimal-invasive Abbauansatz die Perspektive für eine Renaissance des heimischen Bergbausektors.

Die vorgestellten Studien zeigen das vielfältige Ressourcenpotenzial der hydrothermalen Systeme in Deutschland und Chile. Für Deutschland wird das Potenzial der bestehenden geothermischen Kraftwerke zur Li-Gewinnung analysiert und die mögliche Deckung des lokalen Li-Bedarfs quantifiziert. Für Chile wird das allgemeine Rohstoffpotenzial der reichlich vorhandenen geothermischen Systeme des Landes beschrieben.

Um die Herausforderungen zu ermitteln, die sich für DLE aus geothermischen Fluiden ergeben können, werden verschiedene Extraktionstechnologien quantitativ verglichen. Häufig diskutierte Technologien wie die Flüssig-Flüssig-Extraktion, die selektive Extraktion durch

anorganische Sorbentien, elektrochemische Verfahren und Membrantechnologien werden hinsichtlich ihres spezifischen Einflusses auf die physiochemischen Eigenschaften des Wassers (pH, Eh, T, p usw.) bewertet und auf der Grundlage ihres technologischen Reifegrads (TRL) klassifiziert. Schlüsselparameter für das Prozessdesign sind der nutzbare Volumenanteil des geothermischen Fluides und die Extraktionseffizienz.

Auf der Basis des Technologievergleichs werden verschiedene Förderszenarien für die Geothermie in Deutschland entwickelt und in den Kontext der zukünftigen lokalen Nachfrage für die künftige Batterieindustrie gestellt. In Abhängigkeit von der Extraktionseffizienz und der Marktentwicklung könnten die bereits bestehenden geothermischen Kraftwerke in Deutschland bis zu 12 % des zukünftigen Li-Bedarfs decken. In Chile mit seiner bereits großen Lithiumproduktion könnte die Lithiummenge, die in dem einzigen geothermischen Kraftwerk zirkuliert, die Lithiumproduktion des Landes um bis zu 3 % erhöhen.

Zur Analyse des Potenzials bei kontinuierlicher Förderung wurde ein erstes großmaßstäbliches Modell auf der Grundlage der Geologie des Oberrheingrabens in Deutschland entwickelt, das einen 30-jährigen Betriebszeitraum für die Li-Gewinnung simuliert. Die Simulation ergab eine Abnahme der Li Konzentration um 30 - 50 % während des Beobachtungszeitraums, während die Wärmeproduktion konstant bleibt. Dennoch zeigt das Modell auch eine mittlere Li-Produktion von 231 t pro Jahr, was die wirtschaftlichen Aussichten eines geothermischen Kraftwerks erheblich verbessern und, wenn es auf mehrere Anlagen angewendet wird, die Abhängigkeit Deutschlands von weltweiten Li-Importen verringern könnte.

Verbleibende Herausforderungen für die Implementierung von DLE in geothermischen Kreisläufen sind unter anderem unkontrollierte mineralische Ausscheidungen, wie z. B. Si-Scaling, und insbesondere in Chile die generell geringere Mineralisierung vulkanischer geothermischer Fluide. Um diesen Herausforderungen zu begegnen, wurde eine Vorbehandlungsverfahren für geothermische Fluide entwickelt. Das System umfasst eine chemische Vorbehandlung auf der Basis von Kalk/Lauge-Fällung zur initialen Verminderung der Si-Konzentration in dem Fluid. Je nach geothermischen Gegebenheiten werden ein Nach- und ein Vorkonzentrationsschritt implementiert, um die Konzentration der Zielelemente zu erhöhen und gleichzeitig beispielsweise in Chile Süßwasserproduktion zu ermöglichen. Die Kombination von chemischer Vorbehandlung mit Umkehrosiose und Membrandestillation wurde in ein Demonstratorsystem umgesetzt, das im Dauerbetrieb in einem geothermischen Kraftwerk in Deutschland sowie an einer Thermalquelle in Chile getestet wurde. In Deutschland wurde eine erfolgreiche Si-Reduktion von 98 % sowie eine Konzentration der gelösten Mineralien um den Faktor drei nachgewiesen, wobei eine Li-Konzentration von ~500 mg/L erreicht wurde. In Chile wurde die Si-Konzentration im Dauerbetrieb um 50 % reduziert. Die Testphase erzielte hier Konzentrationsraten bis zu einem Faktor von 20 im kontinuierlichen Betrieb und demonstrierte gleichzeitig die Möglichkeit diesen Prozess mit geothermischer Wärme zu betreiben.

Resumen

El cambio climático provocado por el ser humano y la consecuente necesidad de transición en materias de energía y movilidad está creando enormes desafíos y seguirá haciéndolo para las generaciones venideras. Las fuentes energéticas en base a combustibles fósiles, que emiten CO₂, están siendo sustituidas por alternativas renovables. En particular, las fuentes con una alta capacidad de carga base, como el carbón y el gas, dejarán un gran vacío en el panorama energético, un vacío que debe llenarse con energías neutras, más sostenibles y con capacidad de carga base. Además, las nuevas tecnologías emergentes generan una amplia y diversa demanda de materiales de alta tecnología. Particularmente, la electrificación del sector movilidad plantea un reto importante para las cadenas mundiales de suministro de materias primas fundamentales.

A escala mundial, la energía geotérmica demuestra un potencial para el suministro ecológico y económico de calor y energía de carga base, con una capacidad instalada en continuo crecimiento. El gran volumen de los fluidos que circulan constantemente en las centrales geotérmicas, en combinación con el enriquecimiento de elementos específicos, implican, además, un importante potencial en materias primas. Entre los diversos elementos presentes en los fluidos geotérmicos de todo el mundo hay varios definidos como elementos críticos por la Unión Europea (UE), como el litio (Li), el cesio (Cs), el magnesio (Mg), el estroncio (Sr), el boro (B), el silicio (Si), el antimonio (Sb) o el flúor (F).

Un nuevo concepto de sistemas hidrotermales avanzados de usos múltiples que produzcan electricidad, calor y materias primas podría reportar varios beneficios nacionales e internacionales. En países mineros como Chile, este nuevo concepto podría ayudar al sector minero local a transitar hacia una mayor sostenibilidad. Gracias a la energía inherente al agua, se minimizaría el consumo energético externo. Utilizando la Extracción Directa de Litio (DLE), podrían evitarse pérdidas de agua que ocurren en las piscinas de evaporación convencionales para la extracción de Li, eliminando así un típico conflicto de la minería. Además, los recursos recién explotados podrían abrir mayores cuotas de mercado mundial para el sector chileno de litio. Para un país como Alemania, que actualmente importa todo su litio primario, este enfoque minero mínimamente invasivo abre la perspectiva para un renacimiento del sector minero local.

Los estudios presentados describen el potencial de recursos de los sistemas hidrotermales de Alemania y Chile. En el caso de Alemania, se analiza el potencial de las centrales geotérmicas existentes para la extracción de Li y se cuantifica la posible cobertura de la demanda local de Li. En el caso de Chile, se describe el potencial general de materia prima de los abundantes sistemas geotérmicos del país.

Para determinar los retos que puede plantear la DLE a partir de fluidos geotérmicos, se comparan y cuantifican diferentes tecnologías de extracción. Tecnologías discutidas con frecuencia, como la extracción líquido-líquido, la extracción selectiva mediante sorbentes inorgánicos, los métodos electroquímicos y las tecnologías de membrana, se evalúan en función

de su influencia específica sobre las propiedades fisicoquímicas del agua (pH, Eh, T, p, etc.) y se clasifican además en función de su nivel de preparación tecnológica (TRL). Los parámetros clave para el diseño del proceso son la fracción de volumen utilizable del fluido geotérmico y la eficiencia de extracción.

Basándose en la comparación de tecnologías, se desarrollan diferentes escenarios de extracción para el sector geotérmico en Alemania y se sitúan en el contexto de la futura demanda local para la inminente industria de baterías. En función de la eficiencia de extracción y de desarrollo del mercado, las centrales geotérmicas ya existentes en Alemania podrían cubrir hasta el 12 % de la futura demanda de litio. En Chile, con su ya importante producción de litio, la cantidad de litio que circula por la única central geotérmica podría aumentar hasta un 3% la producción de litio del país.

Para analizar el potencial durante la producción continua, se desarrolló un primer modelo a escala real, basado en la geología del Graben del Rin Superior en Alemania, simulando un periodo operativo de 30 años para la extracción de Li. La simulación reveló un agotamiento del Li de entre el 30 y el 50 % durante el periodo de observación, mientras que la producción de calor se mantiene constante. No obstante, el modelo también demuestra una producción media de Li de 231 t al año, lo que podría mejorar significativamente las perspectivas económicas de una central geotérmica y, si se aplica a múltiples centrales, reducir la dependencia de Alemania de las importaciones mundiales de Li.

Los retos pendientes para la aplicación de la DLE en los ciclos geotérmicos son, entre otros, las precipitaciones minerales incontroladas, como la incrustación de Si, y especialmente en Chile la baja mineralización general de los fluidos geotérmicos volcánicos. Para abordar estos retos, se desarrolló un sistema de pretratamiento para fluidos geotérmicos. El sistema incluye un pretratamiento químico basado en la precipitación de cal/soda caústica para reducir inicialmente la concentración de Si en la salmuera. Dependiendo del entorno geotérmico, se implementa una etapa de post y preconcentración para aumentar la concentración de los elementos objetivo y permitir, por ejemplo, la producción de agua dulce en Chile. La combinación del pretratamiento químico con la osmosis inversa y la destilación por membranas se aplicó en un sistema de demostración que se probó en funcionamiento continuo en una central geotérmica de Alemania y en un sistema geotérmico de Chile. En Alemania, se demostró una reducción satisfactoria del Si en un 98 %, así como una concentración de los minerales disueltos en un factor de tres, alcanzando una concentración de Li de -500 mg/L. En Chile, la concentración de Si se redujo en un 50 % en funcionamiento continuo, al tiempo que se alcanzaban tasas de concentración de hasta un factor 20 y se demostraba la posibilidad de un suministro de calor geotérmico para alimentar este proceso.

Table of Contents

Acknowledgments	i
Abstract	iv
Kurzfassung	vi
Resumen	viii
Table of Contents	xi
List of Figures	xiv
List of Tables	xix
1 Introduction.....	1
1.1 Motivation: Energy and Raw Materials – The Social Challenges	1
1.2 Structure of the thesis	4
2 Fundamentals.....	9
2.1 Classification of Geothermal Systems	9
2.2 Development of Geothermal Fluids.....	10
2.3 Processes within Geothermal Reservoirs	13
2.4 Raw Material Extraction from Geothermal Fluids.....	16
2.5 Application of Membrane Processes.....	18
2.6 Scaling.....	20
2.7 Silica Scaling Treatment.....	22
3 Study Areas – Chile and Germany	25
3.1 Germany	25
3.2 Chile.....	30
4 Technology assessment for Direct Lithium Extraction from geothermal fluids.....	36
4.1 Abstract	37
4.2 Introduction	38
4.3 Methods	42
4.4 Extraction Technologies	44

4.5	Current Extraction Projects	53
4.6	Discussion and Conclusion	59
4.7	Acknowledgments	61
5	Potential Evaluation and Production Scenarios for Geothermal Lithium in Germany ...	62
5.1	Abstract	63
5.2	Introduction	64
5.3	Methods	72
5.4	Results	74
5.5	Discussion.....	76
5.6	Conclusions.....	79
5.7	Acknowledgments.....	81
6	Reservoir behavior of lithium-depleted brine in a geothermal reservoir	82
6.1	Abstract	83
6.2	Introduction	84
6.3	Methods	89
6.4	Results	95
6.5	Discussion.....	97
6.6	Conclusions.....	102
6.7	Acknowledgments.....	103
7	Development of a continuous silica treatment strategy for metal extraction processes in operating geothermal plants.....	105
7.1	Abstract	106
7.2	Introduction	107
7.3	Material and Methods	110
7.4	Upscaling continuous Si Precipitation and Fluid Concentration	118
7.5	Results	122
7.6	Discussion.....	130
7.7	Conclusion and Outlook	133
7.8	Acknowledgment	135
7.9	Appendix.....	136
8	The potential of raw material extraction from thermal fluids in Chile	138
8.1	Abstract	139
8.2	Introduction	140
8.3	Potential of geothermal Brine Mining in Chile.....	141

8.4	Pretreatment of thermal waters.....	146
8.5	Outlook and global potential	150
8.6	Conclusion.....	152
8.7	Acknowledgment	153
9	Prototype tests for the treatment of geothermal waters for raw material extraction and freshwater production.....	154
9.1	Abstract	155
9.2	Introduction	156
9.3	Fundamentals.....	157
9.4	Results	161
9.5	Concluding remarks.....	163
9.6	Acknowledgments.....	164
10	Comparison of lime/caustic precipitation mechanisms as pre-treatment in different geothermal fluids	165
10.1	Abstract	165
10.2	Introduction	166
10.3	Material and Methods	166
10.4	Results	168
10.5	Discussion.....	175
10.6	Conclusion.....	178
10.7	Appendix.....	180
11	Conclusion and Outlook.....	184
11.1	Major findings	184
11.2	Outlook	186
	References.....	189
	Declaration of Authorship.....	222
	Appendix.....	225
	Publication list	226
	Curriculum Vitae.....	231

List of Figures

Figure 1:	Global electricity production by source and scenario from 2010 - 2050. STEPS: Stated Policies Scenario; APS: Announced Pledges Scenario; NZE: Net Zero Emissions by 2050 Scenario (Adapted from International Energy Agency, 2022).	1
Figure 2:	Multi-use concept for a deep hydrothermal doublet system. An ideal process would aim for a cascade use of energy. Primary electricity production using the initial high temperatures (>100 °C) is followed by direct heating use. The new concept of a multi-use would then further extract valuable raw materials before reinjecting the fluids into subsurface.	4
Figure 3:	a) Schematic of reverse osmotic equilibrium (1) and reverse osmosis membrane (2) b) schematic drawing of a spiral wound module (adapted from Chian et al., 2007)	19
Figure 4:	Different channel configurations for membrane distillation: direct contact membrane distillation (DCMD); air gap membrane distillation (AGMD); feed gap membrane distillation (FGMD) and feed gap air gap MD (FGAGMD) (Adapted from Schwantes et al., 2019).....	20
Figure 5:	a) Solubility of amorphous silica in NaCl solutions (Data: Appelo, 2015, Chen & Marshall, 1982; Marshall & Warakomski, 1980b). b) Solubility of calcite (displayed by Ca) in double distilled water as a function of CO ₂ partial pressure (Data: Segnit et al., 1962).	21
Figure 6:	Simplified distribution of silica species at 25°C in amorphous silica-saturated NaOH solution excluding polymeric species (Adapted from Eikenberg, 1990).	23
Figure 7:	Overview of the sedimentary thicknesses and major fault systems in Germany. The areas of large sedimentary thicknesses represent also the high potential areas of deep geothermal energy (Adapted from Franz et al., 2018).....	26
Figure 8:	a) Topographic map of the North German Basin with the position of investigated seismic lines (map taken from Mazur & Scheck-Wenderoth, 2005) b) Interpreted geoseismic NNE-SSW cross-section from figure a) across the southern North German Basin. The interpretation is based on seismic reflection lines as well as borehole stratigraphy and the vertical scale is 2-times exaggerated (profile taken from Mazur & Scheck-Wenderoth, 2005).	27
Figure 9:	a) Overview of the Swiss-German Molasse Basin with contour lines of the base of Tertiary sediments (i.e. the Molasse sediments) and major structures. b) N-S profile through the Molasse Basin along the Profile in a) (Map and profile taken from Reinecker et al., 2010).	28
Figure 10:	Schematic cross-section through the Upper Rhine Graben between the Vosges Mountains and the Black Forest north of Strasbourg showing the topographically driven flow system within the sedimentary formations and the fractured crystalline basement (Profile taken from Stober & Bucher, 2015).	29
Figure 11:	Schematic map of South America and the subduction zones of the Nazca and Antarctic plate. Subduction direction and speed are indicated by arrows in cm/yr, and subduction geometry by depth in km to the Wadati-Benioff Zone. The black triangles display quaternary volcanoes (map taken from Stern, 2004).	32
Figure 12:	Schematic drawing of a typical volcanic play type above a subduction zone (adapted after Moeck, 2014).	34
Figure 13:	Geothermal areas in Chile separated into indicated resources, inferred resources, and areas, which are highly favorable, and of interest. The left side shows the Systems in northern	

	Chile, while the right side shows geothermal systems in the south (maps taken from Aravena et al., 2016).	35
Figure 14:	Illustration of a liquid-liquid extraction cycle, adapted after D. Shi et al. (2018). Shown are the four typical extraction steps using a solvent (nL) and a co-extraction reagent, in our example tributyl phosphates (TBP) and FeCl ₄ , respectively. The extraction in the case example is performed from a brine containing lithium and other interfering cations (M ⁺). Right: Principle of incorporation of lithium into a crown ether structure according to Swain (2016).	45
Figure 15:	Principle of lithium extraction with manganese oxides according to Feng et al. (1992). Left: Incorporation of lithium into the structure of manganese oxides. Incorporation takes place via two processes: ion exchange and redox reaction. Right: Redissolution of lithium from the structure by treatment with acid.	47
Figure 16:	Schematic representation of an electrochemical ion pump using manganese oxide as a working electrode for lithium. Adapted from Batisstel et al. (2020). Right: Schematic representation of two different approaches for lithium enrichment using electro dialysis. Approach A is based on a membrane that is permeable for lithium but largely blocks other ions. Approach B uses a lithium-blocking membrane. Adapted from Liu, Zhao, and Ghahreman (2019).	50
Figure 17:	Global annual lithium production as lithium carbonate equivalents (LCE) since 2015 and predictions of different scenarios until 2030 (Data origin: (Martin et al. 2017; Meng et al. 2021; Adams 2020; Jones et al. 2021)). In 2020, 420,000 t of LCE were produced, significantly exceeding earlier projections from 2017	65
Figure 18:	Country and company concentrations of lithium mining production in 2019 (Data origin: DERA 2021a)	66
Figure 19:	Price development for LCE from 2000 to 2021 and forecasts up to 2030 (Data origin:: (Hohmann (2021); Trading Economics (2022); German Lithium Participation (2021))	67
Figure 20:	Location of geothermal sites and of planned battery cell production in Germany. The map shows the lithium content and flow rate of the geothermal sites potentially suited for raw material extraction and indicates the forecasted lithium demand for battery cell production. The demand was calculated based on the planned annual capacities. (Data sources: DERA (2021a), Agemar et al. (2014a) (GeotIS), (2014b))	71
Figure 21:	Theoretically extractable amount of LCE (t/a) from the geothermal systems in the Upper Rhine Graben and the North German Basin for extraction efficiencies of 50% (blue) and 90% (red). Further assumptions for determining potential are a constant lithium concentration over the production period, fluid content usability of 100%, and the availability of geothermal production 90% of the time	74
Figure 22:	a) Preliminary global Li production for 2021 and its global distribution (Data:(Schmidt 2023)). b) Global demand prediction for Li in 2030 for different yearly growth predictions (316,300 t, 426,700 t, 558,800 t) in comparison to the predicted global production scenarios (conservative: 217,890 t, optimistic: 357,680 t) (Data: (Schmidt 2023))	86
Figure 23:	a) 3D-Reservoir model with all implemented geological units. b) Enlarged view of the fault zone and the wells. For clarity, the layers outside the damage zone and the damage zone of the reservoir are not displayed.	90
Figure 24:	a) A general overview of a cross-section of the model containing five layers and a damage and a core zone. The whole model is a box with 12 km × 7 km × 3.5 km extension in x, y, and z directions, respectively. b) A closer view of the mesh size distribution in the adjacency of the injection (red arrow) and production (blue arrow) wells penetrating the damage zone with 250 m width. A 10 m core zone is highlighted in this subplot.	91
Figure 25:	a) Temperature change over time at the production well at different flow rates. b) Maximum pressure changes at the injection and production well after 30 years.	95

Figure 26:	a) Temperature change around the injection well along the fault zone after 30 years in the reference scenario. For clarity, only parts of the fault, the reservoir, and the bottom layer are displayed. The white contour shows the propagation of a temperature drop of -5 K. b) Solute distribution around the injection well along the fault zone after 30 years in the reference scenario. For clarity, only parts of the fault, the reservoir, and the bottom layer are displayed. The white contour shows the spread of a residual solute concentration of 10%.....	96
Figure 27:	Development of the solute concentration at the production well over time for different flow rates and extraction efficiencies.....	97
Figure 28:	a) Productivity of the different scenarios in [t/year]. For all scenarios, the specific product, the amount of extracted Li, was calculated based on the solute concentration for each timestep and normed to one year. b) Accumulated Li_2CO_3 production over time. Based on the productivity and the differences in the timesteps the accumulated Li_2CO_3 production was determined.	100
Figure 29:	Predicted economic values of the products heat and Li_2CO_3 . Reference Li extraction scenario with 80 L/s, 180 mg/L Li initially and an extraction Efficiency of 75 % and Li_2CO_3 prices between 26,200 US\$/t and 61,500 US\$/t. Heat extraction scenario from the same model for an initial temperature at the production well of 160 °C, reinjection temperature of 65 °C and 90 % efficiency at direct heat use with market prices between 6.88 ct/kWh and 12.95 ct/kWh.	102
Figure 30:	Simplified scheme of the power plant Insheim. The scheme displays the major intervention in the fluid properties and the implementation point of the prototype within the systems.	112
Figure 31:	Database validation for the chemical processes of the treatment. The applicability of the thermodynamic data is evaluated with experimental data for temperature, salinity and high pH values for dissolved Ca^{2+} and Si species as well as on CSH phases. a) Simulated solubility of amorphous silica in NaCl waters at different temperatures in comparison to experimental data (Experimental data:(Appelo 2015; Chen and Marshall 1982; Marshall and Warakomski 1980b)). b) Solubility of calcite at different temperatures and NaCl concentrations at a CO_2 partial pressure of 1 kPa (Appelo 2015; Wolf et al. 1989) c) The effect of NaOH addition on aqueous Ca^+ in different saline NaCl solutions at 25°C (Experimental data: (Kutus et al. 2016)). d) Solubility relationship of amorphous silica and in aqueous solutions at 25°C under addition of CaOH (Experimental data: (Greenberg and Chang 1965)). e) The effect of NaOH addition on aqueous Ca^+ in 1 molar NaCl solutions at 25°C, 50 °C and 75 °C (Experimental data: (Duchesene and Reardon 1995; Kutus et al. 2016)).....	117
Figure 32:	Prototype layout and hydraulic scheme. The hydraulic scheme is separated into three major elements: Si-reduction, solid separation, and post-concentration. Major elements for the chemical treatment are the continuously steered tank reactors (CSTR). The Plant can be operated for batch experiments and in a continuous flow mode with additional post-concentration. The possible hydrochemical sampling points are incorporated as S1 to S9.	118
Figure 33:	Schematic representation of the FG-AGMD channel configuration (Figure based on (Schwantes et al. 2019)).....	119
Figure 34:	Demonstration plant operated with natural geothermal fluids on-site at power plant Insheim, Upper Rhine Graben, Germany.....	120
Figure 35:	Results of a PHREEQC simulation of the precipitation behavior in a geothermal fluid induced by a pH shift by NaOH dosing. The plot shows the major concentration changes and mass flows during the pH shift The arrows indicate on which axis the data depend. Fluid starting composition according to URG (Table 12). Constant Temperature at 57 °C. Used PHREEQC Database: Pitzer_CSH.	124

Figure 36:	Reproduction of the treatment strategy developed in the Laboratory. The graph shows the influence of the silica treatment on the 4 major cations. Displayed are four experiments. In the graph, we can see the measured values of the elements and the associated observational errors. Additionally, the upper and lower quartiles from the measurements of untreated water are displayed to judge the effectiveness of the treatment steps.	127
Figure 37:	Development of Cations- Contents over time in the batch operation of the NaOH-induced silica extraction (kinetic mode).	128
Figure 38:	Concentration of treated geothermal fluids. Pre-treated water was concentrated up to almost factor 3. The measured data are presented by the points. The Mean initial Si is the mean measured Si in untreated water samples measured during the sampling campaigns. The black line shows how the Si content of the mean Si would evolve if it would be concentrated at the same rate as the other elements. The red line shows the simulated solubility for Si if untreated water would be concentrated.	130
Figure 39:	Influence of the prototype on the chemistry and temperature of the water. The graph shows the relative change of the geothermal fluid during the continuous operation at 20 l/h with the jacket of CSTR2 heated to 55°C. The results were referred to the initial brine composition sampled at point S1 (see Figure 30).....	136
Figure 40:	The development of Cl concentration during the silica treatment. Chloride as a conservative element is not included in the precipitation reactions and serves as a reference for the quality of the measurement. Generally, the values fluctuate very little and variations are in the range of naturally occurring changes and observational errors.	137
Figure 41:	Distribution of thermal springs in Chile. Marker size indicates the amount of total dissolved solids. The color represents the reservoir temperature. The highlighted springs were selected due to their high values of elements, which are of economic interest in Chile.	142
Figure 42:	Economic potential of selected sites. Different raw materials can be produced from elements in thermal brines in Chile. The left side shows the occurrence of potential target elements. The right side displays the market value of processed products from these elements. Note the logarithmic scale of the market prices. The comparison displays that even elements with minor contents in brines can be lucrative exploration targets. (Bastian 2020; Brioche 2017; Dolley 2017; Tuck 2020b; Tuck 2020a).	144
Figure 43:	Solubility behavior of silica. The plot shows the solubility of different silica polymorphs/phases in dependency of the temperature (Data Source reference (Fournier and Rowe 1966)).	146
Figure 44:	Flow chart summarizing the problem-solving approach in the BrineMine project. Based on the challenge of silica fouling, a treatment strategy was developed in the laboratory. This approach was upscaled first using a numerical design calculation. The simulation results were subsequently reproduced in a technical center leading to the construction of a 1 st generation prototype.	147
Figure 45:	Process scheme and hydraulic/energetic integration strategy for the BrineMine continuous flow demonstrator.	149
Figure 46:	Geothermal power plant Insheim (Source: Pfalzwerke geofuture GmbH).	149
Figure 47:	Prototype installed at the geothermal power plant Insheim. The left picture shows the prototype. Precipitates are shown in the two pictures on the right. (Source: Valentin Goldberg / Sebastian Held).....	149
Figure 48:	Effectiveness of silica treatment. The graph shows the relative change of chosen elements during the prototype testing. Within 5 minutes, the total content of Si is reduced by 98 %. Li as raw material reference stays unaffected and varies within the scope of measurement inaccuracy.....	150
Figure 49:	Preliminary worldwide database of geothermal brines. The database currently contains data of ~10,000 springs and provides the basis for the evaluation of the global economic potential	

	of Brine Mining (Data sources: (Allen et al. 2006; Aquilina et al. 2002; Arnórsson et al. 1983; Cortecce et al. 2005; Giggenbach et al. 1994; Giggenbach 1992; Giggenbach 1978; Gokgoz et al. 2010; González-Partida et al. 2005; Grasby et al. 2000; Karamanderesi and Ölçeno 2005; Karingithi et al. 2010; Kato et al. 2003; Kaya and Kindap 2009; Lowstern et al. 1999; Neupane and Wendt 2017; Nicolau et al. 2014; Özkaya 2007; Ozler 2000; Pauwels et al. 1993; Risacher et al. 2002; Sanjuan et al. 2016a; Sanjuan et al. 2010; Serpen and Aksoy 2010; Simsek 2003a; Simsek 2003b; Tarcan et al. 2000; Tassi et al. 2011; Tekin 2010; Wrage et al. 2017; Yeltekin and Akin 2006; Yildirim et al. 2010)).....	151
Figure 50:	Economic valuable elements in thermal waters. In red: elements that are classified as critical elements by the European Commission (Europäische Kommission 2020). In blue: other elements that are of high economic value and were found to be enriched in the global brine database.	152
Figure 51:	Technical scheme of the demonstrator setup, separated into 4 major sections. The flow diagram displays the associated mass flows in terms of solids and liquids.	158
Figure 52:	a) BrineMine field demonstrator in operation with natural thermal brine in Puyehue, Chile. b) Overview precipitation section. c) Drum filter for separation of CSH precipitates d) Difference CSH Suspension in tank reactor and collected Filtrate.	160
Figure 53:	Influence of the different process steps on the individual element concentration. The figure shows the relative change in element concentrations (Table 19) between all sampling points. This enables to evaluate every single step in its influence on its own. Ca refers to the secondary y-axis (red).	161
Figure 54:	Chemistry and Mineralogy of the precipitates, taken at S6. a) WDX analysis (LOI stands for loss on ignition). b) XRD analysis.	162
Figure 55:	Comparison of the Si concentration and pH value in different flow-through and batch experiments in the two testing phases in Insheim, the pre-study with fluids from BB (Spitzmüller et al. 2021) and from the testing phase in Puyehue, Chile. Markers with the same shape and color result from the same batch or flow-through experiment. The data are displayed in Table 22.	169
Figure 56:	Comparison of the relation between the relative Si reduction, retention time, and the pH value of the different fluids from Insheim, BB (Spitzmüller et al. 2021) and Puyehue. The dashed lines connect markers from the same kinetic experiment. The data are displayed in Table 22.	170
Figure 57:	Heat map on the influence of the fluid chemistry. The figure shows for the batch experiments from Insheim 1 (A, B, J, K, M, O, P, Q, R) the deviation from the standard water which is the average value of the untreated samples from the sampling campaign Insheim 1 (see also Chapter 7). For the kinetic experiments, the relative changes refer to the “T0” measurements.	172
Figure 58:	Mineralogical and chemical composition of the precipitates from Insheim after precipitation at pH 10.5 a) WDX data. LOI = loss on ignition. Analytical error: 1% relative for major and 10% relative for minor elements. b) XRD data (Qualitative determination of the mineralogical composition done with the EVA software of Bruker).	174
Figure 59:	a) BSE image (SEM) of precipitates from experiment G, Reactor 1 at pH 8.4. Euhedral calcite crystals are covered by very tiny grains with anhedral shape. The EDS spectrum illustrates the elevated contents of Si, Ca, Mg, and Na in the grain aggregate. (b) According XRD data(Qualitative determination of the mineralogical composition done with the EVA software of Bruker).	175
Figure 60:	BSE-SEM images of the precipitates at pH 10.5 of experiment M. The precipitates mainly form aggregates of tiny grains, partly displaying a leafy shape (point 8). Locally, amorphous material covers the precipitates (points 4 and 5). Due to the small grain size of the phases, mixture analyses can´t be avoided using SEM-EDS.	182

List of Tables

Table 1:	Different approaches for classifying geothermal systems.....	10
Table 2:	Major and trace element composition of different geothermal fluids. 1-6 compiled by <i>Arnorsson et al., 2007</i> . 1: Steam-heated surficial acid sulfate water, Krísuvík, Iceland (Arnorsson et al. 2007); 2: Carbon-dioxide water, Lýsuhóll well 6, Iceland (Arnorsson et al. 2007); 3: Mixed high-temperature and cool ground water, Nedridalur, Geysir field, Iceland (Arnorsson et al. 2007); 4: Hot spring in silicic volcanics, Ojo Caliente Spring, Yellowstone, Wyoming, USA (Ball et al. 1995); 5: Volcanic geothermal system in basalt, Krafla, well 21, Iceland (Arnorsson et al. 2007); 6: Seawater geothermal system, Reykjanes, well 15, Iceland (Arnorsson et al. 2007); 7: Na-Cl fluid in an andesitic volcanic geothermal system, Cerro Pabellón, well CP_1A, Chile (Cappetti et al. 2020; Giudetti et al. 2020); 8: Na-Cl fluid in granitic fault system of a non-magmatic extensional geothermal system, Insheim, well INSH, Germany (Sanjuan et al. 2016a). ^a pH/temperature of measurement, ^b Total carbonate carbon as CO ₂	12
Table 3:	Fluid chemistry of geothermal fluids from different geothermal regions in Germany	39
Table 4:	Lithium concentrations of different fluids in Germany and South America. Lithium concentrations and extraction conditions of fluids from geothermal, hydrocarbon and hot springs in Germany and salars in Chile and Argentina are compared.	40
Table 5:	Definition of technology readiness levels according to Mankins (1995, 2009), adapted to geothermal systems (De Rose et al. 2017).....	43
Table 6:	Current research projects on and commercial approaches regarding direct lithium extraction from geothermal fluids. Information about the (industrial) projects is not taken from scientifically peer-reviewed publications due to lack of availability but sourced from company communications that cannot be independently verified and evaluated	54
Table 7:	Different technologies for direct lithium extraction from thermal fluids. The table gives an overview of the advantages and disadvantages of the technologies, operating parameters during the extraction process, and an estimation of the technology readiness level (TRL) based on the literature review.	56
Table 8:	Lithium concentration in the fluid, volumetric flow produced, and theoretically extractable amount of lithium for geothermal power plants in the Upper Rhine Graben and the North German Basin. Lithium concentrations are from Sanjuan, et al. (2016a), Regenspurg et al. (2015), Schallenberg (1999) and Naumann (2000). Volumetric flows are taken from the work of Dilger et al. (2021), Egert et al. (2020), and Maurer et al. (2020)	75
Table 9:	Parametrization of the geological reservoir model based on (Q-con GmbH and Deutsche Erdwärme GmbH 2020).*Data not given in the model and added under comparison with additional data source (Stricker et al. 2020).** The fault core was implemented uniformly defined for all geological units as a tight, hydraulic impermeable unit. Data added under comparison with additional data sources (Evans et al. 1997; Stricker et al. 2020).....	92
Table 10:	Parameter variation for the sensitivity analysis and their relative change in comparison to the reference scenario.	94
Table 11:	Results of the different simulation scenarios and their relative influence on Li production parameters on the reference scenario.	99

Table 12:	Mean properties of the initial geothermal fluid in the geothermal power plant Insheim. The mean was calculated from 8 untreated water samples, collected over the range of a month. The standard deviation of the analysis is given as σ	111
Table 13:	Comparison of different thermodynamic datasets for the design calculation.	114
Table 14:	Technical specifications of the FG-AGMD test module.	119
Table 15:	Water analysis of the continuous flow experiments.	125
Table 16:	Sensitivity analysis on the key parameters NaOH, residual Ca content, and residual Si content at pH 10.5 using the design calculation. The varied parameters are highlighted for each simulation are highlighted in bold. Further, the input parameters TDS, Temperature, and HCO ₃ ⁻ as the varied parameters are shown.	133
Table 17:	Typical geothermal production scenario. The scenario assumes a flow rate of 80 L/s and an availability of 90 % of the year (329 days). The extraction rate is a conservative assessment based on the research in lithium extraction.	144
Table 18:	Economic potential of the production scenarios. The circulated amount results from the element content multiplied with the volume of circulated brine and the extraction rate. For boron and lithium, the amount was calculated as resulting compounds that can be produced from the pure element content.	145
Table 19:	Chemical analysis of selected elements over the whole treatment cycle. The referred sampling points (S1-S9) can be located in Figure 51. The last row displays the results of the batch concentration experiment using pre-treated brine.	162
Table 20:	Energetic consideration of the Puyehue spring. The assumptions are based on the site-specific parameters of the source temperature ($\sim 60^{\circ}\text{C}$), the density (983.55 Kg/m ³), specific heat capacity (4.18 kJ/kgK), and different cooling scenarios.	163
Table 21:	Summary of the different precipitation experimental setups.	167
Table 22:	Parameters for characterizing the Si reduction effectivity from the different studies in Germany in Chile.	180
Table 23:	EDS analyses of the measurement spots illustrated in Figure 4 (Experiment M). The data are given in wt.%.	183
Table 24:	XRD Analysis of precipitates of different precipitation experiments at pH 10.5. Qualitative approach using the Bruker EVA software.	183

1 Introduction

Climate change and the associated measures to fight it are currently most urgent challenges, affecting large segments of society. The exit from fossil fuel consumption, as it was decided by several industrial nations, demands a substitution for renewable energies. With these replacements, several challenges arise. The future energy market will be significantly more diverse than it is today (Figure 1) and especially volatile renewable energies will demand storage technologies on a large scale. Moreover, on the end consumer site, several technological changes are on the rise such as electric mobility. This all leads to changes in the global value chains away from hydrocarbons towards various metal raw materials (International Energy Agency 2022; Wellmer et al. 2019).

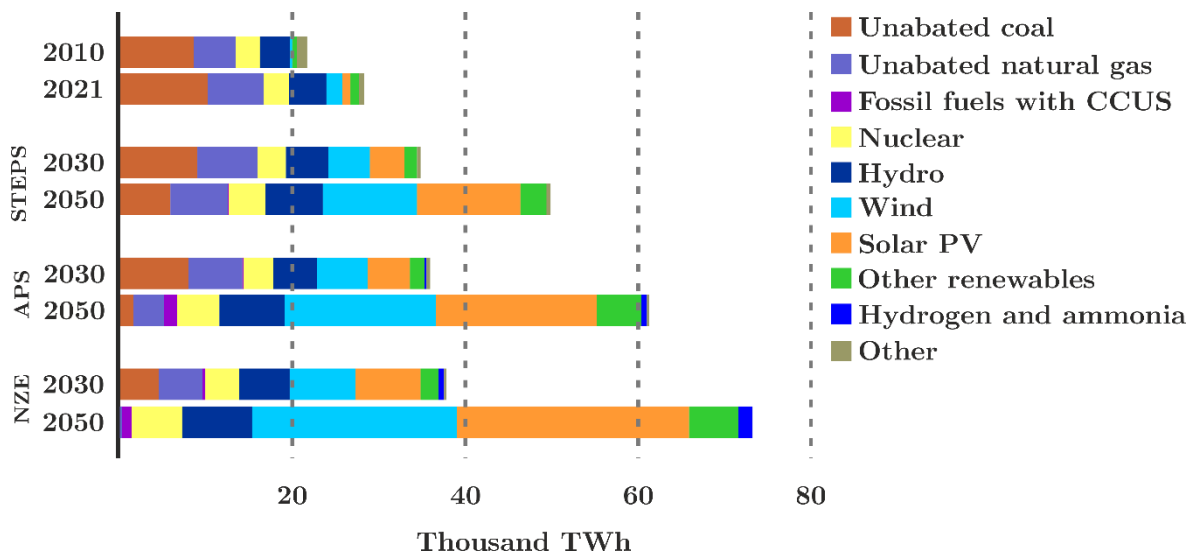


Figure 1: Global electricity production by source and scenario from 2010 - 2050. STEPS: Stated Policies Scenario; APS: Announced Pledges Scenario; NZE: Net Zero Emissions by 2050 Scenario (Adapted from International Energy Agency, 2022).

1.1 Motivation: Energy and Raw Materials – The Social Challenges

Several raw materials necessary for different energy technologies as platinum group elements, indium, tellurium, and rare-earth elements are classified as critical raw materials. Elements are considered critical if they are to a large extent sourced from just one or few countries and if the suppliers are categorized as potentially unreliable. With some exceptions are most of the rare-earth elements defined as critical raw materials because of their high country concentration with 95 % of the global mine production coming from China (Wellmer et al. 2019). For lithium (Li), one of the key elements of today’s state-of-the-art battery technology, also a critical development is foreseen in several scenarios (Greim et al. 2020; Schmidt 2023). Currently, 75 %

percent of the global Li production is sourced by two countries, Australia and Chile (Schmidt 2023; U.S. Geological Survey 2023). Additionally, 76 % of cell and battery manufacturing are located in China (Bridge and Faigen 2022). These two aspects already show poor diversification in the value chain for Li-ion batteries concerning Li. In addition with predictions of the Li supply gap in various scenarios (Greim et al. 2020; Schmidt 2023), the necessity of additional and reliable Li sources becomes apparent. This necessity becomes even more urgent considering the challenges of the largest global Li reserves, centered in the “Li triangle” of the Atacama Desert between Chile, Argentina, and Bolivia. The conventionally applied Li extraction process with a pond system takes between 10 and 24 months to pre-concentrate the salar (salt flat) brines and can thus hardly react to rapid market changes. Moreover, there are controversial discussions about the potential desertification and reduction of flora and fauna resulting from Li extraction in the Salar de Atacama (Schmidt 2023; Vera et al. 2023). Both aspects bear conflicts considering Li being the key element in a fast-growing market that is designed to make our energy supply more sustainable. Two necessary steps can therefore be derived from the volatility of renewable energies such as solar and wind power and the associated need for storage capacities:

1. The expansion of renewable baseload energies that do not require intermediate storage.
2. Development of new sustainable raw material extraction concepts that offer the opportunity to diversify centralized raw material markets.

Geothermal energy shows globally an ecologic and economic provision of baseload heat and energy with continuously growing installed capacity. The worldwide installed renewable electricity capacity of the geothermal sector was 16 GW_e (gigawatt electrical) in 2021 showing a growth of 30 % within 5 years. The installed direct use of geothermal heat suggests an even higher growth by 50 % in the same period, reaching 108 GW_t (gigawatt thermal) in 2020 (Huttrer et al. 2020; Lund and Toth 2021). Despite the large progress in the past years, only a negligible amount of the sheer endless global potential is tapped. In countries with strong volcanic activity such as Chile, the galore of subsurface energy is obvious. But also countries without these natural demonstrations of geothermal power like Germany have large geothermal potential (Agemar et al. 2014b; Aravena et al. 2016).

Concerning deep geothermal energy, hydrothermal geothermal energy is most widespread in both countries. In this type of use, naturally occurring deep fluids are tapped through deep wells and pumped to the surface at high flow rates of up to several hundred litres per second. Here, the fluids drive turbines to generate electricity or directly supply heating grids or industry, before the water is reinjected underground. Due to the temperatures (120 – 260 °C) and pressures (≤ 100 MPa) in the deep reservoirs, water-rock interactions can lead to an enrichment of various elements in the fluids (Cappetti et al. 2020; Sanjuan et al. 2016a; Talybov and Abdulagatov 2021). The baseload nature of geothermal power plants ensures independent and constant energy production and is derived by large fluid volume streams constantly circulating. In combination with the enrichment of specific elements a large raw material potential is derived. Among the elements occurring in geothermal fluids worldwide are various elements defined as critical elements such as Li, magnesium (Mg), strontium (Sr), boron (B), fluorine (F), silicon (Si), or antimony (Sb) (Giudetti et al. 2020; Hauser 1997; Neupane and

Wendt 2017; Sanjuan et al. 2022; Sanjuan et al. 2016a; Warren 2021). Especially for Li the extraction of the raw material using a Direct Li Extraction (DLE) approach for geothermal fluids is widely discussed (Kölbel et al. 2023; Reich et al. 2022; Stringfellow and Dobson 2021a; Weinand et al. 2023).

A new concept of advanced multi-use hydrothermal systems, producing electricity, heat, and raw materials (Figure 2) could bring several national and international benefits. In mining countries such as Chile, the new approach powered by geothermal energy could help to make the mining sector locally more sustainable. Due to the water's inherent energy, the external energy consumption can be significantly reduced, and by using DLE, the conflict-bearing water consumption could be minimized (Flexer et al. 2018; Vera et al. 2023). Moreover, the new untapped resources can open up larger global market shares for the Chilean Li sector.

For a country like Germany, currently importing 100 % regarding primary Li (Schmidt 2023), this minimal-invasive mining approach opens up the perspective for a renaissance of the local mining sector. The dependencies from overseas resources would be reduced as well as the environmental footprint of the raw materials used in Germany.

Considering the challenges of the energy transition and the potential of hydrothermal systems, this study analyses the resource potential of geothermal systems in Germany and Chile. In addition to the raw material potential, different extraction technologies for Li are evaluated with regard to their integrability into geothermal cycles. One of the major challenges identified are the comparatively low element concentrations, especially in volcanic fluids in Chile, while at the same time there is a high risk of silica scaling. Therefore, a silica treatment approach was developed and implemented in a demonstrator, which was tested in Germany and Chile. Finally, a numerical transport simulation was used to analyse the long-term behaviour of potential Li extraction in geothermal systems in Germany.

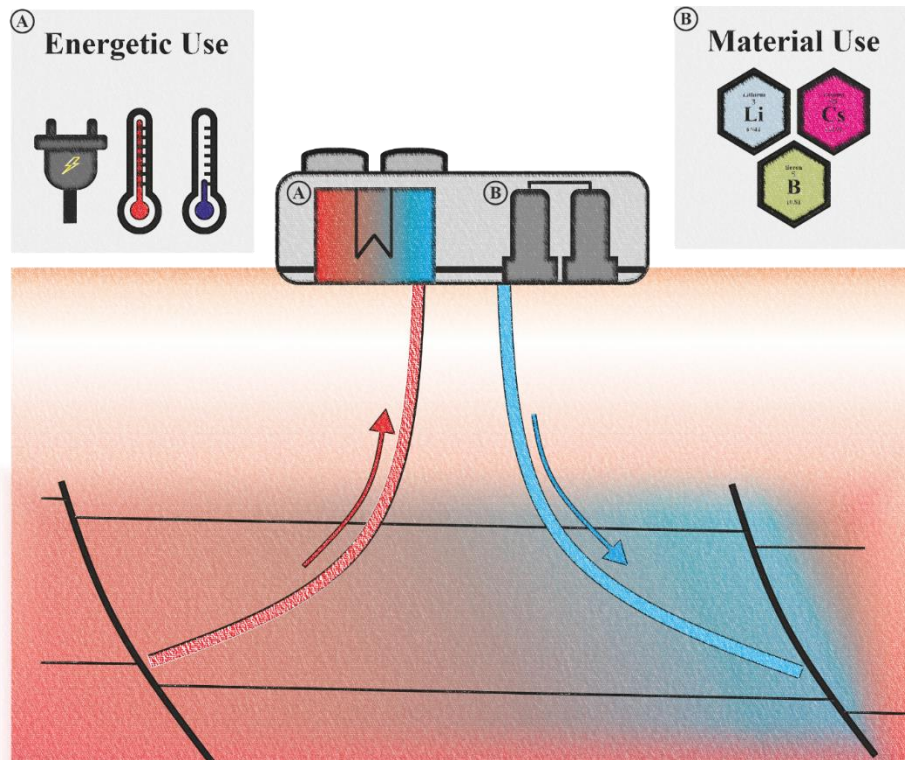


Figure 2: Multi-use concept for a deep hydrothermal doublet system. An ideal process would aim for a cascade use of energy. Primary electricity production using the initial high temperatures ($>100\text{ }^{\circ}\text{C}$) is followed by direct heating use. The new concept of a multi-use would then further extract valuable raw materials before reinjecting the fluids into subsurface.

1.2 Structure of the thesis

This study aims to examine the raw material potential of geothermal systems in Germany and Chile. In Germany, the scope was to analyze the potential of the geothermal sector in terms of Li extraction for the growing demand of the local battery sector. The governing questions were:

- 1) What are the potential technologies for the extraction of Li from geothermal fluids and what are the associated challenges for the integration in geothermal cycles?
- 2) To which extend can the German geothermal sector contribute to the local Li demand?
- 3) How will the Li concentration behave over time in the reservoir during continuous extraction?
- 4) How can the geothermal brine be pre-treated and concentrated for the raw material extraction?

In Chile, having a large active mining sector, the scopes of the research were different. Here the questions were:

- 5) Which raw materials occur in the geothermal systems and Chile and can they be an alternative or addition to the conventional mining sector?
- 6) How can the low-mineralized, but silica-rich volcanic fluids be pre-treated efficiently for raw material extraction?

Knowledge of typical fluid chemistry and fluid-rock interaction is fundamental to understanding the resource potential, the challenges of producing geothermal fluids, and the options for pretreatment. Therefore, Chapter 2 provides an introduction to the different types of geothermal fluids and their development, as well as processes within reservoirs. Different technologies for mineral extraction, scaling treatment and water purification and concentration are also presented. As the geothermal environments in both countries are fundamentally different, Chapter 3 gives a brief overview of the geological settings and geothermal situations in Germany and Chile.

The main results of the conducted research are presented in terms of individual manuscripts that have already been published.

Technology assessment for Direct Lithium Extraction from geothermal fluids (Chapter 4)

This chapter describes and compares frequently discussed technologies for DLE such as liquid-liquid extraction, selective extraction through inorganic sorbents, electrochemical methods, and membrane technologies for their applicability and integration into geothermal power plants. Due to the focus on the geothermal sector in Germany, a brief introduction into geothermal fluids in the German geothermal regions is given. In addition, fluid-rock interactions within geothermal power plants, such as scaling, corrosion, or degassing, are described.

The current state of the art in scientific publications indicates Li extraction efficiencies in laboratory experiments between 50 and 90%. Together with the concentration of Li and the flow rate, the extraction efficiency enables a first estimation of the Li potential of a specific site. Furthermore, the technology comparison enables us to quantify challenges for the incorporation of mineral extraction in geothermal facilities, such as the required extraction time which is in combination with the flow rates directly coupled to the required volumes for the extraction facility and sorbent use. In addition, depending on the extraction method, the physicochemical properties of water (pH, Eh, T, p, etc.) are altered during extraction, which can influence the fluid-rock equilibrium.

This chapter has been published in: Goldberg, V., Kluge, T. & Nitschke, F. (2022a). Herausforderungen und Chancen für die Lithiumgewinnung aus geothermalen Systemen in Deutschland – Teil 1: Literaturvergleich bestehender Extraktionstechnologien. *Grundwasser*. <https://doi.org/10.1007/s00767-022-00522-5>

Potential Evaluation and Production Scenarios for Geothermal Lithium in Germany (Chapter 5)

Chapter 5 takes the results of the technology review from Chapter 4 and combines them with the site-specific parameters from the geothermal sector in Germany and the French part of the Upper Rhine Graben. Additionally, the Li market and predictions for its development are discussed.

Due to the uncertainties of the current state of the technology, different extraction scenarios were calculated. In terms of flow-rate and Li concentration relevant 9 geothermal sites in Germany and France could produce in total between 4,000 and 7,200 t of Li carbonate equivalents (LCE) per year. The German plants alone could produce between 2,600 and 4,700 t of LCE, equivalent to 2 – 13 % of the annual demand for the planned German battery cell production. Large uncertainties remain in terms of the size of the geothermal reservoir, the challenges of the integration of a DLE process on a full scale, and the behavior of the reinjected, Li-depleted brine in the reservoir.

This chapter has been published in: Goldberg, V., Nitschke, F. & Kluge, T. (2022b). Herausforderungen und Chancen für die Lithiumgewinnung aus geothermalen Systemen in Deutschland – Teil 2: Potenziale und Produktionsszenarien in Deutschland. *Grundwasser*. <https://doi.org/10.1007/s00767-022-00523-4>

Reservoir behavior of lithium-depleted brine in a geothermal reservoir (Chapter 6)

Following the potential analysis of German geothermal sites in the previous chapters, Chapter 6 analyzes the long-term behavior of combined geothermal energy and Li extraction from a geothermal reservoir. Based on the geothermal settings of the Upper Rhine Graben, a full-scale 3D geological model is developed. Based on currently planned and operating geothermal power plants, different production scenarios are developed for simulating combined heat and Li extraction over a 30-year operational period.

The hydraulic and thermal models agree with the situation in operating geothermal power plants and the seismic risk assessment for a currently planned one. The chemical model indicates a strong chemical breakthrough in all scenarios. Depending on the scenario the Li breakthrough occurs after 4 to 7 years and leads to a Li depletion at the production well of 30 to 50 %. Nonetheless, the reference model (flowrate of 80 L/s, Li concentration of 180 mg/s, and an extraction efficiency of 75 %) demonstrates that a mean Li production of 1230 t LCE per year over 30 years is possible, equivalent to 0.5 – 3 % of the annual demand for the planned German battery cell production.

This chapter has been published in: Goldberg, V., Dashti, A., Egert, R., Benny, B., Kohl, T. & Nitschke, F. (2023b). Challenges and Opportunities for Lithium Extraction from Geothermal Systems in Germany – Part 3: The Return of the Extraction Brine. *Energies*, 16(16), 5899. <https://doi.org/10.3390/en16165899>

Development of a continuous silica treatment strategy for metal extraction processes in operating geothermal plants (Chapter 7)

Chapter 7 presents the transfer of a silica treatment approach from the laboratory to field demonstrator scale, operated in a geothermal power plant in Germany. The demonstrator combines a chemical pre-precipitation of silica-containing mineral phases with a concentration step using membrane distillation (MD).

For transferring the high alkaline conditions of the chemical treatment ($\text{pH} > 10$) and the high salinities of the geothermal brines ($\text{TDS} > 100 \text{ g/L}$) into the real geothermal environment, a numerical design calculation is conducted. Different existing thermodynamic data-sets were evaluated using experimental data for the validation of the PHREEQC calculation. The existing data-sets showed only poor agreement with the experimental data in terms of relevant TDS, pH, and temperature, making the compilation of a new data set necessary.

The demonstrator was constructed based on the simulation, consisting of three major process steps - 1) Si-removal, 2) liquid/solid separation, and 3) post-concentration using MD. With 98 % Si reduction in the field, the same efficiency like in previous laboratory studies was achieved and is in good agreement with the numerical prediction. The MD enabled Li concentration by a factor of 3 up to $\sim 500 \text{ mg/L}$ while producing fresh water.

This chapter has been published in: Goldberg, V., Winter, D., Nitschke, F., Held, S., Groß, F., Pfeiffle, D., Uhde, J., Morata, D., Koschikowski, J. & Kohl, T. (2023a). Development of a continuous silica treatment strategy for metal extraction processes in operating geothermal plants. *Desalination*, 116775. <https://doi.org/10.1016/j.desal.2023.116775>

The potential of raw material extraction from thermal fluids in Chile (Chapter 8)

Chapter 8 describes the economic potential of dissolved raw materials in thermal spring waters in Chile and provides an outlook on global resources. To describe the occurrence of potentially valuable elements a hydro chemical database was compiled consisting of 10,000 data points worldwide. The data of surface springs are combined with typical parameters of geothermal power plants to calculate different raw material potentials. Based on these data, the economic potentials of these sources are compared.

The analysis shows, that especially in northern Chile the concentration of strategically important elements such as Li, Mg, or Cs is high. Comparing potentially producible amounts and prices revealed further that bulk raw materials with lower specific prices like for example Mg or boric acid have a similar economic potential in the Chilean geothermal systems (4 – 6 Mio. US\$/yr) like trace elements for the high-tech industry such as Li (5 Mio. US\$/yr) with higher specific prices. On a global scale, 12 of 30 elements defined as critical raw materials by the European Commission occur in elevated concentrations within geothermal systems as well as several valuable elements. One of the largest challenges for enabling the extraction from high-temperature geothermal fields in Chile are the typical high silica concentrations and the associated high risk for silica scaling.

This chapter has been published in: Goldberg, V., Winter, D., Nitschke, F., Rath, M., Held, S., Spitzmüller, L., Budach, I., Pavez, M., Morata, D., Koschikowski, J. & Kohl, T. (2021). The potential of raw material extraction from thermal brines – Successful milestones of the BrineMine project. *OIL GAS*, 1, 26–33. <https://doi.org/10.19225/210306>

Prototype tests for the treatment of geothermal waters for raw material extraction and freshwater production (Chapter 9)

The treatment approach and the associated demonstrator developed and described in Chapter 7 is adapted to the described volcanic geothermal settings in Chile described in Chapter 8. Chapter 9 presents the application of the field demonstrator during tests in a geothermal system in the Southern Volcanic Zone of Chile.

The approach is adapted to the lower salinities of the volcanic fluids. The primary step is a pre-concentration using reverse osmosis (RO), followed by a controlled precipitation step for silica reduction, and finalized by a post-concentration step using MD. During continuous operation, the Si reduction was only 50 % and thus lesser than in the previous field studies in Germany. Due to the overall lower salinity, the concentration factor for the dissolved solids reached up to 20 in continuous flow-through conditions underlining the potential of fresh water production in this setting simultaneous with the combined energy and raw material extraction. The geothermally powered MD module demonstrated further already on the prototype scale a 3 times higher efficiency than ideal evaporation for fresh water production demonstrating also the fuel-saving potential. As volcanic geothermal resources are the most widespread in terms of installed capacity, the effective handling of their fluids is a key lever for the global geothermal raw material potential.

This chapter has been published in: Goldberg, V., Winter, D., Eiche, E., Koschikowski, J., Kohl, T., Morata, D., Schwantes, R., Seibt, P., Heboldt, J., Nitschke, F. (2023C). Prototype Tests for the Treatment of Geothermal Waters for Raw Material Extraction and Freshwater Production. *Mining Reports Glückauf*. 06/2023

Comparison of lime/caustic precipitation mechanisms as pre-treatment in different geothermal fluids (Chapter 10)

Chapter 10 discusses in a comparative analysis the influences of the developed Si precipitation approach from the different field studies of Chapter 7, Chapter 9, and from previous studies (Spitzmüller et al. 2021).

The demonstrator tests (Chapter 7) in high saline geothermal brines in Germany showed efficient Si removal by 98 %, while the treatment set up of Chapter 9 in Chile only reached 50 % of Si reduction. In addition to pH being the most important factor for Si reduction, the overall salinity also influences the efficiency of the treatment. Regardless of the setting, Li is not removed by the Si precipitation approach. The precipitating mineral phases are dominated by calcite and portlandite. In addition to the elements of the precipitation reaction (Si, Ca, Mg), metals and metalloids such as Fe, Pb, Mn or Zn are removed from the fluid by the treatment in all geothermal settings. Depending on the downstream process, this reduction beyond Si removal can improve a drinking water use and avoid further their incorporation during the latter DLE processes.

This chapter has not been published before. It represents a summarizing comparison of the different field studies on Si precipitation in Germany and Chile including unpublished data from the different demonstrator field tests.

2 Fundamentals

The presented study analyzes the potential of different geothermal systems regarding combined raw materials and energy production. This was performed in interdisciplinary studies considering the geochemistry of different geothermal systems in Germany and Chile, validation of technological approaches for raw material extraction as well as processing and prevention of scaling. In the following chapters, the fundamentals and state of the art of the individual aspects are presented in more detail.

2.1 Classification of Geothermal Systems

A geothermal system can form in an area where enhanced heat flow in the earth's crust dominates the behavior of groundwater in permeable structures leading to an upflow of hot waters approaching the surface (Arnorsson et al. 2007; Henley and Ellis 1983a). The fluid migration, heating, and ascension of fluid are associated with highly diverse and site-specific processes, such as boiling, degassing, or mineral dissolution or precipitation forming various types of geothermal systems (Arnorsson et al. 2007; Giggenbach 1981; Henley and Ellis 1983b; Nicholson 1993). Therefore, different approaches exist for describing and classifying these systems. Due to this complexity, various classifications and distinctions exist for describing geothermal systems as their heat source, temperature fluid chemistry, reservoir structure, or geothermal use which are all interconnected (Table 1).

Table 1: Different approaches for classifying geothermal systems.

		Reference
Depth	<ul style="list-style-type: none"> - Shallow geothermal energy (< 400 m depth) - Deep geothermal energy (> 400 m depth) 	(Stober and Bucher 2012)
Temperature / Enthalpy	<ul style="list-style-type: none"> - Low: < 120 °C - Intermediate: 120 – 180 °C - High: > 180 °C 	(Hochstein 1988; Nicholson 1993)
Fluid type	<ul style="list-style-type: none"> - Liquid dominated - Vapour dominated 	(Nicholson 1993)
Fluid Chemistry	E.g. by anions: <ul style="list-style-type: none"> - Sulfate type - Bicarbonate type - Chloride type 	(Henley and Ellis 1983a)
Heat Source	<ul style="list-style-type: none"> - Magmatic <ul style="list-style-type: none"> - Volcanic field - Plutonic type - Non-Magmatic <ul style="list-style-type: none"> - Extensional domain - Intracratonic basins 	(Moeck 2014; Nicholson 1993)
Heat transport	<ul style="list-style-type: none"> - Convection dominated - Conduction dominated 	(Moeck 2014; Nicholson 1993)
Heat use	<ul style="list-style-type: none"> - Direct use: <ul style="list-style-type: none"> - Balneology - Agriculture and aquaculture - Hydrothermal systems - Engineered geothermal systems - Indirect use: <ul style="list-style-type: none"> - Geothermal heat pumps - Borehole heat exchanger 	(Lahsen 1988; Stober and Bucher 2012)

An approach for describing geothermal systems is the use of “play types” originating from the oil and gas industry. Applied to geothermal systems it orders geothermal systems by heat source, heat migration pathways, fluid storage capacity, and the potential for recovery of heat (Moeck 2014). The description of the different systems focuses on the areas suitable for potential joint energy- and raw material production in Germany and Chile and is outlined in Chapters 3.1.2 and 3.2.2.

2.2 Development of Geothermal Fluids

For assessing the raw material potential of geothermal systems as well as for identifying pre-treatment and extraction strategies, the governing geochemical water-rock interaction processes are mandatory to be understood. To implement future extraction technologies and treatment strategies, their influences on the fluid chemistry and reservoir properties have to be considered further. Various extensive studies exist about geothermal water genesis and water-rock

interactions and are referred to, such as Arnorsson et al. (2007), Henley and Ellis (1983b), or Nicholson (1993).

Fluids in the subsurface can have various origins and compositions (Table 2). Meteoric water or seawater can percolate into several km of depth by fractures or permeable zones or be buried with sediment rocks as formation or connate waters. Additional sources can be waters that evolved from metamorphic processes (metamorphic waters) or magma (juvenile waters) (Arnorsson et al. 2007; Dugamin et al. 2023; Frape et al. 2014; Kharaka and Hanor 2003). The most common fluid type in deep, intermediate to high-temperature geothermal fields is the “Chloride or Na-Cl – Type”, with Cl as the dominant anion (Table 2, 6-8). They are typically found at the bottom of a geothermal convection system and are the product of fluid-rock interaction as well as the mixing of different fluids. If no water-vapor separation or un-mixing processes have taken place, they are classified as primary waters. In volcanic systems, salinities reach up to 10,000 mg/L, while in sedimentary systems over 300,000 mg/L can be reached (Arnorsson et al. 2007; Henley and Ellis 1983b; Neupane and Wendt 2017). Typically, Na is the dominating cation followed by K in concentrations ten times lower. Furthermore, B is present and Si especially in high-temperature fields, whose solubility correlates with the temperature. Other anions as SO_4^{2-} or HCO_3^- can be present in various concentrations but typically in orders of magnitudes lower than Cl. If the systems are gas-bearing, typically CO_2 and H_2S are present. Trace elements (e.g. Ag, Fe, Cu, Pb, Zn) are typically controlled by sulfide mineral deposition forming cations in solutions. Elements such as Br, I, As, Mo, and W can form large simple anions or oxy-anions resulting also in high mobilities (Arnorsson et al. 2007). The fluids typically form argillic-propylitic alterations, with the following characteristic minerals: silica, (amorphous silica, cristobalite, quartz) albite, adularia, illite, chlorite, epidote, zeolites, calcite, pyrite, pyrrhotite, and base-metal sulfides (Browne 1978; Nicholson 1993; Sanchez-Alfaro et al. 2016).

“Acid-Sulfate Waters” (Table 2, 1) can be formed in different ways. Deep acid-sulfate fluids are found in various geothermal settings, especially in andesitic volcanic systems. Primary acidic-sulfate fluids receive their acidity by transfer of HCl or SO_2 from the magmatic heat source. The main difference in comparison to Cl-fluids is that the pH buffer is $\text{HSO}_4^-/\text{SO}_4^{2-}$ and thus higher concentrations of SO_4^{2-} as well as elements with a pH-dependent solubility such as Fe or Mg. Secondary acid-sulfate waters form typically by the condensation of volcanic gases into oxygenated ground waters (Arnorsson et al. 2007; Taran and Kalacheva 2020). Often these waters are the product of Cl fluids boiling in depths, ascending as vapor and gas, and condensating in more shallow depths. The oxidation of condensed H_2S and the condensation of CO_2 releases H^+ into the fluid phase, causing acidic pH values (Henley and Ellis 1983b; Taran and Kalacheva 2020). The pH values can reach down to 2.8, by the addition of volcanic gases even 2. Cl is present rather as a trace element and due to the dissolution of CO_2 , HCO_3^- is in low concentrations or absent. Volatile elements which tend to separate from deep Cl fluids (such as NH_3 , As, and B), can be also condensed and enriched in these kinds of fluids (Nicholson 1993). The acidic environment in geothermal reservoir rocks can leach silica as well as various cations such as Na, K, Mg, Ca, Al, Fe, Mn, etc. (Aguilera et al. 2016; Ellis 1977; Taran and Kalacheva 2020). The result is typically an advanced argillic alteration, with kaolinite, halloysite, cristobalite and alunite, further silica, anhydrite, hematite, dickite, jarosite, pyrite,

goethite-hematite mixtures, and native/pure sulfur are also commonly found (Aguilera et al. 2016; Henley and Ellis 1983b; Nicholson 1993; Rojas et al. 2022).

In non-oxygenated systems, condensation of gases and vapor in fluids can form “Bicarbonate Waters”. Carbon from mantle, magmatic, or metamorphic origin can mix in volcanic systems or seismic active zones with ground or surface waters. These fluids can be CO₂-rich having close to neutral pH values (Table 2, 2). Sulfate can be present while Cl is rather absent. The most common cation is Na (Aires-Barros et al. 1998; Arnorsson et al. 2007; Nicholson 1993). The CO₂ concentrations of the fluids make them typically reactive by maintaining low pH values, causing a breakdown of hydrothermal sulfide minerals and transport of released metals and metalloids (Thomas et al. 2016). This causes the corrosive and reactive nature leading to elevated mineralizations and typically forms argillic alteration with clay minerals (kaolinite, montmorillonite), mordenite as well as sometimes calcite and silicification (Arnorsson et al. 2007; Nicholson 1993; Thomas et al. 2016).

Between the different types of geothermal fluids, no sharp line can be drawn. Fluids can further be a product of dilution, mixing, or boiling, and are hence strongly dependent on the site-specific conditions.

Table 2: Major and trace element composition of different geothermal fluids. 1-6 compiled by *Arnorsson et al., 2007*. 1: Steam-heated surficial acid sulfate water, Krísuvík, Iceland (Arnorsson et al. 2007); 2: Carbon-dioxide water, Lýsuhóll well 6, Iceland (Arnorsson et al. 2007); 3: Mixed high-temperature and cool ground water, Nedridalur, Geysir field, Iceland (Arnorsson et al. 2007); 4: Hot spring in silicic volcanics, Ojo Caliente Spring, Yellowstone, Wyoming, USA (Ball et al. 1995); 5: Volcanic geothermal system in basalt, Krafla, well 21, Iceland (Arnorsson et al. 2007); 6: Seawater geothermal system, Reykjanes, well 15, Iceland (Arnorsson et al. 2007); 7: Na-Cl fluid in an andesitic volcanic geothermal system, Cerro Pabellón, well CP_1A, Chile (Cappetti et al. 2020; Giudetti et al. 2020); 8: Na-Cl fluid in granitic fault system of a non-magmatic extensional geothermal system, Insheim, well INSH, Germany (Sanjuan et al. 2016a). ^apH/temperature of measurement, ^bTotal carbonate carbon as CO₂.

	1	2	3	4	5	6	7	8
T [°C]	100	60	65	93	238	260	250/260	165
pH/°C ^a	2.55/ 22	6.21/25	7.98/26	8.61/20	8.80/20	5.16/22	6.95/ -	5.23/46.2
Steam fraction							0.36	
Gas/Steam ratio							0.60	
Major elements [mg/L]								
SiO ₂	226	212	176	243	500	669	429	167
Na	27.0	418	210	331	147	9,903	4,452	29,900
K	2.44	30.6	35.9	9.45	18.0	1,314	729	3,816
Mg	68.2	27.2	1.0	0.001	0.0016	1.05	538	99.4
Ca	94.9	99.7	10.0	1.0	2.44	1,548	0.36	7,254
CO ₂ ^b	-	1145	301	-	-	-		
HCO ₃							51	
SO ₄	1,363	41.3	19.9	20.7	291	24.3	28	131
H ₂ S	-	<0.01	0.0	1.1	-	-		
F	0.06	-	4.6	31.6	1.02	0.14	0.5	<1
Cl	5	85.8	20.7	324	73.5	20,534	8,214	64,900
NH ₄								44.0
Trace elements [µg/L]								
Ag								1.04

Al	83,300	40.6	9.4	280	969	91.9		27.7
As	-	40.4	0.4	860	105	156	79,000	11,620
B	-	518.0	396	3980	1670	7,860	293,000	41,100
Ba	8,0	69.5	4.4	<40	0.62	6,650		8,270
Br							7,500	185,000
Cd	-	-	-	<40	<0.002	0.923		24.6
Co								2.86
Cr	108	<0.1	0.07	<90	0.12	0.27		<1
Cs	-	9.6	0.33		9.66	61.6	26,000	14,530
Cu	-	<1.0	0.09	<140	0.18	1.74		372
Fe	101,000	1546	16.90	23.0	2.6	325		25,064
Ga	-	0.02	0.12		4.92	2.29		
Ge	-	21.3	7.45		24.7	23.0		70.4
Hg	-	0.02	0.004		<0.002	0.068		
Li	22.0	21.3	59.2	3960	264	3930	50,000	168,000
Mn	2370	214	5.1	<120	1.59	1500		25,160
Mo	-	10.8	47.5		3.87	92.5		
Nd								0.345
Ni	-							43.2
P	290	<10	6.1		1.25	15.4		1,012
Pb	-	<0.1	0.17	<150	<0.01	<0.1		886
Rb	-	177	61.0		206	4200	6,400	27,200
Sb							1,800	
Sr	89	418	67.9	8.0	5.16	9120	12,800	456,000
Th								0.00016
Ti	23	0.05	0.13		0.18	<0.1		
Tl	-	0.05	0.001		0.011	17.6		
U								0.007
V	376	0.1	1.54		1.73	9.1		
W	-	0.19	4.53		6.41	1.0		
Zn	127	0.5	3.2	<10	0.51	50.9		5,894

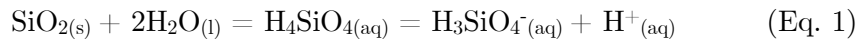
2.3 Processes within Geothermal Reservoirs

Various chemical and physical processes influence the composition of geothermal fluids including mineral-fluid solubility reactions, ion exchange, boiling, cooling, or mixing.

In terms of solubility behavior, certain elements such as Cl, B, Br, As, Cs, Rb, or Li are considered conservative or unreactive. They readily pass into solution before considerable alteration appears and the elements tend to remain in solution and are thus common in most of the high-temperature fluids. In addition, their concentration is just minor influenced by mineral-fluid equilibria or ion exchange processes. But, elements such as As can be influenced by contact of the fluid with different reactants such as H₂S or near-surface ion exchange reactions with clay minerals or iron oxide, making Cl the only truly conservative element (Hawkins and Tester 2018; Henley and Ellis 1983b; Nicholson 1993).

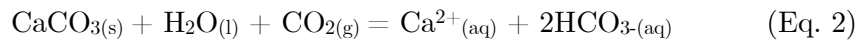
The concentrations of rock-forming species such as Si, Na, K, Ca, and Mg are more likely to be controlled by solubility reactions defining the amount of a species that can be dissolved in

a fluid before precipitation occurs (Hawkins and Tester 2018; Nicholson 1993). Two different processes dominate these reactions – mineral-fluid equilibria (e.g. for SiO_2 and CaCO_3) and ion-exchange reactions (eg. Na and K between feldspars and micas) – producing secondary alteration minerals. Major minerals influencing the fluid composition in terms of solubility equilibria typically are quartz, calcite, and/or anhydrite. The temperature governs the equilibria of these elements. Further pH, pressure or salinity, and other dissolved solids or gases can influence the solubility. One of the most important equilibria in geothermal is the one of silica (Eq. 1) (Alexander 1954; Greenberg and Price 1957; Nicholson 1993).



Silica solubility increases constantly with temperature leading to high Si concentrations in high-temperature fluids. A fluid with 11 g/L NaCl can for instance dissolve at 100 °C 0.37 g/L SiO_2 , at 150 °C 0.61 g/L SiO_2 , and at 200°C 0.94 g/L SiO_2 (Chen and Marshall 1982). This temperature-dependent solubility behavior enables on one site the use of the fluid composition as a geothermometer, but it poses also high challenges in the processing of the fluids. If the temperature is lowered or the SiO_2 concentration is increased by mineral concentrating or in flash steam power plants, the maximum solubility can be overreached (Gunnarsson and Arnórsson 2005; Henley 1983; Iler 1976). Aqueous silicic acid is also a weak acid, dissociating hydrogen ions. Conditions favoring H^+ consumption, as a pH value increases, can enhance the SiO_2 solubility (Dove et al. 2008; Eikenberg 1990; Milne et al. 2014; Nicholson 1993).

Other mineral reactions dominated by solubility reactions are for instance the lime-carbonic acid balance:



In comparison to silicates, carbonatic minerals such as calcite have retrograde solubility, leading to decreasing solubility at increasing temperatures. In addition, the solubility is strongly dependent on the presence of CO_2 and thus the partial pressure of CO_2 (Eq. 2). Accordingly, carbonate minerals can precipitate during ascension and depressurization within a reservoir formation or due to degassing during manufacturing (Hawkins and Tester 2018; Hörbrand et al. 2018; Miller 1952; Nicholson 1993). A fluid with 30 g/L NaCl at 43 °C can dissolve at a CO_2 partial pressure of 1 bar 0.95 g/L of CaCO_3 and at 104 °C at the same pressure only 0.31 g/L. The same fluid can take up 1.9 g/L at 42 °C and 0.88 g/L at 104 °C at CO_2 partial pressure of 20 bars outlining the complex interconnection between pressure and temperature in terms of mineral solubilities (Miller 1952).

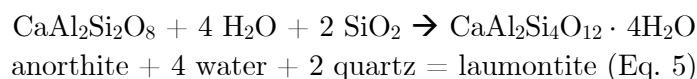
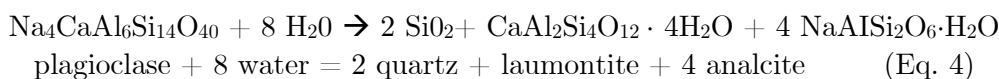
Ion-exchange reactions involve the transfer of ions between the fluid and two or more aluminosilicate minerals and control the ratios of cations in solution, such as H^+ , Na^+ , Ca^{2+} , Mg^{2+} , K^+ , Al^{3+} , or Fe^{3+} . For instance, K is depleted in high-temperature fluids due to the dominance of potassium feldspar over albite. The latter potentially incorporates Na from the solution. The result of ion-exchange reactions is the metasomatic formation of secondary reservoir minerals of primary mineral phases such as feldspar, sulfides, carbonates, silica, and water (Bucher and Stober 2010; Frape et al. 2014; Hawkins and Tester 2018; Nicholson 1993). Typical (secondary) reservoir minerals are serpentine and brucite from olivine dissolution, chlorite or sericite formation, or the conversion of Ca-plagioclase to albite (Frape et al. 2014).

High salinities (100,000 – 300,000 mg/L) are typically found around sedimentary environments. High concentrations of dissolved NaCl can be derived by the dissolution/equilibrium reaction of evaporates. Another factor causing high total dissolved solids (TDS) contents is the water consumption by olivine or feldspar dissolution under for instance the formation of serpentine, brucite, laumontite, or analcite, thus causing a relative increase of the remaining mineral concentration (Frape et al. 2014; Regenspurg et al. 2015a; Stober and Bucher 2000). A general approach is described by the production of high-TDS chloride brines as a consequence of desiccation of pore and fracture space due to water-consuming reactions (Stober and Bucher 2000), as:

unstable "primary" silicate mineral + H₂O-rich dilute solution (low TDS)

→ residual minerals (zeolite, clay, quartz) + H₂O-depleted solution (high TDS) (Eq. 3)

Specific examples of these types of reactions can be the reactions of plagioclase or anorthite under the formation of laumontite or other Ca-zeolites as heulandite or stilbite (Stober and Bucher 2000):



A result of these water-consuming reactions within the reservoir is the relative enrichment of the remaining elements in the fluid. For the effectiveness of this TDS enrichment, Stober & Bucher (2000) give the example of a 1000 cm³ rock with 50 % plagioclase of An₂₀ and 2 % water-filled pores. For consuming half of the water (and thus doubling the TDS concentration) about 70 cm³ of plagioclase is sufficient, forming about 25 cm³ of hydrous minerals (Stober and Bucher 2000).

The enrichment of potentially valuable elements such as Li, Zn, Pb, Cs, and Cu have typically a complex, multi-stage history. Metals such as Ag, Au, Cu, Mo, Pb, Sn, W, and Zn can form complexes with Cl⁻, HS⁻, and OH⁻ during magma crystallization, leading to an enrichment within the magmatic fluid. Due to migration into a reservoir formation, these fluids can enrich a geothermal fluid with metal ions (Arnorsson et al. 2007). Beyond the migration of magmatic fluids, it is also possible that the metals become leached from a host rock by a geothermal fluid. Possible origins for various metals could be for instance sulfide minerals from calc-alkaline intrusions (Hedenquist and Lowenstern 1994). In the geothermal systems of the North German Basin a genesis model postulates that anaerobic conditions in combination with the high salinity in the absence of sulfides can potentially enable metals like Fe, Cu, or Zn to be present as chloride complexes and thus increase their solubility in the reservoir (Regenspurg et al. 2015a; Regenspurg et al. 2010).

For Li different approaches explaining the origin and enrichment mechanisms in fluids are discussed. In general, a correlation between high temperatures and high Cl is associated with high Li concentrations in fluids (Coffey et al. 2021; Dibble et al. 1976; Dugamin et al. 2023; Sanjuan et al. 2022). This leads to the assumption that enhanced water-rock interactions and

leaching processes are a driving force in the enrichment. However, studies further show that just these two factors are not sufficient for explaining the concentrations on their own since highly saline geothermal brines do not necessarily show high Li concentrations (Coffey et al., 2021; Dugamin et al., 2023; Sanjuan et al., 2022).

Due to similar ionic radii, Li can substitute Mg, Fe, Al, or Ti in crystal structures (Horstman 1957). In terms of magmatic rocks, Li can be enriched in granites, especially in granitic pegmatites. Within the pegmatites, incompatible elements for quartz or feldspars, such as Li, become constantly enriched during late-stage crystallization of water-rich magma. Typical Li minerals mined on an industrial scale are e.g. the Si-Al silicates spodumene and petalite found in pegmatites in Australia, China, Zimbabwe, or Brazil (Benson et al. 2017; Grew 2020; Schmidt 2017). Further, in granitic rocks, Li was observed subordinately in tourmaline and feldspars and in increasing concentration in monoclinic pyroxenes, amphiboles, and in micas such as biotite and muscovite (Drüppel et al. 2020; Horstman 1957).

Within clay minerals, Li was observed in elevated concentrations in illite and kaolinite. In terms of kaolinite, it is assumed, that Mg together with Li can replace Al within the octahedral layers (Horstman 1957). Further, Li is dissolved in water as a monovalent cation with a hydrate hull, leading to sorption in outer sphere complexes as well as in the diffuse ion swarms around the negatively charged surfaces (Hoyer et al. 2015).

Water-rock interaction experiments on a laboratory scale show different mechanisms of releasing Li in fluids. Typically, a rapid increase at the beginning of the experiments is observed, indicating the presence of a highly soluble form of Li that becomes mobilized before considerable alteration takes place. Li could be possibly attached to intergranular surfaces or in cracks, be enriched in remnants of original pore fluid, or be released from fluid inclusions that were crushed during the sample preparation (Dibble et al. 1976; Drüppel et al. 2020). After a first rapid increase of Li in the fluid a secondary enrichment over time is observable, most-likely due to the alteration and dissolution of different minerals in volcanic rocks, Li clay beds, or detrital Li-rich phyllosilicates as white micas or illite at high temperatures (Dugamin et al. 2023; Sanjuan et al. 2022). A possible Li source release mechanism can also be high-temperature cation exchange between Li and Mg for instance in smectites (Coffey et al. 2021).

Overall the chemical composition of geothermal fluids can be highly diverse and is moreover site-specific. For the topic of combined geothermal energy- and raw-material extraction this means on one hand large potential of various elements in various systems globally, but on the other hand requires site and brine-specific solutions in terms of extraction technology and scaling pre-treatment.

2.4 Raw Material Extraction from Geothermal Fluids

Extracting raw materials from continental brines is in general by no means a new approach. Several mineral raw materials such as salt (NaCl), potash (KCl), or Mg are typically produced from surface brines. Moreover, deep fluids are also established resources for some commodities.

Beyond the well-known oil and gas production, deep fluids are also a source of elements such as Br (Gunn 2014; U.S. Geological Survey 2023).

Li is also to large amounts produced from brines of the salars in Latin America. The conventional production includes an initial evaporation step, for increasing the Li concentration and pre-precipitation of impurities. In the Salar de Atacama in Chile, for instance, the initial Li concentration of 0.15 % becomes concentrated to 6 % by evaporating over 90 % of the water in solar ponds. During concentration, the brine is pumped from pond to pond to precipitate different minerals selectively in order of their solubility. The result is Li-enriched brine, which is then brought to an industrial plant for further purification and refining using reagents, filtration, or solvent extraction. Li carbonate is precipitated from the final Li concentrate by using soda ash (Schmidt 2017; Warren 2021).

Li production from the salars, especially from the Salar de Atacama, shows the lowest production costs on the market (1800 – 3000 US\$/t LCE). The brine extraction and the pre-concentration using the sun turns out to be more cost-effective than the production of mineral concentrates from hard rock deposits (Schmidt 2017; Sun et al. 2021). Nevertheless, this form of Li production recently received a lot of negative reception due to the intervention in the water system and evaporation of large water volumes in one of the driest deserts on Earth. Ongoing desertification as well as a reduction in the diversity of flora and fauna are discussed as possible results of this type of raw material extraction (Vera et al. 2023). Despite the ecological controversies, further technological limitations are apparent. The concentration using the evaporation ponds takes between 10 and 24 months and can therefore only react sluggishly to rapid market changes (Schmidt 2017; Vera et al. 2023). The overall extracted Li share is only ca. 50 % (Warren 2021), and moreover, the approach of pond precipitation is challenging in brines with high Mg/Li ratios (Li et al. 2019c; Sun et al. 2021; Xu et al. 2021b) making it limited to just a few sites. These different aspects bring DLE more and more in the focus of academia and research for salar brines (Liu et al. 2019; Schmidt 2017; Vera et al. 2023; Xu et al. 2021b) as well as for geothermal fluids (Reich et al. 2022; Stringfellow and Dobson 2021a). An example of the implementation of DLE in Salar brine processing is the Fenix Project in the Salar Hombre Muerto in Argentina, operating for 20 years by a combination of evaporation and DLE (Livent 2023). Research on DLE extraction from geothermal fluids dates back to the 1970s (Reich et al. 2022; Stringfellow and Dobson 2021a). Also, prototypes for continuous DLE were developed and operated in geothermal power plants but never scaled up on a commercial scale successfully (Stringfellow and Dobson 2021a).

Rising Li prices and demand as well as the mentioned conflicts around conventional production are bringing the topic of DLE into the focus again. Moreover, fluids from oil, gas, or geothermal reservoirs containing elevated Li concentrations are globally more distributed than salt flats or large hard rock deposits and offer thus possibilities of independent Li production as a key element of electric mobility for several countries. Additionally, opens the combination with geothermal energy production a perspective of a more environmentally friendly mining approach with associated renewable baseload energy production (Reich et al. 2022; Sanjuan et al. 2022; Stringfellow and Dobson 2021a; Warren 2021).

There are many different approaches to the application of DLE in geothermal systems. These can be fundamentally divided into organic and inorganic sorption, liquid-liquid or solvent

extraction, membrane processes, and electrochemical processes. There are also various approaches combining different technologies. The fundamental principle is that Li is selectively transferred from the natural brine to the extraction medium through contact with the extraction medium, by for instance mixing, flowing through, or suspension. After the loading of the extraction medium with Li a recovery step follows typically. The Li-depleted natural fluid is replaced by a recovery solution such as water or acid. Li is then released from the extraction medium by rinsing, ion exchange, or voltage reversal. The result is a recovery solution relatively enriched in Li in comparison to the initial fluid (Battistel et al. 2020a; Liu et al. 2019; Reich et al. 2022; Stringfellow and Dobson 2021a; Weng et al. 2020; Zhang et al. 2021).

Also in terms of DLE, the challenges are the characteristics of the geothermal fluids and the conditions within geothermal power plants (high temperatures, high pressures, high salinities, etc.), which pose high demands on the extraction facilities.

A detailed description and comparison of the technological approaches can be found in Chapter 4.

2.5 Application of Membrane Processes

Membrane processes are an established method for fluid treatment and have become irreplaceable in several areas in the chemical, environmental, medical, and water purification industries (Melin and Rautenbach 2007). Among the diverse technologies reverse osmosis (RO) is one of the most important worldwide (Biesheuvel et al. 2022; Chian et al. 2007). When a semipermeable membrane separates two fluids with different solute concentrations, water will naturally flow from the side with the lower solute concentration to the site with the higher solute concentration (Figure 3 a) – called osmosis. In RO processes salty water on one side of a semipermeable membrane is exposed to high pressure. This causes a diffusion of pure water through the membrane and thus a relative concentration of the mineral or organic contents within the original fluid and accumulation of fresh water on the other side of the membrane (Figure 3 a). Therefore, the driving factor for this mechanism is the pressure, which is dependent on the salinity. For brackish waters, the RO pressure ranges are 15 – 25 bar, and for seawater between 55 and 85 bar (Chian et al. 2007).

One of the most common configurations of the RO principle is the spiral wound application (Figure 3 b). A spiral wound module consists of several membrane pouches which are closed on three sites and are connected on the open end to the central tube for collecting the permeate. Between the coiled membranes, brine spacers are implemented to ensure proper distance between the two membranes thus enabling uniformly distributed feed brine flow. The spiral configuration has several advantages. It enables the installation of large membrane surfaces at comparably small volumes ($< 1000 \text{ m}^2/\text{m}^3$), has low manufacturing costs, and can be easily cleaned chemically and hydraulically (Chian et al. 2007; Melin and Rautenbach 2007).

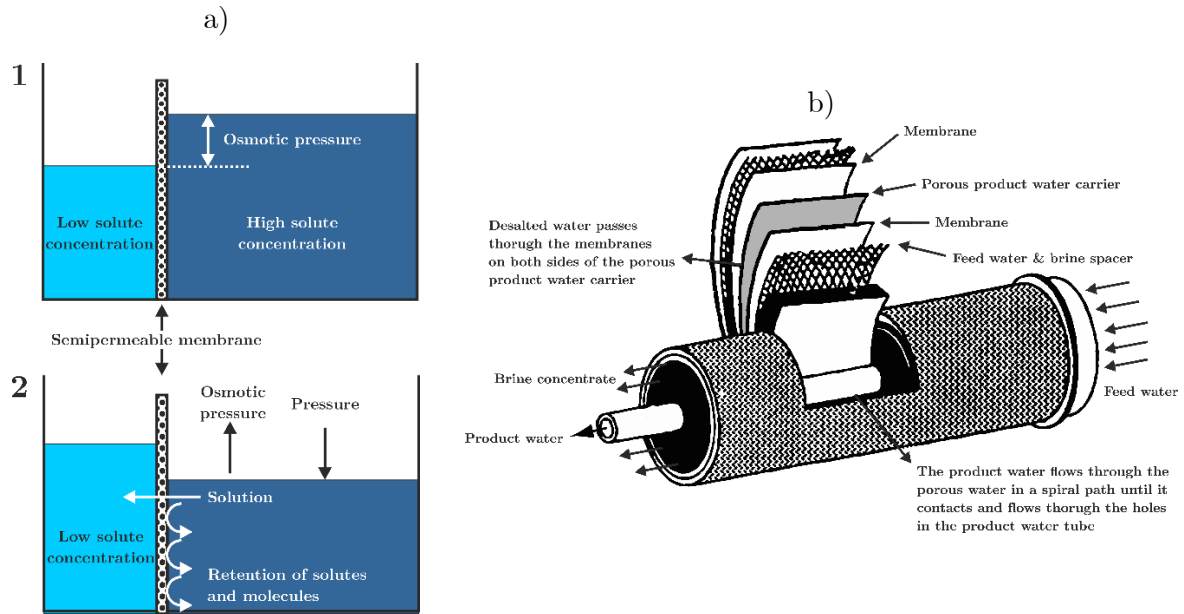


Figure 3: a) Schematic of reverse osmotic equilibrium (1) and reverse osmosis membrane (2) b) schematic drawing of a spiral wound module (adapted from Chian et al., 2007)

Although RO is widely established in the industry, it is limited in terms of economic feasibility to brines with a maximum salinity of 70,000 mg/L of TDS. The main reason for this is the high associated operational costs for the required operational pressures (Tavakkoli et al. 2017). For reaching higher concentration rates for lower saline brines or for the treatment of for instance geothermal brines with salinities $>100,000$ mg/L other methods are required such as membrane distillation (MD). MD can operate fluids up to 350,000 mg/L at temperatures between 30 °C and 90 °C (Schwantes et al. 2019; Tavakkoli et al. 2017; Winter et al. 2011). In the fundamental approach of MD, a heated feed fluid is brought in contact with a hydrophobic membrane. The hydrophobic membrane impedes penetration of the aqueous solution, resulting in a vapor-liquid interface at the pore entrance. This creates a vapor-pressure gradient between the two sides of the membranes which leads to the evaporation of more volatile compounds on the heated site and thus a mass transport by a combination of molecular and Knudsen diffusion to the cold side (Macedonio 2015; Schwantes et al. 2019). The result is a concentration of the remaining solutes on the heated site and permeate accumulation on the cold side. Various approaches exist for configuring the channels of the different solutions involved, such as heating/cooling solution, feed fluid, and permeate (Figure 4, Schwantes et al. 2019). Typically, the different channels are compiled into plate and frame modules or, installed in a spiral-wound module, similar to RO (Schwantes et al. 2019; Winter et al. 2017).

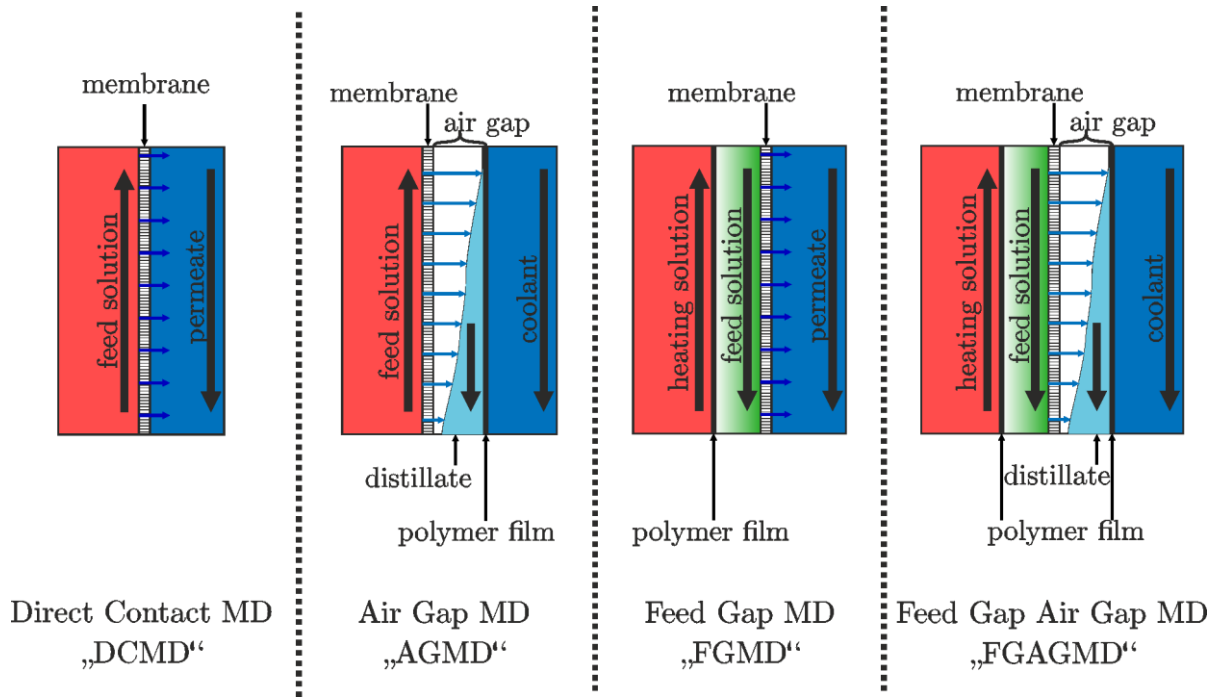


Figure 4: Different channel configurations for membrane distillation: direct contact membrane distillation (DCMD); air gap membrane distillation (AGMD); feed gap membrane distillation (FGMD) and feed gap air gap MD (FGAGMD) (Adapted from Schwantes et al., 2019).

The processes of RO and MD, powered by pressure and heat offer the potential of a cost-efficient integration into geothermal cycles. For lower saline fluids, as from geothermal systems in Chile, RO as a low-cost method offers great potential for a first treatment step. For reaching higher concentrations in these fluids or for treating initially high-saline fluids as from the geothermal systems in the Upper Rhine Graben in Germany, thermally driven MD could serve as a viable and in terms of operation costs, cost-efficient approach.

Due to the strong TDS enrichment by RO or MD, mineral phases can reach their solubility within the fluid and can become oversaturated. Precipitation within a membrane module can clog the pores causing membrane fouling. To avoid mineral fouling and to remove particles, microbiological containments or free oil, feed fluids for membrane processes typically receive a pretreatment before entering the membrane module (Badruzzaman et al. 2011; Lunevich et al. 2016; Tavakkoli et al. 2017; Zhang et al. 2018). The development of the demonstrator and implementing the pretreatment as well as the field tests are in more detail described in Chapters 7, 9 and 10.

2.6 Scaling

The dissolved elements increase the raw material potential on the one hand but pose high challenges in terms of processing on the other hand. Processes leading to an enrichment of elements in the reservoir, such as high temperatures, salinities, or CO₂ contents can be reversed during geothermal energy production. During operation, temperature becomes typically reduced, resulting in lower solubility of several mineral phases such as SiO₂, BaSO₄, CaSO₄, NaCl, and KCl, while others show retrograde solubility such as CaCO₃ or CaMg[CO₃]₂ and

thus an increasing solubility (Appelo 2015; Chen and Marshall 1982; Hörbrand et al. 2018; Marshall and Warakomski 1980a). For silica, the solubility reduces approximately by half from 0.020 mol/kgw at 250 °C to 0.010 mol/kgw at 150 °C in a fluid with 1 mol/kgw NaCl (Figure 5 a). Depending on the fluid composition or the power plant setup and pressure, degassing of non-condensable gases can take place. Degassing of CO₂ for instance strongly influences the solubility of mineral phases such as carbonates (Duan et al. 2006; Duan and Sun 2003; Miller 1952). Moreover, the dissolution of CO₂ in water as carbonic acid or its segregation can strongly influence the fluid's pH value, which again influences the solubility of various mineral phases like silica or carbonates (Duchesene and Reardon 1995; Greenberg 1958; Greenberg and Chang 1965; Kutus et al. 2016; Spitzmüller et al. 2021). A reduction of the CO₂ partial pressure from 60 bar to 10 bar would reduce the solubility of calcite in fluid of 100 °C from about 10 mmol/kg to 5 mmol/kg (Figure 5 a). Furthermore, changes in redox potential can result in the formation of Ba/Sr sulfates or polymetallic sulfides (Nitschke et al., 2014; Regenspurg, mol Feldbusch, et al., 2015).

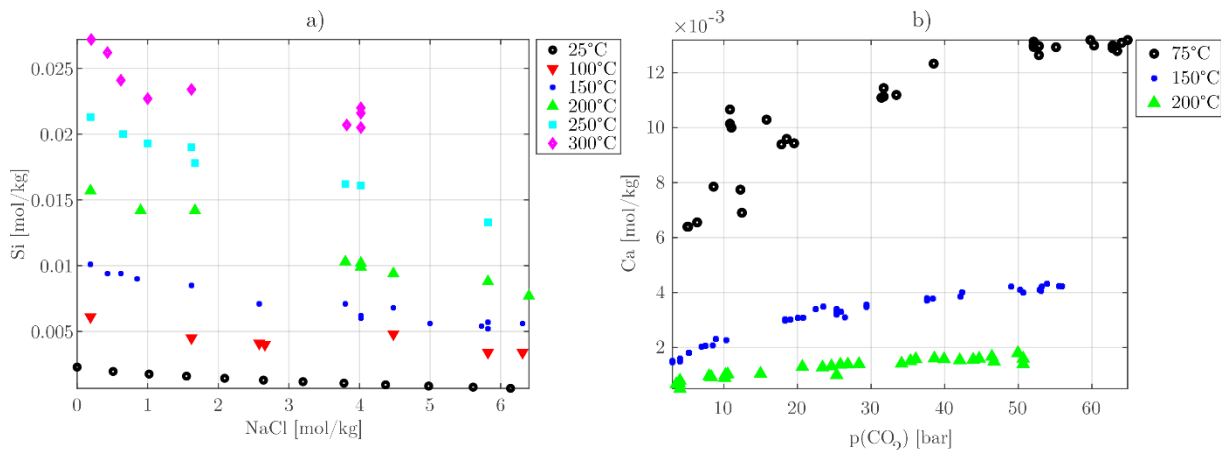


Figure 5: a) Solubility of amorphous silica in NaCl solutions (Data: Appelo, 2015, Chen & Marshall, 1982; Marshall & Warakomski, 1980b). b) Solubility of calcite (displayed by Ca) in double distilled water as a function of CO₂ partial pressure (Data: Segnit et al., 1962).

A result of these interventions (degassing, cooling, etc.) within the fluid dynamics can be the uncontrolled precipitation (“scaling”) of mineral phases (“scales”). The processes of scaling are highly complex and interconnected. Due to the typically high flow rates in geothermal plants, even minor precipitations can accumulate over time and potentially clog wells or installations of the surface energy production facilities, respectively possible raw material extraction plants. Therefore, scales pose one of the major challenges in geothermal energy production independently of the reservoir type (Eggeling et al. 2018; Gunnarsson and Arnórsson 2005; Hörbrand et al. 2018; Nitschke et al. 2014; Regenspurg et al. 2015a; Regenspurg et al. 2015b; Scheiber et al. 2019b; Scheiber et al. 2019a). Similar problems are also known for water treatment processes using membranes (Badruzzaman et al. 2011; Mi and Elimelech 2013; Salvador Cob et al. 2014).

Nevertheless, scaling within geothermal power plants is not an unsolvable obstacle. With targeted measures such as the addition of inhibitors, selective precipitation, or pressure maintenance, scaling is successfully controlled in operating geothermal power plants. Yet it always requires a sound site-specific evaluation which is the subject of ongoing research (Eggeling et al., 2018; EVA-M, 2021; Scheiber et al., 2019a). Concluding, scaling and the

corrosive nature of the geothermal fluids are also some of the major challenges for integrating a continuously operating raw material extraction facility in a geothermal cycle and will require beyond a site-specific moreover a component-specific evaluation. These topics are further also discussed in Chapters 4.2.3 and 7.3.

2.7 Silica Scaling Treatment

For facilitating the pre-treatment using membranes, to enrich the element concentrations in the brines as well as enabling fresh water production, a silica treatment strategy is developed. For water treatment, two paths can be typically distinguished in terms of scaling mitigation: Inhibition and precipitation. Comparative studies on scaling inhibition show limited effectiveness for silica scaling inhibition (Milne et al. 2014; Neofotistou and Demadis 2004). The most common scaling inhibitors are “threshold” inhibitors that prevent or reduce mineral deposition efficiently and cost-effectively. In aqueous solutions, they can inhibit mineral scale growth by using inhibitor concentrations 1000 times less in terms of stoichiometric ratio to the scaling cations (Mpelwa and Tang 2019). Since most of the scaling inhibitors typically aim to prevent crystal formation, their effectivity is reduced in terms of amorphous silica (Milne et al. 2014; Neofotistou and Demadis 2004). Further, organic anti-scalants exclusively designed for silica scaling, can lead to a greater risk of biological fouling during membrane processes (Rahardianto et al. 2007). The approach of combined energy and mineral extraction with additional concentration/water extraction foresees the use of membranes. For this reason, the approach of precipitation is preferred over the approach of inhibition. Therefore, different precipitation approaches were analyzed in a laboratory study to investigate their influence on the Li concentration in artificial and natural geothermal fluids (Spitzmüller et al. 2021).

Silicon dioxide dissolves in water under the formation of silicic acid (H_4SiO_4) (Alexander 1954; Greenberg and Price 1957). The reaction (as displayed in Eq. 6.1) implies that silicic acid and silicon dioxide are in equilibrium with each other resulting in the dependency of the H_4SiO_4 concentration on the SiO_2 solubility (Dove et al. 2008; Eikenberg 1990). Increasing pH values cause ionization of the silicic acid to $\text{H}_3\text{SiO}_4^{1-}$ and further $\text{H}_2\text{SiO}_4^{2-}$. The equilibrium between SiO_2 and H_4SiO_4 is thus shifted in the direction of H_4SiO_4 by increasing pH values (Dove et al. 2008; Eikenberg 1990; Milne et al. 2014).



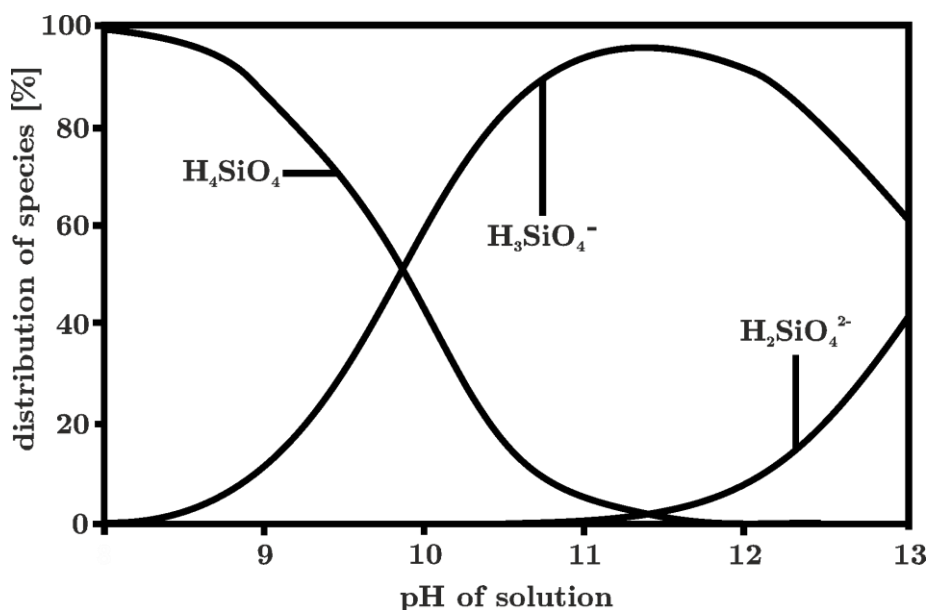


Figure 6: Simplified distribution of silica species at 25°C in amorphous silica-saturated NaOH solution excluding polymeric species (Adapted from Eikenberg, 1990).

Monomeric silicic acid (See Eq. (6.1) – (6.3) / Figure 6) can also be described as reactive silica (Lunevich et al. 2016; Ning 2003). At high pH values hydroxides such as $\text{Fe}(\text{OH})_3$, $\text{Al}(\text{OH})_3$, $\text{Ca}(\text{OH})_2$, and $\text{Mg}(\text{OH})_2$ can be present, causing a copolymerization into anhydrous silicate structures and incorporation of Fe, Al, Ca or Mg (Ning 2003).

The adsorption of divalent cations, e.g. Ca, results in the replacement of a H atom on the surface of the silicic acid by ion exchange (Iler 1976). The resulting positive particle charge is further reduced by attracting a charged ion creating a bridge bond in a Si-O-Ca-O-Si structure (Iler 1976; Maraghechi et al. 2016). The charge balance reduces intramolecular repulsion and thus enhances particle coagulation (Iler 1976). The use of $\text{Ca}(\text{OH})_2$ for silica precipitation causes the additional formation of amorphous C-S-H-phases, such as tobermorite or jennite, or at the presence of Mg talc (Gallup et al. 2003; Richardson 2008).

In the laboratory experiments, the most effective approach for silica reduction was the formation of calcium or magnesium silicate hydrate phases (C/M-S-H) by increasing the pH-value to >10 at molar Ca/Si or Mg/Si ratios >1.25 (Spitzmüller et al. 2021). For the treatment of geothermal fluids the approach was already validated before in geothermal sites in e.g. New Zealand or Japan (Kato et al. 2003; Rothbaum and Anderton 1975; Ueda et al. 2003) and was also used in combination with water treatment using RO (Sheikholeslami and Bright 2002; Tarquin et al. 2020). To analyze its influence on potential target elements for raw material extraction, the approach was tested in laboratory experiments with adapted natural fluids, designed using typical values of a geothermal site in Chile (El Tatio) (Spitzmüller et al. 2021). The experiments showed fast kinetics. In the low saline fluids, the Si concentration fell below saturation concentration within 5 minutes, and after 30 minutes $>90\%$ of silica was removed. Elements being potentially of economic interest (Li, Cs, Rb) were not influenced negatively. The precipitation mechanism can be induced by either just adding $\text{Ca}(\text{OH})_2$ to shift the pH value and adding divalent cations at once or by separately adding NaOH for the pH shift and CaCl_2 for providing the cations (Spitzmüller et al. 2021).

The precipitation mechanisms and their application in the operating systems are further described in Chapters 6.12.2 and 10.

3 Study Areas – Chile and Germany

This binational study examines geothermal systems in Germany and Chile. The potential for both energy generation and potential raw material extraction is highly dependent on the location. The challenges of energy and material extraction are also individual for each site. For this reason, the following chapters provide a basic overview of the different geothermal systems in Germany and Chile.

3.1 Germany

The use of geothermal energy is now widespread in Germany. Concerning thermal baths, there are a total of 168 locations that use geothermal water. In the case of near-surface geothermal energy at depths < 400 m, there are now more than 470,000 systems of geothermal probes or geothermal collectors which, in conjunction with heat pumps, provide approx. 4,700 MW of energy (Bundesverband Geothermie 2023). Deep geothermal energy, which is the focus of this work, is not as widespread. In total, thermal water for energy use from depths > 400 m is currently produced at 42 locations in Germany (Agemar et al. 2014b; Agemar et al. 2014a). Out of these locations, 30 plants are exclusively used as heating plants, two plants exclusively produce electricity and 10 locations use heat and electricity in combination. A total of around 417 MW_t (megawatt thermal) of thermal capacity and 46 MW_e (megawatt electrical) of electrical capacity are installed at an average depth of 2,500 m (Bundesverband Geothermie 2023). The use of deep, hydrothermal geothermal energy is linked to major geological structures, which are explained in more detail below.

3.1.1 Geological setting of Geothermal Systems in Germany

Sites for deep geothermal energy in Germany are generally located within three major geological structures (Figure 7): the active intercontinental rift of the Upper Rhine Graben (URG), the Bavarian Molasse Basin (BMB), and the North German Basin (NGB).

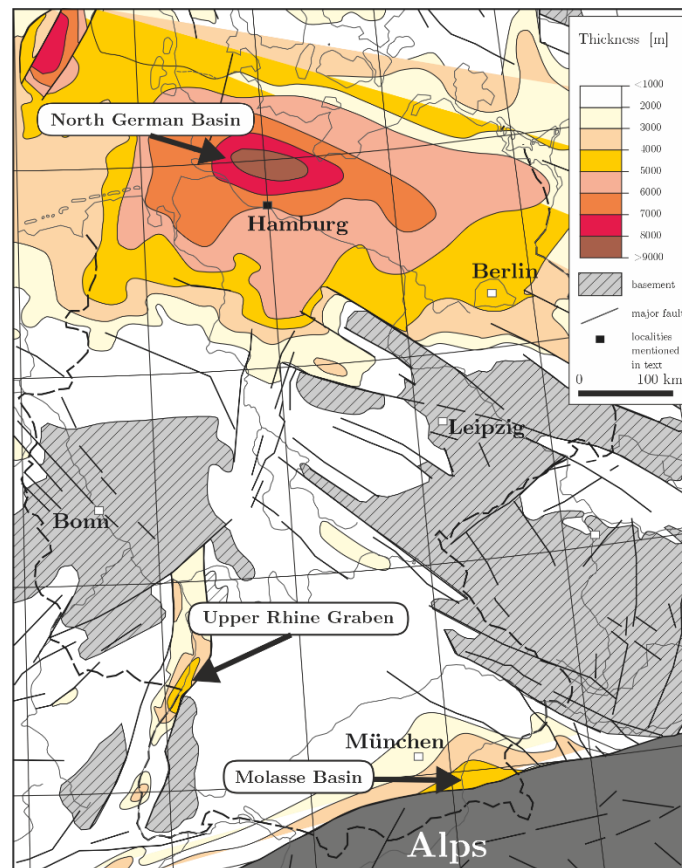


Figure 7: Overview of the sedimentary thicknesses and major fault systems in Germany. The areas of large sedimentary thicknesses represent also the high potential areas of deep geothermal energy (Adapted from Franz et al., 2018).

The NGB represents the central part of the Central European Basin reaching from the North Sea across Europe to Poland, filled with up to 10 km sedimental series from Permian to Cenozoic times (Benek et al. 1996; Feldrappe et al. 2008; Franz et al. 2018). The initiation of the basin formation followed the Variscan orogeny in Late Carboniferous times associated with active volcanism in early Permian times (Lower Rotliegend) and later enforced by thermal subsidence (Upper Rotliegend). The subsidence continued until late Cretaceous times and was ended by a compressive N-S stress field lifting up large parts of the basin (Mazur and Scheck-Wenderoth 2005; Scheck-Wenderoth and Lamarche 2005). The primary volcanic units are overlain by a Mesozoic basin fill of sandstones, clays, and carbonates with intercalations of evaporates. The final phase of basin development during Cretaceous times was dominated by basin differentiation and inversion induced by the collision of the African and European plates. Within this period also salt tectonics was triggered, mobilizing the saline layers of the Zechstein units (Feldrappe et al. 2008; Franz et al. 2018; Mazur and Scheck-Wenderoth 2005). The associated halokinesis led to the formation of large-scale salinary structures such as salt domes and salt diapirs, also causing faulting in their vicinity (Figure 8). The higher thermal conductivity of the enclosed halite and anhydrite formations also leads to higher temperatures at the top of the saline structures in comparison to the surrounding subsurface. The Mesozoic basin fill is crosscut by several fault zones such as the Vorpommern, Fürstenwalde-Guben, or Köris-Merzdorf fault zones with NNW-SSE strike orientations. Prominent structures in the south-west of the Basin like the Altmark-Fläming syncline are WNW-ESE orientated (Feldrappe et al. 2008; Mazur and Scheck-Wenderoth 2005).

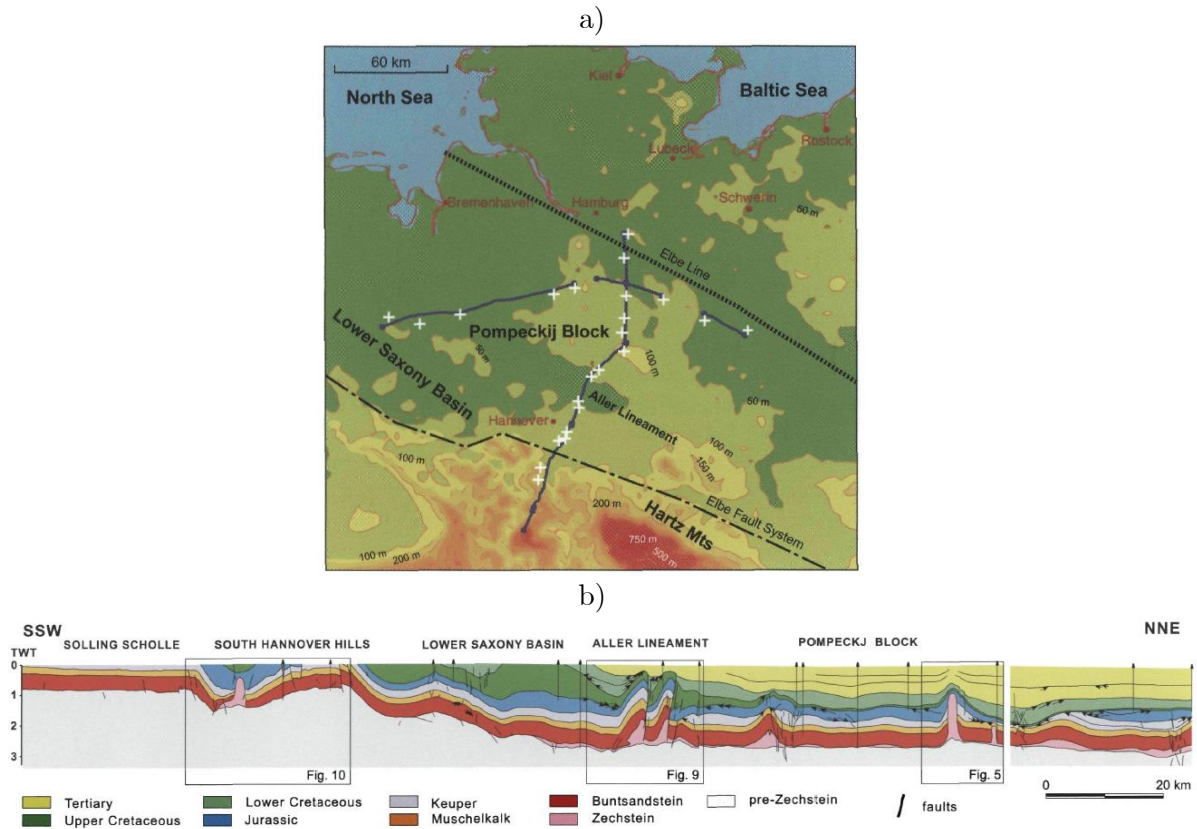


Figure 8: a) Topographic map of the North German Basin with the position of investigated seismic lines (map taken from Mazur & Scheck-Wenderoth, 2005) b) Interpreted geoseismic NNE-SSW cross-section from figure a) across the southern North German Basin. The interpretation is based on seismic reflection lines as well as borehole stratigraphy and the vertical scale is 2-times exaggerated (profile taken from Mazur & Scheck-Wenderoth, 2005).

Another basin structure hosting geothermal potential is the BMB in the south of Germany as a classical foreland basin in front of the Alps. The lateral extension reaches from Lake Geneva in Switzerland over 1000 km to Salzburg in Austria in the east with a maximum width of 130 km in Bavaria (Reinecker et al. 2010). The underground of the basin is formed by Mesozoic sediments covering Variscan granites and gneisses (Bachmann et al. 1987; Maurer 2006). The basin formation and sedimentation are mainly influenced by the north-ward thrusting and isostatic uplift of the alpine nappes caused by the collision with the Adriatic/Apulian Plate (Maurer 2006; Reinecker et al. 2010). The down-bending of the European plate is also causing a typically asymmetric cross-section, with its deepest level situated directly at the Alpine thrust front (Figure 9). The basin fill is composed of up to 5000 m thick successions of late Eocene to late Miocene fluvial fans, deep-marine sandstone marls, and clays. The overthrusting further caused E-W striking synthetic and antithetic normal faults crosscutting the top of the basement, Mesozoic sediments, as well as the bottom of the Tertiary molasses sediments, mostly parallel to the alpine thrust (Dussel et al. 2016; Reinecker et al. 2010).

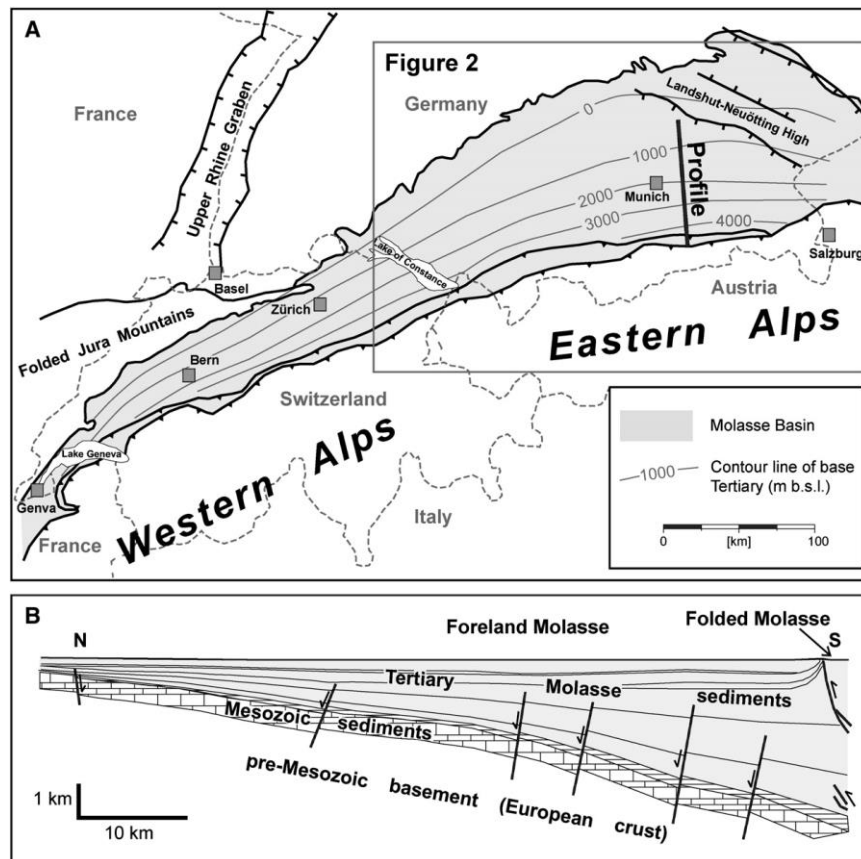


Figure 9: a) Overview of the Swiss-German Molasse Basin with contour lines of the base of Tertiary sediments (i.e. the Molasse sediments) and major structures. b) N-S profile through the Molasse Basin along the Profile in a) (Map and profile taken from Reinecker et al., 2010).

The third large geological structure for deep geothermal energy production is the URG in southwest Germany, a 300 km long and 30-40 km wide NNE-SSW-trending continental rift system (Eisbacher and Fielitz 2010; Geyer et al. 2011). The URG is part of the European Cenozoic Rift System in the foreland of the Alps, whose extension and subsidence initiated during the Eocene (approx. 47 Ma). The margins of the Graben are limited by two main border fault systems separating the uplifted graben shoulders from the sedimentary graben fill (Eisbacher and Fielitz 2010; Grimmer et al. 2017). The Variscan crystalline basement is covered by Permian to Triassic formations in the north and Jurassic formations in the south overlain by up to 3500 m thick successions of Cenozoic sediments. The rifting process accompanied with the subsidence and filling of the Graben structure in combination with the uplift of the Graben shoulders further led to the formation of extensive fault systems (Figure 10). Most prominent are the W-dipping Eastern Main Border Fault and the E-dipping Western Main Border Fault, the graben generating normal faults (Grimmer et al. 2017; Rotstein et al. 2006; Wenzel and Brun 1991).

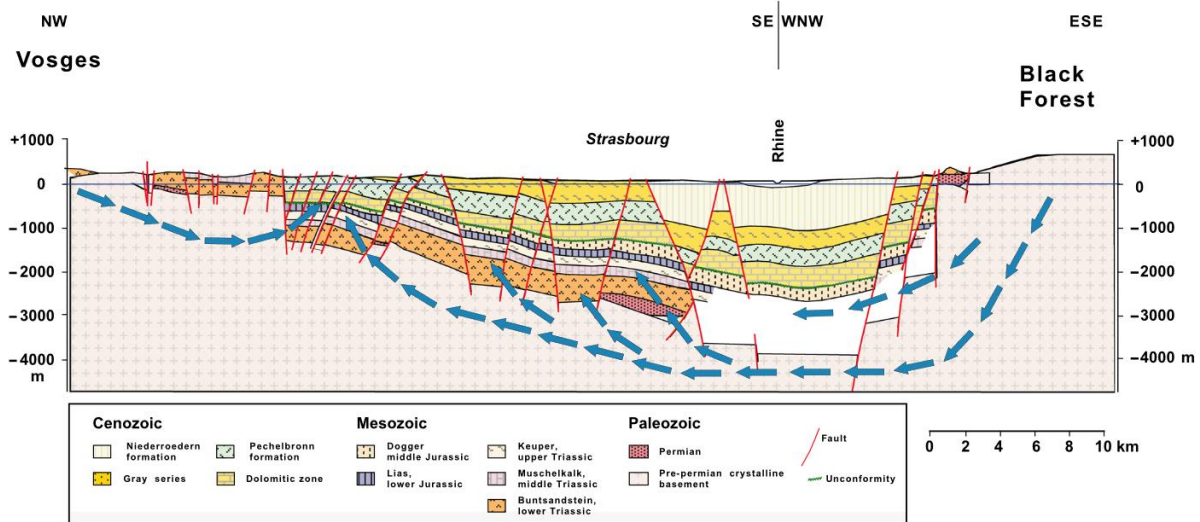


Figure 10: Schematic cross-section through the Upper Rhine Graben between the Vosges Mountains and the Black Forest north of Strasbourg showing the topographically driven flow system within the sedimentary formations and the fractured crystalline basement (Profile taken from Stober & Bucher, 2015).

3.1.2 Geothermal Play Types Germany

In Germany, different systems are currently exploited for deep geothermal use, all of them belonging to the non-magmatic play types. The NGB and BMB as an intracratonic basin type and orogenic belt type show a conduction-dominated heat supply. The hydrothermal systems thus result from fluids, circulating in deep aquifers, warmed by a close to normal heat flow. Locally fault zones can cause additional advective heat flow in fault systems from lower to more shallow geological units (Moeck 2014).

In the BMB, various geological units can be used for geothermal energy production, such as the crystalline basement, Upper Carboniferous – Permian units, Triassic sediments of the Buntsandstein, Muschelkalk, Keuper, and Jurassic Malm and Dogger, as well as Tertiary units. The Tertiary sediments are located at a depth of 2000 m in the Munich area and reach by dipping underneath the Alps depths of up to 5000 m at their margin (Bayerisches Staatsministerium für Wirtschaft Landesentwicklung und Energie 2022). The fluids indicate water-rock interactions of meteoric water with the carbonate reservoir rock, causing only moderate salinity (approx. 2–6 g/L). Gas contents range between 4 and 900 Nm³/L, mostly represented by CO₂ (6–90%), N₂ (5–73%), and CH₄ (3–55%) (Mayrhofer et al. 2014). Multicomponent geothermometers indicate temperatures in the reservoir of 90 – 140 °C (Ystroem et al. 2022).

The NGB as an intracratonic basin is divided into several sub-basins and shows great regional variations in terms of basin fill thickness, structure, and geothermal gradients reaching between 33 and 90 K per km depth (Franz et al. 2018; Moeck 2014). Deep geothermal resources are found in the Paleozoic and Mesozoic groups and reach temperatures of 110 – 150 °C (Franz et al. 2018; Regensburg et al. 2010). The Paleozoic resources are mainly bound to the sediments and volcanic rocks of the Rotliegend Group between 2500 and 5500 m depth. Sandstone reservoirs host the Mesozoic hydrothermal resources in different complexes, such as Middle

Buntsandstein, Lower–Middle and Upper Keuper, Lower and Middle Jurassic, and Lower Cretaceous. Reservoirs in this unit can also reach depths up to 5500 m with the salinity increasing with increasing depth. Reservoirs influenced by highly saline brines, derived by salt dissolution (e.g. from Lower Triassic or Zechstein), can reach pore fluid salinity increases of 20 – 25 g/L per 100 m depth (Franz et al. 2018). Brines from the geothermal site Groß Schönebeck (Rotliegend, 4100 – 4235) show salinities between 193 and 265 g/L TDS. Dominant ions are Ca, Na, and Cl, accounting for 70–98% of the total salinity (Regenspurg et al. 2016; Regenspurg et al. 2010). The gas phase consists mainly of N₂ and CH₄, as well as smaller percentages of He, CO₂, H₂, Ar, and heavy hydrocarbons. The gas–water volume ratio ranges from 1:1 to 1.6:1 (Regenspurg et al. 2010). Water–rock interaction of the high salinity brines with metal-rich permo-carboniferous volcanic rocks is most likely also the cause of high concentrations of different economically valuable elements such as Li concentration of >300 mg/L (Regenspurg et al. 2015a; Regenspurg et al. 2010).

The URG is a non-magmatic extensional domain type. The region shows high temperatures in shallow depth, most likely caused by elevated heat flow at depth because of mantle upwelling and thinning of the lithospheric crust as well as fluid convection along fault zones (Bächler et al. 2003; Guillou-Frottier et al. 2013; Moeck 2014; Stober and Bucher 2015). The extensive fault system in the graben structure, partially connects several fluid reservoirs, including reservoirs in the Paleozoic bedrock and those in the overlying Mesozoic-Cenozoic units, with occasional contributions of surface waters as well (Sanjuan et al. 2016a). Most of the geothermal reservoirs exploited by deep wells are located in fracture networks at the transition zone between the crystalline basement and the sedimentary cover (Vidal and Genter 2018). Fluids typically show high salinities of up to 120 g/L while chemical and isotopic signatures indicate a complex genesis from different fluids as well as several evaporation, mineral precipitation, and dissolution events (Drüppel et al. 2020; He et al. 1999; Pauwels et al. 1993; Sanjuan et al. 2022; Sanjuan et al. 2016a). In the high-salinity fluids, different metals are enriched, possibly due to the interaction of these highly saline waters with sedimentary units of Buntsandstein and crystalline bedrock at high temperatures (225 ± 25 °C) (Drüppel et al. 2020; Pauwels et al. 1993; Sanjuan et al. 2016a). Li concentrations range between 160 – 210 mg/L in deep fluids (Dezayes et al. 2013; Eggeling et al. 2018; Pauwels et al. 1993; Sanjuan et al. 2016a). The brines are characterized as Na-Cl fluids showing high gas contents. The main gas component is typically CO₂ (80-90 Vol%). Secondary are N₂ (6-10 Vol%) and CH₄ (2–7 %) are present in the fluids. The Landau geothermal fluids are exceptions with approximately 48 Vol% N₂ and 44 Vol% CO₂. The gas–water ratio under standard conditions of 1.6:1 is very similar to that of the North German Basin (Eggeling et al. 2018; Sanjuan et al. 2016a).

3.2 Chile

In Chile, the landscape is strongly characterized by the volcanism of the Andes, which is often associated with thermal springs. Due to this widespread volcanic activity, Chile has one of the largest geothermal potentials in the world. The already identified geothermal fields alone indicate a potential of 659 MW_e in terms of indicated and inferred resources (Aravena et al. 2016). Concerning the direct use of geothermal resources, there are a variety of thermal bathing

uses ranging from simple catchments of naturally outflowing springs to large tourist facilities. For the main thermal systems, an installed thermal capacity of approx. 15 MW_t can be estimated for this form of utilization. For the use of shallow geothermal energy utilization by geothermal heat pumps, 29 systems show an installed capacity of approx. 7 MW_t (Morata et al. 2020). Chile commissioned its first power plant using deep geothermal energy in 2017. The Cerro Pabellón power plant, which is also the first in South America, has an installed capacity of 81 MW_e, tapping the reservoir via 13 wells with currently 6 production and 3 reinjection wells in operation (Cappetti et al. 2020; Morata et al. 2020). In the following, the development of the Andes as well as the characteristics of the associated geothermal fields is presented.

3.2.1 Geological setting of Andean Geothermal Systems in Chile

The most prominent geological structure in terms of geothermal systems in Chile is the Andean volcanic arc. It reaches from 6°N in Colombia to 55°S in Chile and hosts at least 12 caldera/ignimbrite systems with over 200 potentially active volcanoes and over 300 geothermal areas (Aravena et al. 2016; Lahsen 1988; Siebert et al. 2010). The Andean volcanic arc developed over 550 Ma. along a 4000 km long continental margin, during 5 tectonic cycles. Extensive studies are documented in the literature, to which reference is made (Charrier et al. 2007; Hervé et al. 2007; Parada et al. 2007; Ramos 2009; Stern et al. 2007; Stern 2004).

A major change in the Andean geodynamics took place at the end of the Jurassic/Early Cretaceous by the detachment of South America and Africa. The ongoing motion to the northwest displays the fifth cycle, the Andean Orogenesis, controlling the Andean crustal thickening and uplift. This change is also the driving force for the distribution of magmatism along the volcanic arc and the origin of the formation of the typical subduction-related mountain belt (Charrier et al. 2007; Ramos 2009). The ocean-continent collision, resulting in the subduction of the Nazca Plate and the Antarctic Plate below the South American Plate, initiated the Andean Arc magmatism ongoing until today (Charrier et al. 2007; Stern et al. 2007).

The occurrence of volcanic systems can be separated into 4 segments the Northern (NVZ; 5°N – 2°S), Central (CVZ; 16–28°S), Southern (SVZ; 33–46°S), and Austral (AVZ; 49–55°S) Volcanic Zones, caused by the variations in the dip and morphology of the subduction (Aravena et al. 2016; Lahsen 1988). For Chile, the largest volcanic occurrences are in the CVZ and SVZ. The northern Chilean volcanic systems in the CVZ reach from the Peruvian border in the North down to Copiapo in the Norte Chico region where the volcanic chain Tres Cruces-Nevaldo Ojos del Salado is located (Stern et al. 2007). The area hosts at least 6 potentially active Quaternary silicic ignimbrite centers and/or caldera systems (Figure 11). The Nazca plate in this area is subducted at 7 – 9 cm/yr with a dip of 25° up to > 400 km depth leading to a crustal thickness of > 70 km. The active strato volcanoes are located here in altitudes of > 4,000 m overlying previous Oligocene and Quaternary volcanism (Stern et al. 2007; Stern 2004). Towards the south, a region of volcanic absence is bordering the CVZ, the Pampean Flat Slap Segment. In this region, the Juan Fernández Ridge is subducted, causing a decrease in the subduction angle (flat-slab), thickening of the lithosphere, and the gap in volcanism (Charrier et al. 2007; Stern

2004). The SVZ (Figure 11) shows again subduction angles increasing from 20° to 25° from north to south, causing a decreasing distance between the trench and volcanic front, a decrease of the depth of the subducted slab as well as a decrease in crustal thickness from > 50 km to 30 km (Stern 2004). One of the most prominent tectonic features in the center of the SVZ is the Liquiñe-Ofqui fault zone (LOFZ, Figure 13). The LOFZ is a 1200 km long $N10^\circ E$ trending strike-slip structure and is assumed to strongly influence the emplacement of the Quaternary volcanism (Charrier et al. 2007; Pérez-Moreno et al. 2021; Sanchez-Alfaro et al. 2016).

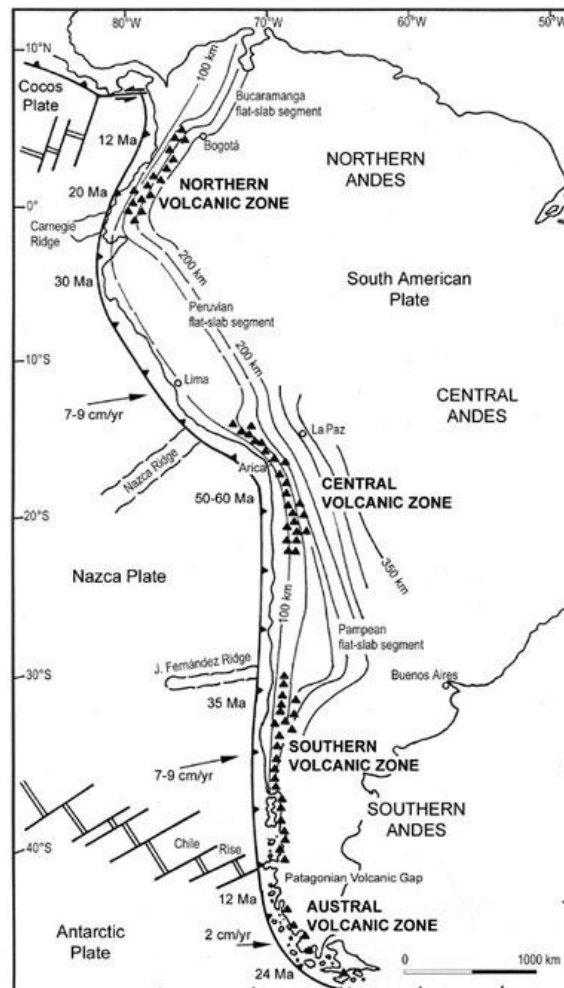


Figure 11: Schematic map of South America and the subduction zones of the Nazca and Antarctic plate. Subduction direction and speed are indicated by arrows in cm/yr, and subduction geometry by depth in km to the Wadati-Benioff Zone. The black triangles display quaternary volcanoes (map taken from Stern, 2004).

The magmatism of the Chilean Andes has taken place since 300 Ma as a consequence of the subduction of the oceanic Nazca and Antarctic plates. The magmatism shows significant spatial and temporal variations with magma sources from the dehydrated, subducted oceanic lithosphere in combination with partly melting of the overlying mantle wedge as well as the participation of continental crust (Parada et al. 2007; Thorpe 1984). Since in Chile, the highest temperatures of springs are located in Quaternary volcanic systems (Lahsen 1988), the focus on the following description of Andean magmatism lies in this episode.

In the southern and central SVZ where the overlying crust is thin, the quaternary eruptions show tholeiitic, high-Al basaltic to rhyolitic signatures (Lahsen 1988; Thorpe 1984). North of 35°S hornblende and biotite andesites and dacites are predominant while south of this latitude olivine and pyroxene basalts and basaltic andesites are most common (Lahsen 1988). The isotopic signatures of Sr, Nd, Be, O, and Pb, as well as different radionuclides (^{226}Ra over ^{230}Th , ^{238}U over ^{230}Th), preclude significant assimilation of continental crust and indicate mafic mantle-derived magma contaminated by fluids of the oceanic lithosphere and sediments without strong interaction with the continental crust (Stern et al. 2007; Stern 2004). Be isotopes indicate a contribution of sedimentary components, and Pb isotopic data indicate further a contribution of subducted Nazca plate sediments to the mantle. The rocks of the central and southern SVZ show high ratios of soluble element groups as large-ion-lithophile-elements to rare earth elements (REE) indicating an enrichment of slab-derived fluids. These indicators of the influence of the slab-derived fluids decrease towards the east along the volcanic front, potentially derived by progressive dehydration of the down-going slab (Stern 2004).

In the CVZ, hornblende and biotite andesites, and dacites are the dominant erupted rock types of quaternary volcanism. This magmatism is associated with stronger contamination of the basaltic magma by the locally thick continental crust, as well as high subduction erosion rates, which are indicated by higher $^{87}\text{Sr}/^{86}\text{Sr}$, lower $^{143}\text{Nd}/^{144}\text{Nd}$ ratios, and relative enrichment of K, Rb, Th, and U in comparison to the SVZ (Parada et al. 2007; Thorpe 1984). The processes are assumed to take place by a combination of intra-crustal assimilation, crystallization, and/or crustal anataxis. Further temporal variation indicates that along with the increase in crustal thickness also the crustal contamination increased. Most of the volcanism and associated hydrothermal springs are located along the western Cordillera of the Altiplano block. During Pliocene and Quaternary times extensional tectonic conditions formed different N-S fault systems inducing differential block uplift and the initiation of small hot water bearing grabens (Lahsen 1988). These fault systems also control the spatial distribution of the volcanic edifices and their hydrothermal systems (Lahsen 1988; Stern 2004)

3.2.2 Geothermal Play Types in Chile

Since most of the geothermal systems are located close to active volcanoes, the Andean magmatism is suggested to be the heat source of most of the geothermal systems in Chile (Lahsen 1988). Due to the heat source, the systems can be typically described as volcanic field type or volcanic geothermal systems. Although every volcanic edifice is unique, there are typical common features in these kinds of systems. The heat transfer from the magmatic heat source is rather convection dominated by deep circulation of fluids beside or above. Fluids can originate from the infiltration of meteoric fluids of higher altitudes and partial mix with magmatic fluids and gases (Arnorsson et al. 2007; Moeck 2014). Due to the typically steep volcanic topography, the systems can be subdivided into an upflow and an outflow zone (Figure 12). Along the site-specific heat source and geological structure, different hydrothermal reservoirs form along the up- and outflow regimes (see also Chapter 2.2 Development of Geothermal Fluids). Deep, rather Cl-rich fluids are heated up reaching temperatures of approximately 300 °C. A rising up in the periphery of the volcanic edifice can form chloride-rich hot springs. Fluids can also rise along the volcanic dome, becoming continuously enriched

with volcanic gases and forming acidic sulfur springs at the summit of a volcano. Pressure relief due to structural changes can also initiate boiling and degassing thus causing a phase separation. This can lead to the formation of a shallower, acidic condensate layer and condensate springs (Arnorsson et al. 2007; Henley and Ellis 1983b; Moeck 2014).

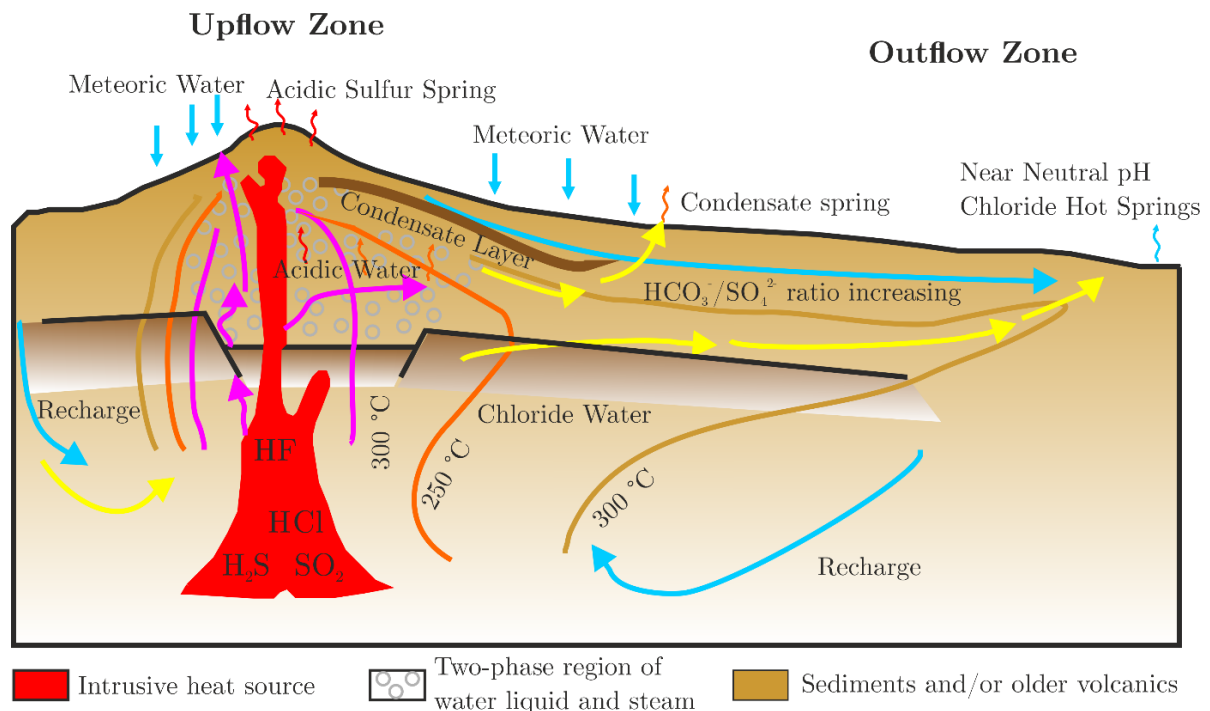


Figure 12: Schematic drawing of a typical volcanic play type above a subduction zone (adapted after Moeck, 2014).

The geothermal occurrences in Chile can be roughly separated into a northern and a southern zone, correlating with the segments of Andean volcanism of the CVZ and SVZ. In northern Chile, hydrothermal activities scatter along the western side of the CVZ and occur typically in NS- and NW-trending graben structures located on altitudes higher than 4000 m (Tassi et al. 2010). These systems manifest partly on the surface by geysers, fumaroles, boiling waters, mud pools, and outflowing springs (Lahsen 1988). The thermal springs at the surface have various chemical compositions. Geothermal systems such as Surire, Puchuldiza-Tuja, and El Tatio show typical Na-Cl composition with salinities up to 10,000 mg/L, Li concentrations up to 39 mg/L, and high SiO_2 concentrations up to 315 mg/L. Other systems such as Pampa Lirima, Pampa Apacheta, or Torta de Tocopuri have rather an acidic-sulfate signature, in comparison to rather low salinities up to 5,000 mg/L and low Li (< 3 mg/L) and SiO_2 (< 90 mg/L) concentrations (Tassi et al. 2010). The dominant gases are CO_2 and H_2S and solute and gas geothermometers indicate high enthalpy resources with temperatures reaching > 300 °C, validated by borehole measurements for singular fields such as El Tatio, Puchuldiza or Cerro Pabellón (Cappetti et al. 2020; Lahsen 1988; Tassi et al. 2010). Furthermore, in northern Chile, the only operating Chilean geothermal power plant, Cerro Pabellón is located (Morata et al. 2020).

Volcanic and associated geothermal systems in the SVZ are spatially and temporally located to the two regional-scale fault systems of the arcparallel (NE- to NNW Striking) Liquiñe-Ofqui Fault System (LOFS) and the Andean Transverse Faults (ATF) striking WNW. The surface

discharges of the geothermal systems show lower overall salinities than in the north ($> 4,000$ mg/L) (Wrage et al. 2017). Also in the south, the geothermometers indicate subsurface temperatures of up to 300 °C for several systems such as Nevado de Chillán, Cordon Caulle, or Tolhuaca. In Tolhuaca these values were also validated by deep borehole temperature measurements (Aravena et al. 2016; Sanchez-Alfaro et al. 2016). Most of the springs show a Na-Cl signature like Termas de Pemehue, Termas de Malleco, or Termas de Aguas Calientes. In addition, acidic-sulfate fluids are present in systems such as Nevado de Chillan, Copahue, or Tolhuaca and only minorly, HCO_3 waters are observed (Pucon Mahuida, Termas de Coyuco). The acidic-sulfate springs show the highest outflow temperatures (< 92 °C) and reach also the highest SiO_2 concentrations (370 mg/L in Nevado de Chillan) while no significant Li concentrations are observed in any of the systems (< 3 mg/L) (Wrage et al. 2017).

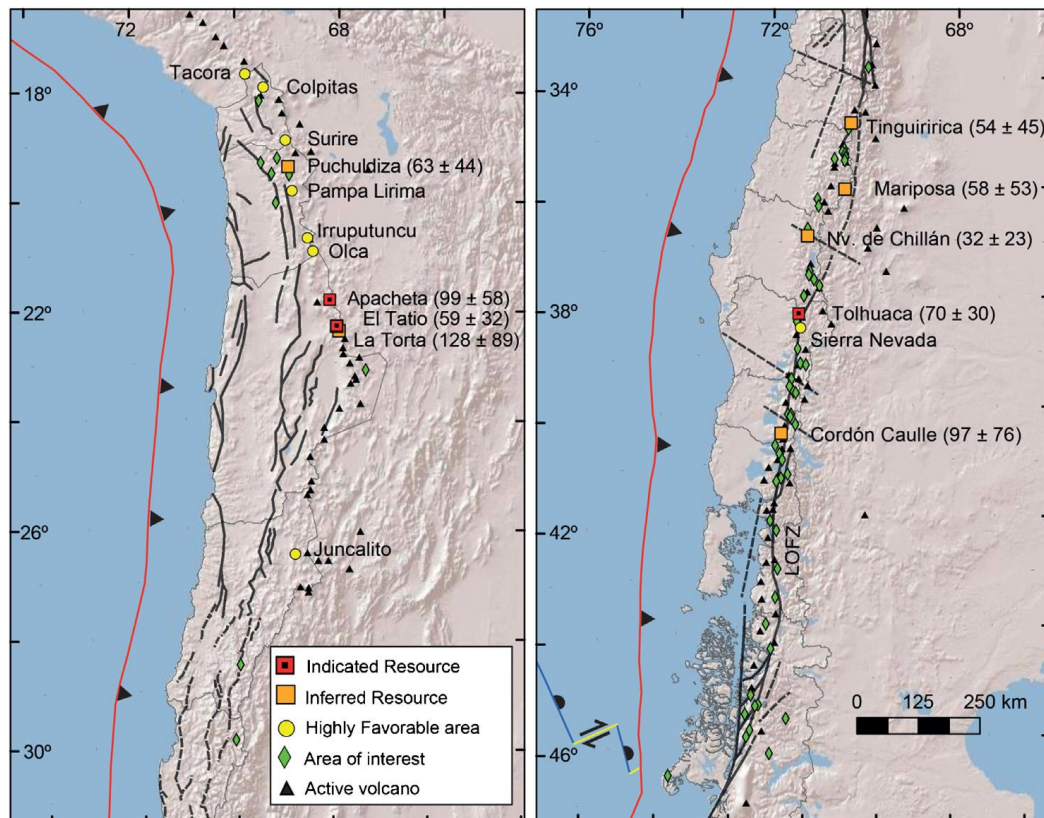


Figure 13: Geothermal areas in Chile separated into indicated resources, inferred resources, and areas, which are highly favorable, and of interest. The left side shows the Systems in northern Chile, while the right side shows geothermal systems in the south (maps taken from Aravena et al., 2016).

4 Technology assessment for Direct Lithium Extraction from geothermal fluids

The following chapter is a translation of the German journal article “*Herausforderungen und Chancen für die Lithiumgewinnung aus geothermalen Systemen in Deutschland – Teil 1: Literaturvergleich bestehender Extraktionstechnologien*” (<https://doi.org/10.1007/s00767-022-00522-5>). It was originally published under an Open Access license in the peer-reviewed journal *Grundwasser*. 27, 239–259 (Goldberg et al., 2022a). The translation was conducted by the original authors of the initial study.

Valentin Goldberg^a, Tobias Kluge^b, Fabian Nitschke^a

^a Institute of Applied Geosciences, Chair for Geothermal Energy and Reservoir Technology, Karlsruhe Institute of Technology, Adenauerring 20b, 76131 Karlsruhe

^b Institute of Applied Geosciences, Chair for Geochemistry & Economic Geology, Karlsruhe Institute of Technology, Adenauerring 20b, 76131 Karlsruhe

4.1 Abstract

This study assesses the status of currently available extraction technologies for lithium recovery from geothermal waters based on recent scientific studies and identifies potential technical challenges. Frequently discussed technologies such as liquid-liquid extraction, selective extraction by inorganic sorbents, electrochemical methods, and membrane technologies are evaluated in terms of their applicability and integrability in geothermal energy production. Current research projects have validated various extraction methods at laboratory and, in some cases, prototype scale. Scaling up to an industrial process does not exist yet. Accordingly, information regarding continuous operation as well as site-specific challenges (water chemistry, volume flow, flow rates, etc.) and actual economic viability is lacking. The amount of recoverable lithium depends primarily on the concentration of lithium dissolved in the water, the extraction efficiency and rate, and the amount of extractant used. The interaction of these factors determines the process technology and the size of the extraction infrastructure. Depending on the chosen Li extraction method, the physiochemical properties of the water (pH, Eh, T, p, etc.) are altered during extraction, which can increase scaling and corrosion potential.

The current state of the art shows an early to mid-technology maturity stage while reaching lithium extraction efficiencies in laboratory experiments of 50 – 90 %. Under the disproportionately higher challenges in the ongoing operation of a geothermal power plant, extraction efficiencies at the bottom of this range are considered realistic.

4.2 Introduction

The current energy transition from fossil fuels to renewable energy sources requires the availability of a variety of strategic raw materials. One of the key metals defined as a critical raw material by the European Commission is lithium (Europäische Kommission 2020). Until the beginning of the 21st century, the main applications for this alkali metal were in the ceramics and glass industries, as a lubricant, or in aluminum alloys. Today, most lithium is used for the production of lithium-ion batteries (Liu et al. 2019; Schmidt 2017). Due to their higher energy density, low discharge rates, long life cycles, and fast charging compared to nickel-metal hydride or lead-acid batteries (Kavanagh et al. 2018; Lee et al. 2011; Schmidt 2017), these batteries first found application in cameras or mobile phones. Today, the main growth market is electric cars. Large electrical storage capacities are needed to compete with the achievable ranges of vehicles with internal combustion engines powered by fossil fuels. This requirement results in correspondingly large batteries (Lee et al. 2011; Srinivasan et al. 2008) with a proportion of pure lithium in an electric car battery of around 10-14 kg (Xu et al. 2020).

Due to high demand and the increase in market price, new lithium sources are being evaluated globally, also to find more environmentally friendly alternatives to conventional mining or extraction from the brines of salt lakes. Currently, lithium extraction from geothermal fluids is being discussed as a new option, which could also make lithium production possible in Germany. This literature review evaluates different technologies proposed for the extraction of lithium from geothermal fluids. Published experimental results are discussed and used to explicate the basic principles of extraction processes and to highlight the technical challenges for integration into a geothermal power plant process. In the second part of this study (Goldberg et al. 2022b), the lithium market is examined in more detail and the potential contribution of geothermal lithium production in Germany is estimated.

4.2.1 Geothermal Fluids in Germany

To evaluate the applicability of existing lithium extraction technologies to geothermal fluids in Germany, the fluid chemistry of relevant geothermal regions is described below (Table 3).

Table 3: Fluid chemistry of geothermal fluids from different geothermal regions in Germany

	Unit	Central Bavarian Molasse Basin	Upper Rhine Graben	North German Basin (example: Groß Schönebeck)
pH	-	6.4–7.5	4.96–7.82	7.05
Na ⁺	mg/L	120–140	827–105,000	33,600
K ⁺	mg/L	16–32	70.9–4,030	2,560
Ca ²⁺	mg/L	35–410	112–11,700	45,400
Mg ²⁺	mg/L	12–58	3.96–1,930	233
Li ²⁺	mg/L	-	4.5–210	212
SiO ₂	mg/L	-	10.7–201	93.7
Cl ⁻	mg/L	120–900	1,480–167,000	138,384
SO ₄ ⁻	mg/L	3.3–16	140–2,730	94.4
HCO ₃ ⁻	mg/L	190–330	124–1,027	-
Reference:	-	(Mayrhofer et al. 2014)	(Sanjuan et al. 2016a)	(Regenspurg et al. 2016)

In Germany, energy from deep geothermal fluids is obtained mainly from three major geological structures: the Upper Rhine Graben (URG), the Bavarian Molasse Basin (BMB), and the North German Basin (NGB). These three regions have low to moderate geothermal reservoir temperatures (120–250 °C) and fall under the category of non-magmatic geothermal systems (Moeck 2014; Sanjuan et al. 2022).

The Malm aquifer in the Bavarian Molasse Basin, especially around Munich, represents one of the horizons with the strongest expansion of geothermal energy production in Germany. However, the fluids there demonstrate no significant lithium concentrations and generally yield only a very low total dissolved solid load (approx. 2–6 g/L) (Mayrhofer et al. 2014).

The North German Basin is a sedimentary basin on a crystalline basement. Its reservoir fluids, however, have fundamentally different chemistry compared to the Molasse Basin (Moeck 2014; Sanjuan et al. 2022). For example, at the Großschönebeck geothermal site solution contents > 300 g/L are reached. The main ions of the fluids are Ca, Na, and Cl, which account for 70–98% of the total salinity (Regenspurg et al. 2016; Regenspurg et al. 2010). In addition, the fluids contain high amounts of non-condensable gases in a gas-water volume ratio of 1:1 to 1.6:1 (Regenspurg et al. 2010). The main components of the gas phase are N₂ and CH₄ and in smaller amounts He, CO₂, H₂, Ar, and heavy hydrocarbons (Regenspurg et al. 2010).

The geothermally utilized reservoir fluids in the Upper Rhine Graben exhibit salinities of up to 120 g/L. These Na-Cl fluids have gas-water ratios of up to 1.6:1, making them similar to the fluids in the North German Basin (Eggeling et al. 2018; Sanjuan et al. 2016a). A gas fraction of 0.13 wt% was measured at the site of Soultz-sous-Forêts, and about 0.5 wt% at the Bruchsal site (Eggeling et al. 2018; Sanjuan et al. 2016a). The main gas component is typically CO₂ with 80–90 vol.%. In addition, N₂ (6–10 vol.%) and CH₄ (2–7 vol.%) were measured in the fluid. At the Landau site, nitrogen is the main component with about 48 vol.% whereas the share of CO₂ is 44 vol.%.

4.2.2 Geothermal Fluids as a Lithium Resource

Lithium occurs in relatively high concentrations in the geothermal fluids of the URG and NGB, though at levels not comparable to the highest concentrations of the salars in South America

(Table 4). The lithium concentration, reservoir size, and flow rate considered economically sufficient for extraction depends on the level of technology readiness level, the extraction process, and the world market price. Seawater contains only 0.18 mg/L of lithium (Stoffyn-Egli and MacKenzie 1984). Moderate lithium concentrations >1 mg/L are found in Europe in a few select regions. In addition to the URG and NGB, those regions include Cornwall in northern England, the Massif Central in France, the Paris Basin, and the western Apennines (Sanjuan et al. 2022). Little has been published on the concentration of lithium in geothermal fluids from other European regions. As a result, the potential in other European regions cannot be assessed conclusively.

In Germany, the highest Li concentrations and flow rates are reached mainly in reservoirs developed by deep drilling (Table 4). The highest concentrations approach the lower limit of the concentration range of salars in Argentina, where lithium is already being commercially produced. With an effective technological approach, these fluids could be an environmentally sound and economically viable resource in Germany.

Table 4: Lithium concentrations of different fluids in Germany and South America. Lithium concentrations and extraction conditions of fluids from geothermal, hydrocarbon, and hot springs in Germany and salars in Chile and Argentina are compared.

Region	Extraction Conditions	Li Concentrations	References
Upper Rhine Graben Insheim, Landau, Bruchsal (D) Soultz-sous-Forêts, Rittershoffen (F)	Geothermal wells: Temperatures: ≤ 165 °C Flow rates: ≤ 80 L/s Depth: 2500–5000 m	160–190 mg/L	(Dilger et al. 2021; Sanjuan et al. 2016a; Uhde 2021)
North German Basin Groß-Schönebeck	Research well: Temperature: 150 °C Flow rate: < 15 L/s Depth: ≤ 4240 m	212 mg/L	(Dilger et al. 2021; Regenspurg et al. 2016)
North German Basin Altmark	Gas field formation fluid: Depth: ≤ 3500 m	50–375 mg/L	(Lüders et al. 2010)
Southwest German Molasse Basin	Hydrocarbon wells: Temperature: 50–100 °C Depth: 1400–2500 m	0–150 mg/L	(Stober 2014)
Taunus Mountains Bad Nauheim	Hot spring: Temperature: ≤ 33 °C Flow rate: ≤ 9 L/s Depth: 180 m	≤ 12 mg/L	(Kirnbauer 2008; Loges et al. 2012)
Chile Salar de Atacama	Li extraction projects: Flow rates: 600–1600 L/s	600–5000 mg/L	(Garcés and Alvarez 2020)
Argentina Salar de Cauchari, Salar de Olaroz, Salar Hombre Muerto, Salar Rincon	Li extraction projects	340–900 mg/L	(Xu et al. 2021a)

4.2.3 Water-Solid Interactions in Geothermal Power Plants

In a geothermal power plant circuit, the water-gas-solids equilibrium is affected in different ways, which can lead to uncontrolled mineral precipitation. This process is referred to as "scaling," and the mineral precipitates are termed "scales." An important driver of scaling is the temperature reduction required for energy production. Mineral phases such as amorphous SiO_2 , BaSO_4 , CaSO_4 , NaCl , and KCl show a decrease in solubility in water with decreasing temperatures (Appelo 2015; Hörbrand et al. 2018). One group of minerals that pose a particular challenge, especially in high-temperature systems, are amorphous silicate phases (Goldberg et al. 2021; Gunnarsson and Arnórsson 2005; Spitzmüller et al. 2021). In a fluid containing around 2.6 moles of dissolved NaCl (about 150 g/L), on the order of salinities in the URG, approximately 200 mg/L Si are soluble at 150 °C, 110 mg/L at 100 °C, and about 40 mg/L at 25 °C (Chen and Marshall 1982; Marshall and Warakomski 1980a). In the case of barite (BaSO_4), solubility in water containing 3 moles of NaCl (TDS of approximately 180 g/L) changes from approx.. 100 mg/L at 150 °C to approx.. 77 mg/L at 95 °C and to approx.. 44 mg at 50 °C (Monnin 1999; Templeton 1960). Mineral phases such as CaCO_3 or $\text{CaMg}[\text{CO}_3]_2$, on the other hand, demonstrate retrograde solubility behavior, i.e. improved solubility with decreasing temperature.

The solubility of CO_2 also increases in the presence of decreasing temperatures (Appelo 2015; Hörbrand et al. 2018). However, CO_2 solubility deteriorates significantly with decreasing system pressure, which is of significance for the (surface) depressurization of water. In water at 150 °C with 2 mol NaCl (about 120 g/L), ca. 42 g CO_2 (4.2 wt%) is soluble at a pressure of 300 bar in a geothermal reservoir. At the same pressure and salinity, the solubility changes to approx. 40 g/L at 60 °C. When this water is depressurized at 150 °C to 100 bar, the solubility drops to approx. 21 g/L and at 10 bar to approx. 1.5 g/L. At 10 bar and a temperature of 60 °C, comparable to conditions in a geothermal power plant after energy production, 5 g/L (0.5 wt.%) of CO_2 is soluble (Duan et al. 2006; Duan and Sun 2003). The outgassing of CO_2 dissolved in water as carbonic acid leads to an increase in pH and a shift in the speciation of dissolved inorganic carbon (DIC). Pure water can dissolve 0.88 g/L CaCO_3 at a CO_2 partial pressure of 100 bar at 100 °C. When the CO_2 partial pressure is reduced to 10 bar at the same temperature, the solubility decreases to 0.51 g/L (Miller 1952). However, at the same CO_2 partial pressure of 10 bar, 0.99 g/L CaCO_3 is soluble again at 60 °C due to the retrograde solubility of CO_2 and CaCO_3 (Miller 1952). Consequently, water-mineral interactions must be considered not only site-specifically, but also section-specifically (with regards to the pumping and reinjection of the fluid and processing during extraction) in a geothermal system.

Equally complex is the dissolution behavior of SiO_2 as a function of pH and dissolved ions in water. In pure water at pH 7, approximately 61 mg/L of Si is soluble as SiO_2 at 25 °C (Marshall and Warakomski 1980a). As pH increases, the solubility of amorphous SiO_2 increases steadily to approx. 260 mg/L at a pH of 10.4 (Marsh et al. 1975). In the presence of Ca and pH >10, the amount of aquatic Si species is greatly reduced due to the precipitation of calcium silicate hydrate (CSH) phases (Greenberg and Chang 1965; Spitzmüller et al. 2021). In the presence of Ca, the solubility at 25 °C and pH 10.5 is only approx. 41 mg/L, and at pH 11.4 it is as low as

7.1 mg/L (Greenberg and Chang 1965). In addition, the change in redox potential and pH can result in the formation of BaSr sulfates and polymetallic sulfides. In this process, ^{226}Ra and ^{228}Ra can be incorporated into sulfates and ^{210}Pb into sulfides (Nitschke et al. 2014; Regenspurg et al. 2015a).

Those processes described are challenging in particular due to the prevailing flow rates in geothermal power plants in the URG of up to 80 L/s. Even relatively low mineral precipitation per liter can cause larger amounts of solids to accumulate over time and lead to damage to the aboveground facility, reduction of the well diameter, or even loss of a well, as well as clogging of pathways in the injection area of a reservoir. Therefore, scales present one of the major challenges in geothermal energy production regardless of reservoir type (Eggeling et al. 2018; Gunnarsson and Arnórsson 2005; Hörbrand et al. 2018; Nitschke et al. 2014; Regenspurg et al. 2015a; Regenspurg et al. 2015b; Scheiber et al. 2019a). Nevertheless, scales do not constitute an uncontrollable constraint on geothermal energy production. With appropriate measures (addition of inhibitors, pressure maintenance), scaling can be controlled, though these interventions always require a site-specific evaluation and are subject to ongoing research (Eggeling et al. 2018; EVA-M 2021; Scheiber et al. 2019b). Accordingly, uncontrolled precipitation in geothermal or extraction systems is also regarded as a major challenge for the planned extraction of valuable elements (Goldberg et al. 2021; Spitzmüller et al. 2021).

4.3 Methods

4.3.1 Standardized Technology Assessment – Technology Readiness Level

The Technology Readiness Level (TRL) scale was used to quantify the status of different technologies. This scale was developed by NASA in the 1970s to systematically classify the technological maturity of developments and make the status of different technologies comparable (Mankins 2009; Mankins 1995). The TRL scale continues to be used in the European Union's Horizon 2020 program to define funding targets. For this purpose, the European Commission has tested, confirmed, and adapted the applicability of the TRL scale to energy issues and explicitly to geothermal energy. This adapted scale deviates slightly from the original version in some respects (De Rose et al. 2017). The different levels of maturity and their definitions are provided in Table 5.

The (financial) expenditure required to reach the individual stages is by no means linear and moreover technology-specific (Mankins 2009; Mankins 1995; Straub 2015). In the first three TRL stages, the costs and effort are low to moderate compared to any later system application (Mankins 2009; van der Spek et al. 2017). The development and validation of initial system components for TRL 4 represent a significant first leap that can be many times the investment required to reach TRL 3 (Mankins 2009). Moderate to high costs must be assumed for reaching TRL 5, similar to those for reaching TRL 4 or a multiple thereof (Mankins 2009; van der Spek et al. 2017). Reaching an initial demonstrator of final size and capability (TRL 6/7) usually represents an escalation of expenditure and constitutes a significant portion of the total

development cost. Due to the significantly more complex level of detail, this stage brings a large number of unforeseeable technical issues that require additional adjustments. This level of development usually cannot be achieved by regular research facilities alone (Mankins 2009; van der Spek et al. 2017). Completing and implementing a first production facility of its kind in the target environment (TRL 8) represents the end of system development with an estimated effort equivalent to five to ten times the cost of all previous stages (Mankins 2009; van der Spek et al. 2017). TRL 9 describes the successful operation of the new technology. Costs for reaching TRL 9 can still be high, depending on the technology, but are generally much lower than for reaching TRL 8 (Mankins 2009; van der Spek et al. 2017).

On the basis of the TRL scale, different lithium extraction technologies were evaluated and compared using a standard case (a flow rate of 80 L/s and a lithium concentration of 200 mg/L). These values correspond to a best-case assumption for known geothermal reservoirs in Germany.

Table 5: Definition of technology readiness levels according to Mankins (1995, 2009), adapted to geothermal systems (De Rose et al. 2017).

TRL	Requirements
TRL 1	Basic principles observed and documented (Mankins 2009; Mankins 1995; De Rose et al. 2017) Geothermal-specific: theoretical concepts, applications, and barriers identified (De Rose et al. 2017)
TRL 2	Formulation of technological concept and/or application (Mankins, 2009; Mankins, 1995) Consideration of interfaces and commercial offerings (De Rose et al. 2017) Geothermal-specific: first simulation of the model (De Rose et al. 2017)
TRL 3	Basic function proven by experimentation or analysis/proof of concept (De Rose et al., 2017; Mankins, 2009; Mankins, 1995) Geothermal-specific: simulation concept validated (De Rose et al. 2017)
TRL 4	Validation of individual components in a laboratory environment (Mankins 2009; Mankins 1995; De Rose et al. 2017) Small-scale demo with auxiliary systems tested in laboratory (De Rose et al. 2017) Geothermal-specific: prototype ready for testing phase (De Rose et al. 2017)
TRL 5	Validation of individual components in a relevant environment (Mankins, 2009; Mankins, 1995) Large-scale demo with auxiliary systems completed, concretized economic consideration (De Rose et al. 2017) Geothermal-specific: Prototype tested and additional functions integrated (De Rose et al. 2017)
TRL 6	Model or prototype tested in a relevant environment (Mankins, 2009; Mankins, 1995). Technological pilot plant in relevant environment, manufacturing strategy (De Rose et al. 2017). Geothermal-specific: Full-size prototype tested (De Rose et al. 2017).
TRL 7	System prototype tested in the target environment (Mankins, 2009; Mankins, 1995) Demo in operating environment, manufacturing approach demonstrated (De Rose et al. 2017) Geothermal-specific: Full-size prototype installed on-site and connected (De Rose et al. 2017)
TRL 8	Actual system completed and confirmed by testing and demonstration in the target environment (Mankins, 2009; Mankins, 1995). Geothermal-specific: Technology has reached the final stage and technically successful application is possible; economic and financial problems have been solved; marketing measures are underway (De Rose et al. 2017).
TRL 9	Actual system confirmed through successful operation in the target environment (Mankins, 2009; Mankins, 1995) System is fully operational concerning production, profitability, and the market (De Rose et al. 2017)

4.4 Extraction Technologies

When raw materials are extracted from fluids, the extraction technique should alter the chemical state of the brine in the power plant and reservoir as little as possible while achieving a high extraction efficiency. Any change in fluid composition should neither adversely affect the surface installations nor the downhole area around the injection well. The criteria used in this study to evaluate the extraction technologies were ion selectivity, the ratio of material cost to lithium yield, the chemical properties of the required material (cycle stability), and the required energy input. The goal of our comparison is to identify which technology aspects present particular challenges for use in geothermal power plants. In addition, we provide a derived technology maturity level based exclusively on scientifically peer-reviewed studies. In general, it should be noted that direct comparison and evaluation of extraction technologies are hampered by inconsistent data (Battistel et al. 2020b; Liu et al. 2019; Stringfellow and Dobson 2021a).

4.4.1 Liquid-Liquid Extraction

In the case of liquid-liquid extraction, dissolved substances of a liquid starting medium are transferred into a liquid solvent (hence the term solvent extraction) (Liu et al. 2019). The basic prerequisite is that the starting medium does not mix with the solvent but exchanges the substance to be extracted on contact. Organic solvents can take up relevant amounts of lithium chloride and also show selectivity toward other cations (Liu et al. 2019; Stringfellow and Dobson 2021a). Promising approaches for recovering lithium from high-salinity fluids include the use of tributyl phosphates (TBP) diluted with methyl isobutyl ketone or kerosene (Liu et al. 2019; Nguyen and Lee 2018; Shi et al. 2018; Xiang et al. 2017; Xiang et al. 2016; Yu et al. 2019), the use of crown ethers (Liu et al. 2019; Swain 2016; Zhang et al. 2021), or the use of ionic liquids (Liu et al. 2019; Park et al. 2014; Shi et al. 2017).

For extraction by TBP, a co-extraction reagent, e.g. FeCl_3 , is used in addition to the solvents. A complex is formed from the FeCl_3 in chloride-rich fluids together with the solvents, which binds the lithium via a cation exchange process (Figure 14). For this process, the two liquids and the coextraction reagent have to reach chemical equilibrium. Subsequently, the phases are separated again and the lithium is recovered from the solvent complex utilizing highly concentrated acid. Finally, the solvent and coextraction reagent are regenerated using caustic solutions (Liu et al. 2019; Nguyen and Lee 2018; Shi et al. 2018; Xiang et al. 2016).

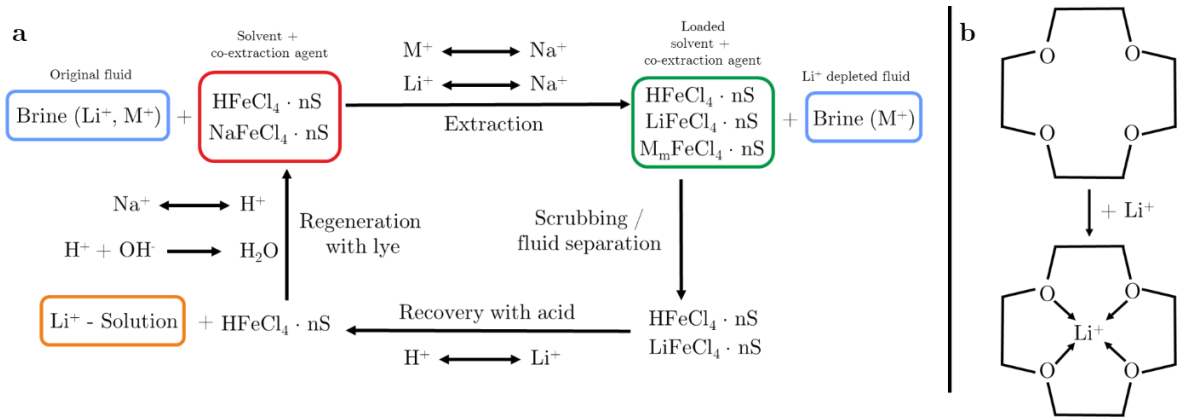


Figure 14: Illustration of a liquid-liquid extraction cycle, adapted after D. Shi et al. (2018). Shown are the four typical extraction steps using a solvent (nL) and a co-extraction reagent, in our example tributyl phosphates (TBP) and FeCl_4 , respectively. The extraction in the case example is performed from a brine containing lithium and other interfering cations (M^+). Right: Principle of incorporation of lithium into a crown ether structure according to Swain (2016).

The function of crown ethers is based on the “Hard and Soft Acids and Bases” concept (HSAB/Pearson concept) (Pearson 1963; Swain 2016). According to this concept, strong acids preferentially bind to strong bases and weak acids to weak bases (Pearson 1963). In crown ethers, oxygen acts as a donor atom, forming a strong base and showing very good reactivity with dissolved alkali metal cations such as lithium, which in turn represent a strong acid (Liu et al. 2019; Swain 2016; Zhang et al. 2021). The cations are thus bound in the center of the crown ether structure (Figure 1, (Boulatov et al. 1999; Itoh et al. 1991)). After the uptake of the lithium, the organic ether phase can be separated from the water phase, such as via centrifugation, and the lithium can be redissolved from the ethers with acid (Itoh et al. 1991; Zhang et al. 2021). Competing ions such as Na, K, Mg, or Ca can be incorporated into the ether structure at the same scale as lithium (Itoh et al. 1991; Zhang et al. 2021). Therefore, the recovery of Li from the ethers proceeds in several steps. Na and K can be dissolved from the ethers at a pH of 7–8, since Li is released only at a lower pH. Ca and Mg remain in the organic phase (Itoh et al. 1991).

Ionic liquids are salts with melting temperatures below 100 °C that consist of organic cations and organic or inorganic anions (Park et al. 2014; Shi et al. 2017). For targeted raw material extraction, they can serve directly as extractants or be used in combination with other organic solvents as co-extractants (Liu et al. 2019; Shi et al. 2017; Stringfellow and Dobson 2021a; Swain 2017). This approach also requires the ionic liquids to first be separated from the lithium-bearing fluid and subsequently treated with acid for lithium extraction (Shi et al. 2017).

During the application of liquid-liquid extraction, up to 90% of the lithium contained was extracted from aqueous solutions in the laboratory (Liu et al. 2019; Yu et al. 2019). In extraction using TBP, an extraction efficiency of 90% was achieved after five extraction passes. For single contact, the rate was approximately 40% (Yu et al. 2019). For the most part, the solvents discussed can be regenerated and reused after lithium extraction. This requires large amounts of acid to mobilize the lithium, as well as mostly caustic soda for regeneration (Liu et al. 2019; Shi et al. 2017; Yu et al. 2019). Accordingly, material consumption must be included in the economic analysis, and the residual acids and caustic solutions need to be considered in terms of their ecological footprint. In addition, small amounts of solvent are lost during contact with the carrier fluid as well as during subsequent reprocessing (Liu et al. 2019; Shi et al. 2017).

In addition, the corrosiveness of acids and bases puts high demands on the material of reaction vessels and piping in an extraction plant. Another challenge is the volumetric flow rates for liquid-liquid extraction. Depending on the solvent, geothermal fluid-to-solvent ratios vary from 1:1 to 1:2.5 (Flexer et al. 2018; Garrett 2004; Shi et al. 2017; Yu et al. 2019; Zhang et al. 2021). This requires a correspondingly high solvent input for the high flow rates in geothermal power plants, but the solvents require sufficient contact time with the source fluid of at least 10 to 30 min (Shi et al. 2017; Yu et al. 2019). A continuous flow system with flow rates of 80 L/s would require a reaction volume of 48–144 m³ to achieve appropriate retention times for the geothermal fluid. For extraction, the volume of the solvent must also be provided. Assuming a 1:1 ratio of solvent to geothermal fluid, between 96 m³ and 288 m³ would be required for retention times of 10 to 30 min.. Separation of the phases again requires a reaction time of the same order of magnitude but can be shortened by the use of centrifuges (Liu et al. 2019; Shi et al. 2018; Swain 2017). The dissolved ions in the redissolution water can also pose a challenge as they can negatively affect Li recovery and redissolution (Yu et al. 2019).

Generally, liquid-liquid technologies offer high potential and have achieved very good extraction efficiencies in the laboratory. The series of experiments most closely corresponding to the reality of a geothermal power plant was conducted in the laboratory at room temperature with a geothermal fluid. The fluid was concentrated to about 350 g/L total salinity before the experiments and contained 700 mg/L Li (Yu et al. 2019). As a result, the basic function was experimentally demonstrated and tested in a laboratory setting corresponding to a TRL of 3–4 (Mankins 2009; Mankins 1995; De Rose et al. 2017). However, for technical application at the scale of a geothermal power plant, different parameters such as reaction time, required flow rate, and chemical use should be optimized to enable economic application. Solutions also need to be developed for the maintenance of pressure and temperature required in a geothermal cycle.

4.4.2 Selective Extraction by Sorption

Different approaches and materials are being explored for the use of inorganic sorbents for selective ion separation, such as titanium oxides, manganese oxides, aluminum hydroxides, or zeolites. The current focus of research projects is to optimize the performance of sorbents concerning their loading capacity and reusability (Liu et al. 2019; Stringfellow and Dobson 2021a). The basic principle is based on ion exchange and physical adsorption and absorption. In the processes, the dissolved raw material is bound to a solid that is added to or passed through the fluid. After contact between the sorbent and the raw material to be recovered, the latter must be redissolved from the loaded sorbent. Depending on the application, the solid is first filtered off for this purpose, or the flow cell in which it is located is treated directly.

Titanium oxide-based sorbents are very similar to manganese oxide sorbents regarding their reaction mechanisms, but show higher stability over multiple loading and unloading cycles and are less selective (Liu et al. 2019; Stringfellow and Dobson 2021b). For an optimal pH range of 8–13, their loading capacities are in the range of 20–30 mg/g (Liu et al. 2019).

Lithium extraction with aluminum hydroxides is based on the incorporation of lithium into octahedral gaps of layered aluminum hydroxide minerals (e.g. gibbsite) with the formation of lithium aluminum double hydroxide chloride (LADH-CL) (Isupov et al. 1999; Paranthaman et al. 2017; Stringfellow and Dobson 2021a; Wu et al. 2019). At the same time, chloride is bound between each layer, which facilitates lithium chloride production during redissolution (Jiang et al. 2020; Wu et al. 2019). Compared to the above sorbents, the loading is much lower, reaching less than 8 mg/g (Isupov et al. 1999; Jiang et al. 2020; Stringfellow and Dobson 2021a). No acid is required for desorption, which minimizes the loss of sorbent. However, this requires large amounts of water at a water:sorbent ratio of 100:1 (Isupov et al. 1999). In a sensitivity analysis (Jiang et al. 2020), an optimal pH of 7 was determined, as well as a loading time of 60 min for 50% loading and 600 min for reaching equilibrium. Considering these parameters, up to 90% of lithium could be recovered from brines in the laboratory (Isupov et al. 1999; Wu et al. 2019).

Another method is the extraction of lithium using natural and artificially synthesized zeolites. These achieve loading capacities of 5 mg/L via incorporation by ion exchange and are still in the early stages of development for use in thermal fluids (Stringfellow and Dobson 2021a; Wisniewska et al. 2018).

Direct lithium extraction using sorbents is among the best-investigated methods. Of those sorbents, manganese and titanium sorbents achieve the highest loading capacities (Liu et al. 2019; Stringfellow and Dobson 2021a). Nevertheless, the material input at loadings of max. 40 mg/g sorbent is not insignificant if fluids with lithium concentrations of up to 200 mg/L are to be treated at flow rates of 80 L/s. To achieve the sometimes long reaction times of 24–120 h (Liu et al. 2019; Ryu et al. 2019; Zandevakili et al. 2014) for full loading, very large reaction vessels are required for continuous volume flow. Even if the extraction is not part of the geothermal energy production unit, it must be possible to integrate appropriate reaction vessels, retention times, etc. into the thermal water loop. Another specific challenge for this type of sorbent is that they are degraded during desorption, which further increases material consumption. The consequences of introducing manganese or titanium into the geothermal reservoir must also be considered. In this context, dissolution rates vary between 1–7% during the first use of a freshly synthesized sorbent and are about 1% per cycle thereafter (Ryu et al. 2016; Zandevakili et al. 2014). For the optimal extraction range with high pH values, bases are necessary to buffer the system. These buffers further increase the material input. In basic pH ranges, there is also the risk of carbonate and CSH scales that could reduce the effectiveness of the sorbent. In addition, the incorporation of competing ions, such as Na, into the crystal lattice may also occur (Zandevakili et al. 2014). Material consumption also increases due to the acid required to redissolve the lithium.

LADH-CL require bases (or more rarely acids) to buffer the system if the optimum pH range of 7 is to be achieved. Disadvantages are the low loading of maximum 8 mg/g and the high water requirement. According to Jiang et al. (2020), to achieve an extraction rate of 50%, a reaction time of approximately 60 minutes is required. The reaction volume must be able to

hold the flow rate of at least 60 min, which would correspond to 288 m³ at 80 L/s. Thus, for fluids with a concentration of 200 mg/L lithium, 57,600 g of lithium would circulate. To extract 50% of this within one hour, a total capacity of 8 mg/g would require about 7.2 t of aluminum hydroxide sorbent and 100 times this amount, i.e. 720 t of water, for redissolution. Even though this water can be used in the next cycle after treatment, the volume is still a key parameter for the dimensions of the plant. The high volume of water also results in a low lithium content in the extracted solution, which requires concentration and water recovery before further processing.

In summary, the different sorbents and their functions are very well investigated in the laboratory setting and achieve efficient results. Experiments with geothermal fluids have demonstrated the high potential of the sorbents. The technological readiness level of manganese and titanium sorbents is assumed to be between 3 and 4 based on the available literature, as individual components and the basic function have already been tested in experiments. According to reports of successful field tests (Rettenmaier et al. 2021; Stringfellow and Dobson 2021a), the technology readiness level of aluminum hydroxides is estimated to be higher. For the usage of titanium or manganese sorbents with real fluids in a geothermal power plant, stability needs to be improved. In the case of aluminum hydroxide, the loading capacity is the focus of development. In general, for sorbents, the kinetics where lithium uptake occurs will need to be improved. Since retention times significantly affect the size of the reaction vessels required, given the high flow rates in geothermal power plants, rapid partial loading of the sorbents is preferable to high-rate (or even complete) but significantly slower loading. Furthermore, long retention times introduce new problems of temperature maintenance and kinetic reactions.

4.4.3 Electrochemical Methods

The basic principle of the electrochemical extraction of lithium is based on the selective attraction of positively charged lithium cations to a working electrode under the application of a voltage. Anions and interfering elements are bound to a counter electrode (Battistel et al. 2020b; Calvo 2019; Liu et al. 2019). Similarly to sorbents, manganese and titanium oxides can be used as working electrodes (Battistel et al. 2020b; Calvo 2019; Liu et al. 2019; Stringfellow and Dobson 2021a). The major advantage of the electrochemical approach is the rapid binding of lithium and redissolution without the use of chemicals (Battistel et al. 2020b). The electrochemical methods show good selectivity even at low initial lithium levels starting at 7 mg/L, but are limited to a maximum concentration of about 350 mg/L lithium (Battistel et al. 2020b; Palagonia et al. 2017). The most commonly discussed methods are the electrochemical ion pump and electrodialysis methods. Both techniques use a working electrode that can bind lithium. The maximum loading coefficients are 30–40 mg/g (Battistel et al. 2020b; Calvo 2019; Liu et al. 2019; Stringfellow and Dobson 2021a).

In the case of ion pumps, Li is bound by applying a voltage to the working electrode and chloride is bound to the counter electrode, which is made of nickel or silver, for example (Figure 16; (Battistel et al. 2020b; Liu et al. 2019; Romero et al. 2021). In the next step, the fluid is flushed from the chamber and replaced with a recovery solution (seawater or brine). In a third step, the bound lithium is released by voltage reversal (Battistel et al. 2020b; Liu et al. 2019).

Electrodialysis combines electrochemical and membrane-based methods (Figure 16) and additionally uses ion-selective membranes (Li et al. 2019a; Liu et al. 2019; Mroczek et al. 2015; Stringfellow and Dobson 2021a). These membranes selectively separate lithium cations and chloride anions when a voltage is applied, thus allowing for enrichment (Mroczek et al. 2015). In a second step, a voltage reversal can be used to deliver the recovered raw material back to a carrier solution (Battistel et al. 2020b; Li et al. 2019a; Liu et al. 2019). The technology has been tested for low-salinity geothermal fluids in the laboratory (Mroczek et al. 2015). For higher-salinity fluids, multiple bipolar membranes have been connected in sequence in laboratory tests, allowing for the incremental removal of ions from the fluid phase (Calvo 2019; Li et al. 2019a).

Since electrochemical extraction methods are based on the same mechanisms as in lithium-ion batteries, the processes are well understood (Liu et al. 2019). Loading times are generally lower (< 20 min) than for inorganic sorbentia (Battistel et al. 2020b). No chemicals are needed for redissolution or regeneration as applying a corresponding voltage is sufficient. Depending on the method, the required energy varies from 1 to 60 Wh/mol, without considering pump energy (Battistel et al. 2020b; Liu et al. 2019). In a geothermal power plant with a flow rate of 80 L/s and 200 mg/L lithium, 8300 moles of lithium (about 0.31 t/h LCE) circulate in one hour. For a complete extraction, this would require 8.3–498 kWh of energy. At the defined geothermal power plant standard case with a flow rate of 80 l/s, the electrical power is about 4 MW, which means that the extraction would require 0.2–12.4% of the electrical energy produced, without taking into account the required pump energy.

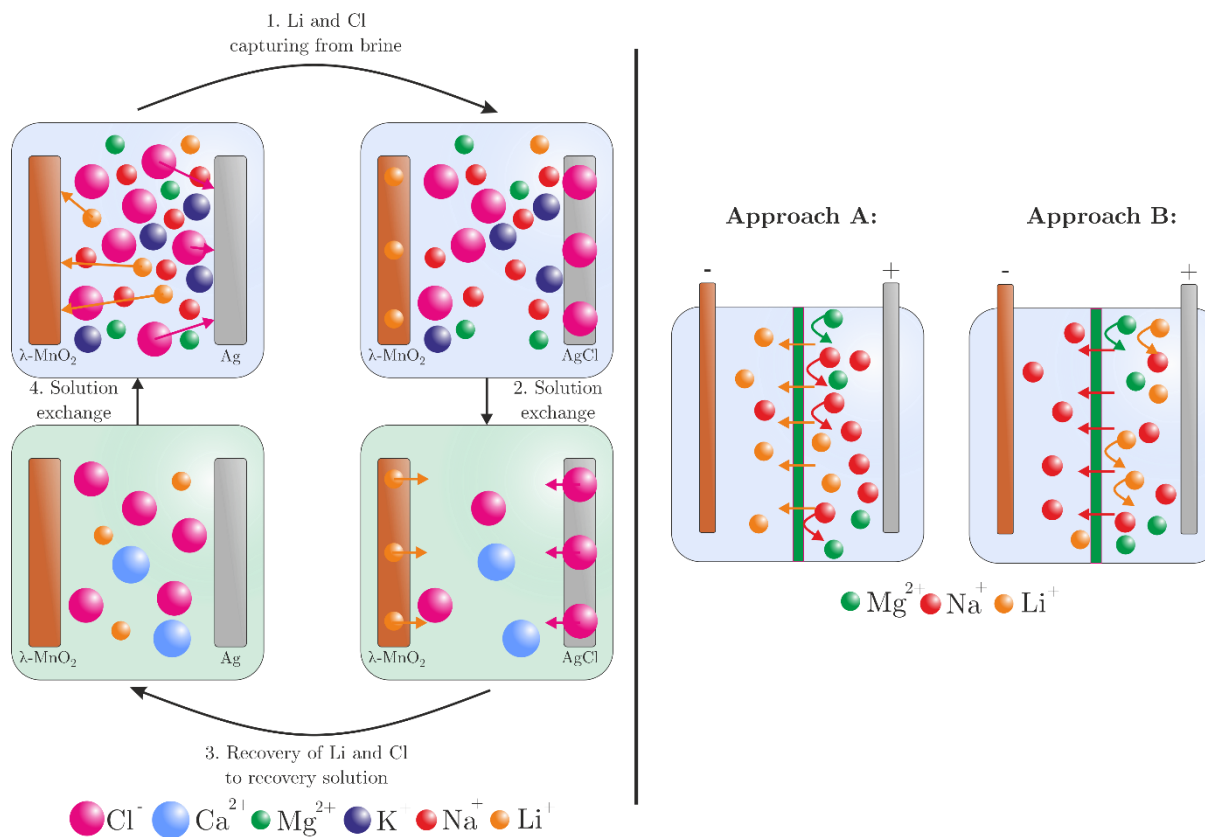


Figure 16: Schematic representation of an electrochemical ion pump using manganese oxide as a working electrode for lithium. Adapted from Battistel et al. (2020). Right: Schematic representation of two different approaches for lithium enrichment using electrodialysis. Approach A is based on a

membrane that is permeable for lithium but largely blocks other ions. Approach B uses a lithium-blocking membrane. Adapted from Liu, Zhao, and Ghahreman (2019)

In a comparison of electrochemical methods, the ion pump is assumed to be more effective (Battistel et al. 2020b). Electrodialysis has been successfully tested on a small scale with geothermal fluids (Kano et al. 1993; Mroczek et al. 2015), but the durability of the selective membranes poses a challenge for scaling up to a plant scale (Li et al. 2019a). One issue is the maximum loading capacity of the working electrodes of 30–40 mg/g. Therefore, for effective deployment in a geothermal power plant, the technical design of the reaction cell is of utmost significance (Battistel et al. 2020b; Calvo 2019; Zhao et al. 2019). The corrosive nature of thermal fluids is a threat to the integrity of the electrodes and can affect performance (Calvo 2019). In addition, electrochemical water treatment processes have been found to cause pH fluctuations that can trigger uncontrolled mineral precipitation (Arulrajan et al. 2021; Dykstra et al. 2017; Mroczek et al. 2015; Obata et al. 2020). In particular, the accumulation of divalent cations such as Ca^{2+} , Mg^{2+} , Fe^{2+} , and the formation of carbonate precipitates can affect performance and longevity (Arulrajan et al. 2021). When membranes are used in electrodialysis, there is an additional risk that they will become clogged by precipitates (Li et al. 2019a; Zhang et al. 2018).

Despite many unresolved issues, electrochemical methods are considered to have high potential for commercial use at a plant scale, mainly due to short loading time and the low need for chemicals (Battistel et al. 2020b; Calvo 2019; Liu et al. 2019). Based on initial successful laboratory tests, the technology readiness level is estimated to be between 3 and 4.

4.4.4 Membrane Technologies

Like electrodialysis, pure membrane technologies are based on the use of lithium-selective membranes. Selective separation can be achieved by ion size, surface charge, or chemical and physical properties (Stringfellow and Dobson 2021a). There is a wide variation in membrane technologies, where the membrane itself can cause separation or be the carrier for solvent or sorbents (Li et al. 2019a).

Nanofiltration, one example of membrane technology, enables selective separation of multivalent from monovalent ions (Li et al. 2019a; Li et al. 2019b; Sun et al. 2015). Nanofiltration treatment is particularly useful for magnesium-rich fluids, as Mg competes with Li in many methods due to similar ionic radii (Schmidt 2017; Sun et al. 2021). Separation occurs in a pressure-driven process via pore size as well as membrane charge (Li et al. 2019a; Li et al. 2019b; Sun et al. 2015). Nanofiltration systems are already available on an industrial scale and are also used for water treatment. The technique has been tested for lithium extraction from complex fluids (Li et al. 2019a; Li et al. 2019b; Sun et al. 2015). In the context of lithium removal, nanofiltration is always used in combination with a pre- or post-treatment to separate the interfering ions since other monovalent cations such as Na or K also pass through the membrane (Li et al. 2019b; Somrani et al. 2013; Sun et al. 2015).

Another approach is to combine membrane distillation and crystallizers. Membrane distillation is a temperature-driven process that facilitates contactless concentration to the crystallization limit via a water-repellent membrane (Li et al. 2019a; Quist-Jensen et al. 2016b; Quist-Jensen

et al. 2016a). The temperature-driven process enables net energy-neutral treatment of water for geothermal systems. In this process, a warm input solution is conveyed past a hydrophobic membrane with a cold permeate stream on the other side, creating a vapor pressure gradient along the membrane. The water can pass through the membrane as vapor and condenses in the permeate stream. The removal of water molecules in the form of the separated vapor results in the relative enrichment of solids in the input fluid stream (Quist-Jensen et al. 2016a; Winter et al. 2017). The permeate water stream could even be used to recover fresh water as a co-product (Liu et al. 2019; Macedonio 2015). Similarly to nanofiltration, membrane distillation only allows for the enrichment of mineral phases up to the saturation limit. Large-scale plants for water treatment using membrane distillation have already been tested in continuous operation with seawater (34 g/L salinity) (Winter et al. 2017) and at a prototype scale at the Insheim geothermal power plant in the URG (Goldberg et al. 2021). The economic viability of water extraction by membrane distillation has been demonstrated for high-salinity fluids (about 100 g/L) from shale gas extraction (Tavakkoli et al. 2017). A separate process or crystallizer must be used for actual Li extraction (Li et al. 2019a; Quist-Jensen et al. 2016b; Quist-Jensen et al. 2016a).

In the supported liquid membrane method, membranes are loaded with solvents used for liquid-liquid extraction (Li et al. 2019a; Sharma et al. 2016). These membranes can then be permeated like other membrane systems (Ma et al. 2000). This preparation combines the advantages of liquid-liquid treatment with significantly reduced solvent and space requirements. Under laboratory conditions, this approach was tested for lithium extraction with low-salinity solutions and achieved extraction rates of over 90% in recirculating processes within 120 min at pH values of 9.5 and 12.5, respectively (Ma et al. 2000; Sharma et al. 2016).

Membranes can also be equipped with ion sieves, which facilitates application at plant scale (Li et al. 2019a). This combines the large surface area and selectivity of the sorbents with the advantages of the membrane, which keeps the sorbent stationary and ensures low energy consumption (Li et al. 2019a). Membranes loaded with the sorbents were able to achieve loadings of 30 mg/g. Most of the loading in this approach occurs within the first 60 min of contact time, showing comparatively fast kinetics (Li et al. 2019a; Sun et al. 2016).

Membrane processes can be used for various applications in the recovery of raw materials from thermal fluids. Nanofiltration and membrane distillation are effective methods for concentrating dissolved components in the fluids and can be very well integrated into a geothermal cycle via their pressure- or temperature-driven process. Concentration can also bring low-salinity fluids to lithium concentrations that enable the extraction of raw material. Membrane technologies for direct lithium separation, combining the sorbent or solvent with membranes, are still at a developmental stage. Selective extraction has been successfully performed in laboratory testing, but has not yet expanded to a plant scale (Li et al. 2019a; Li et al. 2019b; Ma et al. 2000; Sharma et al. 2016; Sun et al. 2016). The technology readiness level ranges from 3 to 4. The combinations have improved the performance of each extraction method in some areas, but challenges such as lithium redissolution with acids or sorbents or solvent degradation remain. In addition, there are new membrane-specific challenges such as clogging of the membranes by mineral precipitates in the pores. One exception is membrane

distillation, which shows a lower propensity for clogging. Other challenges include the complexity of membrane production and the high costs associated with it (Li et al. 2019a).

4.5 Current Extraction Projects

Research is being conducted worldwide on techniques for direct lithium extraction from salar brines or thermal fluids with high lithium concentrations (Table 4). Examples include work by Livent in Catamarca (Argentina) and by several companies in Qinghai (China) (Grant 2020). Pilot work by Livent (formerly FMC) dates back to the 1990s (Grant 2020). Commercial production with direct lithium extraction using sorption technology (sorbents not specified) has existed since the 2000s in Catamarca (Argentina) (Grant 2020). The first attempts to apply this technology to thermal waters were conducted in the Salton Sea region (Imperial Valley, USA). Following initial laboratory studies of lithium extraction by precipitation of lithium aluminate complexes (Bertold and Baker 1976) and lithium carbonate (Palmer et al. 1975), thermal waters there were taken into consideration as an important resource for lithium (Bertold and Baker 1976). However, what was actually implemented was the extraction of other elements such as K and Ca, Mn and Fe (1965-1990, various companies) or Zn (CalEnergy, 2000) (Stringfellow and Dobson 2021a). SimbolMaterials completed the setup for commercial lithium production from geothermal fluids in the 2010s (Stringfellow and Dobson 2021a). However, due to the volatility of the market, companies there were under severe financial pressure, and most projects had to be abandoned prematurely. Increasing demand and rising market prices for lithium (Schmidt 2017) have brought in new players who say they expect to start production in the Salton Sea geothermal field beyond the pilot stage as early as 2024 (Energy Source Minerals 2022). Several projects dealing with direct lithium extraction from thermal fluids are also underway in Europe (Table 6).

Table 6: Current research projects on and commercial approaches regarding direct lithium extraction from geothermal fluids. Information about the (industrial) projects is not taken from scientifically peer-reviewed publications due to lack of availability but sourced from company communications that cannot be independently verified and evaluated

Project	Partner Company	or	Funding	Extraction Method	Details	References	
In Europe							
URG	Unlimited	EnBW, Universität Göttingen, Bestec, Hydrosion	KIT, BMWK, million	€2.7	Selective sorbents, mainly manganese oxides	Prototype tests According to the project consortium, up to 20,000 car batteries could be produced per year from the lithium theoretically extracted at the Bruchsal geothermal power plant (URG)	(Unlimited 2022)
URG	EuGeLi	Eramet Ideas, BASF, BRGM, Chimie Paris Tech, Eifer, Electricité de Strasbourg, VITO, Universitet Brussel	EIT Materials	Raw	Unspecified sorbents	In a pilot project at the Rittershoffen geothermal power plant (URG), sorbent application was adapted to the temperature and fluid chemistry of the URG. Lithium could be extracted at operating pressure and temperature. Recovery through low-salinity eluate	(Eramet 2022a; Eramet 2022b; Rettenmaier et al. 2021)
Germany	Li+fluids	BGR, Fraunhofer IEG, Fraunhofer UMSICHT	BMWK			Evaluation of the potential of lithium extraction in Germany and assessment of the extraction methods known so far. Lithium release rates from the deep rock will be determined together with a utility analysis of co-production in geothermal operation	(Stechern 2021)
URG	Vulcan Energy Resources	Australian-German company	Commercial		Aluminum hydroxide with pretreatment to remove competing ions	A demonstrator is to start direct lithium extraction at the Landau or Insheim (URG) sites. Objective: Pure lithium chloride concentrate. Commercial lithium production is planned for 2024. Vulcan Energy Resources holds several exploration licenses in the URG and has signed several offtake agreements for the lithium to be produced with Umicore, LG, Renault Group, Stellantis, and Volkswagen. Committed to deliver 179,000–225,000 t of LiOH (276,000–347,000 t of Li ₂ CO ₃) between 2025 and 2031	(Vulcan Energy Resources 2021a; Vulcan Energy Resources 2021b; Vulcan Energy Resources 2021c; Vulcan Energy Resources 2021d; Vulcan Energy Resources 2021e; Vulcan Energy Resources 2021f; Wedin 2022; Wedin and Harrison 2021)
France	Geolith (Sustainable)	French company; partners: Mines Paris Tech, ADEME	Commercial		Sorbents fixed to microfibers	Geolith promises economic production from a lithium concentration of 50 mg/L. A mobile test plant has been available since 2021	(Geolith 2022)

France	Lithium Solutions) Adionics		French company	Commercial	“Thermal Swing Salt Absorption” (variant of liquid-liquid extraction)	“Thermal Swing Salt Absorption” technique developed and patented. The aim is the direct extraction of LiCl from salars and geothermal fluids	(Adionics 2022)
Salton (USA)	Sea						
	Energy Minerals	Source	US-American company	Commercial	Sorbents	Current projects at John L. Featherstone geothermal power plant, projected capacity of 20,000 t LiOH (31,000 t LCE) per year.	(Energy Source Minerals 2022)
	Controlled Thermal Resources		US-American company	Commercial	Sorbents, ion exchange	Current projects at Hell’s Kitchen geothermal power plant, projected capacity of 20,000 t LiOH (31,000 t LCE) per year.	(Controlled Thermal Ressources 2022)
	Berkshire Hathaway Renewables		US-American company	Commercial, \$6 million California Energy Commission, \$14.9 million DOE	Ion exchange	The plan is to build a demonstrator for LiOH extraction by spring 2022 and start commercial production by 2024.	(Lithium Valley 2021)

Table 7: Different technologies for direct lithium extraction from thermal fluids. The table gives an overview of the advantages and disadvantages of the technologies, operating parameters during the extraction process, and an estimation of the technology readiness level (TRL) based on the literature review.

Method	Technologies	Advantages	Disadvantages	Extraction Parameters	TRL
Liquid-liquid extraction	Tributyl phosphates as solvent	Short loading time Extraction agent recyclable	High consumption of chemicals for redissolution and regeneration	Extraction efficiency: 40–90%	3–4
	Crown ether as solvent Ionic liquids as solvent or for co-extraction		Large space requirement for the required fluid flows High costs (for crown ethers) Possible corrosion due to acids and bases used for redissolution, regeneration, and buffering	Loading time: 10–50 min Solvent-brine ratio: 1:1–1:2.5	
Inorganic sorbents	Manganese and titanium sorbents (ion screens)	High loading capacities	Sorbents are degraded by use and regeneration (approx. 1% per cycle) pH change can lead to scaling Long loading time Corrosion may occur due to acids and bases used for redissolution, regeneration, and buffering	Extraction efficiency: 40–95% Loading capacity: 20–60 mg/g Ideal pH value during extraction: 10–13 Loading time: 60 min–120 h	3–4
	Aluminum hydroxide	Low chemical consumption Good recyclability	Low loading capacity Large stationary volume of water required for redissolution	Extraction efficiency: 50–90% Loading capacity: < 8 mg/g Ideal pH value during extraction: 7 Loading time: 60 min–10 h Water requirement for stripping: ~100 times the amount of sorbents	

Electrochemical methods	Ion pump Electrodialysis	Short loading time	Additional energy demand	Loading capacity of the working electrode: 30–40 mg/g pH value fluctuations due to method used: ± 2 Loading time: < 20 min Additional power demand: 1–60 Wh/mol lithium	3–4
		No chemical consumption	pH effects of the process can lead to scaling		
		Processes related to those in a battery	Can only be used up to a lithium content of 350 mg/L		
		Works efficiently even at low lithium levels			
Membrane technologies	Nanofiltration/membrane distillation	Energy-efficient	Integrity of the membranes is compromised by scaling	-	3–4
		Can be well integrated into geothermal cycles	Without additional processes, lithium is only relatively enriched and not selectively extracted		
		Known for water treatment and used industrially			
		Additional possibility of water extraction			
	Supported Membrane	Liquid -	Very high pH values required for optimum conditions pH value change can lead to scaling Possible corrosion due to the use of acids and bases for redissolution, regeneration, and buffering	Extraction rate: 90% Loading time: 120 min pH value: 9.5–12.5	3–4
	Combination with ion screens	High loading capacities Faster kinetics than sorbents alone	Sorbent is degraded by lithium recovery pH value change can lead to scaling Long loading time	Loading capacity: 30 mg/g Loading time: < 60 min.	

Possible corrosion due to acids and bases used for redissolution, regeneration, and buffering

Other parameters analogous to manganese & titanium sorbentia:

Extraction efficiency: 40–95%

Ideal pH value for extraction: 10–13

4.6 Discussion and Conclusion

From a technical standpoint, direct extraction of lithium from thermal fluids is not trivial, yet it has been successfully achieved in the laboratory on multiple occasions. The next hurdle is to implement the technologies in field demonstration units and test them in the operational environment. A comparison of the technologies (Table 7) shows that all methods have hurdles to overcome when integrated into a power plant process, but also present individual advantages. The main challenges for achieving technological readiness can be summarized in four main points:

- **Retention time/space requirements:** Retention time is a decisive parameter for integration into a power plant process, as it has a significant influence on the size of the reaction infrastructure. Electrochemical methods and liquid-liquid extraction stand out favorably, as high extraction efficiencies of 90% are achieved in short periods (< 60 min) with these methods. In contrast, the different sorbents can only achieve low extraction rates (e.g. 50%) at similar periods (\approx 60 min). Contact durations of several hours to days are required to fully load the sorbents. These periods can be shortened, such as by combination with membrane processes. Large space requirements may also arise from the quantity of extraction or redissolving substances needed. This quantity is significantly influenced by the specific loading capacity Q of the substances used:

$$Q = \frac{(c_0 - c_e) * V_{fluid}}{m_{sub}}$$

Q = loading capacity [mg/g]

c_0 = initial lithium concentration [mg/L]

c_e = lithium concentration after extraction [mg/L]

V_{fluid} = processed volume of thermal fluid [L]

m_{sub} = mass of extraction substance used [g]

- Liquid-liquid extraction solvents are required for effective extraction at a ratio of one to two and a half times the thermal fluid flow, which is a substantial space requirement and thus a disadvantage. For lithium aluminum double hydroxide chloride (LADH-CL), a large stationary water volume is required, amounting to several 100-1000 tons including processing equipment.
- In particular, the large reaction volumes are a challenge for power plants where the thermal water loop is kept under pressure to avoid scaling. Depending on the extraction method, an enormous pressure content product can arise due to the pressure level and volume flow. This can result in significant demands on the extraction infrastructure and technical implementation.
- **Material decomposition/requirements:** The decomposition of extraction substances and the chemicals needed during operation are important factors in the economic implementation of a method. Electrochemical methods and extraction using

aluminum hydroxide sorbents are the only methods that do not require additional chemicals for extraction in laboratory tests (Battistel et al. 2020a; Isupov et al. 1999). All other solvents and sorbents require acids and bases for lithium redissolution and regeneration and for setting an ideal pH range during extraction. In addition, partial dissolution of the extraction substances was also observed in the sorbents.

- **Scaling potential:** The scaling potential (risk of uncontrolled mineral precipitation) is significantly influenced by pH value, temperature, and the duration of interaction with the extraction materials. In the technologies described with long retention times (> 60 min), kinetic reactions can occur that would not be observed with a short retention time (Setiawan et al. 2019). The risk of precipitation may be increased by potential cooling during the contact time with the sorbent. Adjusting pH to improve extraction conditions alters fluid chemistry and can induce scaling. In electrochemical processes, the application of voltage can cause local pH changes of ± 2 that can induce scaling (Arulrajan et al. 2021; Dykstra et al. 2017; Mroczek et al. 2015; Obata et al. 2020). The sorbents as well as the supported-liquid membranes have an ideal pH range that is only reached by buffering. The best efficiencies have been experimentally demonstrated at pH 9-13 for manganese and titanium oxide (Liu et al. 2019) and pH 7 for LADH-CL. At high pH (>10), different mineral phases, such as CSH phases, supersaturate and can lead to precipitation (Goldberg et al. 2021; Greenberg and Chang 1965; Spitzmüller et al. 2021).
- **Energy consumption:** Energy consumption influences the economic viability of combined energy and raw material production. With an electricity-generating power plant, the amount of electricity that can be fed into the grid is reduced, but is available in a CO₂-neutral and reliable manner. In the case of a thermal-only power plant, the electricity would have to be additionally purchased. All methods involve additional energy consumption by pumps, stirring vessels, centrifuges, or control technologies. In the case of the electrochemical methods, additional energy is needed for extraction.

Comparison of the different technologies shows that selective extraction of lithium from geothermal fluids is technologically possible and has been validated in the laboratory. However, transfer to a prototype or plant scale is no trivial matter. Extraction efficiencies of 90% were achieved in idealized laboratory tests at room temperature, steady-state operation, and mostly only with long retention times. However, long retention times are very difficult to achieve in a geothermal power plant due to large volume flows. For implementation, lower extraction efficiencies in support of faster kinetics are therefore preferable, or else working on a partial stream, as otherwise a significantly higher material input and space requirement must be planned for. Achieving 50% efficiency requires a 60-minute retention time for various methods (Jiang et al. 2020; Yu et al. 2019), which presents a challenge with respect to flow rates of 80 L/s or higher. This is particularly true since the thermal fluids are immediately returned to the subsurface during energy production and thus normally have a short surface retention time (Brasser et al. 2014; Schilling et al. 2022).

Extraction is complicated by the corrosion and scaling potential of the fluids, which is a known issue from geothermal energy production. However, this can be controlled with a targeted treatment strategy (Eggeling et al. 2018; Nitschke et al. 2014; Scheiber et al. 2019b; Scheiber et al. 2019a). Corrosion and scaling issues increase as a result of fluid concentration processes,

cooling during the reaction time, or pH changes to improve extraction efficiency. How this affects lithium extraction at a production scale in detail, however, can only be evaluated in a long-term in-situ plant test (TRL 7–8). Spot prototype tests provide only limited information. Grant (2020), for example, highlights that a simple transfer of findings from one plant to other sites is not possible without limitations due to differences in the thermal fluid composition. The efficiency of extraction in ongoing operations thus remains speculative due to the lack of large-scale demonstration cases. The extraction efficiencies achieved in the laboratory were 50–90% under ideal conditions with very long retention times in some cases. Since the demands on material, technology, and volume capacity of the reactors are disproportionately higher in ongoing plant operations with real fluids and high flow rates, comparably high efficiencies cannot be expected. Therefore, with the current status of technology, extraction efficiencies during ongoing operation are more plausibly at the lower end of the range seen in laboratory experiments, rather than the frequently discussed, more optimistic scenarios.

4.7 Acknowledgments

The authors would like to thank the Helmholtz Association for research funding under the Geoenergy subtopic in the MTET (Materials and Technologies for the Energy Transition) program of the research field "Energy". The BMBF (Federal Ministry of Education and Research) Client II is thanked for funding within the BrineMine project (grant number 033R190B). Special thanks are also due to the chair of Geothermal Energy and Reservoir Technology, headed by Professor Dr. Thomas Kohl, and the chair of Geochemistry and Economic Geology, headed by Professor Dr. Jochen Kolb, at the Institute of Applied Geosciences at KIT for making this work possible and for the lively scientific exchange. Furthermore, this work grew through many technical discussions, for which we would like to especially thank Dr. Joachim Koschikowski, Dr. Daniel Winter, Gerrit Fuelling, and Klemens Slunitschek. We thank the anonymous reviewers and the editors for their constructive suggestions for improvement.

5 Potential Evaluation and Production Scenarios for Geothermal Lithium in Germany

The following chapter is a translation of the German journal article “*Herausforderungen und Chancen für die Lithiumgewinnung aus geothermalen Systemen in Deutschland Teil 2: Potenziale und Produktionsszenarien in Deutschland*” (<https://doi.org/10.1007/s00767-022-00523-4>). It was originally published under an Open Access license in the peer-reviewed journal *Grundwasser*. 27, 261–275 (Goldberg et al. 2022b). The translation was conducted by the original authors of the initial study.

Valentin Goldberg^a, Fabian Nitschke^a, Tobias Kluge^b

^a Institute of Applied Geosciences, Chair for Geothermal Energy and Reservoir Technology, Karlsruhe Institute of Technology, Adenauerring 20b, 76131 Karlsruhe,

^b Institute of Applied Geosciences, Chair for Geochemistry & Economic Geology, Karlsruhe Institute of Technology, Adenauerring 20b, 76131, Karlsruhe

5.1 Abstract

This study provides background information to estimate the potential of future lithium production from geothermal fluids in Germany. Growing demand and the dependence on poorly diversified overseas sources points towards a high strategic importance of domestic resources. Furthermore, potentially lower CO₂ emissions and reduced areal use during lithium production are additional aspects that need to be considered.

Based on the technology comparison for direct lithium extraction from geothermal fluids and the current state of geothermal energy production in Germany and the French part of the Upper Rhine Graben, different scenarios for the extractable amount of lithium carbonate were calculated. In the most optimistic scenario, taking into account all currently active wells, a maximum production of 7200 t/a of lithium carbonate equivalent is expected. This could cover 5 - 19 % of the annual demand of the planned German battery cell production.

Key parameters for the process design are the usable volume fraction of the geothermal fluid and the extraction efficiency. The uncertainties in the resource assessment regarding its size and sustainability of its management are still considerable. To exploit the great potential of this technology, these key issues need to be addressed.

5.2 Introduction

The most important field of application for lithium today is the production of lithium-ion batteries (Liu et al. 2019; Schmidt 2017). The market with the largest growth potential is the use of lithium in electric vehicles, which can be competitive with combustion engine vehicles due to the low discharge rates of lithium-ion batteries, their long life, and their comparably short charging times. To achieve a sufficiently long range, a large storage capacity in the region of 60–100 kWh is needed, resulting in battery sizes of 600–800 kg and volumes of 0.4–0.6 m³ (Lee et al. 2011; Srinivasan et al. 2008; Xu et al. 2020). The amount of pure lithium required for such a storage capacity amounts to 10–14 kg (Xu et al. 2020).

Due to the development of electromobility, a great increase in lithium demand can be expected. (Adams 2020; Jones et al. 2021; Martin et al. 2017; Meng et al. 2021; Schmidt 2017). Alternatives to conventional mining or extraction from the brines of salars in South America are being evaluated around the globe to find new ways to meet this demand. One important focus has been placed on environmentally friendlier alternatives to make the automotive industry more sustainable in at least one part of its value chain. A much-discussed approach is lithium extraction from geothermal fluids. The successful realization of domestic lithium production from geothermal fluids could make Germany less dependent on global markets for raw materials, offer an opportunity to buffer global price fluctuations with regional supply chains, and cushion against global supply shortages. Additionally, the combined material and energetic utilization of a geothermal reservoir could lead to a symbiosis with positive economic effects for the geothermal sector, all while rendering the extraction of raw materials more sustainable. The combination of renewable energy with raw materials production requiring only small amounts of land and having a minimal environmental impact represents a great opportunity for a modern and future-oriented use of resources in Europe and Germany.

There are several technical approaches worth considering for extracting lithium from geothermal waters, which were compared in the first part of this study (Goldberg et al. 2022a). Lithium extraction from brines is possible and has been demonstrated in the laboratory and with small-scale prototype systems (Battistel et al. 2020b; Liu et al. 2019; Ma et al. 2000; Mroczek et al. 2015; Sharma et al. 2016; Wu et al. 2019; Yu et al. 2019; Zandevakili et al. 2014). However, the integration of this extraction into the process of a geothermal power plant results in several challenges that need to be examined in long-term testing procedures. In particular, the chemistry of the geothermal fluids and the high flow rates, elevated temperatures, and pressures in geothermal cycles result in specific requirements for extraction agents and system components. Furthermore, extraction efficiencies determined in the laboratory need to be continuously tested and adjusted during system operation. It is uncertain whether the same efficiencies can be reached on an industrial scale as under laboratory conditions. In view of the current state of the art, no exact prediction can be made about the costs of extraction, which will depend to a great extent on the exact technology used. Nevertheless, geothermal reservoirs can potentially contribute to cushioning rising lithium prices and ensuring a domestic supply of raw materials. The contribution of lithium production from brines to the regional market at the current state of technology will be further explored in this study.

5.2.1 The Market and Projections

The development of annual global lithium production (*Figure 17*), measured in lithium carbonate equivalent (LCE), indicates a strong upward trend in the last twenty-five years from approx. 40,000 t in 1995 to 420,000 t in 2020. By the end of 2021, a production of 520,000 t is expected. Although 2008 showed a clear decline in production due to the global economic crisis, in 2010 the market had already recovered and reached record highs (German Lithium Participation 2021; Hohmann 2021; Trading Economics 2022). The political decision to transition towards electromobility, as seen in major markets such as Europe and China, has resulted in a stronger increase in growth since 2015 than in prior decades. In recent years, electromobility has expanded to such an extent that even the optimistic projections of the 2017 Electric Vehicle Scenario as well as those made in 2019 were significantly exceeded in 2021 (Martin et al. 2017; Meng et al. 2021). If growth remains unchanged, a doubling of lithium demand is predicted by 2025, reaching 1,000,000 t LCE (Adams 2020; DERA 2021a; Jones et al. 2021). A comparison of predicted demand with the maximum global lithium production capacity of 640,000 t LCE in an optimistic scenario (Schmidt 2017) indicates a risk of a global lithium deficit of 360,000 t LCE in 2025. For 2030, a deficit of up to 1,000,000 t LCE is predicted (Schmidt 2021).

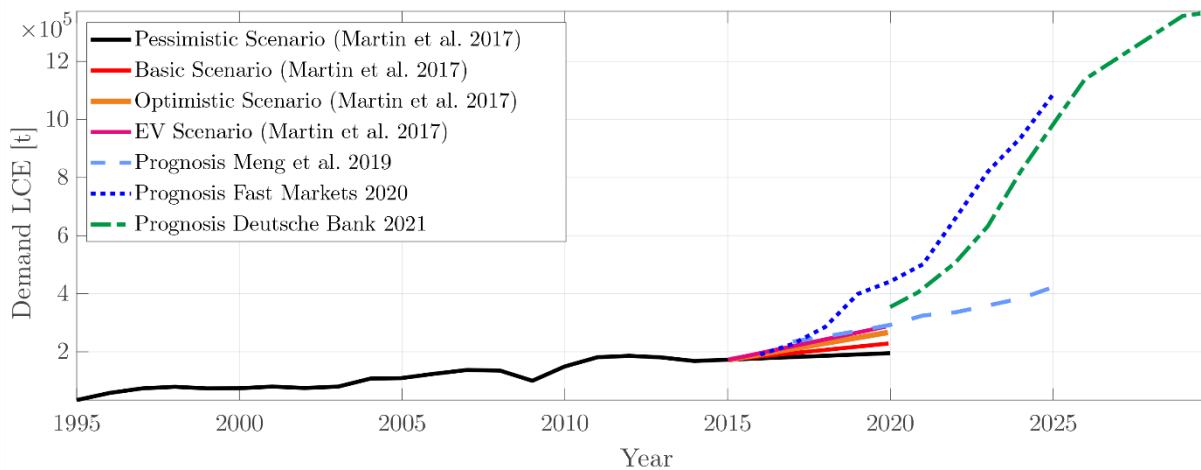


Figure 17: Global annual lithium production as lithium carbonate equivalents (LCE) since 2015 and predictions of different scenarios until 2030 (Data origin: (Martin et al. 2017; Meng et al. 2021; Adams 2020; Jones et al. 2021)). In 2020, 420,000 t of LCE were produced, significantly exceeding earlier projections from 2017

Global lithium production is mainly concentrated in only three countries and four companies (Figure 18). The largest lithium producer by far is Australia, where lithium is mined in the form of the mineral spodumene and mostly exported to China (DERA 2021a; Schmidt 2021; Schmidt 2017). Chile and Argentina are the second- and third-largest producers, respectively (DERA 2021a). Lithium is obtained there via evaporation and precipitation from the brines of salars. This small number of lithium-producing countries is seen as problematic for European imports, especially since there is virtually no European lithium production. While there is only a medium risk associated with the number of countries and the weighted risk due to the safety and stability of the producing countries (DERA 2021b), it should be noted that geological availability is not synonymous with free availability for global industries. Of the concentrates

extracted from material mined in Australia, for instance, 95% will go to China due to long-term supply contracts and is therefore unavailable to Europe or Germany as a raw material (DERA 2021a; Schmidt 2021).

The planned expansion of battery cell production beginning in 2022 at nine production sites in Germany is projected to produce a total capacity of 55 GWh in the medium term and reach up to 215 GWh at its completion. This increase in battery production would result in an additional lithium demand of 7,000–28,000 t annually (equaling 37,000–149,000 t LCE/a) (DERA 2021a). To meet this demand, Germany would need 3–15% of the predicted global demand in LCE in 2025 without an existing domestic production at its disposal.

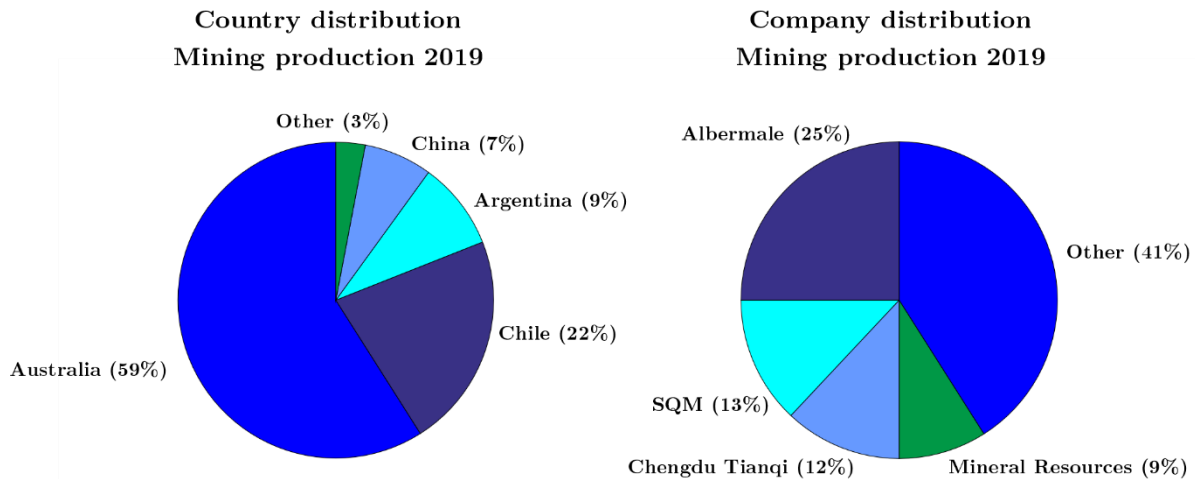


Figure 18: Country and company concentrations of lithium mining production in 2019 (Data origin: DERA 2021a)

Changes in supply and demand also have strong effects on the development of lithium prices (Figure 19). Production costs vary depending on the production type. While the mining costs of lithium ores are rather low compared to the market price for lithium (US\$250–400/t), the processing costs to reach battery quality are higher than those of extracting lithium carbonate from brine (Schmidt 2017). Production costs for one ton of lithium carbonate in battery quality from the world’s largest lithium mine (Greenbushes, Australia) are around US\$4,500, higher than the costs of producing lithium carbonate from the salt lakes of the Atacama Desert, which are currently US\$2,500–3,000 (Schmidt 2017).

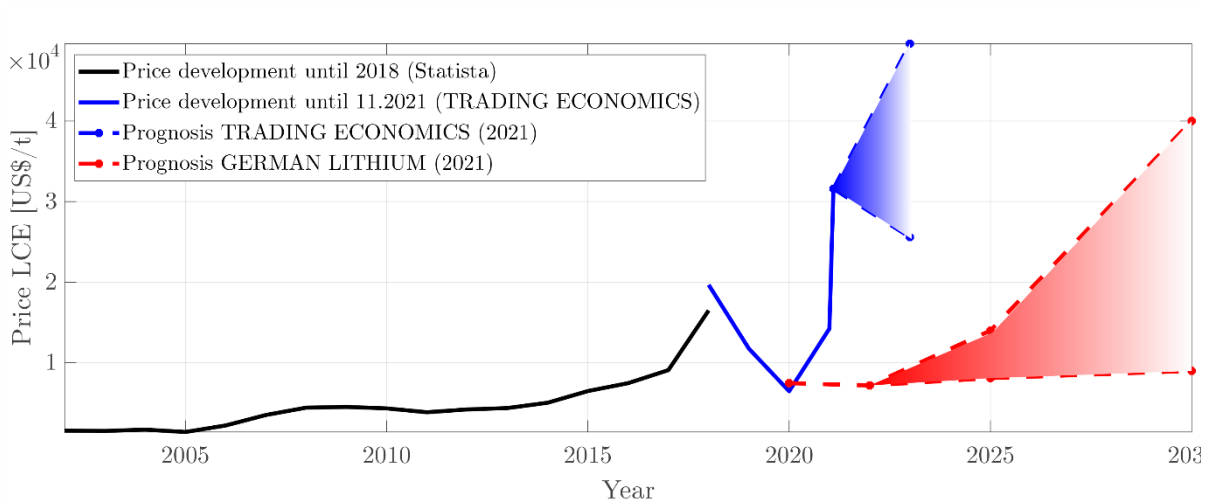


Figure 19: Price development for LCE from 2000 to 2021 and forecasts up to 2030 (Data origin:: (Hohmann (2021); Trading Economics (2022); German Lithium Participation (2021))

Since 2002, prices for lithium carbonate have increased from US\$1,590/t to more than US\$30,000/t in 2021 (Figure 19). The expansion of production in Australia in particular is the result of the strong price increase between 2016 and 2018. It led to a temporary oversupply which, in combination with delayed demand, caused prices to fall in 2020 (DERA 2021a). However, lithium prices recovered quickly and reached a new record in the fourth quarter of 2021. Different scenarios predict further growth in the lithium market (Adams 2020; Jones et al. 2021; Martin et al. 2017; Meng et al. 2021; Schmidt 2017). According to a study from the German Mineral Resources Agency (DERA) (Schmidt 2017), an annual growth in demand between 7.3% and 12.8% is expected. The conservative model for the minimum case (7.3%) would result in a 23% surplus of supply (109,000 t LCE) in 2025, making a rise in the lithium carbonate price unrealistic. In 2017, a supply deficit of 19% (121,000 t LCE) was estimated for the maximum case of a 12.8% growth in demand, causing a corresponding increase in prices (Schmidt 2017). With recent predictions indicating an even larger deficit (36% or 360,000 t LCE), continued price increases are very likely. Forecasts differ on price developments (Figure 19): In 2020, a development between US\$8,000 and US\$14,000/t LCE was expected for 2025 due to the temporarily low prices (German Lithium Participation 2021). On the other hand, studies from 2021 predict prices in 2023 to be between US\$25,600 and US\$49,600/t LCE (Trading Economics 2022) and between US\$9,000 and US\$40,000/t LCE in 2030 (German Lithium Participation 2021), expecting a considerably greater increase when taking the current values into account.

5.2.2 Lithium in the Geosphere

The percentage of lithium in the Earth's crust amounts to $1.8 \cdot 10^{-3}$ % by weight (Hans Wedepohl 1995). Elements with similar percentages are niobium ($1.9 \cdot 10^{-3}$ %), nitrogen, gallium ($1.5 \cdot 10^{-3}$ %), scandium ($1.6 \cdot 10^{-3}$ %), cobalt ($2.4 \cdot 10^{-3}$ %), and lead ($1.5 \cdot 10^{-3}$ %) (Hans Wedepohl 1995). Like all other alkali metals, lithium is highly reactive due to its free valence electron. It therefore never occurs in elemental form but only bound with minerals. Furthermore, lithium has the highest hydration enthalpy of all alkali metals and is hygroscopic. The melting point of lithium is 180.5 °C, its boiling point 1342 °C, and it has a very low density of 0.534 g/cm³ (at 25 °C) (Lide 2005). A look at the electrochemical properties of lithium reveals very positive

properties for applications in electrical engineering. Its electrochemical potential of 3.05 V is the highest of all metals. (In comparison, sodium is 2.71 V and zinc 0.76 V.) The ionic radius of lithium is 60 pm (Li^+), allowing it to substitute ions of similar ionic radius in metals like magnesium or aluminum (Kavanagh et al. 2018).

5.2.3 Potential Hydrothermal Plays for Lithium Extraction in Germany

Sites for deep geothermal energy in Germany are generally located within one of three major geological structures: the active intercontinental rift of the Upper Rhine Graben (URG), the Bavarian Molasse Basin (BMB), and the North German Basin (NGB). The latter two are sedimentary basins on top of a crystalline basement. All three major structures are non-magmatic play systems with low to medium temperatures of 120–250 °C (Moeck 2014; Sanjuan et al. 2022).

In 2021, a total of forty-two sites were operational in Germany producing thermal water from depths of >400 m (Figure 20, geothermal production data from GeotIS; Agemar et al. 2014a; Agemar et al. 2014b). Thirty of these sites are used solely for heat generation, three geothermal sites generate electricity, and nine sites are used for both heat and electricity production. In total, they provide approximately 350 MW of heating capacity and 47 MW of electrical capacity. The lithium concentration in deep waters in Germany ranges widely, from <2 mg/L up to 400 mg/L (Lüders et al. 2010; Sanjuan et al. 2022; Stober 2014). For the higher concentrations within this range, extraction at a reservoir of sufficient size appears profitable. It is important to stress that water composition can vary widely according to the specific geological conditions of the site and even in different parts of the same geological structure or at a short geographic distances. The concept of lithium extraction from deep geothermal fluids proposes accessing the resource via deep drilling analogously to geothermal production of heat and electricity. Current efforts focus on the shared use of existing thermal water production.

Although hydrocarbon drilling into the Muschelkalk formation of the southwestern BMB geological structure has occasionally indicated high lithium concentrations (> 150 mg/L; Stober 2014), geothermal fluids used from the Malm aquifer in the BMB show no significant potential for lithium extraction. As a result of the interaction between meteoric water and the carbonate reservoir rock, these waters are only moderately saline (approx. 2–6 g/L). They contain 4–900 Nmol/L of gases, the most common being CO_2 (6–90%), N_2 (5–73%), and CH_4 (3–55%) (Mayrhofer et al. 2014).

Fluids from the sedimentary NGB, however, are fundamentally different compared to the BMB. For example, brine from the geothermal site at Groß Schönebeck (NGB) contains a lithium concentration of >300 mg/L, presumably due to the evaporation of sea water or the solution of evaporites in the sedimentary units of the Rotliegend, combined with the subsequent interaction of water and rock in the metal-rich permo-carboniferous vulcanites (Regenspurg et al. 2016). Dominant ions are Ca, Na, and Cl, accounting for 70–98% of the total salinity (Regenspurg et al. 2016; Regenspurg et al. 2010). The gas phase consists mainly of N_2 and CH_4 , as well as smaller percentages of He, CO_2 , H_2 , Ar, and heavy hydrocarbons. The gas–water volume ratio ranges from 1:1 to 1.6:1 (Regenspurg et al. 2010). The anaerobic environment in

combination with the high salinity and the absence of sulfides potentially enables metals like Fe, Cu, or Zn to be present as chloride complexes, increasing their solubility in the reservoir and eventually leading to high concentrations in the thermal fluid and scaling issues during geothermal energy generation. (Regenspurg et al. 2015b).

The thermal water reservoirs in the URG are influenced by the rift system, which caused subsidence and sedimentary infilling. This led to an extensive fault system that partially connects several fluid reservoirs, including reservoirs in the Paleozoic bedrock and those in the overlying Mesozoic-Cenozoic rock, with occasional contributions of surface waters as well (Sanjuan et al. 2016a). For the deep reservoir fluids, a salinity of up to 120 g/L and the corresponding fluid chemistry and isotope values generally indicate a very complex genesis from different fluids as well as several evaporation, mineral precipitation, and dissolution events. Dilution by meteoric waters further influences the fluid evolution. Interaction of these highly saline waters with sedimentary units of Buntsandstein and crystalline bedrock at high temperatures (225 ± 25 °C) leads to an accumulation of metallic ions (Sanjuan et al. 2016a). The related brines are characterized as Na-Cl fluids and are dominated by high gas contents. CO₂ typically constitutes the main component of the gas phase (80-90 Vol%). Secondary gas components of the fluid are N₂ (6-10 Vol%) and CH₄ (2-7 %). The geothermal site at Landau is an exception with approx. 48% N₂ and 44% CO₂. The gas-water ratio under standard conditions of 1.6:1 is very similar to that of the North German Basin (Eggeling et al. 2018; Sanjuan et al. 2016a).

Differences between the geological plays in Germany and the variable distribution of their lithium concentration raises new questions regarding the exploration, resource evaluation, and exploitation of geothermal reservoirs for combined material and energy utilization. The origin of the lithium in deep fluid reservoirs remains a major open question. Furthermore, consistent fluid genesis models for the different plays and geothermal sites are yet to be developed and are still subject to active research. High lithium concentrations cannot be explained by high temperatures or reservoir depths alone, which becomes apparent when comparing the Muschelkalk and Malm aquifers of the Molasse Basin (Stober 2014). High lithium concentrations are instead the result of the interplay of seawater evaporation, fluid mixing, and rock-water interaction, particularly at elevated temperature and high chloride concentration (Regenspurg et al. 2016; Regenspurg et al. 2015; Sanjuan et al. 2022; Sanjuan et al. 2016a).

Looking at the properties of the reservoir rock can provide helpful clues with respect to lithium in geothermal brines. Experiments on the fluid-rock interaction show that specific types of reservoir rocks in the URG or in the Rotliegend sandstone of the NGB have a higher potential for lithium emission into the formation water (Drüppel et al. 2020; Regenspurg et al. 2015b). Experiments on the fluid interaction with granite confirm a significant correlation between the lithium solution potential and the salinity of a fluid (Drüppel et al. 2020).

Three major mechanisms are expected to influence the genesis of fluids containing high lithium concentration in the URG and NGB:

- Initial lithium accumulation during the evaporation of seawater. This fluid remains in the respective layer after the initial phase and is potentially diluted by other fluids.

Lithium accumulation has been observed during the experimental evaporation of seawater (e.g.(Babel and Schreiber 2014)).

- Subsequent interaction of the fluid with the surrounding minerals in the reservoir at increased temperatures, e.g. the crystalline bedrock or lower Triassic sandstone (Sanjuan et al. 2022). The interaction with the granite bedrock leads to an alteration of layered silicate, especially muscovite, biotite, and chlorite, and to a release of lithium into the fluid (Drüppel et al. 2020). This lithium-rich fluid then remains in the respective layers and could in a later stage be diluted by other fluids.

In a more complex formation scenario, deep thermal brines integrate fluids from different depths and reservoirs through mixing via fluid circulation through fault zones (Burisch et al. 2018). End-members are seawater, highly saline waters from halite dissolution, and a meteoric component. If the saline fluids interact with the reservoir rock over a long period of time (multiple 100 ka) and at increased temperatures, lithium and other minerals with affinity to chloride can accumulate. It remains unknown which other types of reservoir rocks and sedimentary layers apart from granite, Triassic Buntsandstein, Rotliegend, or Zechstein can contribute to significant lithium concentrations by interaction with the initial brine.

Geothermal Projects

- In operation
- ● In operation with power generation
- Under construction
- ● Under construction with power generation
- Planning stage
- ● Planning stage with power generation
- Research
- ● Research with power generation

Upper Rhine Graben:

1. Landau
Flowrate: 70 L/s
Lithium content: 181 mg/l
2. Insheim
Flowrate: 80 L/s
Lithium content: 168 mg/l
3. Bruchsal
Flowrate: 28 L/s
Lithium content: 163 mg/l
4. Soultz-sous-Forêts
Flowrate: 30 L/s
Lithium content: 173 mg/l
5. Rittershofen
Flowrate: 70 L/s
Lithium content: 190 mg/l

North German Basin:

6. Groß Schönebeck
Flowrate: 15 L/s
Lithium content: 215mg
7. Neustadt-Glewe
Flowrate: 35L/s
Lithium content: 10 mg/
8. Waren
Flowrate: 17 L/s
Lithium content: 2,7 mg
9. Neubrandenburg
Flowrate: 28 L/s
Lithium content: 1,7 mg

(Planned) Battery cell production

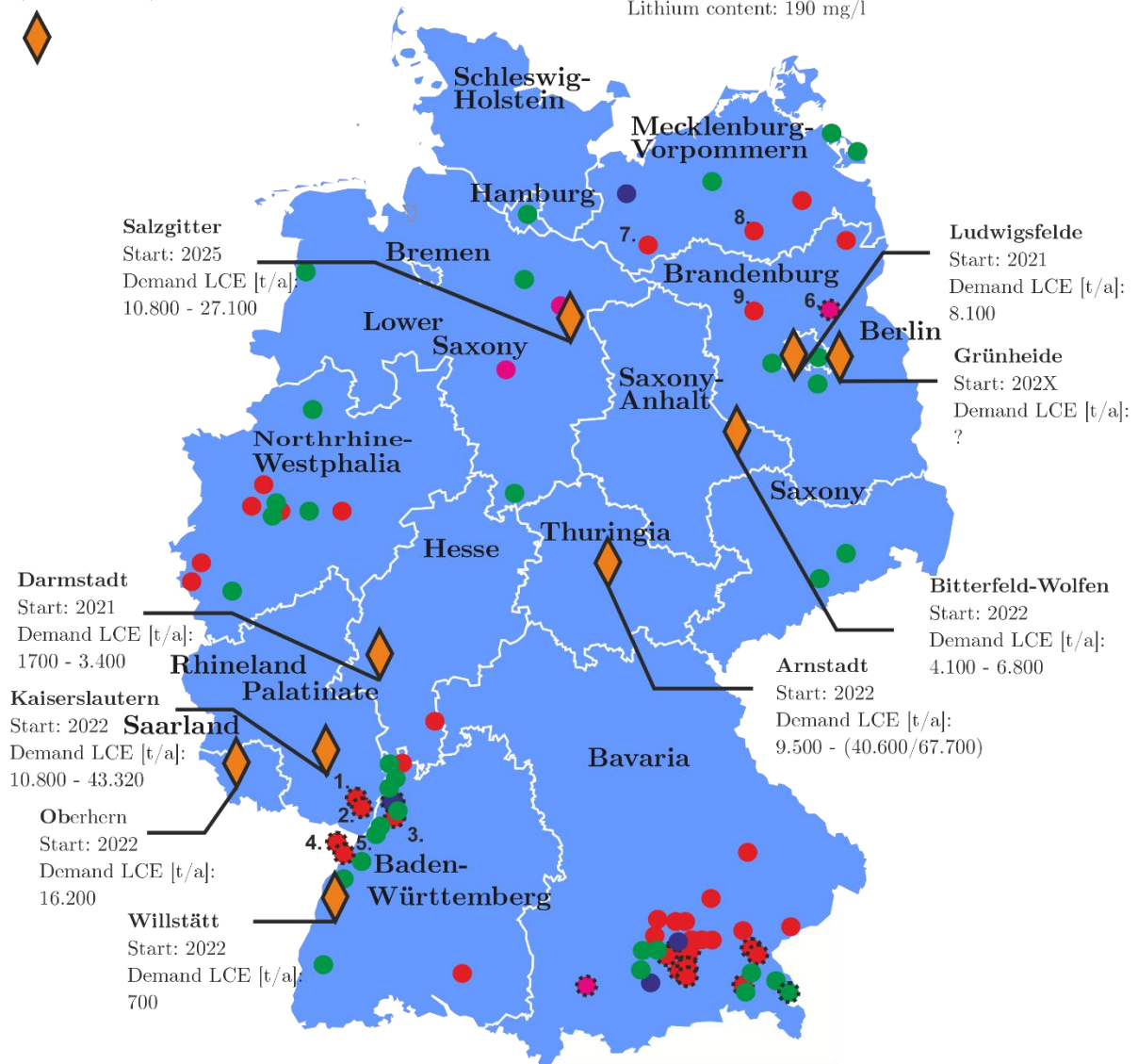


Figure 20: Location of geothermal sites and of planned battery cell production in Germany. The map shows the lithium content and flow rate of the geothermal sites potentially suited for raw material extraction and indicates the forecasted lithium demand for battery cell production. The demand was calculated based on the planned annual capacities. (Data sources: DERA (2021a), Agemar et al. (2014a) (GeotIS), (2014b))

5.3 Methods

Two site-specific scenarios were considered during the calculation of a first estimate of the maximum amount of lithium that could theoretically be extracted from the geothermal power plants operational in Germany as of December 2021. The scenarios were calculated only for geothermal power plants with a lithium concentration of >1 mg/L (see Figure 20). The lithium concentrations $c \left[\frac{mg}{L} \right]$ were taken from literature sources (Naumann 2000; Regensburg et al. 2015b; Sanjuan et al. 2016a; Schallenberg 1999) and the flow rates $Q \left[\frac{L}{s} \right]$ of the respective heat and power generating plants derive from information provided by the German Geothermal Association (Dilger et al. 2021) and other literature data (Egert et al. 2020; Maurer et al. 2020).

Merely multiplying the lithium concentration of the water with the flow rate of a geothermal plant led to an overestimation of the raw material production potential. The following factors must be considered for a more realistic estimate of the extractable amount of lithium from geothermal reservoirs:

- System availability of the geothermal power plant (**A = Availability** [%]): The most reliable geothermal plants generate power 80–95% of the time (Faltlhauser 2016; Uhde 2021). However, for some sites dealing with scaling and corrosion problems due to a complex fluid composition, a much lower availability must be expected. For a starting approximation, we orient ourselves by the availability of power-generating plants and assume an optimistic value of 90% availability.
- Exploitable partial flow rate **q_q** [%]: Some facilities in the URG with large extraction potential have flow rates of 70–80 L/s (Dilger et al. 2021). The extraction procedure (see accompanying article by Goldberg et al. 2022a) requires sufficient time for efficient extraction as well as large amounts of extractants in the form of sorbents, solvents, or water. The necessary volume and infrastructure must be reconciled with the requirements of a geothermal plant, potentially allowing for extraction from only a portion of the total flow (Goldberg et al. 2022a). This constraint cannot be quantified without a large-scale demonstrator of element extraction. Therefore, we base our calculations on 100% of the flow rate and note that a lower fraction will likely be used in practice.
- Lithium concentration over time: The geothermal utilization of deep fluids in Germany is based on doublet systems (or similar configurations). Tracer tests show that parts of the fluid return from the injection well into the production system during the monitoring period (Egert et al. 2020; Sanjuan et al. 2016b). As a consequence, lithium concentration will diminish over time when extracting lithium. Without detailed information *a priori* and because of the high dependency on site conditions, this factor is difficult to calculate. We therefore assumed a constant lithium concentration for a first approximation but also note here that changes in the lithium concentration over time are likely, depending on hydrogeological conditions in the sub-surface.

- Resource extraction efficiency ε [%]: In laboratory experiments, up to 90% lithium extraction from waters has often been achieved. Upscaling and integration of extraction processes into the operations of a power plant are likely to result in lower efficiencies due to the following reasons: competing ions in the selective extraction process, insufficient retention times of the geothermal fluid in the extraction system (e.g. due to high flow rates), high temperatures unsuitable for certain techniques, and more. For this reason, two different extraction efficiencies—50% and 90%—were used for the calculations (Table 8). This mirrors the range of extraction efficiencies achieved in the laboratory using different extraction methods (Goldberg et al. 2022a).

Based on flow rates, the lithium concentration of the related fluid, and the reducing factors, we calculated the site-specific amount of lithium that could theoretically be extracted per year and converted it into lithium carbonate (Li_2CO_3), as ($m = \text{Lithium mass (LCE)} \left[\frac{t}{a} \right]$):

$$m = Q \cdot A \cdot c \cdot q_Q \cdot \varepsilon$$

Eq. (1)

$$m = \text{Lithium mass} \left[\frac{t}{a} \right]$$

$$Q = \text{Flow rate} \left[\frac{L}{s} \right]: \text{ (site-specific)}$$

$$A = \text{Availability: Assumption 90\% (329 days)}$$

$$c = \text{Lithium concentration} \left[\frac{mg}{L} \right]: \text{ (site-specific)}$$

$$q_Q = \text{Exploitable partial flow rate: Assumption 100\%}$$

$$\varepsilon = \text{Extraction efficiency: Assumption 50 and 90\%}$$

Eq. (1) was used to calculate an extraction scenario of 50% and another of 90% for all power plants listed in Table 8. This was then combined with different price predictions, creating a worst-case scenario with the lowest prediction (US\$9,000/t LCE) and the 50% extraction scenario, as well as a best-case scenario with the highest price prediction (US\$50,000/t LCE) and the 90% extraction scenario. It should be noted, however, that even the worst-case scenario is based on very optimistic assumptions of a constant lithium concentration in the geothermal reservoir during the production period, 90% availability of the production fluid, and utilization of the entire flow rate.

5.4 Results

5.4.1 Potential of Existing Power Plants for Lithium Extraction

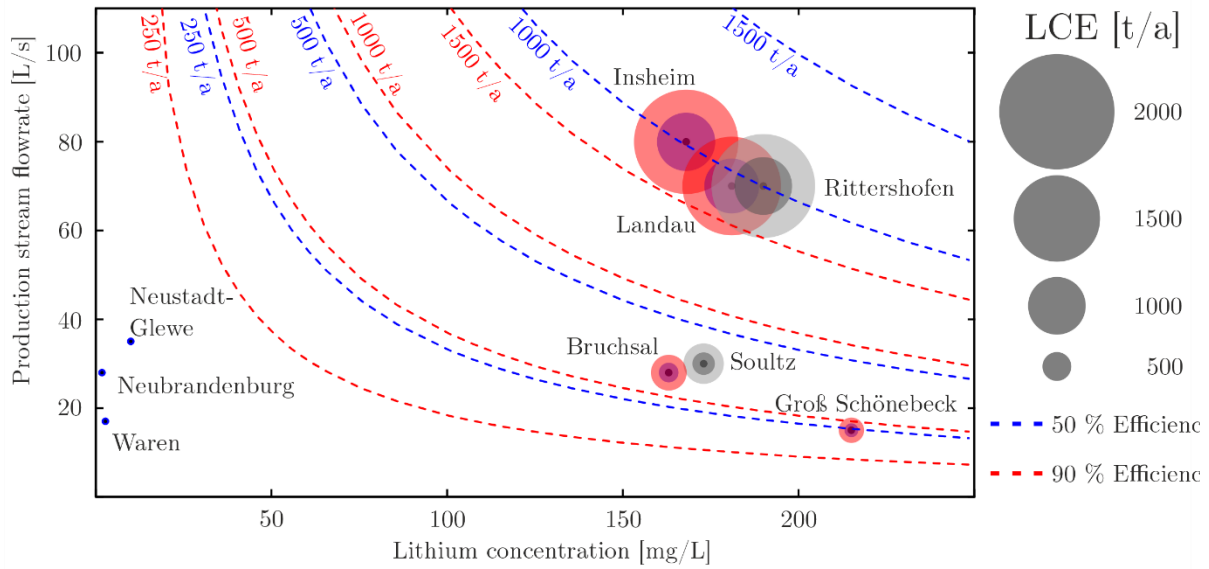


Figure 21: Theoretically extractable amount of LCE (t/a) from the geothermal systems in the Upper Rhine Graben and the North German Basin for extraction efficiencies of 50% (blue) and 90% (red). Further assumptions for determining potential are a constant lithium concentration over the production period, fluid content usability of 100%, and the availability of geothermal production 90% of the time

The high lithium content in some geothermal fluids and the large volume of their respective reservoirs represent a promising resource (Figure 21). The combined fluid volume produced by currently operational geothermal wells in the German parts of the URG and the NGB known for a high Li concentration amounts to around 270 L/s. When the French sites in the URG at Sultz-sous-Forêts and Rittersshoffen are also taken into consideration, the total amount reaches 370 L/s of lithium-rich thermal fluids (Table 8). These values form the basis for the calculation of the extraction scenarios according to Eq. (1).

For the geothermal power plant at Insheim, Eq. (1) results in a maximum quantity of 1000 to 1800 t/a LCE depending on the extraction efficiency. Similar quantities are found for the plants at Rittersshoffen (1000 to 1800 t/a) and Landau (950 to 1720 t/a). Due to lower flow rates, the sites at Sultz-sous-Forêts and Bruchsal allow for a potential lithium extraction of only 390 to 700 t/a LCE and 350 to 620 t/a LCE, respectively. At the Groß Schönebeck site, which contains the highest lithium concentration (215 mg/L), the theoretical flow rate of only 15 L/s results in 240 to 440 t/a LCE. The three other sites in North Germany (Neustadt-Glewe, Waren, and Neubrandenburg) have a lithium concentration between only 1 and 10 mg/L, resulting in much smaller quantities of <50 t/a LCE, respectively.

In a 50% efficiency scenario, the total production volume of all sites together, including those in in the French URG, amounts to approx. 4000 t LCE per year (assuming 90% availability of

geothermal power plants and 100% utilization of flow rates). This would equate to 3–11% of the total demand for battery cell production planned in Germany. Depending on price predictions (US\$9000, US\$25,600, or US\$50,000/t LCE), the production volume would have a market volume of US\$36, 102, or 200 million. With global production reaching 420,000 t LCE in 2020 (Figure 17), the total amount of extractable LCE from the geothermal plants listed above could add around 1% (2% with 90% efficiency) to the world market, close to the amount of Europe’s entire current production (Kavanagh et al. 2018).

Table 8: Lithium concentration in the fluid, volumetric flow produced, and theoretically extractable amount of lithium for geothermal power plants in the Upper Rhine Graben and the North German Basin. Lithium concentrations are from Sanjuan, et al. (2016a), Regenspurg et al. (2015), Schallenberg (1999) and Naumann (2000). Volumetric flows are taken from the work of Dilger et al. (2021), Egert et al. (2020), and Maurer et al. (2020)

Geothermal Power Plant	Li-conc. Fluid [mg/L]	Volumetric Flow Q [L/s]	Extractable Amount of Li At efficiencies: 50% / 90% LCE [t/a]	Market value	
				Worst-Case: 50% extraction at US\$9,000 /t LCE (German Participation 2021)	Best-Case: 90% extraction at US\$50,000 /t LCE (German Lithium Participation 2021)
Bruchsal	163	28	345 / 620	\$3,105,000	\$31,000,000
Insheim	168	80	1015 / 1826	\$9,135,000	\$91,300,000
Landau	181	70	957 / 1722	\$8,613,000	\$88,600,000
Soultz sous Forêts	173	30	392 / 705	\$3,528,000	\$35,250,000
Rittershoffen	190	70	1004 / 1807	\$9,036,000	\$90,350,000
Groß Schönebeck	215	15	243 / 438	\$2,187,000	\$21,900,000
Neustadt-Glewe	10	35	26 / 48	\$234,000	\$2,400,000
Waren	2.7	17	3 / 6	\$27,000	\$300,000
Neubrandenburg	1.8	28	4 / 7	\$36,000	\$350,000
SUM	-	373	3989 / 7229	\$35,901,000	\$361,450,000

5.5 Discussion

The calculated scenarios represent production volumes that would be globally measurable and make a relevant contribution to lithium production in Germany and Europe. It should be noted that German industry is transitioning from buying batteries elsewhere towards having its own battery cell production, which entails increased demand for lithium as a raw material. The planned expansion of domestic cell production is confronted with nonexistent lithium extraction and processing, resulting in complete dependency on the global lithium market. The time frames for developing lithium extraction from geothermal fluids are relatively long due to the long lead times for the construction of geothermal power plants. With exploration and approval procedures and the subsequent construction phase, it can take five to eight years until a power plant begins operations (Geothermie Unterhaching 2021; Uhde 2021). Nonetheless, this development is crucial to tap into additional reservoirs of lithium-rich geothermal fluids.

Our results show that high flow rates are essential for extracting sufficiently large amounts of lithium. As existing sites only have a limited ability to extend their flow rates due to the reservoir hydraulics, new wells and geothermal power plants are the most decisive factors to ensure relevant lithium production from geothermal fluids in Germany.

5.5.1 Extraction Scenarios

At the current state of research and technology, estimates are subject to large degrees of uncertainty and simplified assumptions. Important factors for the potential amount of extractable lithium are the availability of the geothermal fluid flow and the percentage of lithium that can actually be extracted from it. The operational availability of geothermal systems was assumed to be 90%. However, an availability of 90% is a very high estimate corresponding to electricity-generating geothermal systems (Faltlhauser 2016; Uhde 2021). Heat-generating geothermal plants (for instance in the NGB) often have a significantly reduced availability of 30–60% due to the seasonal nature of demand for heating (Sandrock et al. 2020). As the availability of the geothermal fluid flow equals the resource availability and linearly affects the calculations, the full load hours of the heat-generating plants limit the lithium production. This reduces the expected lithium production by one- to two-thirds if it is not adjusted for cases of combined heat and power generation.

Extraction efficiency has so far been derived only from laboratory tests and small-scale demonstrators. On a laboratory scale, multiple methods were successfully validated and mostly yielded high efficiencies of in part >90%. Successful upscaling to an industrial process has yet to occur. Available documentation accounts for a Technology Readiness Level (TRL) of around 3-5 for most lithium extraction techniques (Battistel et al. 2020b; Liu et al. 2019; Ma et al. 2000; Mroczek et al. 2015; Sharma et al. 2016; Wu et al. 2019; Yu et al. 2019; Zandevakili et al. 2014). The nine-level scale of the Technology Readiness Level was developed by NASA to classify the maturity level of new technologies in development (Mankins 2009; Mankins 1995). In this scale, TRL 4-5 describes the initial prototype testing. The communication from some central players in the URG includes reports of on-site demonstrators, indicating a TRL of 5 (Eramet, 2021; Vulcan Energy Resources, 2021). It should be noted that the next step towards

a demonstrator that reaches the dimensions and efficiency of an industrial installation (TRL 6/7) represents a much greater obstacle than all earlier stages (Mankins 2009; van der Spek et al. 2017; Straub 2015). Scaling an installation requires a much higher level of detail than previous prototypes, often causing complications that increase costs and other expenditures (Mankins 2009; van der Spek et al. 2017; Straub 2015). The costs of this stage are usually between the same amount and up to more than twice as much as for reaching all previous Readiness Levels (Mankins 2009; van der Spek et al. 2017). The subsequent construction and implementation of the first real industrial installation (TRL 8) then requires five to ten times as much financial investment as all previous steps combined, depending on the technology (Mankins 2009; van der Spek et al. 2017). As the advanced TRL stages have not yet been reached to our current knowledge, it is not possible to determine the extraction efficiency actually achievable during future continuous extraction operations, nor to estimate the exact costs.

5.5.2 Reservoir and Resource Evaluation

One major factor for investment in the extraction of valuable elements from geothermal fluids is the available reservoir volume in combination with the concentration of the target element. In contrast to conventional mining, schematized practices for resource evaluation were rarely applied until now. An estimation of the resource size of lithium in geothermal fluids was carried out by Vulcan Energy. In the Ortenau license area, a resource size of 13.2 million tons of LCE was estimated (Vulcan Energy, 2019). However, the estimation was graded with the highest degree of insecurity (“inferred resource”) available for a resource. A classification of the Australian Joint Ore Reserves Committee Code (JORC) from 2012 was used for the evaluation. A more precise estimation of the resource size of a deep geothermal reservoir is challenging, as many parameters specific to each reservoir must be determined which are in part still being evaluated in ongoing research projects:

- Volume of the fluid reservoir
- Porosity
- Natural and artificially modified permeability in the aquifer
- Possible aquitards and filled fractures reducing or impeding permeability
- Fractures and fault zones connecting to aquifers below or above, allowing for an exchange between reservoirs in different stratigraphic units
- Details of natural fluid circulation in the geothermal reservoir
- Connections of the power plant’s geothermal circulation to the fluid circulation in the reservoir (What percentage of the geothermal reservoir is connected to the deep wells and its fluid circulation? Do the production well and the injection well form a short circuit, and if so, to what extent?)
- Origin of the lithium and potential additional accumulation in the reservoir; depletion rate during extraction

To operate a lithium extraction installation that is economically viable, the behavior of the fluid chemistry over time is of crucial importance, followed by the resource size. In the case of a hydraulic short circuit between the production well and the injection well that resulted in an extraction of injected water volume after just a few weeks, the lithium concentration would

quickly drop (in the course of weeks or months) to a point where production would become unprofitable. A well-established connection of the production well to the deep geothermal reservoir with only a minor percentage of injected water contributing to the production is therefore essential. At the Soultz-sous-Forêts site, tracer tests showed that after ninety days, 25% of the injected water is extracted again. Furthermore, the highest tracer concentration was observed after only thirteen days (Egert et al. 2020; Sanjuan et al. 2016b). In contrast, at the Rittershofen geothermal site, the tracer return after twenty-five days was only around 0.2% (Sanjuan et al. 2016b). If completely lithium-free water was pumped back into the reservoir at the injection well (equivalent to an extraction efficiency of 100%), the stated tracer return would correspond to the dilution of the lithium concentration in the given time frame. This dilution would lead to a continuous decrease of the extractable lithium over time and would negatively impact the amount of lithium that could be produced. In addition, the system parameters would have to be continuously adapted to the changing lithium concentrations, negatively affecting the extraction performance. The wide range of 0.2–25% return of the injected fluid during the tracer tests demonstrates how site-specific this factor is and that the reduction in fluid lithium concentrations over time strongly depends on the system design and hydrogeologic parameters. For instance, at Soultz-sous-Forêts, the system was designed as an EGS (Enhanced/Engineered Geothermal System), a design that necessitates a high fluid return rate. Consequently, an estimation of the potential for lithium extraction cannot simply be transferred from one site to another without taking site-specific changes in hydrogeology, fluid chemistry, and characteristics of the geothermal production site (T, p, flow rate, injection T,..) into account.

In this context, the aspect of a possible “recharge” of lithium as a cause of water-rock interactions remains undetermined. Due to the current lack of operational in-situ lithium extraction, no empirical knowledge is available. Estimations can only be based on laboratory experiments and simulations and remain simplified as they cannot fully reflect the conditions in an aquifer. A study by Drüppel et al. (2020) investigated the leaching behavior of granite when exposed to fluids at 70 °C and at 200 °C with 2 molar NaCl solution. At 70 °C, lithium is released to the lithium-free fluid amongst other things from the alteration of layered silicates like muscovite, biotite, and chlorite. In experiments at 200 °C with granite and monzonite, the leaching solution had a lithium concentration of 1-2 mg/L at the end of a thirty-six-day test period. This result shows that a lithium recharge from the reservoir is possible under high temperatures. For a more precise estimate of the magnitude of this effect in an exploited thermal water system, flow paths and interaction time with reservoir rock as well as the rock-water ratio must be taken into account. This approach may allow for an estimation of the scale of lithium concentration in a fluid that would be injected lithium-free and left in the thermal water aquifer for a specific time until it is extracted again.

In general, further detailed research and models are needed regarding the behavior of water that is depleted of lithium and potentially other ions hindering an extraction and injected back into a geothermal reservoir. Selective extraction will disturb the chemical equilibrium between the geothermal fluid and the minerals in the reservoir. After re-injection of the lithium-poor and chemically altered fluid after selective extraction, the fluid attains a new chemical equilibrium by water-rock interaction that could cause mineral precipitation or dissolution in the geothermal reservoir and therefore affect production sustainability.

Another relevant aspect is the potential presence of radionuclides in deep, high-salinity thermal fluids (Eggeling et al. 2018; Nitschke et al. 2014; Regensburg et al. 2014; Scheiber et al. 2019a). Lithium extraction attempts to very selectively separate lithium from the rest of the fluid, making enrichment of radionuclides unlikely due to their very different physical properties (e.g. significantly larger ionic radii of radionuclides). However, changes in the element concentration of the fluid, temperature reduction, or changes in Eh-pH conditions can enhance the formation of scales. Among minerals occurring during scaling, BaSr-sulfates and polymetallic sulfides can incorporate radionuclides. In the sulfates, ^{226}Ra and ^{228}Ra and in the sulfides ^{210}Pb are incorporated (Nitschke et al. 2014). Due to the lack of direct contact, the resulting radioactivity normally does not pose a hazard to humans or the environment during plant operations. Over time, however, the mineral precipitates can accumulate on pipe walls or filters, which must be separately disposed of after removal. Pipes from sites in the URG have been classified as “metal waste contaminated by hazardous substances” (AVV-170409), which could be cleaned of radionuclides by melting and thus be recycled (Eggeling et al. 2018). Radionuclides are not a direct obstacle to extraction, but the costly disposal of mineral precipitates with possible radionuclide contents must be included in a holistic economic consideration.

5.6 Conclusions

Global lithium demand will continue to grow at a strong pace. The main driver for this is the increasing need for lithium-ion high-performance energy storage, for the expansion of e-mobility in particular. In this context, the German lithium market will change significantly due to the large-scale battery production in planning for at least nine production sites. The current import of ready-manufactured batteries will have to be replaced by the import of raw materials. The proposed battery production would meet up to 15% of global demand in 2025, with a planned use of 37,000–149,000 t LCE for battery cell production in Germany. Rising demand could create a global lithium deficit of 360,000 t LCE (36% of global demand) in that same year, which may have a particular impact on new players on the market due to existing long-term contracts with companies and countries already producing batteries (such as China).

Until now, lithium production has been poorly diversified, with more than 80% of all lithium being produced in Australia and Chile. Lithium extraction and processing in Germany (or at least in Europe) is advisable from a geostrategic standpoint, especially since the processing of mineral ores is mostly conducted in China. In addition, extraction has been associated with environmental impacts, which are magnified by the long transport distances to battery cell manufacturing facilities. Domestic production from geothermal fluids could set new standards in terms of minimizing the CO₂ footprint and the extent of environmental impacts.

In Germany, lithium occurs in high concentrations in deep geothermal fluids. Concentrations at relevant sites in the Upper Rhine Graben range between 160 and 190 mg/L. In the North German Basin, concentrations in the Groß Schönebeck well reach up to 215 mg/L. In fluids of the Rotliegend, concentrations of close to 400 mg/L were detected in isolated cases. Access to these deposits has so far been achieved only by deep drilling. The co-production of lithium at

currently operational geothermal energy production sites has the potential to make the first contribution to covering Germany's growing demand for lithium. In Germany and France, there are nine actively productive deep wells at lithium-relevant locations (the URG and NDB). Cumulatively, a volume flow of about 370 l/s is produced at these sites. From this total flow, a maximum of 7200 t/a LCE could be produced in a very optimistic forecast scenario (extraction efficiency 90%, availability 90%, constant lithium concentration in the geothermal fluid, and a usable fluid fraction of 100%). The value of this simplified estimate corresponds to about 5–19% of the annual demand of planned battery cell production in Germany. This is a purely theoretical, highly simplified potential estimate. Nevertheless, it shows the potential for responsible, independent raw material production in Germany, which could play an important role especially in the case of an impending lithium shortage.

The adaptability of the specific extraction technology to the characteristics of the geothermal fluid and power plant operation and the question of potential changes in lithium concentration due to re-circulation of injected fluid are critical for the actual feasibility. Should the breakthrough to an industrial process succeed, the following site-specific techno-economic key questions, which could not be taken into account in the very optimistic consideration carried out here, must still be clarified for implementation:

- How large is the geothermal fluid reservoir and how sustainably can it be managed?
- How does the lithium concentration behave over time during production?
- Based on fluid chemistry, which extraction method is best suited?
- Can extraction efficiency and surface fluid retention time be optimized at the site? Can such design be integrated into the operating plant process?
- How large are the volume flows resulting from the process engineering treatments? Can these be handled? What material input is necessary at what price?
- What infrastructures need to be built?
- Do plant operating parameters (temperature, pressure, full load hours) need to be adjusted for extraction?
- What are the energy requirements for selective lithium extraction?
- How does the scaling potential in all plant components develop through coupling with lithium extraction?
- What influence does the extraction (possibly with pretreatment) have on the chemical composition of the fluid? How does this affect the reservoir and the existing plant components?
- Which substances are added to the fluid (inhibitors, extraction media, etc.) and removed (raw material, co-precipitate, scaling)? Is this compatible with legal requirements?
- What substances and quantities are generated for waste disposal? What are the related costs?

Due to the complexity of the topic, the exceptional importance of future raw material supply, as well as increasing interest on the part of society, scientific support should continue to be provided for this process. More cooperation between researchers and the industrial sector would be highly constructive for achieving efficient technological progress.

5.7 Acknowledgments

The authors would like to thank the Helmholtz Association for research funding within the Geoenergy subtopic in the MTET (Materials and Technologies for the Energy Transition) program of the Energy research field. Thank you to the BMBF (Federal Ministry of Education and Research) Client II for funding the BrineMine project (Grant Number 033R190B). Special thanks are also due to the chairs of Geothermal Energy and Reservoir Technology and Geochemistry and Economic Geology at the Institute of Applied Geosciences at the KIT, headed by Prof. Thomas Kohl and Prof. Jochen Kolb, for making this work possible, and for the lively scientific exchange. Furthermore, this work grew through many technical discussions, for which we would like to especially thank Dr. Joachim Koschikowski, Dr. Daniel Winter, Gerrit Fuelling, Klemens Slunitschek, Rebekka Reich, and Michael Schmidt. Last but not least, we would like to thank the anonymous reviewers and the editors for their constructive suggestions for improvement.

6 Reservoir behavior of lithium-depleted brine in a geothermal reservoir

This manuscript has been published in *Energies*. 16, 5899 (2023), under the title:

Challenges and Opportunities for Lithium Extraction from Geothermal Systems in Germany - Part 3: The Return of the Extraction Brine

Valentin Goldberg^{a,b}; Ali Dashti^a, Robert Egert^c; Binil Benny^d; Thomas Kohl^a; Fabian Nitschke^a

^a Institute of Applied Geosciences, Chair for Geothermal Energy and Reservoir Technology, Karlsruhe Institute of Technology, Adenauerring 20b, 76131 Karlsruhe,

^b Department of Geology and Andean Geothermal Center of Excellence (CEGA), Facultad de Ciencias físicas y Matemáticas, Universidad de Chile, Santiago, Chile.

^c Energy and Environment Science and Technology Directorate, Idaho National Laboratory, Idaho Falls, USA

^d Department of Civil and Environmental Engineering, Environmental Engineering, Bochum University of Applied Sciences, Am Hochschulcampus 1, 44801 Bochum,

6.1 Abstract

Lithium (Li) is considered a crucial element for the energy transition due to its current irreplaceability in Li-ion batteries, particularly in electric vehicles. Market analysis indicates that Germany's future automotive sector and planned battery cell production will necessitate significant quantities of global lithium production. At the same time, only 1% of the world's Li production is currently sourced from Europe.

Recently, geothermal brines in Germany have gained attention as a potential local raw material source. These brines exhibit elevated Li concentrations and substantial flow rates in geothermal plants, suggesting the possibility of viable local production. However, a comprehensive full-scale Li extraction process from geothermal brines is yet to be established, and uncertainties persist regarding its long-term behavior. To address this, a generic model based on the geothermal settings of the Upper Rhine Graben was developed, simulating a 30-year operational period for Li extraction. The simulation revealed a 40% depletion of lithium during the observation period, while heat production remained constant. Nonetheless, the model also demonstrated a mean Li production of 231 tons per year (equivalent to 1230 tons per year of lithium carbonate equivalent), which could significantly enhance the economic prospects of a geothermal power plant and, if applied to multiple plants, reduce Germany's dependence on global lithium imports.

The primary factor influencing productivity is the achievable flow rate, as it directly impacts access to the raw material. Hence, emphasizing the importance of detailed reservoir exploration and development in optimizing future lithium production from geothermal brines.

6.2 Introduction

The importance of lithium (Li) has tremendously increased in the past years. Formerly mostly used in the ceramic industry or lubricants, Li is the main component of today's state-of-the-art rechargeable Lithium-Ion-Batteries (LIB) and therefore one of the key materials of the energy transition. 67 % of the global Li demand in 2020 was used for batteries mostly for battery electric vehicles (Schmidt 2023; Schmidt 2017). This sector represents also the most important and very rapidly growing market (Martin et al. 2017; Meng et al. 2021). Recent sharp rises in Li market prices are projections of a near-future worldwide Li shortfall even within optimistic market scenarios (Goldberg et al. 2022b). The EU plans foresee to decarbonize individual transport and light cargo transport by banning the sale of combustion engine vehicles after 2035 (Europäisches Parlament 2022). With this, Li-batteries and their raw materials become a crucial and critical aspect of the climate goals. At the same time, Li is defined as a critical raw material in the EU since 2020 (Europäische Kommission 2020).

The situation becomes even more challenging since Europe's and especially Germany's battery sector is in a transition. Until today Li-commodities, in particular batteries, are mainly imported from China as ready-manufactured products (Schmidt 2023). To become more independent and remain competitive, a transformation of the battery value chain is being pursued by establishing local Li conversion and battery cell production facilities (DERA 2021a). This foresees importing fewer battery cells but manufacturing Li products in Germany. The associated necessity for imports of Li as a raw material leads to new dependencies upon global suppliers. Relying widely on one of the largest automotive sectors in the world, an undisrupted and sufficient Li supply is essential for local supply chains and the entire German economy. Therefore, domestic Li resources dissolved in deep geothermal brines get more and more into focus recently.

In Germany numerous research studies and industrial development projects are working on improving, implementing, and upscaling the technology called direct Li extraction (DLE) from geothermal brines (Goldberg et al. 2022b; Reich et al. 2022; Rettenmaier et al. 2021; Sanjuan et al. 2022; Schmidt 2023; Stringfellow and Dobson 2021a). The first scenario analyses have shown that already the currently existing geothermal power plants in Germany could theoretically cover up to 13 % (880 T Li) of the Li demand caused by the planned local battery cell production. This would substantially contribute to partial supply independence (Goldberg et al. 2022b).

However, besides technical challenges associated with the extraction process itself also key questions of reservoir management are still unsolved. In particular, so far no study exists clarifying the long-term Li concentration development during production. Therefore, it is not clear if a geothermal reservoir can be managed sustainably over the typical periods geothermal reservoirs are operated. It is known, that the thermal signal of the injection well can reach the production well in a so-called thermal breakthrough after several years of operations (Bauer et al. 2014). We bring up the hypothesis that a similar effect can occur analogous in a chemical breakthrough of the reinjected Li-depleted brine returning to the production well. This will be a crucial factor for the economics of a planned combined energy and raw material use of

geothermal reservoirs, which has not been addressed in scientific reservoir models before. In terms of reservoir and resource characterization, conventional mining assessment is not sufficient but it requires the methods of hydraulic transport modeling known from geothermal energy. For quantifying this transient process and its sensitive parameters for the first time, a numerical modeling study is conducted using a generic geological model based on the geology of the Upper Rhine Graben (URG) for different operation scenarios. The URG is a hotspot for geothermal energy as well as the developments of geothermal Li extraction in central Europe (Dilger et al. 2021; Goldberg et al. 2022a; Sanjuan et al. 2022) and was thus targeted for this case study.

6.2.1 The market and projections

The production of Li, as well as its processing for battery production, is poorly diversified globally. China is producing 76 % of the global battery capacities as well as conducting 60 % of the global refining of battery grade Li (Bridge and Faigen 2022). The largest Li producer is Australia with over 50 % of the global Li are produced from hard rock mines (cf. Figure 22a). It is followed by Chile (25 %) and China (13 %) which took over more and more market shares over the past years (DERA 2021a; Schmidt 2023; Schmidt 2017). The only European producer of Li is Portugal with only 1%. While in 2021 the global Li production was about 100,000 t, the global demand is predicted to grow between 316,307 t and 558,780 t in 2030. Compared to global production scenarios, even including Li recycling, only in the combination of the lowest expected Li market growth and the most optimistic prediction of Li production, the Li market in 2030 will be covered. All other scenarios result in a Li deficit (cf. Figure 22b) (Schmidt 2023). The forecasted production relies on primary production as well as on the secondary sector involving battery recycling. The primary supply is determined by considering current mining output, planned operational expansions, and upcoming mining projects, including their annual extraction capacities and projected production starting dates. The data for operational expansions are project numbers from mining and exploration companies. The demand scenarios are based on various forecasts of compound annual growth rates (Schmidt 2023).

For Europe, the yearly demand in 2020 was 4,600 t while the prognosis predicts 2030 a demand between 77,000 and 195,000 t (Fraunhofer ISI 2022; Schmidt 2023). The planned battery cell productions at 9 sites in Germany will require 7,000 to 51,400 t/year, depending on the success and the speed of ramp-up (DERA 2021a; Fraunhofer ISI 2022). For fulfilling this goal, Europe and especially Germany accordingly will require large amounts of global Li production. Predictions for European Li production foresee, including recycling, production of 26.250 t in 2030 (Schmidt 2023). The existing geothermal plants in Germany could produce 490–880 t per year in an ideal scenario (Goldberg et al. 2022b). The large difference between the planned local Li production and the demand shows, that current politics just shift the dependency from relying on battery imports to relying on Li (and other raw material) imports for supplying the European automotive industry. If no new Li exploration projects are started in Europe or if the geothermal production, and the associated access to Li-bearing reservoirs, are not significantly pushed forward, there are no possibilities to improve this situation in the future.

The criticality becomes more apparent if prices and volatility of the market are considered. Developments of the past 20 years are in more detail described in previous studies (Goldberg

et al. 2022b). From 2020, due to the global high demand for e-mobility, prices strongly increased, leading to an all-time high of up to 87,000 US\$/t for Lithium Carbonate Equivalents Li_2CO_3 (LCE) in November 2022 (Trading Economics 2023; Trading Economics 2022). Since then prices decreased to 47,000 US\$/t LCE (Trading Economics 2023). Reasons for this decrease might be inflation-caused regression of sales, and insecurities due to measures against the Covid pandemic in the sales and production in China (Schmidt 2023). The development shows high volatility of the Li market. The current prognosis for the Li price varies between 26,200 and 61,500 US\$/t LCE (Steiger et al. 2022). The high prices show great potential for local unconventional resources. However, the volatility in the past years in short periods also shows that robust economic planning is necessary with price fluctuations of 50% within half a year.

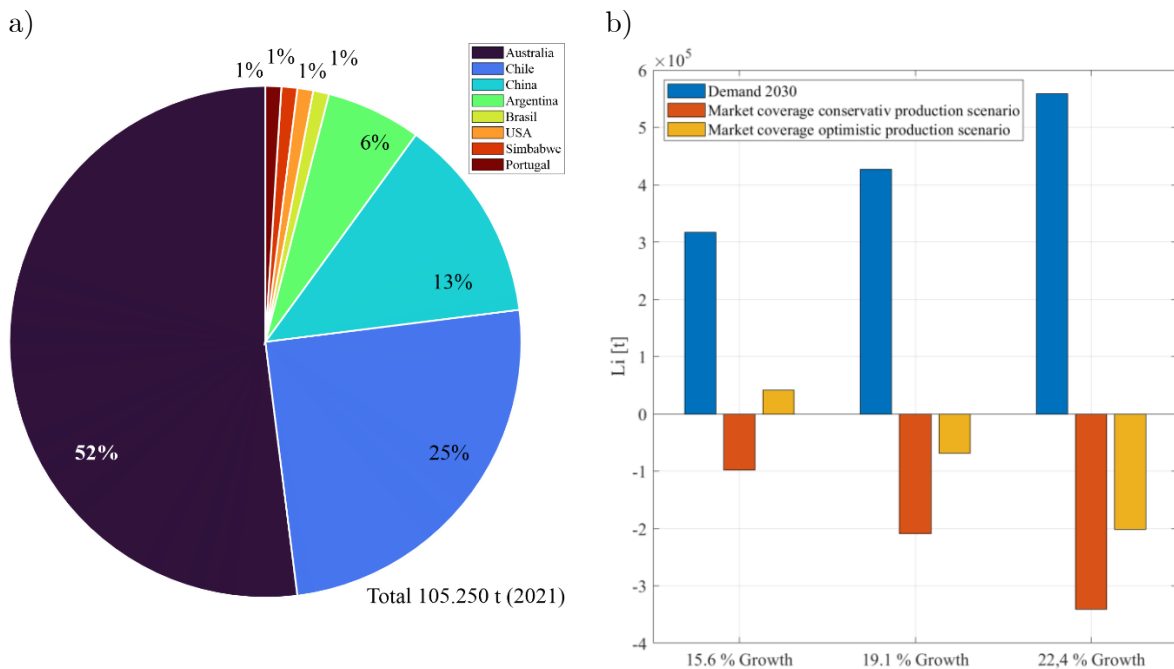


Figure 22: a) Preliminary global Li production for 2021 and its global distribution (Data: (Schmidt 2023)). b) Global demand prediction for Li in 2030 for different yearly growth predictions (316,300 t, 426,700 t, 558,800 t) in comparison to the predicted global production scenarios (conservative: 217,890 t, optimistic: 357,680 t) (Data: (Schmidt 2023))

6.2.2 Geothermal reservoirs in the Upper Rhine Graben

The URG is a 300 km long and 30-40 km wide NNE-SSW-trending continental rift system (Eisbacher and Fielitz 2010; Geyer et al. 2011). The extension and subsidence of the system initiated during the Eocene (approx. 45 Ma) and are limited by two systems of main border faults, separating the graben shoulders from the sedimentary graben fill (Eisbacher and Fielitz 2010; Grimmer et al. 2017). The Cenozoic sedimentary graben fill reaches thicknesses up to 3500 m and covers the graben floor consisting of Permian to Triassic formations in the north and Jurassic formations in the south overlaying the Variscan crystalline basement (Grimmer et al. 2017).

The rifting process was accompanied by the subsidence and filling of the graben as well as the uplift of the graben shoulders, which led to the formation of an extensive fault system. The

fracture network connects several fluid reservoirs, including reservoirs in the Paleozoic crystalline basement and those in the overlying Permo-Mesozoic and Cenozoic rocks, with occasional contributions of surface waters as well (Sanjuan et al. 2016a). Major reservoir targets occur in the sedimentary sandstones of the Triassic Buntsandstein. Fault systems in the sedimentary units of the Buntsandstein were explored by existing wells e.g., in Cronenburg, Bruchsal, Insheim, or Brühl (Vidal and Genter 2018), and are also currently in the visor of newly planned or ongoing projects (Q-con GmbH and Deutsche Erdwärme GmbH 2020; Vulcan Energy 2023). The geothermal play can be described as a non-magmatic extensional domain which is for example also found in the Great Basin in the United States, or Western Turkey (Moeck 2014).

The brines with salinities of up to 120 g/L are characterized as Na-Cl fluids and are dominated by high gas contents. In most fluids, CO₂ is the dominant component with gas–water ratios up to 1.6:1 reaching under standard conditions (Eggeling et al. 2018; Sanjuan et al. 2016a). The geothermal exploited reservoirs of the URG are in depths of 2500-5000 m and show fluid temperatures between 120 and 200°C. Existing deep wells produce with flowrates between 28 and 80 L/s and Li concentrations of 160 – 190 mg/L (Dilger et al. 2021; Sanjuan et al. 2016a; Uhde 2021).

The source of Li and other metals is yet not fully clear. Studies of the brines in the URG indicate an origin by water-rock interaction in sandstones or granitic basement causing mica dissolution with further influences by illite, chlorite, or tosudite precipitation at high temperatures (225 ± 25 °C) (Sanjuan et al. 2022; Sanjuan et al. 2016a). Beyond the temperature influence, high salinities, especially high chloride concentrations seem to correlate with high Li concentrations (Drüppel et al. 2020). The high salinity could be derived from the evaporation of seawater, which shows in evaporation experiments also enrichment of Li (Babel and Schreiber 2014). But several competing hypotheses regarding these kinds of brines origins are discussed, e.g. freshwater evaporation and dissolution of evaporites or influences of former high-temperature and pressure geothermal systems (Sanjuan et al. 2022). The genesis of the URG brines likely took place in a complex multi-stage mixing history of different fluids such as seawater, meteoric water, and saline brines from halite dissolution, with different precipitation and leaching events in different lithologies (Aquilina et al. 2002; Burisch et al. 2018). A final assessment of the provenance is currently the subject of research.

Regarding the sustainability of Li production from thermal waters, the question arises of how the Li concentration behaves over time and develops as a consequence of extraction. Tracer experiments in the Upper Rhine Graben reveal that the reinjected fluids may break through and can be at least partially reproduced at the production well. This observation is very site-specific and additionally dependent on the reservoir geometry and operation configuration. At the Soultz-Sous-Forêts site, 25% of the tracer was recovered at the production well after 90 days, and at the Rittershofen site 0.2% after 25 days (Egert et al. 2020; Sanjuan et al. 2016b). This has important implications for the long-term performance of future Li production. If a 100% Li-depleted brine would be reinjected into the reservoir and no Li recharge occurs in the reservoir, the Li content would decrease equally to the tracer recovery at the production well. The remaining percentage represents the lateral inflow of fresh brine at the production well from the geothermally uninfluenced parts of the reservoirs.

Leaching experiments using rock material from geothermal reservoirs and saline brines showed that water-rock interaction processes can result in a Li release from minerals into the brines (Drüppel et al. 2020; Regenspurg et al. 2016). This suggests that there may also be a Li recharge from the reservoir during Li production. For a meaningful estimation of the recharge extension, long-term and time-resolved water-rock interaction experiments are needed. A definite statement on reservoir scale, however, will only be possible with full-scale long-term production.

6.2.3 Li extraction from geothermal fluids

The product of produced flowrates and Li concentrations in geothermal plants in the URG defines the theoretic raw material potential of the geothermal systems. Considering these two factors only, the URG geothermal plants with high flow rates (70-80 L/s) such as Rittershoffen, Insheim, or Landau circulate every year about 400 t of Li that could be used for the production of approx. 2100 t LCE. The research in the field of Li extraction from geothermal brines is ongoing for almost 50 years (Bertold and Baker 1976; Palmer et al. 1975). Various approaches (e.g. liquid-liquid-extraction, inorganic sorbents, electrochemical methods, and membrane technologies) are functional on laboratory and small prototype scale (TRL 4/5), but yet a full industrial implementation of DLE for geothermal brines is missing worldwide (Goldberg et al. 2022a; Goldberg et al. 2022b; Reich et al. 2022; Stringfellow and Dobson 2021a).

Liquid-liquid extraction approaches aim for transferring one dissolved substance of a liquid medium to a liquid solvent. This approach requires that the two media can transfer the target elements but are not miscible for later separation. As such, organic solvents open up promising approaches for raw material extraction from high salinity geothermal brines, such as tributyl phosphates (TBP) diluted with methyl isobutyl ketone or kerosene (Liu et al. 2019; Nguyen and Lee 2018; Shi et al. 2017; Xiang et al. 2017; Xiang et al. 2016; Yu et al. 2019), the use of crown ethers (Swain 2017; Zhang et al. 2021), or the use of ionic liquids (Park et al. 2014; Shi et al. 2017).

Regarding inorganic sorbents, different materials and approaches are investigated for selective ion separation. Promising and currently widely discussed approaches are for instance titanium oxides, manganese oxides, or zeolites (Reich et al. 2023; Stringfellow and Dobson 2021a). Typically ion exchange, physical adsorption, and absorption are the extracting mechanisms. The raw material in the solution is bound to a solid that is added to or exposed to the fluid, in the first loading stage. After contact between the sorbent and the raw material to be recovered, a stripping stage follows, exchanging the initial solution with a recovery solution and desorbing the elements from the loaded sorbent (Goldberg et al. 2022a).

Electrochemical extraction methods are based on the principle that positively charged Li cations are selectively attracted to a working electrode under the application of a voltage while anions and interfering elements are bound to a counter electrode (Battistel et al. 2020b; Calvo 2019; Romero et al. 2021). The electrode material can be similar to inorganic sorbents built of manganese or titanium with the major advantage of rapid electrochemical binding and desorption in this application (Battistel et al. 2020b). A benefit is also that the methods are based on similar mechanisms as in the widely used lithium-ion batteries and are thus well understood (Liu et al. 2019).

Membrane processes are based on the use of lithium-selective membranes, separating by ion size, surface charge, or chemical and physical properties (Stringfellow and Dobson 2021a). Beyond this, membranes can also be used for keeping other approaches as liquid-liquid extractions or sorbents stationary (Li et al. 2019a)

The described methods showed promising results with individual positive and negative aspects for their industrial application. The technologies were overall able to extract 40 – 95 % of the initially dissolved lithium from the brines under well-controlled laboratory conditions. This proportion describes how much of the total Li dissolved in the could in theory be extracted during the operation of a future plant and is further referred to as extraction efficiency (Goldberg et al. 2022a).

In Germany and on the French site of the Upper Rhine Graben, several industrial and research projects are working currently on this topic for applying different technological approaches as well as scaling up the processes to an industrial scale (Adionics 2022; Eramet 2022b; Geolith 2022; Unlimited 2022; Wedin 2022). The main challenges are the high flow rates in combination with the chemical composition of the fluids, leading to high scaling and corrosion potentials, which are typical challenges during geothermal energy production. The addition of chemical reaction agents, pH changes, degassing, cooling, or kinetic effects during extraction processes increase these challenges significantly and pose high demands on the extraction material, the process technology as well as the construction materials (Goldberg et al. 2023b). The extraction efficiency will linearly lower the theoretically producible amount in comparison to the theoretically circulated Li amount which is a function of Li concentration and flow rate. Further aspects that will decrease the Li output are for instance downtimes for maintenance work. From 400 t of circulated Li per year only 180 to 320 t (950 – 1700 t LCE) will be extractable depending on the success of the upscaling of the extraction processes (Goldberg et al. 2022b). The quantification of further markdowns which might occur over time due to the dilution of Li in the reservoir is quantified with the following model and simulation.

6.3 Methods

6.3.1 Geological Model

To assess the development of the Li concentration in the reservoir during raw material production, a generic model was developed, based on the existing geothermal settings in the URG (Figure 23a). The bottom layer with impermeable parameters represents the variscan crystalline basement and/or an aquitard. On top of the basement, a reservoir layer is defined (e.g., Buntsandstein). The reservoir is covered by further Triassic sediments (Upper Buntsandstein, Muschelkalk, Keuper) and the top layer displays Paleogene, Neogene, and Quaternary sediments. The model extends from the top layer in a depth of 1500 m down to 5000 m. In the center of the model, the top layer has a thickness of about 1300 m, Keuper approx. 300 m, Muschelkalk ca. 170, Upper Buntsandstein approx. 100 m, Buntsandstein (Reservoir) approx. 360 m and a ground layer of about 1,250 m. The thicknesses of the layers

and the resulting inclination changes are based on published data for currently planned geothermal wells in the URG (Leiter and Elsner 2020).

The fault zone crosscutting all layers is slightly inclined for representing one of the URG typical normal faults (Grimmer et al. 2017; Vidal and Genter 2018). Fault cores in the Triassic sandstones can be fully or partly sealed (Bauer et al. 2015; Vidal and Genter 2018). In this simplified scenario, a uniform sealed core was assumed, with a thickness of 10 m following surface analogs (Bauer et al. 2015). Damage zones in the URG are reported to expand over several dozen of meters from the fault core (Bauer et al. 2015; Vidal and Genter 2018). For the model, a damage zone of 125 m width in each direction from the fold core was assumed. The chosen width of the damage zone could result, independently from the lithology, from a fault displacement between 200 and 600 m (Choi et al. 2016) which is a realistic value for normal faults in the URG that could even reach > 2 km (Grimmer et al. 2017).

Only the open hole sections of the two geothermal wells are implemented in the model as the hydraulically connected part to the reservoir. Being deviated the tops of the well's open hole sections are separated by 700 m of distance and by 1690 m at the bottom hole depth. The open hole sections start at the top of the described reservoir layer on one side of the fault, crosscut the damage zones and the fault core and reach their final depth at the bottom of the reservoir layer at 3735 m at the other side of the fault (Figure 23b).

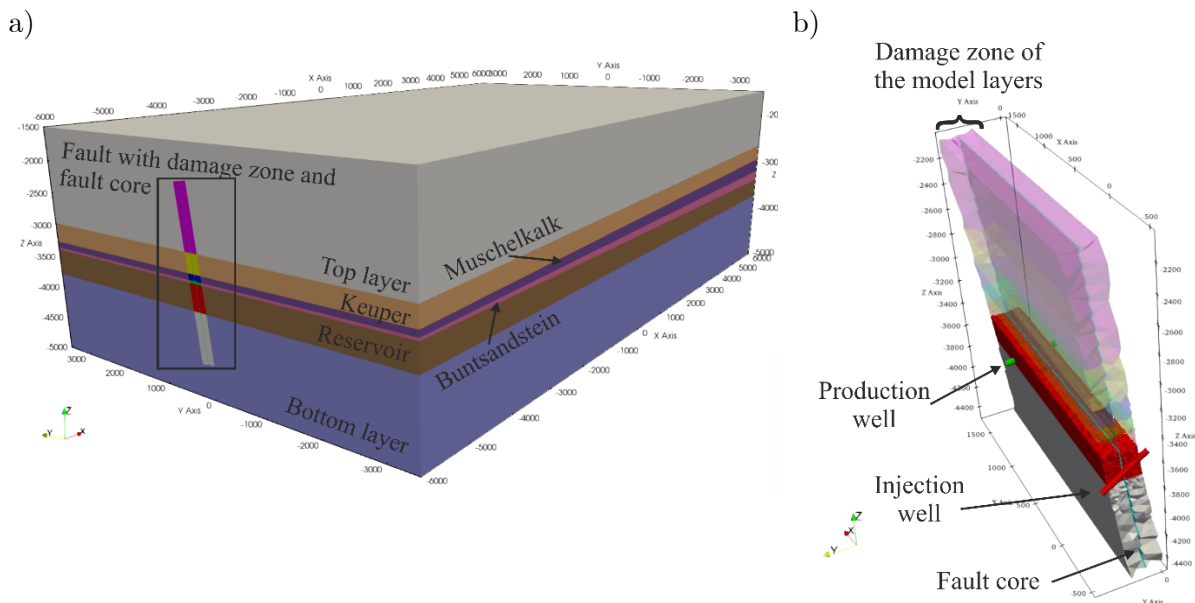


Figure 23: a) 3D-Reservoir model with all implemented geological units. b) Enlarged view of the fault zone and the wells. For clarity, the layers outside the damage zone and the damage zone of the reservoir are not displayed.

6.3.2 Mesh Generation

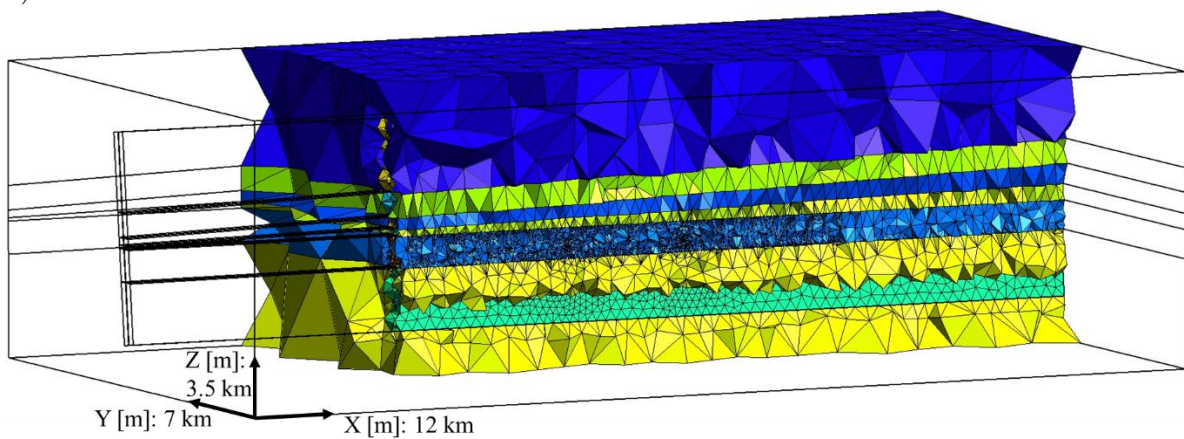
For creating the mesh the open-source mesh generator GMSH (Geuzaine and Remacle 2009) was used. The model geometry is defined as a box with a lateral extension of $12 \text{ km} \times 7 \text{ km}$, large enough to avoid any effects of boundaries on simulation results (Figure 24a). The model comprises six geological formations with a total thickness of over 3500 m in the vertical

direction. 2D flat planes represent the contact of the formations. The tilted fault damage/transmissive zone is recreated with a 3D element. In the middle of a damage zone, a 3D block with a width of 10 m represents the tight core zone. 1D elements as shared edges are used to create the injection and production sections of the wells with deviated open-hole sections. The line elements are approx. 300 m long and have a given scale factor of 21.5 cm representing an 8,5“diameter borehole.

Due to the diversity and intersection of the geometrical elements (five 2D surfaces and several 1D lines passing through the two boxes), it is challenging to maintain mesh conformity where elements are arranged in a way that two of them intersect, sharing a face, an edge, or a node. The thick damage zone box splits into two zones due to the existence of the thin core zone in the middle. Each 2D flat plane generated as a boundary of the layers also splits into five ones due to intersecting the damage and core zones in the middle. Available functionalities like boolean operations in GMSH allow for a global intersection of the model taking care of the whole intersections, new elements generation, and embedment.

A multi-level mesh refinement in the model is carried out through several available functions in GMSH. Distance, Threshold, Constant, Restrict, and Box fields allowed for a gradual mesh size increase of 4 to 750 m from the target points, lines, and surfaces toward the exterior. Figure 24 visualizes the refinement trend in the model. Mesh size in the damage and core zones and wells is forced to be kept as fine as possible. These fields are intermingled in a way that converges to the most efficient refinements with the least number of nodes and elements. The mesh contains 164'499 nodes and 1'181'197 elements.

a)



b)

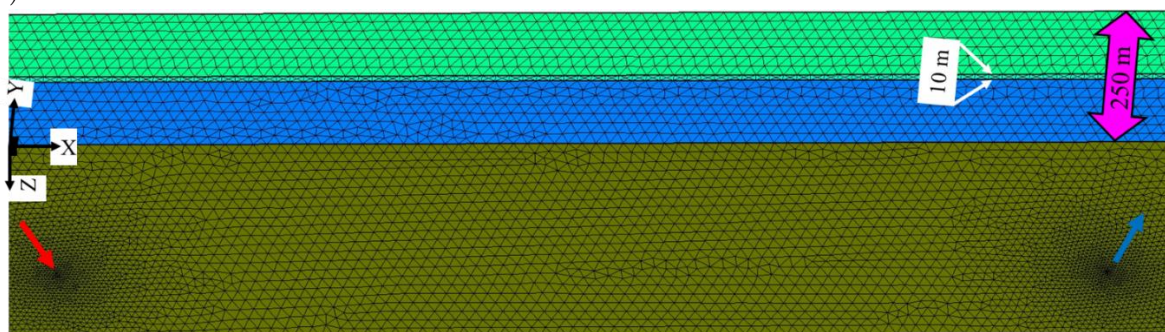


Figure 24: a) A general overview of a cross-section of the model containing five layers and a damage and a core zone. The whole model is a box with $12 \text{ km} \times 7 \text{ km} \times 3.5 \text{ km}$ extension in x, y, and z directions,

respectively. b) A closer view of the mesh size distribution in the adjacency of the injection (red arrow) and production (blue arrow) wells penetrating the damage zone with 250 m width. A 10 m core zone is highlighted in this subplot.

6.3.3 Parametrization

The thermo-hydraulic parameters (cf. Table 9) are based on published reservoir model data from the URG (Q-con GmbH and Deutsche Erdwärme GmbH 2020; Stricker et al. 2020):

Table 9: Parametrization of the geological reservoir model based on (Q-con GmbH and Deutsche Erdwärme GmbH 2020). *Data not given in the model and added under comparison with additional data source (Stricker et al. 2020). ** The fault core was implemented uniformly defined for all geological units as a tight, hydraulic impermeable unit. Data added under comparison with additional data sources (Evans et al. 1997; Stricker et al. 2020).

Layers	Porosity [%]	Permeability [m ²]	Thermal conductivity [W/(m.K)]	Matrix density [kg/m ³]	Specific heat capacity [J/(kg.K)]
Top layer		*7e-14			
Top layer damage zone	4	*2.71e-13	2.5	2400	730
Keuper		5.42e-16			
Keuper Damage zone	4	2.71e-15	2.5	2400	730
Muschelkalk		1.29e-15			
Muschelkalk Damage zone	3	6.46e-15	2	2400	730
Upper Buntsandstein		2.3e-15			
Upper Buntsandstein damage zone	9	1.15e-14	3	2300	710
Buntsandstein (reservoir)		2.3e-15			
Reservoir damage zone	9	1.21e-13	3	2300	710
Basement		3.45e-18			
Basement damage zone	0.5	1.73e-17	3.4	2600	900
Core zone	**0.5	**3.45e-18	**2.5	**2400	**730

The fluid viscosity (0.00025 Pa·s) and density (1030 kg/m³) were defined for a fluid with a salinity of 150 g/L (comparable to the salinities in the URG) and the reservoir temperature based on literature data (Francke and Thorade 2010), solute diffusion was taken from tracer models in the URG (4e⁻¹⁰) (Egert et al. 2020). The Li content is implemented as a solute representing a conservative tracer with an initial value of 100 % in the fault zone and reservoir layer. Quantification of the Li production with the simulation results is later fulfilled by multiplying the output parameters of the solute dilution with Li concentrations between 160

and 200 mg/L as measured in reservoirs of the Upper Rhine Graben (Sanjuan et al. 2022). For the initial pressure conditions a function for the hydrostatic pressure is implemented, calculating a linear pressure increase as a function of depth. For the temperature also a depth-dependent temperature gradient was applied and calibrated so that the production well has the URG typical production temperature of 160 °C (Sanjuan et al. 2016a). The flow rate was set to 80 kg/s at both wells according to existing plants in the URG (Dilger et al. 2021) and a lifetime of 30 years is projected.

For giving an outlook on the economics of future Li production in comparison to conventional geothermal heat extraction, a simplified scenario for energy output was calculated. For the specific heat capacity a representative value for saline brines of 3600 J/kg·K was assumed (Ramalingam and Arumugam 2012; Toner and Catling 2017). Further, an availability of 90 % (as for the Li extraction) of the plant and an efficiency of 90 % for the heat transfer, as reported for geothermal heating plants (Schneider 2023), was assumed. The heat production was calculated based on the difference between the injection temperature (65 °C) and the temperature signal from the production well of the reference scenario as well as its mass flow.

6.3.4 Numerical Modeling

The thermo-hydro-chemical coupled simulations are performed using the finite element (FE) open-source application TIGER (THMC simulator for GEoscientific Research) (Egert et al. 2020; Gholami Korzani et al. 2020). The code is based on the MOOSE (Multiphysics Object-Oriented Simulation Environment) framework (Permann et al. 2020) and has been previously successfully applied to multi-physical and multi-dimensional problems in geothermal reservoirs and wellbores (Egert et al. 2021; Stricker et al. 2020; Yan et al. 2022).

6.3.5 Governing Equations

The approach solves the flow of reservoir brines coupled with the solute transport and heat in the geothermal reservoir and damage zone. It assumes a Representative Elementary Volume (REV) for the porous media where interaction between the coupled processes and the liquid and solid phases can occur. The hydraulic field is solved for the pore pressure and using the balance of mass and momentum (Eq. 1 and Eq. 2)(Bear 1972):

$$bS \frac{\partial P}{\partial t} + \nabla \cdot b\mathbf{q} = Q \tag{Eq. 1}$$

$$\mathbf{q} = \frac{k}{\mu_f} (-\nabla P + \rho_f \mathbf{g}) \tag{Eq. 2}$$

where S is the mixture-specific storage [1/m]; P is the pore pressure [Pa]; t is the time [s]; Q is the source term for injection/production [kg/s]; \mathbf{q} is the fluid or Darcy velocity vector [m/s]; k is the permeability tensor [m²]; μ_f is the brine dynamic viscosity and combined known as the mobility term [Pa·s]; ρ_f is the brine density [kg/m³]; \mathbf{g} is the gravitational vector [m/s²] and b is a scale factor [-] for considering missing dimensions in lower-dimensional elements like fractures (2D) and wells (1D).

The non-reactive transport of Li and other dissolved minerals (Eq. 3.1), as well as heat (Eq. 3.2), is described by the well-known advection(-dispersion)-diffusion-equation (Bear 1972) and assumes thermal/concentration equilibrium between the liquid and solid phases:

$$b \frac{\varphi \partial C}{\partial t} + b(-\nabla \cdot D \nabla C + q \nabla \cdot C) = Q \quad \text{Eq. 3.1}$$

$$b \rho C_p \frac{\partial T}{\partial t} + b(-\nabla \cdot \lambda \nabla T + (\rho C_p)_f q \nabla \cdot T) = Q \quad \text{Eq. 3.2}$$

where C is the Li/solute concentration [-]; φ is the porosity [-]; D is the sum of molecular diffusion and dispersion [m^2/s] (Dashti et al. 2023). ρC_p and λ are the heat capacity [J/K] and thermal conductivity [$\text{W}/\text{m}\cdot\text{K}$] of the mixture, respectively. $(\rho C_p)_f$ represents the heat capacity of the fluid.

According to equations 3.1 and 3.2, the dissolved Li is moving by advection due to the brine flow and along this fluid propagation front, it mixes diffusively following the concentration gradient. The open-hole section of the borehole is included as a lower-dimensional feature sharing edges with the reservoir and representing the zone of active hydraulic connection to the reservoir. The flow rates are implemented as Dirac kernels on top of the open-hole section for injection and extraction. On the margins of the model function Dirichlet boundary conditions are applied for temperature and pressure.

A reactive Li recharge or discharge (source or sink term) by water-rock interaction is not implemented in the model.

6.3.6 Model Scenarios

Different model scenarios are calculated to assess the sensitivity of operational parameters on the Li output (Table 10). The impact of extraction efficiency and flow rate were evaluated in separate simulations. Values for the extraction efficiency are varied based on the technological comparison (55, 75, and 95 %) of prototype results in the intended environment (Goldberg et al. 2022a) (see Chapter 6.2.3). For the flow rate data covering the range of existing projects as well as predicted higher flow rates of future projects were used (60, 80, and 100 L/s) (Dilger et al. 2021; Q-con GmbH and Deutsche Erdwärme GmbH 2020; Vulcan Energy 2023). The sensitivity of the Li concentration is done by multiplying the solute output as a fraction of 100 % from the reference case with varying Li concentration in the range of values measured in the URG (160, 180, and 200 mg/L) (Sanjuan et al. 2022).

Table 10: Parameter variation for the sensitivity analysis and their relative change in comparison to the reference scenario.

Model name	Extraction efficiency [%]	Flowrate [kg/s]	Li concentration [mg/s]
Reference Model	75	80	180
55% Ex	55 (-27 %)	80	180
95% Ex	95 (+27 %)	80	180
60 L/s	75	60 (-25 %)	180
100 L/s	75	100 (+25 %)	180
160 mg/L	75	80	160 (-11 %)
200 mg/L	75	80	200 (+11 %)

6.4 Results

The maximum overpressure at the injection well shows 17 bars for the reference scenario (80 L/s) and 14 and 21 bar for 60 and 100 L/s (Figure 25b). As expected, the pressure has a strong flow rate dependence and is in the order of magnitude measured at hydraulic tests in the Upper Rhine Graben at similar flow rates (Baujard et al. 2017). Regarding the temperature, we see in all 3 scenarios initially a heating up at the production well, caused by water being drawn in from deeper reservoir domains being hotter due to the geothermal gradient. After reaching the aquitard at the bottom layer, the withdrawal propagates also more upward along the fault zone causing a slight temperature decrease below the initial temperature after 2 years due to the influence of water intrusion from more shallow and subsequently cooler domains. Following this time step, the temperature is stable for two decades in all scenarios. After 22 years we can see a clear thermal breakthrough in the 100 L/s scenario with the arrival of the injection-related cold temperature signal at the production well. Also, in the 80 L/s scenario, a slight hydraulic breakthrough is observable at the end of the observational period of 30 years, while the 60 L/s remains stable (Figure 25a). The temperature models are in good agreement with typical projected geothermal plant lifetimes of 20-30 years (Bauer et al. 2014; Egert et al. 2021; Held et al. 2014) in which no breakthrough of the injection temperature should occur. The calculation of heat output of the reference scenario derives a thermal capacity of 21-22 MW_t, which is a typical value for a plant of this size.

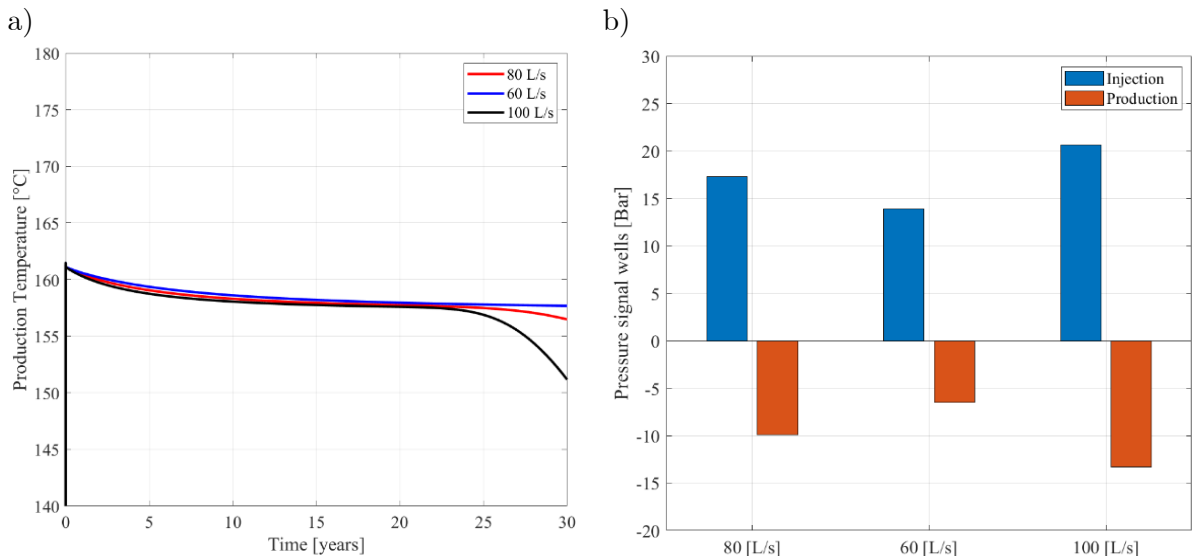


Figure 25: a) Temperature change over time at the production well at different flow rates. b) Maximum pressure changes at the injection and production well after 30 years.

If we compare the propagation of the temperature and the solute (representing the Li concentration) drawdown (Figure 26) it becomes apparent, that the solute is faster propagating than the temperature signal. Both signals propagate along the damage zone in the reservoir layer following the pressure gradient between the injection and the production well but the solute is showing a lower diffusion rate in comparison to the temperature. The damage zones between both wells are almost totally depleted in solute in the reference scenario after 30 years (Figure 26b). Also in the opposite lateral extension, the Li depletion signal propagates up to 2000 m along the fault zone. In comparison, the temperature signal (Figure 26a) just arrives

at the end of the observational period at the production well. Also in the other direction, the temperature shows a far lower extension of just 1000 m lateral propagation along the fault zone. Especially in the temperature signal, the sealing effect of the fault core is further observable. Further, due to the impermeable parametrization of the bottom layer vertical propagation of temperature and solute occur mainly upward.

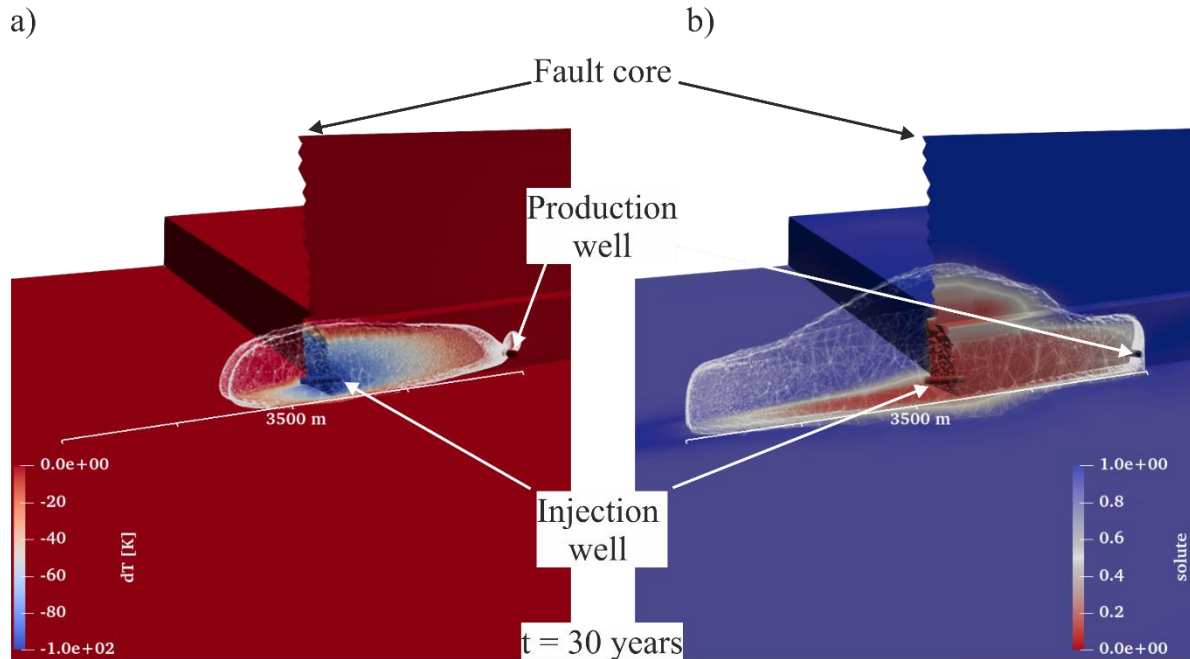


Figure 26: a) Temperature change around the injection well along the fault zone after 30 years in the reference scenario. For clarity, only parts of the fault, the reservoir, and the bottom layer are displayed. The white contour shows the propagation of a temperature drop of -5 K. b) Solute distribution around the injection well along the fault zone after 30 years in the reference scenario. For clarity, only parts of the fault, the reservoir, and the bottom layer are displayed. The white contour shows the spread of a residual solute concentration of 10%.

In the first 5 years, there is only a minor solute concentration decrease at the production well (Figure 27) for all scenarios. After this period, the solute developments start to vary strongly. A decrease by 5 %, for example, arrives firstly in the 100 L/s scenario already after 6 years, in the reference scenario after 7 years, and with 60 L/s after 9 years. For the first 13 – 16 years, the flow rate shows the largest influence of the solute concentration. Thereafter, the 95% Ex and the 55 % Ex scenario form the margins of the predictions of solute development. The flow rate has a larger influence on the slope of the breakthrough front but in the long run, the extraction efficiency shows a larger influence on the concentration. In the reference scenario, 57 % residual solute concentration is predicted at the production well after 30 years. The 95% Ex scenario draws down to 50 %, the 55 % Ex scenario stabilizes at 65 %. The variation of the flow rate by 25 % from the reference scenario causes for the final solute concentration a relative change of 5 %. The extraction efficiency variation of 27 % causes in the 55% Ex scenario a 14 % relatively higher value and in the 95 % scenario a 12 % relatively lower concentration in comparison to the reference case.

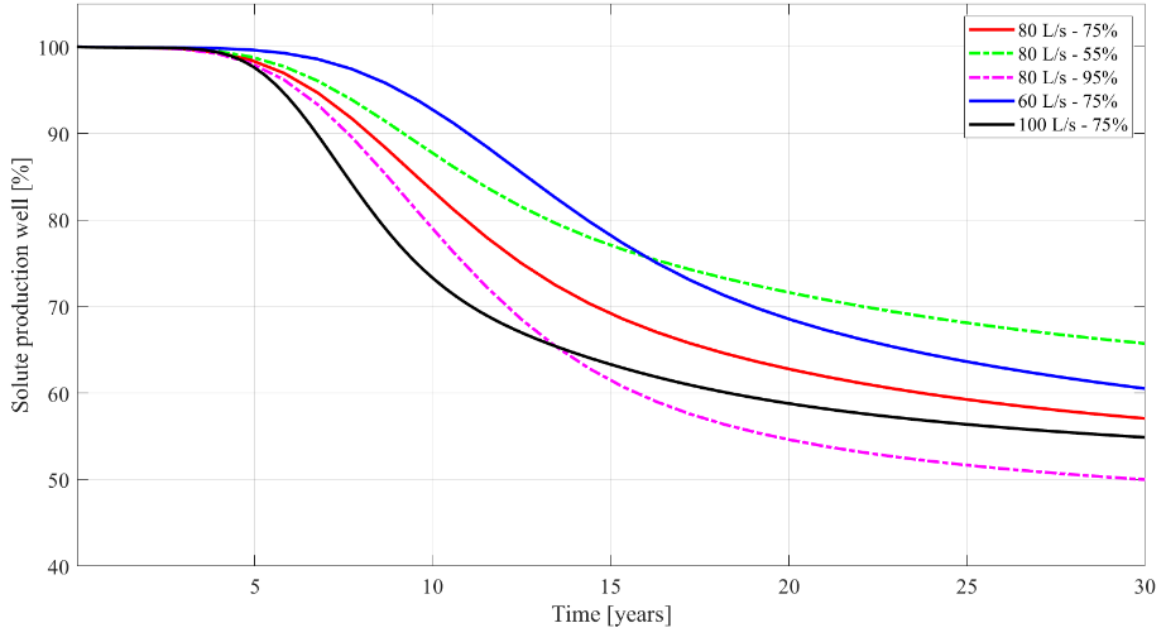


Figure 27: Development of the solute concentration at the production well over time for different flow rates and extraction efficiencies.

6.5 Discussion

For making the numerical results comparable the Li productivity and the accumulated producible Li amount were computed (cf. Table 11, Figure 28). For calculating the productivity Eq. 4 (Goldberg et al. 2022b) was applied.

$$m = Q \cdot A \cdot c \cdot q_Q \cdot \varepsilon \quad \text{Eq. 4}$$

$$m = \text{Li mass} \left[\frac{t}{a} \right]$$

$$Q = \text{Flow rate} \left[\frac{L}{s} \right]: \text{Model specific}$$

$$A = \text{Availability}: \text{Assumption } 90\% \text{ (329 days) (Faltlhauser 2016; Uhde 2021)}$$

$$c = \text{Lithium concentration} \left[\frac{mg}{L} \right]: \text{Input from numerical model and scenarios}$$

$$q_Q = \text{Exploitable partial flow rate}: \text{Assumption } 100\% \text{ (Faltlhauser 2016; Uhde 2021)}$$

$$\varepsilon = \text{Extraction efficiency}: \text{Model specific}$$

The numerical model gives as an output the solute concentration of the production well in terms of the scenario analysis for flow rate and extraction efficiency. For all time steps, the difference between the solute concentration at the production and the following injection is taken from the model as the function of the residual Li concentration and the extraction efficiency at the production. The solute difference is then multiplied with the different initial concentrations from the scenarios, the flow, and the availability and is integrated over time and normed to tons per year (Figure 28a). Beyond the reference concentration of 180 mg/L, the influence of Li concentration differences in the reservoir was analyzed by using the

numerical output from the reference scenario and two alternative concentrations (160 mg/L and 200 mg/L).

At the initial period, all scenarios show the same Li output as the shear static estimation of a function of flow rate, availability, extraction efficiency, and the initially measured Li concentration as previous calculations (Goldberg et al. 2022b). All parameters are linear factors in the productivity function (Table 11). The reference scenario shows an initial productivity of 307 t per year, and all parameters influence linearly with their initial variation from the extraction scenarios (see Table 10 and Table 11). At the time steps where the solute is reducing the dynamics and importance of the simulation becomes apparent as the productivity is consequently decreasing. With the stronger Li dilution in the 95 % Ex scenario after 13 years the 100 L/s scenario becomes the most productive one until the end of the observation period. On the opposite, the performance of the 60 L/s scenario becomes overtaken by the 55% Ex scenario with the higher flow rate. While extraction efficiency shows the strongest influence on solute development, the flow rate has the highest influence on productivity. The initial productivity of the reference scenario decreases over time from 307 – 175 t/a Li (1630 – 930 t/a LCE) by 43 %. The strongest decrease in productivity comes from the 95 % scenario with 50 %. The importance of the flow rate as a function of the reservoir connection becomes also apparent if we compare the 160 mg/L (80 L/s) scenario with the 60 L/s (180 mg/L) scenario. Over the whole observational period, the “lower quality brine” scenario with 160 mg/L scenario shows better performance than the “low flow” scenario with 60 L/s.

The accumulation of the produced Li over time (Figure 28) shows a similar tendency. The highest amount of Li is also produced in the 100 L/s scenario, slightly more than in the 95 % Ex scenario. The head start of the “high extraction” scenario is just caught up at the end of the observational period. In a longer observation period, this difference would become larger. Again, it is shown that within the reported range of values for flow rates, Li concentrations, and extractions efficiencies, the Li concentration in the reservoir shows the lowest influence on the raw material output.

Over the observational period, the reference scenario produces 6,920 t Li (36,834 t LCE). The higher extraction efficiency and flow rate cause in the end 18 % higher output of 8,150 t Li while the lowering of both parameters at the same quantity causes a decrease by 20 %. The results show that the output is not increasing linearly with the improvement of the technical parameters (flow rate and extraction) but approaching a limited value.

From a technological point of view high extraction scenarios are very challenging, causing higher retention times of the brine on the surface or higher material demand and accordingly higher operational costs (Goldberg et al. 2022a). With higher flow rates, better results are achieved in the long run and thus emphasize investing initially in reservoir exploitation rather than trying to increase the last percentage points of extraction efficiency. Moreover, these investments would also influence positively the energy output. Since existing wells showed the best-case flow rates of 70–80 L/s, the biggest lever for enhancing Li output is the number of wells.

Table 11: Results of the different simulation scenarios and their relative influence on Li production parameters on the reference scenario.

Model name	Initial Productivity [t/a]	Final Productivity [t/a]	Accumulated Li Production [t]	Mean Output over 30 years [t/a]
Reference Model	307	175	6920	234
55% Ex	225 (-27 %)	148 (-15 %)	5465 (-21 %)	185 (-21 %)
95% Ex	388 (+27 %)	194 (+11 %)	8148 (+18 %)	275 (+18 %)
60 L/s	230 (-25 %)	139 (-21 %)	5554 (-20 %)	188 (-20 %)
100 L/s	383 (+25 %)	210 (+20 %)	8150 (+18 %)	275 (+18 %)
160 mg/L	272 (-11 %)	156 (-11 %)	6151 (-11 %)	208 (-11 %)
200 mg/L	340 (+11 %)	195 (+11 %)	7689 (+11 %)	260 (+11 %)

A large uncertainty, which so far is not considered in the model, is a Li recharge from the rocks to the reinjected Li-depleted brine. Alteration experiments with 2- molal NaCl-solution at 200 °C and granites from the Schwarzwald as URG reservoir analog, showed a Li release of up to 3 mg/L after 36 days (Drüppel et al. 2020). This implements, that there will be a Li recharge to some certain amount but since there are no time-resolved data it cannot be anticipated how large a transient recharge will affect the results in approx. 5 years from injection to the first arrival of the chemical signal at the production well. In addition, in comparison to the alteration experiments, the reinjection brine is not Li-free but remains at a Li concentration of 45 mg/L in the reference scenario with 75 % extraction efficiency and 180 mg/L Li initially. Considering also the highly complex genesis of the initial waters, the uncertainties were considered too large for implementing a recharge function in the model based on the current knowledge.

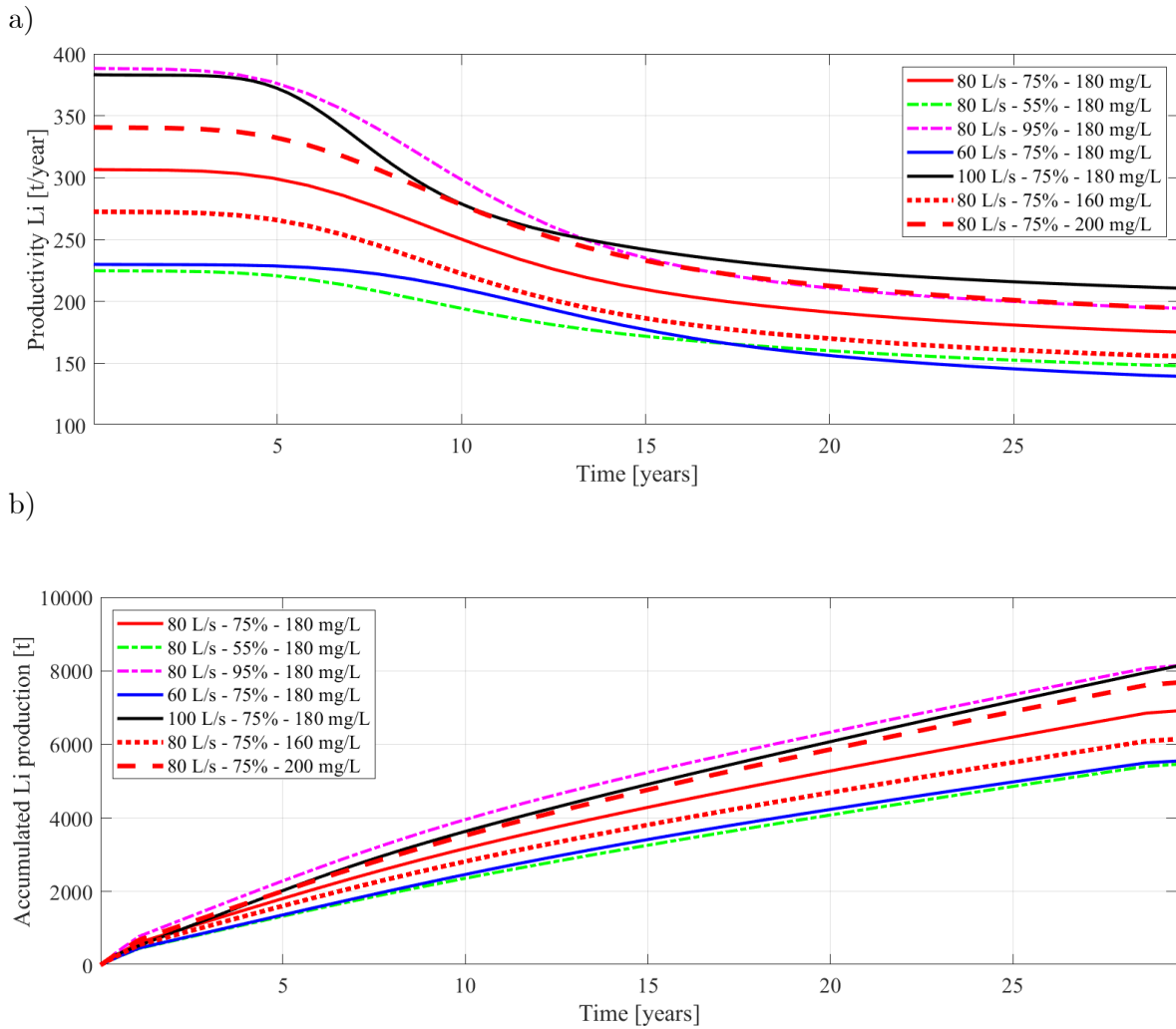


Figure 28: a) Productivity of the different scenarios in [t/year]. For all scenarios, the specific product, the amount of extracted Li, was calculated based on the solute concentration for each timestep and normed to one year. b) Accumulated Li₂CO₃ production over time. Based on the productivity and the differences in the timesteps the accumulated Li₂CO₃ production was determined.

Along with this, the uncertainties related to the reservoir itself pose the largest dependencies. Faults between the two wells as e.g. given in Bruchsal (Vidal and Genter 2018), or a connection of the fault into the crystalline basement could tremendously delay a solute breakthrough. Further, the presented models favor a strong fluid flow along the fault due to the permeability contrast between the matrix and the fault. A more homogenous permeability distribution in the reservoir would most likely also delay or weaken a Li breakthrough (Ghergut et al. 2023). Nevertheless, with the temperature breakthrough after 30 years and pressure signals comparable to existing URG plants, the model is plausible from a geothermal energy point of view but with the absence of Li recharge and the circulation of the brine on the same fault, maybe conservative from a Li extraction point of view. However, even in this scenario, a Li production over 30 years is possible without a total depletion of the resource. In comparison to the static model of constant Li concentration, flow rate, and extraction efficiency (Goldberg et al. 2022b) the mean output of the reference scenario over 30 years is lowered by 24 % (from 307 to 234 t/a Li) due to the decreasing Li concentration over time.

Comparing the new Li resource with other metal resources, show that the depletion or concentration decrease is common in raw material projects. Copper mines for instance,

independent if they have high or low ore grades, show a decrease in the ore grades over the years. A comparing study of 25 copper mines shows an average copper ore grade decrease of 25 % within ten years but also decreases up to 60 % in just 6 years are observed (Calvo et al. 2016).

Also, fluid-type deposits such as oil fields show similar behaviors. A ramping up of the production is followed by a plateau of constant oil output, followed by a long decline period down to the economic limit of production. However, the mechanisms in this sector are different. In the case of oil deposits, two different immiscible fluids (water and oil) are present. The depletion of the oil content can thus be compensated by an enhanced water injection. This leads to the observation that the decline in raw material concentration is quite early observable while the decline in daily oil production comes delayed due to the increase of the water cut. This enhancing method is not transferable to the geothermal sector, since here the raw material is dissolved in the water and thus adding more water would only dilute the concentration. The timeframe of reaching peak oil production after 7-10 years followed by declining production is similar to the presented Li depletion model (Höök et al. 2014a). Although the time frame is similar, the decline rates can be steeper. Within 10 years after the peak production, the daily output was observed to decrease up to 50 – 80 % for fields in the U.S. or Denmark. (Höök et al. 2014b). Important aspects for improving the reservoir behavior are the field size, number of wells, enhancing methods, and the initial oil in place. For maintaining or improving a future Li output these aspects should be transferred to the combined geothermal energy and Li production. For upcoming projects, concepts should be developed for a Li in place determination, enhanced Li recovery methods as well as sustainable multi-well field development. Also, in terms of multi-well field development, the value of the presented study becomes apparent. The outreach of the Li propagation signal (Figure 26b) indicates a reasonable distance if, for example, multiple wells should target one fault zone. Considering the chemical outreach of 2000 m a proper safety distance to a next doublet system should be ensured.

Transferring these aspects of established raw material processes to the new potential raw material resources of geothermal brines different aspects become apparent. The Li depletion has to be taken into account for economic consideration but is by no means a show-stopper for this promising raw material extraction approach but shows that with the experience from the known extraction industries, meaningful project life cycles can be developed. A large benefit in comparison is that the combined geothermal energy and raw material extraction have moreover the advantage of additional energy output over the whole raw material extraction period.

For comparing the economic potentials of the “products” energy and Li the determined capacity of 22 MW_t was compared to the Li productivity. For deriving the economic value of the energy output, the produced energy over time for the specific capacities was calculated and multiplied with historical mean annual low (6,88 ct/kWh - 2005) and high (12,95 ct/kWh - 2022) prices for district heating in Germany (Destatis 2023). The prices were normed to US\$ (1€=1.06 US\$ 16.03.2023) making it comparable to the Li value (Figure 29). For simplified Li value estimations, the accumulated Li production of the reference scenario was calculated into LCE and multiplied with the current price predictions for Li in the future of 26,200 US\$/t LCE and 61,500 US\$/t LCE (Steiger et al. 2022).

The consideration only displays the simplified economic value of theoretically producible Li and heat, without considering any production costs. It only demonstrates the high economic potential that Li bears, despite the decrease in Li productivity over time. Even in the worst price scenario, Li derives a value of 1000 Mio. US\$ over 30 years, exceeding the economic value of the scenario with the highest energy prices of 800 Mio. US\$ by 20%. Whether it will be more profitable is a question of technical feasibility, but the sheer economic value of the mineral offers great potential for the economics of geothermal energy and the domestic raw material sector.

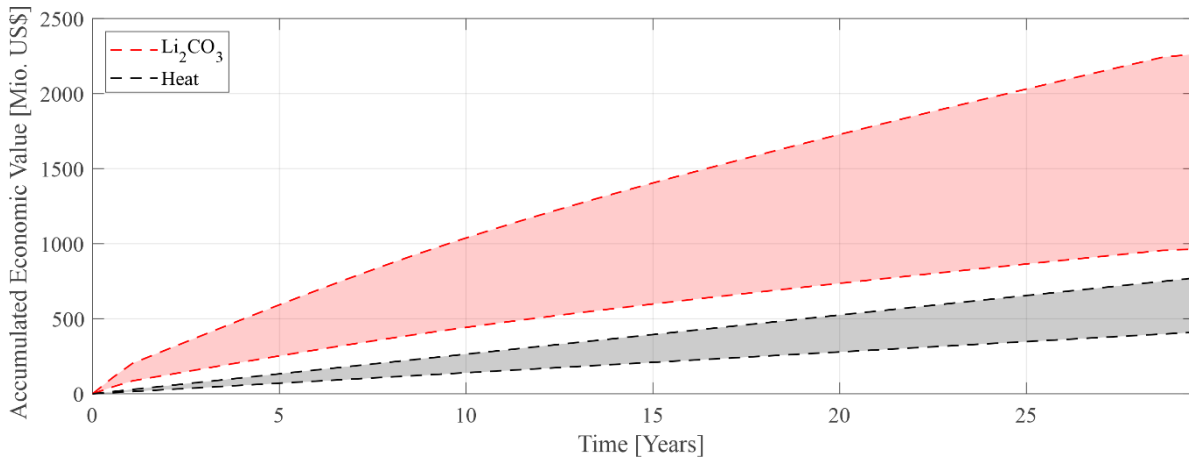


Figure 29: Predicted economic values of the products heat and Li_2CO_3 . Reference Li extraction scenario with 80 L/s, 180 mg/L Li initially and an extraction Efficiency of 75 % and Li_2CO_3 prices between 26,200 US\$/t and 61,500 US\$/t. Heat extraction scenario from the same model for an initial temperature at the production well of 160 °C, reinjection temperature of 65 °C and 90 % efficiency at direct heat use with market prices between 6.88 ct/kWh and 12.95 ct/kWh.

6.6 Conclusions

The Li market situation will become more and more acute globally during the next decade. Europe and Germany in particular are plunging into new dependencies on international imports with the planned ramp-up of their battery industry without having significant Li production. Considering the importance of battery supply for the automotive sector, this has to be seen as critical. Raw material supply must be long-time secured for keeping the industry crisis-proof and internationally competitive. Li extraction from geothermal brines could contribute to partial independence from the global market and could help to balance out price fluctuations. Yet transient reservoir analysis of continuous combined energy and Li extraction were missing.

For analyzing the influences on long-term productivity, this study presents the first 3D numerical reservoir case study based on geological features and geothermal production data from the URG. The geothermal model setup represents a typical non-magmatic extensional system. Therefore, the findings in the fluid behavior do not just apply to the URG but could also be transferred to other geothermal regions with similar settings.

In the generic model, the temperature development just shows a clear breakthrough after 25 years in the 100 L/s scenario and a beginning breakthrough after 30 years in the 80 L/s scenario. Regarding the raw material output, the formulated hypothesis of a chemical Li

breakthrough is confirmed in all scenarios under the given model assumption. The breakthrough occurs between 5-10 years causing a decrease in Li output over time, lowering the Li output up to 50 %. In comparison to previous static scenarios based just on flow rate and a fixed Li concentration, the mean Li output is 24 % lower in the given simulation. In terms of productivity, it is pointed out, that higher flow rates are more decisive than higher initial Li concentrations. That raises the attention to detailed exploration for finding highly permeable structures as well as the necessity of more geothermal wells for enhancing resource availability. For improving the predictions on the long-term behavior, the research about the Li origin will be crucial as well as analyzing Li recharge from the reservoir or recharge enhancing methods.

However, even without Li recharge and despite the chemical breakthrough it is demonstrated, that under the given model parameters, the production of Li from a geothermal reservoir can be possible in the long term additionally to constant energy production over 30 years. A mean output of 234 t Li, as in the reference scenario, could provide Li for about 17,000 – 23,000 electric vehicles per year (considering a Li demand of 10-14 kg per battery (Xu et al. 2020)). With this output, 30 – 220 geothermal doublets (60 – 440 wells) of this quality would be necessary for covering the whole predicted Li demand for Germany (7,000 – 51,000 t/a (DERA 2021a; Fraunhofer ISI 2022)). At small or intermediate market developments a coverage of large market shares with local Li could be achieved providing 0.5 – 3 % of market coverage with every doublet system of the given mean production per year. Every project potentially leads to more independence from global imports for this key element for electrification and by the co-production of geothermal energy also to more independency from imports of energy raw materials. If the upscaling of the extraction process is successful in terms of technical and economic feasibility, the resulting economic value of the accumulated LCE after 30 years, ranges between 1 – 2.3 billion US\$. This additional value could significantly improve the economics of geothermal plant and could be a pull factor for investments in this renewable energy technology.

To be able to investigate the long-term behavior, closely monitored long-term extraction tests on large volume flows within operating geothermal power plants are now needed. It became apparent that this new approach has indeed similarities with established raw material productions, but for a reasonable characterization and use of these resources, new approaches as presented in this study, are necessary along the whole value chain. Only then the potential of a combined heat and raw material production from thermal fluids can be finally evaluated for Li, but potentially also for other dissolved elements.

6.7 Acknowledgments

The authors would like to thank the Helmholtz Association for research funding within the Geenergy subtopic in the MTET (Materials and Technologies for the Energy Transition) program of the Energy research field. Further, the BMBF (Federal Ministry of Education and Research) is thanked for funding the BrineMine project (Grant Number 033R190B) in the Client II framework. We would also like to thank Prof. Bastian Welsch from the University of Applied Sciences Bochum for fruitful discussions and a lively exchange of ideas. Further, we

want to thank the GDMB Society of Metallurgists and Miners for enabling a brought discussion about this study. This paper is an extended and revised version of our paper published in the Proceedings of the European Metallurgical Conference 2023, Düsseldorf, Deutschland, June 11-14 June 2023. Finally, three anonymous reviewers are thanked for improving this manuscript through their intensive and constructive discussion.

7 Development of a continuous silica treatment strategy for metal extraction processes in operating geothermal plants

This manuscript has been published in *Desalination*. 564, 116775 (2023).

Valentin Goldberg^{a,f}, Daniel Winter^b, Fabian Nitschke^a, Sebastian Held^c, Florian Groß^b, Daniel Pfeiffle^d, Jörg Uhde^e, Diego Morata^f, Joachim Koschikowski^b, Thomas Kohl^a

^a Institute of Applied Geosciences, Division Geothermal Energy and Reservoir Technology, Karlsruhe Institute of Technology, Adenauerring 20b, 76131 Karlsruhe, Germany

^b Fraunhofer Institute for Solar Energy Systems ISE, Heidenhofstraße 2, 79110 Freiburg, Germany

^c Formerly at Institute of Applied Geosciences, Division Geothermal Energy and Reservoir Technology, Karlsruhe Institute of Technology, Adenauerring 20b, 76131 Karlsruhe, Germany

^d SolarSpring GmbH, 79114 Freiburg, Germany

^e Stadwerke Speyer, Georg-Peter-Süß-Straße 2, 67346 Speyer

^f Department of Geology and Andean Geothermal Center of Excellence (CEGA). Facultad de Ciencias Físicas y Matemáticas, Universidad de Chile, Plaza Ercilla 803, Santiago, Chile

7.1 Abstract

The extraction of rare metals like lithium (Li) from geothermal fluids is a promising alternative to conventional mining. Membrane distillation (MD) could support energy-efficient fluid treatment enabling further freshwater production. For the operation of geothermal plants and MD uncontrolled precipitation of silica (Si) represents a major hurdle. Herein, we demonstrate the transfer of a Si treatment from lab to field demonstrator scale, tested under conditions of an operating geothermal power plant.

For the treatment, lime precipitation was chosen showing good Si reduction rates using artificial fluids. The high alkaline conditions of this process ($\text{pH} > 10$) in combination with the high salinities of the geothermal brines ($\text{TDS} > 100 \text{ g/L}$) are transferred into real geothermal environment with a newly developed numerical design calculation. The resulting demonstrator consists of three major process steps - 1) Si-reduction, 2) liquid/solid separation, and 3) post-concentration using MD. The Si treatment efficiently reduced 98 % of Si in less than 5 minutes reaction time, without influencing the lithium concentration negatively. The MD resulted in Li concentrations of $\sim 500 \text{ mg/L}$ while producing fresh water. Beyond the approval of the concept, neuralgic points for improvement were identified expanding fundamental knowledge about the material use of geothermal fluids.

7.2 Introduction

7.2.1 Motivation

The energy transition is generating a large demand for non-energy, raw materials used for the generation and storage of energy, but also in the high-tech industry in general. For sustainable energy production, the supply of these strategic raw materials must be secured sustainably along the entire value chain. A potential resource for elements such as lithium (Li), which is recently under consideration, are geothermal fluids in the earth's crust (Goldberg et al. 2022b; Goldberg et al. 2021; Kavanagh et al. 2018; Neupane and Wendt 2017; Paranthaman et al. 2017; Spitzmüller et al. 2021; Stringfellow and Dobson 2021a; Toba et al. 2021). The combined use of geothermal fluids – for energy production and raw material extraction – could derive new possibilities in terms of sustainable energy and raw material production. Due to the special properties of deep geothermal fluids, their processing is still challenging and leads to the requirement of new methods for economical use as an alternative to conventional extractive mining methods.

The hydrochemistry of geothermal fluids is governed by their origin and their history. In particular important for the trace metal content is the water-rock interaction with the reservoir rock which is mainly depending on lithology, temperature, pressure, and the regional flow system in the subsurface (Neupane and Wendt 2017; Stober and Bucher 2015; Stober and Bucher 2012). Depending on the geothermal play type, the reservoir depths are varying between several hundred meters in volcanic geothermal systems and more than 5 km in petro-thermal systems (Stober and Bucher 2012) and can reach temperatures up to 500 °C (Baccarin et al. 2019). These conditions can lead to the enrichment of various strategic chemical elements as e.g. silicon (Si), Li, zinc (Zn), boron (B), cesium (Cs), or antimony (Sb) (Bourcier et al. 2005; Eggeling et al. 2018; Finster et al. 2015; Goldberg et al. 2021; Hauser 1997; Neupane and Wendt 2017; Sanjuan et al. 2016a; Stober and Bucher 2012; Toba et al. 2021). The economic potential of these elements in terms of extraction results from their concentrations in the fluid in combination with the targeted production flow rates (Bourcier et al. 2005; Finster et al. 2015; Goldberg et al. 2022b; Goldberg et al. 2021; Neupane and Wendt 2017). The flow rate of a hydrothermal doublet power plant is ranging between 20 l/s (Egert et al. 2020) and 150 l/s (Stober and Bucher 2012) and can reach up to 500 l/s if numerous wells are combined operating a geothermal field (DiPippo 2015). Other decisive factors are processability and extraction technology (Goldberg et al. 2022a; Goldberg et al. 2022b). The fluids can contain total dissolved solids (TDS) from several mg/L to more than 400 g/l (Neupane and Wendt 2017) as well as dissolved gases (Sanjuan et al. 2016a; Stober and Bucher 2012). Interventions in the chemical equilibrium as cooling, depressurizing, or concentrating change the saturation of different mineral phases within the fluid and can cause mineral scaling (Eggeling et al. 2018; Goldberg et al. 2022a; Nitschke et al. 2014; Stober and Bucher 2012).

In terms of geothermal energy extraction in high enthalpy geothermal fields, silica (SiO₂) scaling in the geothermal power plant or the reinjection well is the most limiting factor for efficiency (Gunnarsson and Arnórsson 2005). Geothermal fluids can contain high silica concentrations since its solubility increases with temperature, e.g. 201 mg/L SiO₂ in Soultz-sous-Forêts in

France or 509 mg/L SiO₂ in the Geysir field in Iceland (Arnórsson et al. 1983; Fournier and Rowe 1966; Gunnarsson and Arnórsson 2005; Sanjuan et al. 2016a; Spitzmüller et al. 2021). This affects major parts of the geothermal industry worldwide with about 16 GW_e installed capacity in high-enthalpy geothermal power plants (Huttrer et al. 2020). The reservoir fluids are assumed to be in equilibrium with quartz, the most common SiO₂ mineral, at reservoir conditions. Cooling of the fluid, as it is intended in the power plant, or an increase of the silica content (e.g. by concentrating) can lead to supersaturation of the fluid with respect to the different SiO₂ minerals following their solubility behavior: quartz, chalcedony, cristobalite and amorphous silica. If the solubility of the most soluble SiO₂ phase (amorphous silica) is reached, precipitation of silica scales can be the consequence (Fournier and Rowe 1966; Gunnarsson and Arnórsson 2005).

Also for water treatment processes using membrane processes, such as membrane distillation (MD), silica fouling is a recovery and efficiency-limiting scalant (Badruzzaman et al. 2011; Mi and Elimelech 2013; Salvador Cob et al. 2014; Zhang et al. 2018). During water treatment processes, the feed fluid is concentrated during the production of pure water permeate. In silica-containing waters, this can lead to super saturation of the feed water with amorphous silica. The uncontrolled precipitation can block the pores of the membranes and reduces their efficiency (Badruzzaman et al. 2011; Mi and Elimelech 2013; Salvador Cob et al. 2014; Zhang et al. 2018). Especially at high salinities, as it is given in geothermal brines in Germany in the Upper Rhine Graben (URG) or the North German Basin ((Regenspurg et al. 2015a; Sanjuan et al. 2022)), the silica solubility is reduced (Marshall and Warakowski 1980b). During the concentration of this kind of brines using membrane processes, precipitation occurs (Lunevich et al. 2016; Zhang et al. 2018) and can thus cause significant flux declines during MD processes (Zhang et al. 2018).

In terms of raw material extraction from brines the scaling potential is further increased by measures for enhancing the efficiency of various technological approaches. Typical measures are concentrating the mineral content in the brine or buffering the fluid at alkaline pH values of 8-11. (Goldberg et al. 2022a; Liu et al. 2019; Ma et al. 2000; Reich et al. 2022; Ryu et al. 2016; Sharma et al. 2016).

The challenges of mineral scaling known from geothermal and water treatment processes like MD as well as expected from the mineral extraction technologies show the necessity of a pre-treatment for paving the way to combined geothermal power, raw material and water production. For this purpose, an interdisciplinary treatment strategy was developed within the framework of the German-Chilean BrineMine Project¹. The project strives for exploring geothermal brines as an alternative technology to conventional extractive mining, as is the case in the Chilean Atacama Desert in terms of Li.

7.2.2 Achievements on Laboratory Scale

One of the most promising regions in Germany for combined energy and raw material production using geothermal brines in Germany, is the URG (Goldberg et al. 2022b; Sanjuan et al. 2022). The fluids of the URG reservoirs are typically supersaturated after cooling with

¹ <https://geothermics.agw.kit.edu/brinemine.php>

several mineral phases (Eggeling et al. 2018; Nitschke et al. 2014; Stober and Bucher 2012). Regarding combined thermal and raw material use a treatment strategy must meet several requirements. It must be implementable within a geothermal power plant cycle, valid in the associated temperature and pressure ranges, environmentally compatible, and finally must not affect the targeted raw materials for extraction. In this study, Li serves as the target and reference material for raw material extraction. Subsequently, the chemical background of the treatment process is displayed as well as the associated thermodynamic requirements for a simulation tool and compared to the results from the field demonstrator.

In general, two major strategies in terms of silica treatment systems are established – specific precipitation and scaling inhibition. Since the silica treatment serves as a pre-treatment for later membrane concentration processes, the method of precipitation was chosen. By reducing silica initially, downstream supersaturating during concentration shall be avoided. Further existing studies showed that inhibition of silica scalings during MD processes can be hindered at high Ca and Mg concentrations as is the case in the study area (Zhang et al. 2018).

In a previous study (Spitzmüller et al. 2021) different methods on their applicability for raw material extraction were compared, the lime precipitation, the caustic precipitation, and the seed-induced precipitation. The methods were evaluated in the laboratory using synthetic and natural fluids. The study revealed two main factors required for successful silica treatment; An increase of the pH value >10 combined with high calcium (Ca) concentrations (molar ratio of $\text{Ca/Si} > 1.25$) (Spitzmüller et al. 2021). An increase in the pH value transfers the dissolved, aqueous silica predominantly into the H_3SiO_4^- species (Eikenberg 1990; Iler 1976). This negatively charged species enhances the adsorption of divalent cations like Ca^{2+} and enhances their agglomeration and can lead to the formation of aqueous Calcium-Silicate-Hydrate (CSH) phases (Gaboriaud et al. 1999; Iler 1976; Maraghechi et al. 2016; Spitzmüller et al. 2021). At high pH values, the CSH phases supersaturate and tend to precipitate (Spitzmüller et al. 2021). CSH phases are amorphous and poorly ordered phases with high variability in their chemistry (Jennings 1986; Richardson 2008). They form a mixed series between amorphous silica (SiO_2) and portlandite (Ca(OH)_2) depending on the ionic strength of the reactants (availability of Si and Ca), the pH value, and the temperature. (Blanc et al. 2010a; Jennings 1986). The effect of this precipitation process is especially known from the hardening process of portland cement (Blanc et al. 2010a; Thomas et al. 2003) but not yet established in the geothermal environment. The previous experiments, showed an effectiveness of 98 % in the reduction of silica, while not affecting the Li content negatively (Spitzmüller et al. 2021).

This study is displaying the fulfilled steps for the successful upscaling of this laboratory scale achievements on a flow-through demonstrator in the intended environment. Beyond silica precipitation, a pre-precipitation at a pH value of 8.3 is evaluated in this study. At \approx pH 8.3 the negatively charged HCO_3^- is the dominant aquatic carbonate species (Bethke 2008; Zarga et al. 2014). Thus, it was evaluated how a pre-treatment at this pH value would influence further silica treatment.

7.3 Material and Methods

7.3.1 Geochemical sampling and analysis

For monitoring the treatment, the hydrochemistry of the geothermal fluid is the decisive variable. Therefore, the fluid was sampled during continuous operation and different parameters were measured in the field. Further, the chemical brine analyses served as the base for the numerical design calculation. During the field operation, fluid temperature and pH values were measured using a compact precision handheld meter (WTW Multi 340i). The bicarbonate (HCO_3^-) concentration of the initial fluid was determined via titration using an alkalinity test kit (Merck MColorTest™). The titration was conducted in the field during the sampling process, which is described in the following paragraph.

For avoiding the contamination of the fluid sample with solids that could potentially dissipate, all fluid samples were filtered with a syringe filter using a cellulose acetate filter ($0.45\ \mu\text{m}$). To avoid precipitation or further reactions after the sampling process, all samples are directly diluted by a factor of 1:10 using distilled water. For measuring trace elements and metallic cations, separate samples, also diluted by a factor of 1:10, were additionally acidified using highly pure (37 %) hydrochloric acid (Hydrochloric acid 37 & AnalR NORAMPUR). The main cations were measured with an inductively coupled plasma optical emission spectrometry (ICP-OES, Varian 715-ES), and the anions were measured via ion chromatography (IC, Metrohm 930 Compact IC Flex). For determining the uncertainty, the limit of detection, and the limit of quantification, standard solutions and blind samples were measured in parallel. The precipitation products were pre-dried in the field using a Büchner Funnel and dried in the oven overnight at 105°C . The dried precipitates were analyzed with X-ray diffraction (XRD, Bruker D8), SEM (Tescan Vega), and EDS (Inca X Act).

7.3.2 Test site: Geothermal power plant Insheim

The prototype testing campaign was conducted at the geothermal power plant Insheim, at that time operated by the Pfalzwerke geofuture GmbH. The plant is located in the Upper Rhine Graben, has an installed capacity of $4.8\ \text{MW}_e$, and could further provide $6\text{-}10\ \text{MW}_t$. The geothermal reservoir is tapped by a doublet system and located at a depth of about 3600 m reaching $165\ ^\circ\text{C}$. The inflow has contributions from several geological units as the granite basement of the Saxothuringian unit, Rotliegend and Buntsandstein, and Muschelkalk (Vidal and Genter 2018). Being in operation since 2012 the Insheim plant is the longest continually producing industrial geothermal project in the Upper Rhine Graben. The geothermal fluid circuit is established by one production and one reinjection well, which are connected to the reservoir, forming a subsurface heat exchanger. At the surface, the heat is transferred via a heat exchanger from the geothermal fluid to an organic rankine cycle. In this second circuit, an organic fluid evaporates in a controlled manner and expands above a turbine in a closed loop, which drives a generator to produce electricity.

The reservoir fluid has a salinity of about $105\ \text{g/l}$ and is characterized as a sodium-chloride (Na-Cl) water type. The coupling point for the prototype was on the cold side of the primary

cycle behind the heat exchanger as schematically shown in Figure 30. For determining the reference chemistry of the fluid and subsequently the effectiveness of the silica treatment, eight untreated samples were taken from the bypass where the prototype was coupled over the period from 22.07.2020 to 18.08.2020. The mean element concentrations of the water samples were defined as reference fluid (see Table 12) and served as the input for the numerical design calculation. The standard deviation shows that the fluid is influenced by fluctuation derived among others from flow rate, environmental temperature, and analytical error.

Table 12: Mean properties of the initial geothermal fluid in the geothermal power plant Insheim. The mean was calculated from 8 untreated water samples, collected over the range of a month. The standard deviation of the analysis is given as σ .

Parameter	Unit	Insheim Inflow $\pm \sigma$
pH	-	5.3 ± 0.19
Temperature	[°C]	57 ± 2.8
TDS	mg/L	105255 ± 3137
Lithium (Li ⁺)	mg/L	164 ± 10.7
Sodium (Na ⁺)	mg/L	28937 ± 1538
Potassium (K ⁺)	mg/L	4290 ± 230
Calcium (Ca ²⁺)	mg/L	7566 ± 359
Magnesium (Mg ²⁺)	mg/L	119 ± 7.4
Silicon (Si)	mg/L	87 ± 8.2
Chloride (Cl ⁻)	mg/L	63692 ± 1479
Sulfate (SO ₄ ²⁻)	mg/L	143 ± 5.4
Bromine (Br ⁻)	mg/L	179 ± 4.2
Fluorine (F ⁻)	mg/L	16 ± 0.09
Bicarbonate (HCO ₃ ⁻)	mg/L	188 ± 11.3

In addition, non-condensable gases (NCG) are present in the fluid, which were not measured during the sampling campaign. The gas:water ratio in geothermal brines in the Upper Rhine Graben can reach at normal conditions up to 1.6:1 (Eggeling et al. 2018). 85 % of the gas phase in Insheim consists of carbon dioxide (CO₂) (Sanjuan et al. 2016a). To avoid the degassing of the NCGs the power plant is operating at a pressure of 20 bar. Beyond the pressure maintenance, further measures from the power plant operator are conducted to avoid unwanted mineral precipitation or corrosion. Prior to the heat exchanger, scaling and corrosion inhibitors are added to the fluid to avoid Ba-Sr sulfate and Pb-Sulfide scaling as they are common in the Upper Rhine Graben geothermal power plants (Eggeling et al. 2018; Nitschke et al. 2014; Scheiber et al. 2019a; Scheiber et al. 2019b). The inhibitors are commercially available products whose exact composition is confidential.

Especially the degassing of CO₂ can influence fluid chemistry since the segregation leads to an increase in the pH value and influences the lime-carbonic acid equilibrium which can lead to scalings. The influence of the degassing was experimentally determined, showing an increase to a pH value of 5.3 to 6.3 if the water is continuously stirred throughout 2.5 h in the reaction tank.

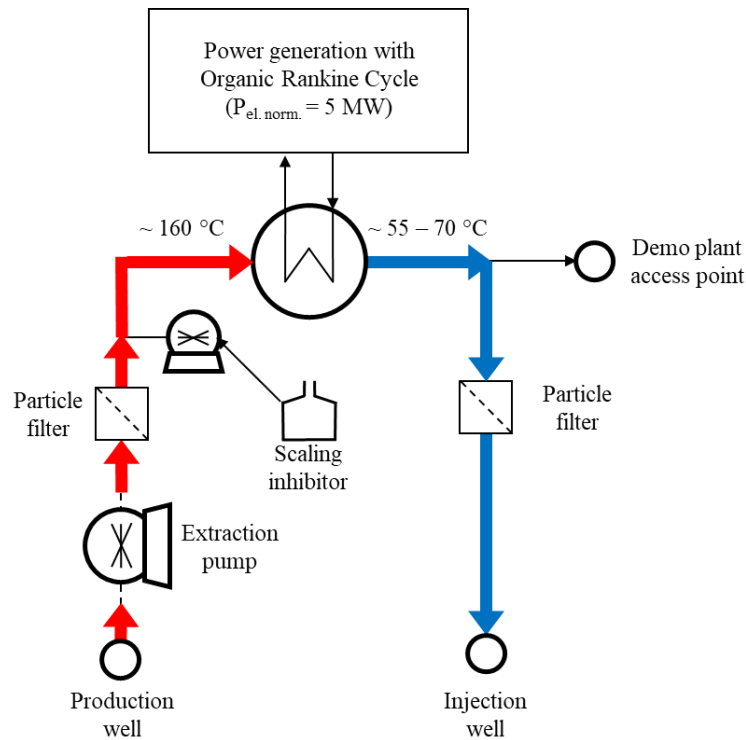


Figure 30: Simplified scheme of the power plant Insheim. The scheme displays the major intervention in the fluid properties and the implementation point of the prototype within the systems.

7.3.3 Performance Parameter

The fluids at the test site are characterized by high contents of total dissolved solids (see Chapter 7.3.2) and high contents of Ca^{2+} ions, which are mandatory for the precipitation process. Subsequently, only sodium hydroxide (NaOH) as a reactant was used to adjust the pH value. The addition of divalent cations, as in the previous laboratory experiments, was not necessary since the initial concentration Ca/Si is already $\gg 1.25$ being sufficient for an effective silica reduction using lime precipitation. For transferring the laboratory experiments to the real-life environment, a numerical design calculation is developed (Chapter 7.3.4). The calculation helps to dimension the prototype as well as predict the chemical parameter sensitivity of the process.

The key performance parameters of the process are defined as follows:

- Si reduction factor:
Comparison of aqueous Si before and after the treatment to quantify the effectiveness of reduction.

$$R_{\text{Si}} = \frac{c_{\text{Si}_{\text{init}}}}{c_{\text{Si}_{\text{final}}}} [\%]$$

- Li loss factor:
Comparison of aqueous Li before and after the treatment to quantify the influence of the treatment on the target element.

$$R_{\text{Li}} = \frac{c_{\text{Li}_{\text{init}}}}{c_{\text{Li}_{\text{final}}}} [\%]$$

Passive performance parameters:

- NaOH material use:
Comparison of the aqueous Na⁺ before and after the treatment for quantifying the NaOH consumption for pH adjustment.
- Ca²⁺ reduction:
Comparison of the aqueous Ca²⁺ before and after the treatment for quantifying the Ca²⁺ consumption during precipitation.

The most relevant operational parameters that are adjusted and reported are:

- Residence time:
The reaction time is the time available for the chemical precipitation to take place and is an important scale for a later industrial application since it is a function of the size of the reaction vessel and the flow rate of the fluid.
- Temperature:
The temperature of the heating jacket of Vessel 2.
- Mixing:
Rotations per Minute of the Stirrers.
- Final pH

7.3.4 Design simulation

The purpose of the design calculation is to apply the chemical treatment process in the first step numerically on the chemistry of the chosen test site. Therefore, the model is based on the chemical and thermodynamic data of the target power plant (Chapter 7.3.2). The resulting information (Chapter 7.5.1) aligned with the defined performance parameters (Chapter 7.3), is validated using published experimental data and served then upscaling the necessary mass flows of the process on the demonstrator scale and the configuration of the reaction vessels. Moreover, a sensitivity analysis was conducted using the numerical tool, to discuss the influence of varying operation parameters and to estimate the economics of the treatment (Chapter 7.6.2). For the numerical design calculation the hydrochemical modeling software PHREEQC (Parkhurst and Appelo 2013), version 3.6.4, was used.

PHREEQC offers the possibility to perform various aqueous geochemical simulations. The basis for the calculation are thermodynamic datasets for the different aqueous models as the PITZER specific-ion-interaction aqueous model or the Specific Ion Interaction Theory (SIT) (Appelo 2015; Hörbrand et al. 2018; Parkhurst and Appelo 2013). The datasets contain mineral phases, aqueous species of dissolved ions, and gas phases for calculating fluid-rock interactions. The applicability in terms of temperature and TDS range or included minerals is variable (Hörbrand et al. 2018). Therefore, before conducting a model calculation, the thermodynamic dataset must be evaluated on its appropriateness for the given hydrochemical system and process (Appelo 2015; Hörbrand et al. 2018).

For calculating the silica treatment process, the relevant parameters, which must be covered by the thermodynamic data, are the relevant mineral phases as well as the temperature and TDS range. In the given case, the important temperature range is the outflow temperature of the cold side of the power plant: > 70°C. The TDS range is defined by the initial salinity of 105 g/L TDS and the saturation limit of the water with respect to NaCl during the

concentration process (approx. 350 g/L). Therefore, a molality range from about 2 to 5 mol/l of NaCl must be covered. Further, the dataset must be valid at a pH range of 5 to 11, to display the treatment process. Four different datasets (PITZER, Thermoddem, ThermoChimie, PSI/NAGRA TDB) are compared to evaluate if and how they can be used for the fluid treatment processes at high salinities and pH values (Table 13).

For the evaluation of the applicability of the datasets to the desired process, experimental laboratory data were collected, covering the described ranges of the given parameters. The laboratory experiments described in the literature were then replicated numerically to evaluate the reliability of the different data sets on the process.

Table 13: Comparison of different thermodynamic datasets for the design calculation.

Data set	Application	Confidence Zone	Activity models	Source
Pitzer.dat Version: PHREEQC 3.6.4	Basic salt solutions in a wide p, T, c range No CSH-Data included	Ionic strength: < 6 mol/kg Temperature: 0 – 200 °C Pressure: 1 – 1000 atm	PITZER interaction model Peng-Robinson equation of state	(Appelo 2015; Hörbrand et al. 2018; Peng and Robinson 1976)
Thermoddem Version: V1.10 Code version 1.07_2.06	Environmental processes Water-rock interaction and pollutant behavior in waste material management	Ionic strength: 0.1– 3 mol/kg Temperature: 10 – 100 °C Pressure: 1 Bar	Benson-Helgeson convention Isocoulombic/isoelectric approach PITZER interaction model Debye-Hückel activity model	(Blanc 2017; Blanc et al. 2012; Blanc et al. 2010b; Blanc et al. 2010a; Hörbrand et al. 2018)
ThermoChimie Version: 10a, 26 th September 2018	Chemical behavior of radionuclides and other pollutants in the nuclear waste repository	Ionic strength: < 10 mol/kg Temperature: 15 – 80 °C pH: 6 -14	Specific Interaction Theory (SIT)	(Colàs et al. 2019; Giffaut et al. 2014; Sipos 2008)
PSI/NAGRA TDB Version: TDB 12/07, last modifications 11 th June 2015	Safety assessment for radioactive waste storage No CSH-Data included	Ionic strength: < 3 mol/kg Temperature: < 350 °C pH: < 12,2		(Thoenen et al. 2014)
PITZER_CSH Compiled of: PITZER PHREEQC 3.6.4 and Thermoddem V1.10 Code version 1.07_2.06	Simulation of CSH – Mineral reaction at high salinities, pH and temperatures		Calculation model as at pitzer.dat CSH-Phases from Thermoddem added Native parameters of Portlandite were exchanged by Portlandite data from Thermoddem	This study

For evaluating the data for silica and carbonate solubility in high saline waters (Figure 31a & b) the simulations with the Pitzer dataset by Appelo (Appelo 2015) were used and expanded to the other datasets. Amorphous silica is equilibrated with waters of different salinities and temperatures within the experimental range (Appelo 2015; Chen and Marshall 1982; Marshall and Warakowski 1980b). The results (Figure 31a) show for 25 °C the best fit to the experimental data by the simulation conducted with the `pitzer.dat`. For 100 °C, the results are similar for Pitzer, Thermochem and ThermoChimie. At the closest data point to the initial values of the experimental water at 1.63 mol/kg, the Pitzer database overestimates the solubility by about 20 % and ThermoChimie with the best fit by about 16 %. At the next closest point of 2.58 mol/kg, Pitzer gives the best fit with an overestimation of 13 %. At higher salinities as 5.82 mol NaCl, the results based on `pitzer.dat` underestimate the solubility while ThermoChimie is giving the best fit. The pH value was not adjusted separately and was not reported for the data from the literature individually. Therefore, the simulated pH values could not be validated for these experiments.

For evaluating the applicability on high saline Ca-containing waters the simulations were compared to experimental data (Appelo 2015; Wolf et al. 1989) over a broad TDS and temperature range (Figure 31b). To a salinity of about 0.5 ‰, all databases give sufficient results. The simulation results show further, that only the Pitzer dataset gives a good agreement to the experimental data representing all tendencies properly.

To predict the solubility of portlandite within the treatment, the simulations equilibrate the mineral phase with different saline solutions at varying temperatures (Figure 31c & e). For determining the influence of a pH value increase, literature data of experiments fulfilling NaOH addition were chosen (Duchesne and Reardon 1995; Kutus et al. 2016). The experiments displayed in Figure 31c, were conducted at a temperature of 25 °C and different initial NaCl concentrations of 0, 1 and 4 mol NaCl. Then NaOH was added, raising the pH value and consequently leading to a further increase of the Na⁺ content. For the experiments, the datasets give all a good performance over the salinity ranges from 0, 1 and 4 mol NaCl. At increasing temperatures (Figure 31e) a weakness in the conventional Pitzer database becomes apparent. While the solubility is decreasing at higher temperatures in the experimental data, the dataset indicates an increase in solubility and thus a false reverse tendency. The substitution of the thermodynamic data in the Pitzer dataset by the data from Thermochem to the new `Pitzer_CSH` dataset gives overall temperature and salinity ranges the best fit compared to the experimental data exceeding the precision of the established datasets.

The solubility behavior for silica, if the pH value is increased with an alkaline calcium hydroxide (CaOH) solution, is displayed in Figure 31d. Experimental data (Greenberg and Chang 1965) were numerically reproduced by equilibrating an aqueous silica phase and a calcium hydroxide solution at various pH values with amorphous silica and a CSH phase. For the Thermochem and `Pitzer_CSH` datasets, the same mineral phase C0.9SH has shown the best fit, for the ThermoChimie dataset CSH0.8. The PSI/NAGRA TDB was not included due to the lack of CSH data. For the initial experiment, a pH value of 7.06 is given resulting in a possible solubility of 0.00165 mol Si and 0.00011 mol of Ca²⁺. At this pH value, `Pitzer_CSH` deviates the most. At the pH value of 10.5, it gives the best results with a deviation of 25 % for Si solubility. At higher pH values the experimental and laboratory results coincide better again.

In general, the solubility behavior is correctly represented by all databases, but especially in a pH range from 9.5 to 10.5, the values deviate for all thermodynamic datasets, with PITZER_CSH giving the best fit.

The compiled PITZER_CSH gives an overall a brought confidence interval in terms of temperature, TDS and pH value for the required mineral phases. Therefore, this dataset was chosen, for making the design simulation.

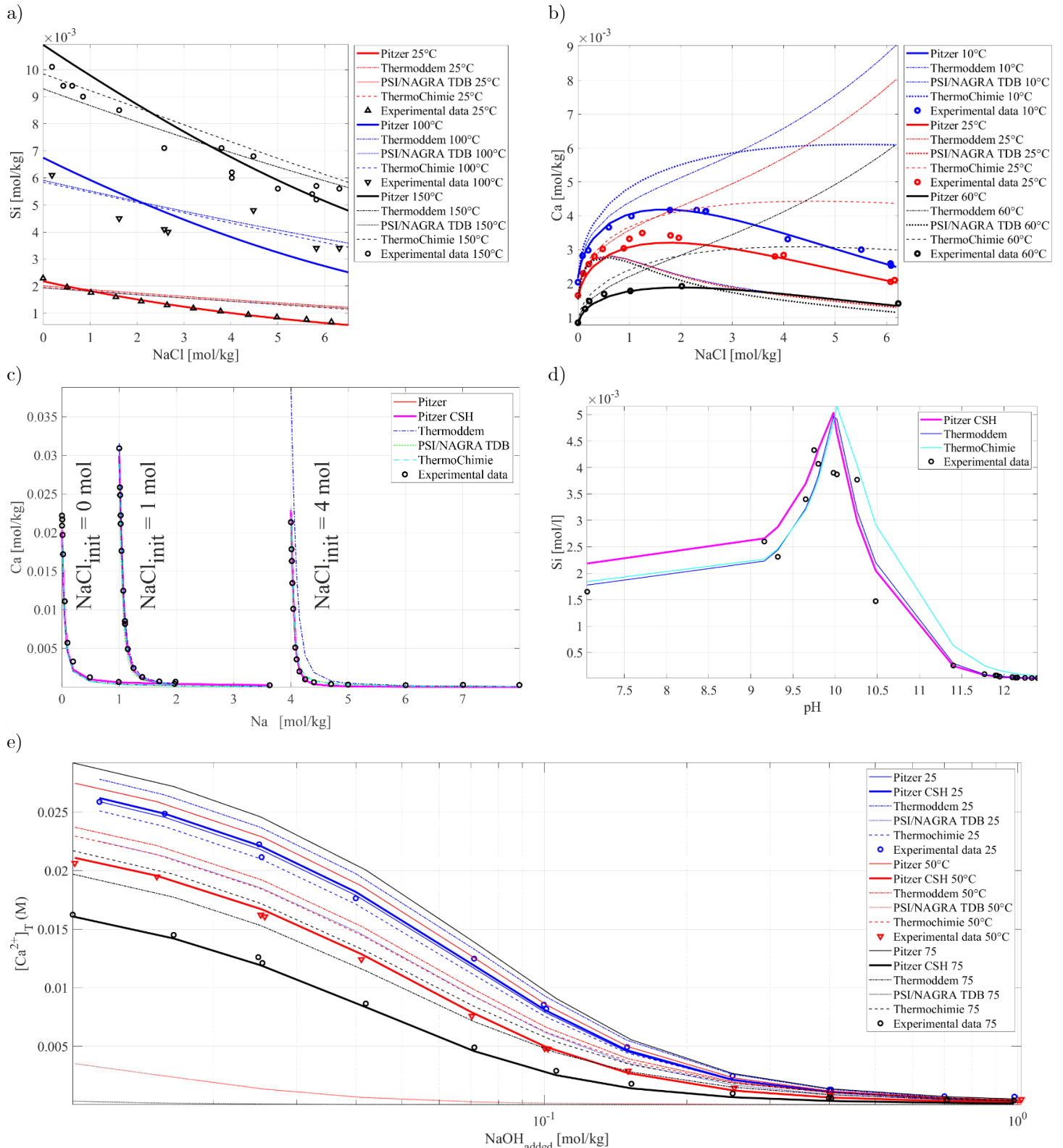


Figure 31: Database validation for the chemical processes of the treatment. The applicability of the thermodynamic data is evaluated with experimental data for temperature, salinity and high pH values for dissolved Ca^{2+} and Si species as well as on CSH phases. a) Simulated solubility of amorphous silica in NaCl waters at different temperatures in comparison to experimental data (Experimental data:(Appelo 2015; Chen and Marshall 1982; Marshall and Warakomski 1980b)). b) Solubility of calcite at different temperatures and NaCl concentrations at a CO_2 partial pressure of 1 kPa (Appelo 2015; Wolf et al. 1989) c) The effect of NaOH addition on aqueous Ca^{2+} in different saline NaCl solutions at 25°C (Experimental data: (Kutus et al. 2016)). d) Solubility relationship of amorphous silica and in aqueous solutions at 25°C under addition of CaOH (Experimental data: (Greenberg and Chang 1965)). e) The effect of NaOH addition on aqueous Ca^{2+} in 1 molar NaCl solutions at 25°C, 50 °C and 75 °C (Experimental data: (Duchesene and Reardon 1995; Kutus et al. 2016)).

7.4 Upscaling continuous Si Precipitation and Fluid Concentration

7.4.1 Technical Set-Up

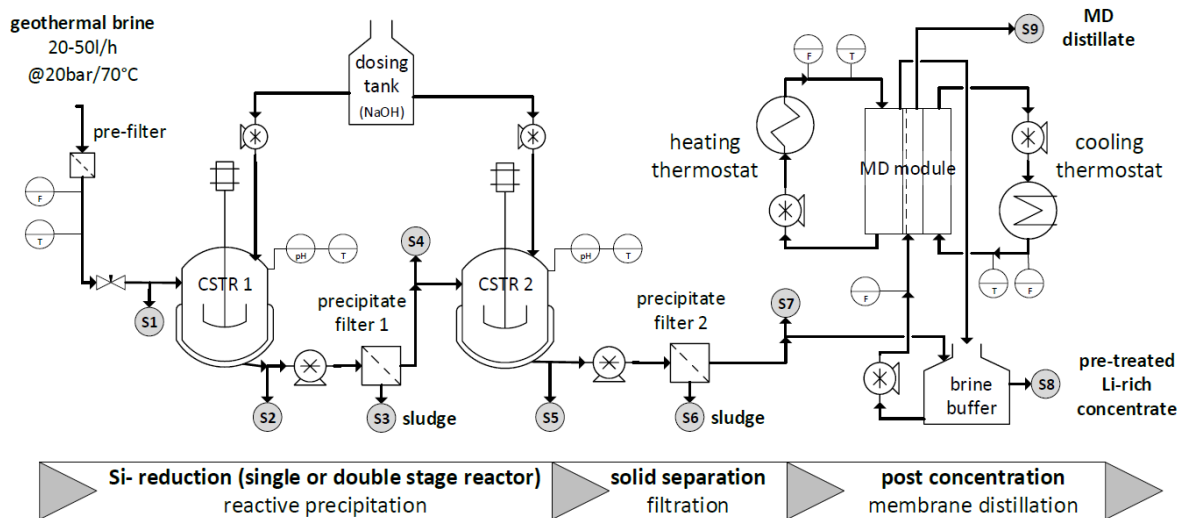


Figure 32: Prototype layout and hydraulic scheme. The hydraulic scheme is separated into three major elements: Si-reduction, solid separation, and post-concentration. Major elements for the chemical treatment are the continuously stirred tank reactors (CSTR). The Plant can be operated for batch experiments and in a continuous flow mode with additional post-concentration. The possible hydrochemical sampling points are incorporated as S1 to S9.

A demonstration plant for continuous operation was developed and built according to the process flow diagram given in Figure 32. The hydraulic schematic represents three major subsequent process steps: Si-reduction, liquid/solid separation, and post-concentration. The demonstrator is hooked up to the pressurized geothermal fluid circuit of the power plant according to the access point shown in Figure 30. At this point, the geothermal fluid has a temperature of about 55-70°C and a pressure of 20 bar. The water flow rate is adjusted in a range of 20-50 L/h by the inlet valve, in which water pressure is relieved to atmospheric level. The flow rate is measured by a magnetic inductive flow indicator, allowing the precise derivation of the residence time in the reactors. The water passes two subsequent continuously stirred tank reactors (CSTR) of 10 L nominal volume. Both reactor vessels incorporate pH and temperature probes that allow an individually controlled dosing of an alkaline reactant, here NaOH. The second reactor (CSTR 2) has a thermostat jacked to limit the heat losses and consequently the temperature drift during operation. An individual precipitate filtration system is installed after each reaction vessel for solid separation and to avoid precipitates to get entrained into subsequent process steps. The filtration media has a nominal pore size of 5µm. The pre-treated fluid goes into a buffer tank.

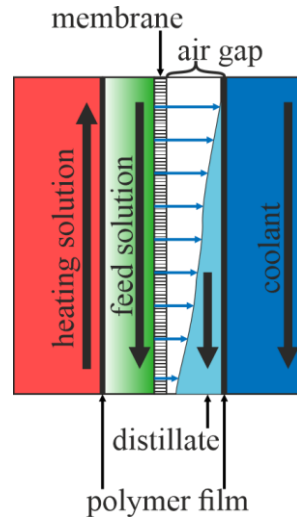


Figure 33: Schematic representation of the FG-AGMD channel configuration (Figure based on (Schwantes et al. 2019))

Following the chemical pre-treatment, the fluid gets concentrated by the evaporative extraction of pure water in a MD system (Winter et al. 2017). Here a plate-and-frame type of air gap MD test module (FG-AGMD) with 4 separate internal hydraulic channels (feed solution, distillate, heating and cooling water) is used (Schwantes et al. 2019). The specifications of the MD module, manufactured by SolarSpring GmbH, are summarized in Table 14. The driving thermal energy is introduced by the heating solution (water), which is separated from the feed by an impermeable polymer film (Figure 33). The feed is heated and water is evaporated through the microporous, hydrophobic membrane, condensing on the cold wall of the impermeable film in the air gap. Forced by gravity, the distillate exits the membrane module on the bottom part. The plate-and-frame arrangement allows easy adaptation of the channel geometry and membrane exchange. Here, for the purpose of scientific demonstration, the heating and cooling water streams are re-circulated through electrically operated thermostats. However, it is worth mentioning that in a potential commercial application, the heat source would be the low-exergy part of the power plant's thermal brine circuit, which perfectly meets the temperature requirements of an MD concentrator.

Table 14: Technical specifications of the FG-AGMD test module.

membrane type	ePTFE on PP scrim backing (L-020A-S (Winter et al. 2013))	
nominal pore size	[μm]	0.2
porosity	[%]	80
membrane thickness	[μm]	70
backing porosity	[%]	50
backing thickness	[μm]	280
membrane surface	[mm^2]	670x330
feed channel width	[mm]	1.0
air gap width	[mm]	2.0
heating and cooling channel width	[mm]	2.0
impermeable film	[μm]	100

The demonstrator includes 9 sampling points, indicated with S1 to S9 that allow a chemical characterization of water and solids in all relevant process steps. The demonstrator on site is shown in Figure 34.



Figure 34: Demonstration plant operated with natural geothermal fluids on-site at power plant Insheim, Upper Rhine Graben, Germany

7.4.2 Operational configurations for the Demonstrator

For the conduction of the here presented experimental field study, the demonstration plant is used in five different operational modes that are described as follows:

Experimental Mode 1: Reference experiment for continuous flow at nominal operational conditions:

Since the chemical equilibrium of thermal fluid changes by the relaxation of the pressure level in the inlet section, where substantial degassing of NCGs occur, and by a shifting temperature during flow-through, a “blank” reference experiment was performed. In this way, the experimental observations of the later tested water treatment strategies can be clearly addressed to those. For the reference experiment, the demonstrator is operated in a double-stage CSTR arrangement at its nominal conditions which are defined by a flow rate of 20 l/h with resulting nominal residence times of 30 min in CSTR 1 and 30 min in CSTR 2; a reactor stirring speed of 300 rpm, no reactant dosing; jacked flushing in CSTR 2 with water at 55°C.

Experimental Mode 2: Continuous operation of silica extraction with a water relaxation stage:

The demonstrator is operated with both CSTR stages. CSTR 1 is acting as a passive relaxation stage without chemical dosing. Fundamentally, CSTR 1 introduced a passive residence time of 30 min allowing proper degassing and equilibration of the fluid after pressure relaxation before the actively induced pH shift to the target pH of 10.5 by NaOH dosing in subsequent CSTR 2, which is operated with a residence time of 30 min.

Experimental Mode 3: Continuous operation of silica extraction with a double-stage precipitation approach:

The demonstrator is operated with both CSTR stages. NaOH dosing is activated in CSTR 1 and CSTR 2. The first precipitation in CSTR 1 is targeted at a pH of 8.3 and a residence time of 30 min. The precipitates are extracted by filtration before the fluid is forwarded to CSTR 2. In CSTR 2 the pH is increased to the final value of 10.5 with a residence time of 30 min. Both reactors are stirred at 300rpm.

Experimental Mode 4: Batch operation of silica extraction with single-stage precipitation - kinetic mode:

For the performance of kinetic experiments, a CSTR is operated in a batch precipitation mode. CSTR 2 is rapidly filled with natural fluid. When completely filled, the pH is adjusted to the desired value by controlled dosing of NaOH under continuous stirring at 300rpm. The CSTR outlet line is closed. Further, the temperature of the heating jacket was adjusted to 55 °C. Frequent sampling of the fluid allows a detailed characterization of the involved reaction kinetics and thus identification of the suitable residence time.

Experimental Mode 5: Operation of MD post-concentrator:

The MD post-concentrator may be operated either directly fed with untreated geothermal fluid from CSTR 1 in non-dosing relaxation mode or with pre-treated fluid from the filtered effluent of CSTR 2 in active precipitation mode. Due to the limited sizing of the MD set-up, the MD post-concentrator is operated in a batch mode to reach substantial concentration factors, recirculating the fluid from the fluid buffer tank. In this study, the heating water was controlled to 70°C, and the cooling water was controlled to 20°C.

7.5 Results

7.5.1 Simulation Results for Prototype System Layout

During conducting the design calculation, 3 potential areas of precipitation in dependency on the pH were defined. Directly after the inlet of the demonstrator, a pH increase due to a pressure relief-induced CO₂ degassing is expected. Further, a two-staged pH-depending treatment, with a first precipitation stage at pH 8 – 9, and the main precipitation at pH values 10-11, defines two more areas (Figure 35).

For the calculations, the chemistry of the reference fluid was used as input data (Table 12). The pH value is incrementally increased using NaOH. Since divalent cations are already contained in surplus in the fluid, the treatment consists only of a pH value increase by NaOH. The mineral precipitation is quantified by keeping the mineral phases portlandite, calcite, CSH and amorphous silica equilibrated with the fluid. As the CSH phase, the C0.7SH of the thermoddem database included in the Pitzer_CSH was used. That phase was chosen because CSH studies have shown that at high Ca and Si contents and short reaction times, the CSH formation process is best described by metastable CSH phases with small Ca/Si ratios (Blanc et al. 2010b; Chen et al. 2004; Stronach and Glasser 1997). The simulation considers a direct mixing without any kinetic effects. Since initially high contents of divalent cations are present and the temperature is constant, the pH value was identified as the decisive influence of the process (Figure 35).

The model predicts that amorphous silica is supersaturated and tends to precipitate at the initial conditions when entering the prototype. After equilibration of the reference fluid with the involved mineral phases, the aqueous Si content is reduced by 12 % from 87 mg/L to 77 mg/L, resulting in the precipitation of 21 mg/L of amorphous silica. At a pH value of about 5.8 calcite starts to precipitate and continues till a pH value of 7 is reached. Within the pH value change by degassing this results in a reduction of the Ca²⁺ ions by 102 mg/L (1.3 %) in comparison to the initial value. In terms of mineral precipitation, an amount of 252 mg/L calcite precipitation is calculated. Consequently, without any treatment, just by the natural equilibrium of the initial water and the degassing 274 mg/L of mineral scalings as a sum of silica and calcite are predicted.

For the first precipitation stage, a pH range between pH 8 and 9 is considered. For reaching that pH range a NaOH addition between 236 mg/L and 364 mg/L is required. The amorphous silica and calcite precipitation are not influenced anymore (< 1mg/L). At a pH value of about 8.2, the CSH precipitation initiates leading to a strong relative decrease in the Si content. Between the initiation and pH 9, the aqueous Si is reduced by 62 mg/L to 15 % of the initial value and Ca²⁺ by 63 mg/L to 97.5 % of the initial value. The reduction of these two ions results in a predicted formation of 244 mg/L of CSH phases considering the molar mass of the given molecular formula of C0.7SH of the parameter file.

For the main silica treatment, the previously determined pH range > 10 (Spitzmüller et al. 2021) was observed up to a value of 11. The Si content is strongly decreasing until a pH value of 10.5 when it reaches a residual dissolved amount of 2.8 g/L which corresponds to an

extraction efficiency of $R_{Si} = 97\%$. Until the pH value of 10.5 in total 282 mg/L, CSH phases precipitate. For reaching this pH value an amount of 676 mg/L NaOH is required. Calcite is slightly further reduced until a pH value of 10.8 where it finally reaches 308 mg/L of total precipitates.

From a pH value of 10.5 to 11 the fluid chemistry stays relatively constant. At a pH value of 10.9, the formation of portlandite initiates. The reaction is extremely pH-sensitive and reaches already 707 mg/L of mineral precipitation at a pH value of 11. Here, about 8 % of the initial Ca in the solution is precipitated. Further, the formation is a buffer reaction consuming in comparison to the pH increase up to this level by far more NaOH. For shifting the pH value from initial to 10.9, 976 mg/L NaOH are consumed. For the next step to a pH value of 11, the consumption increases by further 328 mg/L. This is also accompanied by a really strong decrease in Ca^{2+} ions.

The simulation shows that even without influencing actively the chemistry, precipitation of amorphous silica and calcite can be expected by the natural supersaturation of the fluid at the bypass and further the CO_2 degassing in the prototype. Since these reaction processes can be fast, the configuration of a first pre-precipitation reactor vessel was considered in the flow-through demonstrator experiments to avoid an impairment of the actual silica treatment installation. Two reactors enable further fundamental pre-treatment experiments at the pH range of 8.3 as a neuralgic value of the aqueous carbonate species. Regarding the silica treatment, a pH value of 10.5 could be identified as a sweet spot for the reduction of aqueous Si. At this point, nearly the total aqueous Si phase is removed at a comparatively low material usage. At a pH value of 11 the material usage increases, as well as the reduction of the Ca^{2+} ions from the aqueous phase. Consequently, the intervention in hydrochemistry increases but also a possibility for Ca^{2+} reduction, which can also form mineral scales, is identified.

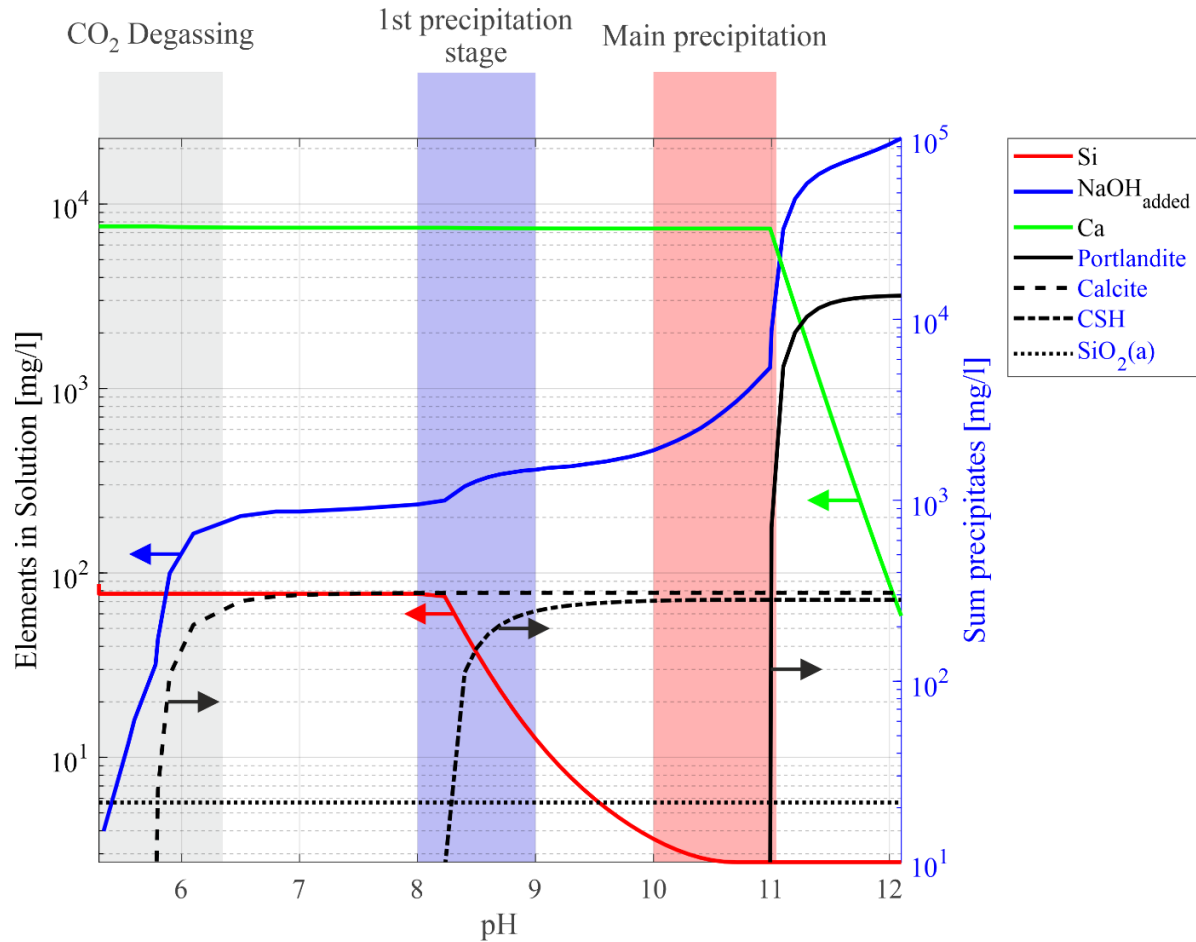


Figure 35: Results of a PHREEQC simulation of the precipitation behavior in a geothermal fluid induced by a pH shift by NaOH dosing. The plot shows the major concentration changes and mass flows during the pH shift. The arrows indicate on which axis the data depend. Fluid starting composition according to URG (Table 12). Constant Temperature at 57 °C. Used PHREEQC Database: Pitzer_CSH.

7.5.2 Results of continuous operation for silica treatment and reproduction of the laboratory experiments

7.5.2.1 Continuous Blank Operation of Demonstrator

In the first step, the impact of the prototype itself on the fluid chemistry was determined (see Experimental Mode 1). Therefore, a flow-through experiment was conducted without adding the reaction agents. The perspective was to evaluate the effectiveness of the chemical treatment in comparison to the influence of the dynamical intervention in the chemistry of the fluid by degassing, stirring, filtering and the retention time in the demonstrator. The results are displayed in Figure 39 in the appendix. The plots show the main anions and cations of the fluid as well as the pH value and temperature. The reference data to which the measurements were normalized are sampled at the sampling point before entering the prototype (S1). The flow rate was 20 l/h and the filling volume of the tanks was 10 l each, resulting in a residence time of 30 minutes per reactor. The temperature is slightly decreasing till it reaches heated CSTR 2. After CSTR 2 it increases again due to the heating jacket of the vessel before it decreases again while

passing by the second filter unit. The fluid finally leaves the demonstrator with 5 K less compared to the inlet temperature. Regarding the pH value, a minor change can be presumed by changing the pH from 5.56 to finally 5.73. The largest deviations in the chemistry are shown for HCO_3^- . These fluctuations can be explained by the measurement that was determined in the field by titration manually and is, therefore, more error-prone than a laboratory measurement. The other chemical components are deviating by a maximum of 2 %, which indicates no clear influence beyond the observational error. Consequently, all changes in the water chemistry that are found in the subsequent chemically induced precipitation trials are directly associated with the chemical induction, here NaOH dosing.

7.5.2.2 Continuous Operation of Silica Precipitation

Table 15: Water analysis of the continuous flow experiments.

Parameter	Unit	Reference	Experiment A		Experiment B		Experiment C (J)		Experiment D (K)	
Reactor		-	R1	R2	R1	R2	R1	R2	R1	R2
pH	-	5.5	5.18	10.45	8.39	10.49	5.16	10.45	8.42	10.49
Temperature	[°C]	57	60	55	70	59	61	60	61	53
TDS	mg/L	102596	104896	102275	104806	106237	111779	107886	104598	111258
Inhibitors	-		Yes		Yes		No		No	
Li ⁺	mg/L	159	176	166	175	172	181	171	166	175
Na ⁺	mg/L	27482	28279	32970	28984	34654	32141	32173	30764	36634
K ⁺	mg/L	4020	4152	3908	4146	4126	4663	4469	4328	4624
Ca ²⁺	mg/L	7234	7670	3020	7092	2948	8285	6995	7139	5023
Mg ²⁺	mg/L	110	114.37	0.13	71.76	0.25	120.88	1.21	66.85	3.62
Si	Mg/L	77	78	1	22	1	89	2	20	1
SiO ₂	mg/L	166	167.07	2.91	47.82	2.90	191.24	3.22	43.04	2.62
Cl ⁻	mg/L	63179	64094	61899	64017	64040	65942	63746	61815	64479
SO ₄ ²⁻	mg/L	141	140	127	108	107	155	137	111	122
Br ⁻	mg/L	177	177	171	176	176	187	180	176	184
F ⁻	mg/L	16	16	12	13	12	16	13	13	13
HCO ₃ ⁻	mg/L	186	201				88			

For evaluating the applicability of the process in the field several continuous operation parameters are evaluated (Table 15). In the following paragraph, the behavior of the fluid composition concerning the target elements Si, Na, Li, and Ca for four key experiments is outlined. Experiment A shows the basic treatment of silica at a pH value of 10.5 in CSTR 2, while CSTR 1 acts as a relaxation vessel. Experiment B represents a combination of a first precipitation stage in CSTR 1 at a pH of 8.4 before the main silica treatment in CSTR 2. The standard operation scheme of the power plant includes the application of scale inhibitors, which are consequently also present in the experiments. To study the effect these scale inhibitors could have on the precipitation results, the experiments were repeated without scale inhibitors by deactivation of the inhibitor dosing in the plant temporarily (Experiments C and D). All experiments were conducted at the same operational parameters; the flow rate was adjusted to 20 l/s, the heating jacket of CSTR 2 was thermostated to 55 °C and the stirrers were rotating at 300 rpm. The influence of the chemical treatment on the main cations is displayed in Figure 36. To correctly illustrate the significance of the results the observational error of the measurements is displayed as error bars. Further, since the fluid is subject to natural

fluctuations, the upper and lower quartile of the background measurements of each element (see Chapter 7.3.2) are displayed as light background regions.

The results show that for all displayed experiments, Si is reduced to about 1.3 mg/L ($R_{Si} = 98\%$) at the treatment in CSTR 2 (Figure 36a). The measured Si concentrations are below the corresponding limit of detection in experiments A and B (1.59 mg/L) and slightly above the detection limit in experiments C and D (0.78 mg/L) (the detection limit is individually determined for each measuring run, therefore it varies for different experiments and elements). Further, all measured values are underneath the value of quantification. A comparison of the experiments with and without scale inhibitors shows that the scaling inhibitors do not influence the Si content in the fluid beyond the natural fluctuation and observational error. If the precipitation is subdivided into two stages, the Si content is reduced by about 75% in the first stage, reaching the final value of about 98% reduction in the second stage. It is worth mentioning that a similar reduction rate is also achieved for Mg (see Table 15).

The Li content (Figure 36b) shows similar behavior in all 4 experiments. It is not influenced by the pH shift in the tested range neither at single or double-stage precipitation nor in the presence of the scaling inhibitors. The variation is ranging within the natural fluctuation and observational errors.

In comparison, Ca (Figure 36c) is strongly influenced by the inhibitors and shows a variation in the different treatments with or without inhibitors. In the single-stage precipitation strategy with relaxation (Experiment A and C) the Ca content in CSTR 1 shows no clear influence. In the two-stage precipitation method, (Experiment B and D) at pH 8.4 the Ca content reduces in both cases slightly by about 6%. The larger changes took place in CSTR 2. The two experiments with scaling inhibitors (Experiment A and B) show a reduction of Ca by about 60% from 7566 mg/L to approx. 3000mg/L in CSTR 2, independent from the applied reactor arrangement. In the retrials without scaling inhibitors, Experiment C shows a small reduction of Ca by about 7% in CSTR 2. In Experiment D operated with pre-precipitation the Ca content is finally reduced by 30%.

The change in the Na content (Figure 36d) is the indicator for the required amount of NaOH for the pH adjustment. The standard experiment with inhibitors and only silica treatment (Experiment A) shows an increase of Na of 4000 mg/L in CSTR 1 in comparison to the reference fluid (Table 12). This is equivalent to an addition of about 7000 mg/L of NaOH. The pre-precipitation in Experiment B requires a minor addition of NaOH to reach the aimed pH value. In comparison to the reference fluid (Table 12), the addition of Na in CSTR 1 disappears in the background noise and the measurement error with 47 mg/L. For reaching the treatment level in CSTR 2 an additional Na increase of 5717 mg/L is measured. The pure silica treatment without scaling inhibitors (Experiment C) shows no clear results due to the larger measurement error of these specific measurements. The initial measurement in CSTR 1 without any treatment shows a value about 3200 mg/L higher than the reference value (Table 12). However, considering the observational error it is in the range of the background noise. The measured value for the treatment in CSTR 2 is almost the same. Regarding the observational error, the addition is ranging between the initial reference value and an increase of about 6500 mg/L for the pH adjustment. The pre-treatment experiment without inhibitor (D) shows an increase of Na of about 1800 mg/L in CSTR 1 and 7700 mg/L in CSTR 2.

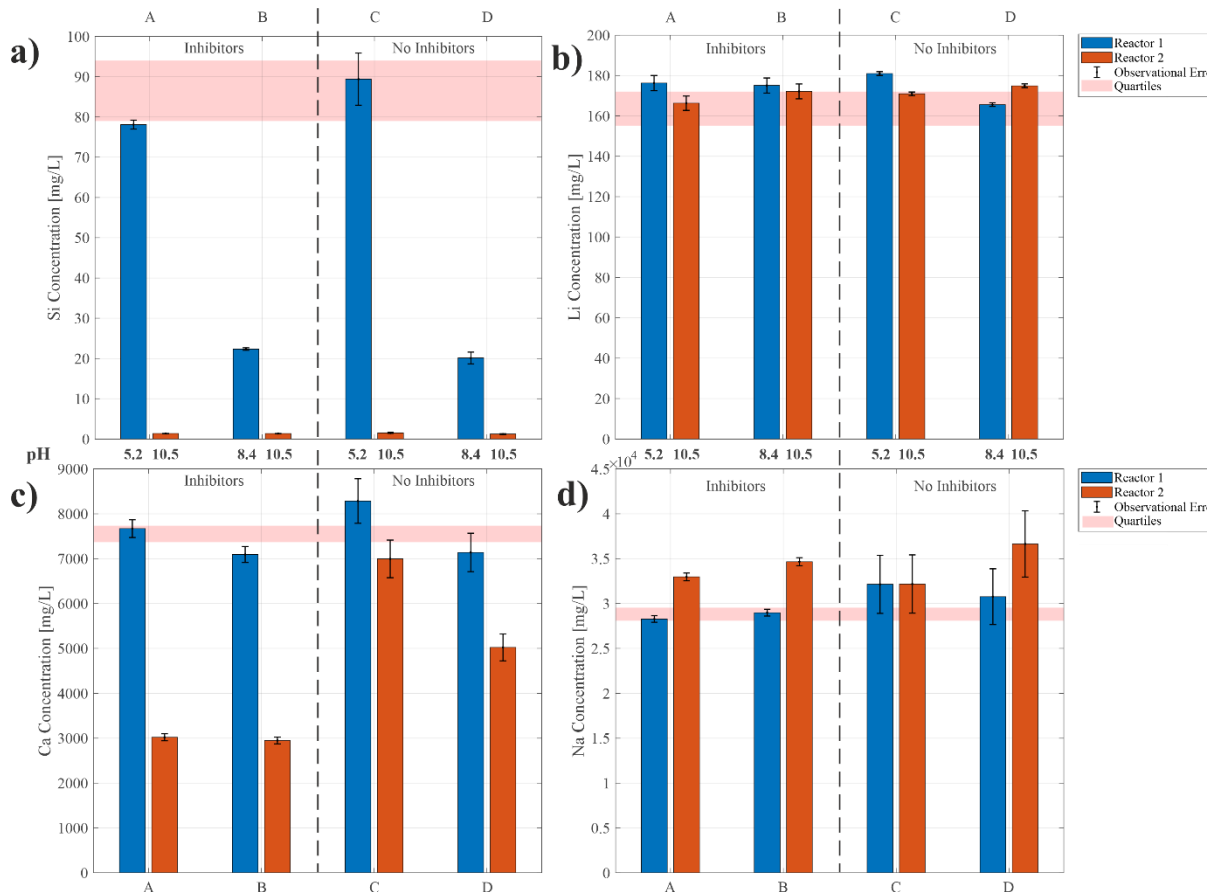


Figure 36: Reproduction of the treatment strategy developed in the Laboratory. The graph shows the influence of the silica treatment on the 4 major cations. Displayed are four experiments. In the graph, we can see the measured values of the elements and the associated observational errors. Additionally, the upper and lower quartiles from the measurements of untreated water are displayed to judge the effectiveness of the treatment steps.

Chloride as a conservative element that is not included in the chemical equilibrium of the treatment serves as a reference for the quality of the sampling (Figure 40 in the appendix). As can be seen, the values generally vary only marginally as a function of natural fluctuation and observational errors. After subtraction of the measurement error, all measurements stay in the range of the background noise.

7.5.3 Results and effects of the treatment on the geothermal fluid and downstream processes

Beyond the reproduction of the laboratory experiments, the demonstrator operation aimed to analyze the behavior of the geothermal fluid in more detail. Further, the applicability of subsequent concentration processes should be evaluated.

7.5.3.1 Batch operation of Silica Precipitation – Identification of Reaction Kinetics

For the batch experiments (see Experimental Mode 4), a fixed amount of fluid was fed into the tank reactor without inflow or outflow. It was conducted under the normal operating conditions of the power plant which includes the addition of scaling inhibitors to the fluid. The pH value is adjusted and kept at a pH of 10.5 under continuous stirring and temperature is maintained at 55 °C using a heating jacket.

The results (Figure 37) show that the reduction of Si and Mg, which is described for the continuous operation before (Chapter 7.5.2.2), takes place during the first 5 minutes after the addition of NaOH. In this time step Si is reduced by 98 %, and Mg by 99.7 % to their detection limits while adding an amount of 1865 mg/L of Na in the form of NaOH. Again, it is observed that the Li concentration stays unaffected. During the whole observational period of 60 minutes, its concentration is fluctuating in the range of the observational error. Ca is reduced by 6.5 % (484 mg/L) in the first five minutes.

From minutes 5 to 30, the water chemistry remains almost unchanged. Between the time steps at 30 and 60 minutes, the data show that the fluid again changes in a relevant manner. In this period Ca is reduced by 4107 mg/L to 36 % of the initial content. The associated precipitation process was leading to a pH value decrease requiring further NaOH addition for keeping up the pH value. In this time step, Na increased by 3207 mg/L to a total increase of 6683 mg/L. Also in this time step, no decrease of Li is observed regarding the initial value.

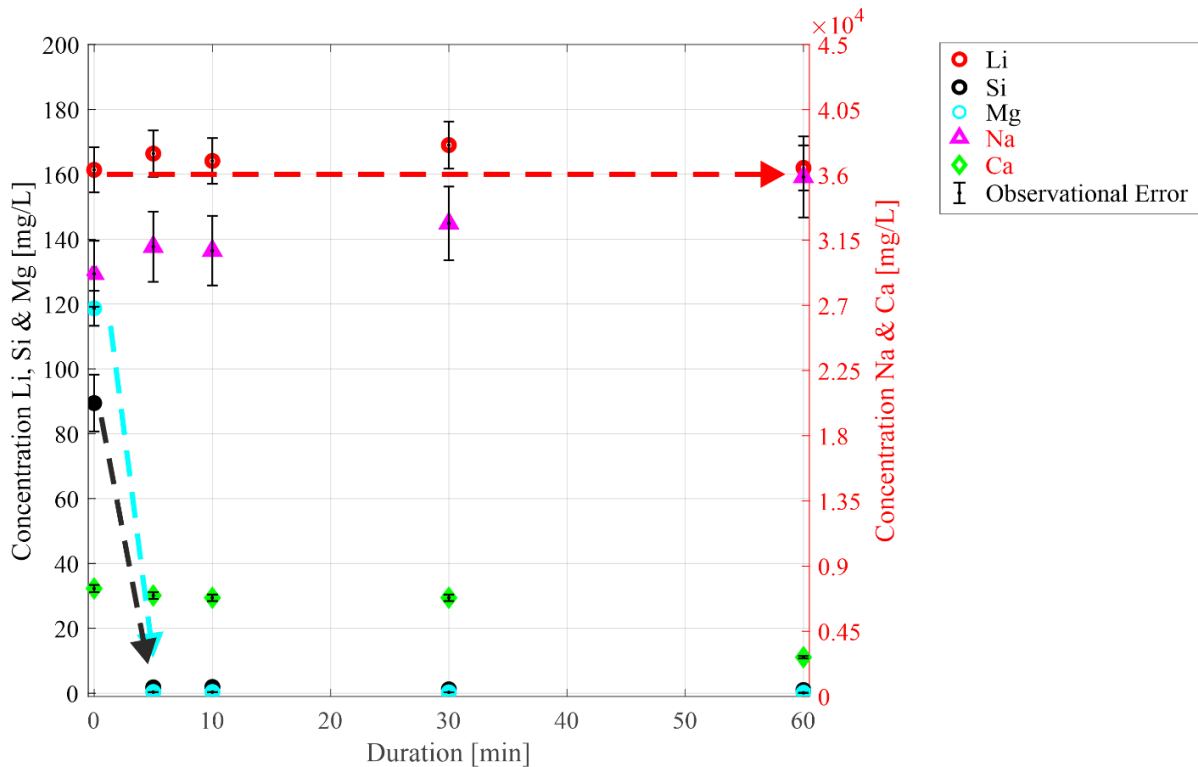


Figure 37: Development of Cations- Contents over time in the batch operation of the NaOH-induced silica extraction (kinetic mode).

7.5.3.2 Post Concentration of the fluid with Membrane Distillation

The purpose of the brine treatment is to enable the concentration of the natural geothermal brine using membrane technologies as MD without causing silica fouling. For evaluating the effectiveness of the Si treatment the treated brine was further processed in the membrane distillation plant. Subsequent to the separation of the solid precipitates after CSTR 2 the treated brine was taken into a buffer tank from which the MD module was operated in a batch mode.

During the batch operation (Figure 38) the initial concentration of the total dissolved solids of 103,053 mg/L is increased by a factor of 2.8 to 291,179 mg/L. Na and Li concentrate analogously to the total dissolved solid content. Li reaches at the final concentration factor about 469 mg/L. Ca shows up to a concentration rate of about 1.4 similar concentration rates as the TDS. Afterward, the total dissolved solids reached a concentration rate of 1.65 while Ca shows an enrichment of 1.55. At the last measurement, Ca reaches 2.44 and a total content of 7988 mg/L hence a difference of 0.35 in enrichment in comparison to the allover concentration. The decrease in the Ca enrichment rate is accompanied by a change in the pH value. Starting at initially 11.15 after the filtration of the treated brine, the pH value reaches its maximum at a concentration rate of about 1.6 with 11.26. Afterward, it drops to about 10.90.

In comparison, Si stays at low a low concentration during the concentration steps. Just at the final concentration rate, it overcomes clearly the limit of detection by reaching a final value of 4.01 mg/L. The measured Mg contents are below the detection limit for the whole concentration process.

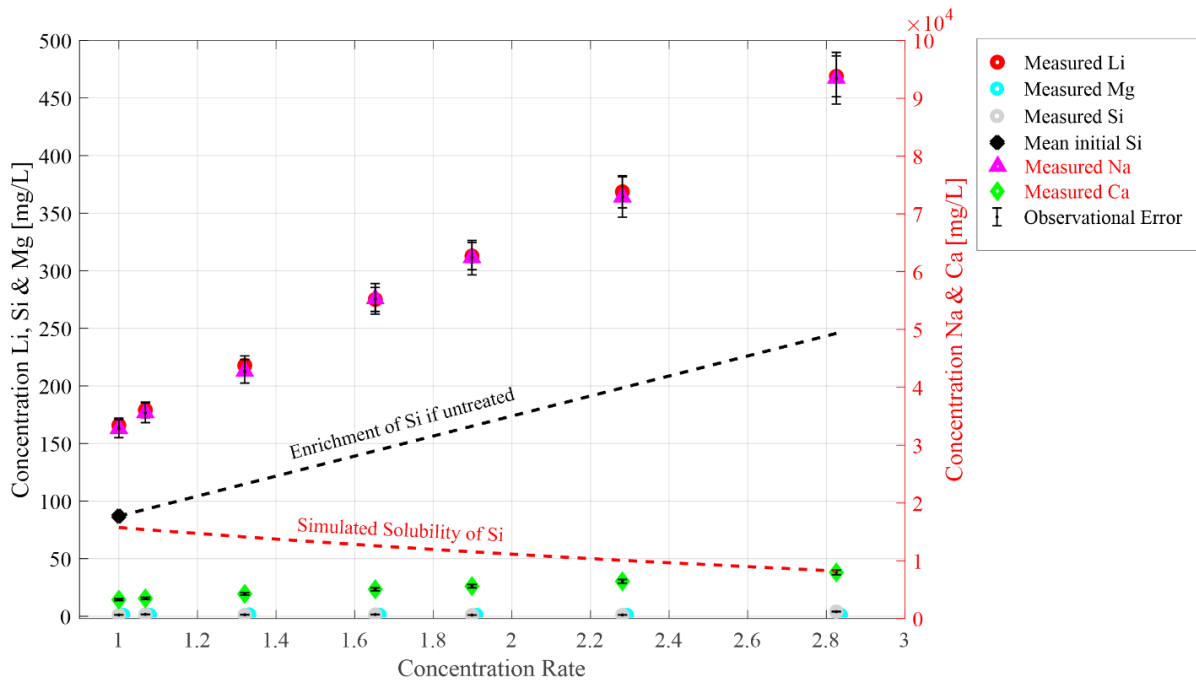


Figure 38: Concentration of treated geothermal fluids. Pre-treated water was concentrated up to almost factor 3. The measured data are presented by the points. The Mean initial Si is the mean measured Si in untreated water samples measured during the sampling campaigns. The black line shows how the Si content of the mean Si would evolve if it would be concentrated at the same rate as the other elements. The red line shows the simulated solubility for Si if untreated water would be concentrated.

Figure 38 shows the theoretical increase in Si if it would be concentrated as the total mineral content. It shows that without treatment at the final concentration step, it would reach a content of 246 mg/L. Further, the saturation for amorphous silica, simulated with the developed approach in Chapter 7.5.1 was determined in untreated water at the respective concentration rates. As shown in Figure 35 the brine is initially oversaturated with respect to amorphous silica. In untreated brines this increases with every concentration step since on the one hand the silica content is increased by the concentration process and further the possible solubility is decreasing due to a higher total dissolved solid content (i.e. salting-out effect). Subsequently, the theoretical Si content if untreated and the maximum possible solubility are diverging with every step. At the final step, the difference is 206.3 mg/L representing a large silica scaling potential during concentration without any treatment as observed in other MD experiments using NaCl-brines (Zhang et al. 2018). Due to the treatment the measured Si content is still far beyond the determined solubility.

7.6 Discussion

7.6.1 Validation of the Field Experiments

To classify the transferability and the success of the results, both the numerical and the experimental applications and results will be discussed in the following. The results of the field tests show that the content of the aqueous Si is reduced down to the limit of detectability at the final treatment steps (pH 10.5) in all operational modes. With these results, the laboratory

results (Spitzmüller et al. 2021) as well as the simulation results could be transferred and validated in the intended environment. In addition, the expectation that Li is not affected by the reaction could be confirmed with the natural geothermal brine. The kinetics experiments show fast precipitation of the Si-containing phases within 5 minutes after the addition of NaOH. With these fast kinetics, the reaction exceeds the speed of the reaction with the lower saline fluids in the lab (Spitzmüller et al. 2021). The fast kinetics are beneficial for a large-scale application, enabling smaller reaction tanks for reaching the required hydraulic retention time. For the used 20 L/h flowrate of the demonstrator therefore a reaction volume of 1.67 L would be enough for the total silica reduction, for the full flowrate of the power plant Insheim a reaction volume of 24 m³ would be required. With the same kinetics, also Mg is removed from the brine. This is also beneficial for downstream Li extraction processes since Li and Mg are competing ions in different extraction technologies. In fact, the Mg/Li separation as a pretreatment prior to Li extraction from salt lake brines is a challenging, multistage process opening up its own research field (Li et al. 2019c; Sun et al. 2021; Xu et al. 2021b). Application of the introduced silica pre-treatment would enable avoiding this treatment step in a later downstream extraction process. The process can also be optimized by reducing the first precipitation stage and slimming down the treatment to one reaction vessel. A first precipitation at pH 8.4 did not show any advantage regarding silica reduction or NaOH consumption. Also, the purity of the CSH precipitates in CSTR 2 could not be substantially enhanced by a double-stage process.

Regarding geothermal energy production, it is shown that the mandatory scaling inhibitors do not influence the process negatively, regarding the Si reduction and the Li content. Therefore, the process is also compatible with the safe state-of-the-art operation of a geothermal plant. Only the Ca reduction is enhanced at the presence of scaling inhibitors.

After the chemical precipitation, the concentration of the brine was tested, enabling a total concentration of the brine up to a factor of 2.8. Si is only above the detection limit at the last concentration step with 4 mg/L. In comparison to the simulation, a maximum solubility for Si would be reached at about 40 mg/L (Figure 38). Considering the simulation, the threat of silica scaling within the membrane module is eliminated. In terms of silica, by far higher concentration factors could be achieved resulting in higher Lithium concentrations. The comparison with MD experiments in the literature using similar saline and silica-containing, artificial brines at 65°C shows silica concentration limited by a silica “pseudo-solubility” at about 205 mg/L. The higher apparent solubility is explained by insufficient time for dissolved silica to precipitate to its true solubility (Zhang et al. 2018). The findings of the mentioned study underline that in the case of the natural brines used in this study, scaling would occur since the untreated concentration of Si would by far exceed even compared to the higher “pseudo-solubility” (Figure 38). A further strong benefit of the used approach is the associated Mg removal from the brine. In the presence of Mg, the risk of the formation of magnesium silicate on the membrane surface is given (Zhang et al. 2018). Since Mg is reduced along with Si by the chemical treatment, also this hurdle is not given anymore. In terms of scaling treatment, in the literature, the approach of scaling inhibitor use was evaluated. The results show also good effectiveness, but only for brines with low Ca and Mg concentrations (Zhang et al. 2018). Since the brines of the URG show high concentrations of these elements, the mentioned inhibition is not transferable to the test site. In addition to the proven effectiveness,

this methodological comparison further demonstrates how promising the presented approach is for continuous fluid treatment.

The measurements showed that Ca enriches less in comparison to the total dissolved solids at a certain concentration factor of about 1.5. Leading to the assumption of precipitation of Ca from the brine. For reaching higher concentration factors in high-Ca brines, further Ca-specific treatment should be considered. Another opportunity is to re-adjust the pH value prior to the concentration since the solubility of calcite and portlandite increase at low pH as the simulation and the literature data (Duchesene and Reardon 1995; Kutus et al. 2016) showed.

The comparison of the simulation and the field results in terms of the NaOH consumption and precipitation results show, that it was not possible to adjust the pH value exactly to 10.5. For the adjustment to a pH value of 10.5, the simulation predicted a demand of 675 mg/L NaOH while from the increase of aqueous Na in the brine a consumption of 6500 – 7000 mg/L (Experiment A & C) can be inferred. According to the simulation with this addition, a pH value of about 11 would be reached. This leads to the assumption that the pH value was effectively higher than that indicated by the built-in pH probe. This is supported by the dominance of portlandite within the precipitates, which forms according to the simulations at pH values higher than 11. Laboratory studies even report higher pH values for the formation of Portlandite in classical cement (Blanc et al. 2010b; Šiler et al. 2016). The higher pH values indicated by the simulations and brine chemistry can be derived from two major effects. The corrosive nature of the brines led to fast degradation of the installed pH probes leading to a negative measurement pH shift that was documented by a reference handheld multi-parameter probe. Therefore, the probes were frequently exchanged, an influence of the automated dosing could nevertheless still not fully be avoided. A further explanation is the occurrence of local pH peaks at the direct contact of the concentrated NaOH at the dosing point due to insufficient local micro-mixing while adjusting the pH value in the geothermal fluid. This could lead to local pH peaks forming portlandite before mixing totally in the brine and thus consuming additional NaOH in advance.

7.6.2 Numerical sensitivity Analysis

The comparison of the simulation results and the field results showed how sensitive the system for the pH value is and is further displayed in the simulation results (Figure 35). A pH difference between adjusting the pH to 10.5 or 11.1 can lead to a difference in NaOH consumption of one order of magnitude from 676 mg/L to 7321 mg/L. To outline further sensitive parameters, a numerical sensitivity analysis was conducted (Table 16) using the developed design calculation and the background measurement. The chemical data from the background measurement (Table 12) served as input parameters for the standard scenario and analog to the field study, the pH was adjusted to 10.5 using NaOH. The resulting performance parameters of the standard case (Table 16, Column 3) are then compared to the resulting parameters of the different scenarios. The varied parameters are the total salinity of the brine, the inlet temperature, and the HCO_3^- in the range of the acquired field data.

The sensitivity analysis shows that besides the pH value, the temperature shows the largest influence. With increasing temperatures, the portlandite precipitation starts at lower pH values

due to the lower solubility at high temperatures. Thus, the NaOH consumption increases since the portlandite precipitation consumes the NaOH and more has to be added to reach the higher pH values. Here lower temperatures improve the process. Less NaOH must be consumed, which will lower the costs of a future continuous process. Also, the residual Ca content stays a little bit higher, resulting in fewer precipitates and in general a lower intervention in the brine chemistry. This shows good compatibility with geothermal power production since lower temperatures also enhance the extractable amount of energy. In terms of the chemical input parameters, the HCO_3^- content shows the clearest influence. The lower value also lowers the NaOH demand by about 2 % while the higher value leads to an increase of the same magnitude. The other parameters change minor. Regarding the HCO_3^- lower contents would be favorable. The HCO_3^- is a function of the dissolved CO_2 in the brine. It is assumed that due to the open outflow in the demonstrator, some part of the CO_2 is already degassed from the brine. That is usually avoided within geothermal cycles to avoid CO_2 release into the atmosphere as well as precipitation of carbonate minerals. Therefore, in a full-scale plant, the operation should be conducted in a closed, pressurized loop. Without the degassing the HCO_3^- will be most likely higher and thus more NaOH will be required for the treatment. But still, the influence of the higher contents is quite low in comparison to the overall required amount of NaOH. According to the standard model, 676 mg/L of NaOH would be required for continuous treatment. If the process is normed to one liter of brine, independent of scale and flow rate, NaOH costs are less than 1 % of the economic Li value. The chemical for treating one liter of brine would be 0.00017 to 0.00034 US\$ (250 – 500 US\$/t, (Alibaba.com 2022)) compared to a Li carbonate value of 0.022 – 0.044 US\$ (25,000 – 50,000 US\$/t Li_2CO_3 (German Lithium Participation 2021; Trading Economics 2022) in the same amount of brine. Depending on the required silica reduction a cost-optimized scenario could also be feasible. For example, the reduction of 50 % of the Si at a pH value of 8.40 using only 296 mg/L of NaOH.

Table 16: Sensitivity analysis on the key parameters NaOH, residual Ca content, and residual Si content at pH 10.5 using the design calculation. The varied parameters are highlighted for each simulation are highlighted in bold. Further, the input parameters TDS, Temperature, and HCO_3^- as the varied parameters are shown.

	Initial (Measured)	Standard	TDS _{low}	TDS _{high}	T _{low}	T _{high}	HCO_3^- low	HCO_3^- high
NaOH Consumption [mg/L]	0	676	672	680	600	756	664	692
Ca _{Residual} [mg/L]	7566	7367	7092	7838	7372	7362	7374	7359
Si _{Residual} [mg/L]	87	2.8	2.8	2.7	2.9	2.7	2.8	2.8
TDS _{input} [mg/L]		105192	101440	111780	105192	105192	105192	105192
Temperature _{input} [°C]		57	57	57	52.8	60.7	57	57
HCO_3^- input [mg/L]		188	188	188	188	188	177	201

7.7 Conclusion and Outlook

As silica scaling is one of the major hurdles in geothermal energy production and water treatment processes, it is accordingly a major challenge for the promising approach of combined geothermal energy and raw material production. However, the risk of scaling is further

enhanced by the characteristics of various direct raw material extraction technologies. Therefore, a specific pretreatment of these waters is of utmost importance to bring this scientific approach into practical application.

The used chemical approach is based on the precipitation of the aqueous Si as CSH phases by adjusting the pH value to a value larger than 10. Scaling inhibitors showed not to be effective in existing studies for the conditions met at the study site. The therefore chosen geochemical reactions are typically known from cement hardening processes but are not common in the geothermal sector. For upscaling the approach, a site-specific numerical design simulation was developed. For the calculations, a new thermodynamic dataset had to be compiled because the existing datasets could not derive sufficient calculation results for displaying this new approach numerically. The data set enabled the transfer of the cement process to the hydrochemistry of the brine of the geothermal power plant in Insheim, Germany. The simulation was used to quantify the volumetric streams of the process and to estimate the demand for the reaction agents for designing the demonstrator. Moreover, the developed numerical tool enabled a parameter sensitivity analysis and further will enable the transfer to different geothermal fluids.

The demonstrator was successfully tested in the field in a continuous flow system for silica reduction and post-concentration of the remaining dissolved solids. The silica reduction showed an effectiveness of 98 % in the field which is in agreement with the lab experiments and simulation results. The onsite application revealed further fast reaction kinetics of less than 5 minutes for the silica reduction. This facilitates the latter processability of big volume streams for geothermal energy production itself or combined energy and raw material production. In addition, the treatment enabled a concentration of the minerals in the brine up to a factor of 2.8 under the production of freshwater using membrane distillation. Another result in terms of system design is, that single-stage precipitation is sufficient for the goal of silica reduction making a slimmed-down operation with one tank reactor possible.

The field tests further revealed several challenges for a brought application of raw material extraction facilities in geothermal cycles. The post-analysis of the field tests showed, that the pH value could not perfectly be adjusted to the target value due to local pH peaks at the contact point of the reaction agent as well as due to the fast degradation of the pH probes due to the corrosive fluid. This material challenges in combination with the absence of complete thermodynamic datasets for the implementation of the technology outlined the necessity of further research on this topic as well as the importance of long-term on-site tests. The field tests allowed us to identify these critical points. The brine used at the Insheim power plant is representative at least for the geothermal region of the Upper Rhine Graben and allows in this regard the transfer to other locations locally. The field results can thus be used to optimize the technical facility as well as to scale up the process on a full scale, especially including a downstream Li-extraction. Finally, the new dataset and the mobile demonstrator can further be used to transfer the approach also to other geothermal systems globally, e.g. in high enthalpy fields, as they are present in Chile. The implementation of the developed (numerical) approaches is recommended if the geothermal systems show high concentrations of valuable, dissolved metals and at the same time high silica concentrations that tend to precipitate during energy production, concentration, or raw material extraction processes. Further, in high-enthalpy geothermal systems, where silica scaling is a common problem, especially enhanced

by steam flashing, the described process of a preventive pre-precipitation, could enhance the energy production efficiency, minimize maintenance times and avoid damage on the surface facilities.

7.8 Acknowledgment

The authors gratefully acknowledge research funding by BMBF Client II for the BrineMine Project (Federal Ministry of Education and Research, FKZ: 033R190B). Further, the authors would like to thank the Helmholtz Association for research funding within the subtopic “Geoenergy” in the MTET (Materials and Technologies for the Energy Transition) program of the research field “Energy”. We thank Dr. E. Eiche, Chantal Kotschenreuther, Maya Denker and Beate Oetzel of the Department of Geochemistry & Economic Geology (Karlsruhe Institute of Technology, Division of Applied Geosciences) for the support in developing the measurement strategy and the access to laboratories and equipment, as well as for fruitful discussions. The team of Pfalzwerke geofuture GmbH is thanked for enabling the prototype implementation at the powerplant Insheim and for the pleasant cooperation during sampling. Finally, we appreciate the support of the Chilean ANID-Fondap program (projects 15090013 and 15200001).

The three anonymous reviewers are also thanked for improving the manuscript through their critical and productive discussion of the manuscript.

7.9 Appendix

7.9.1 Samples continuous blank operation

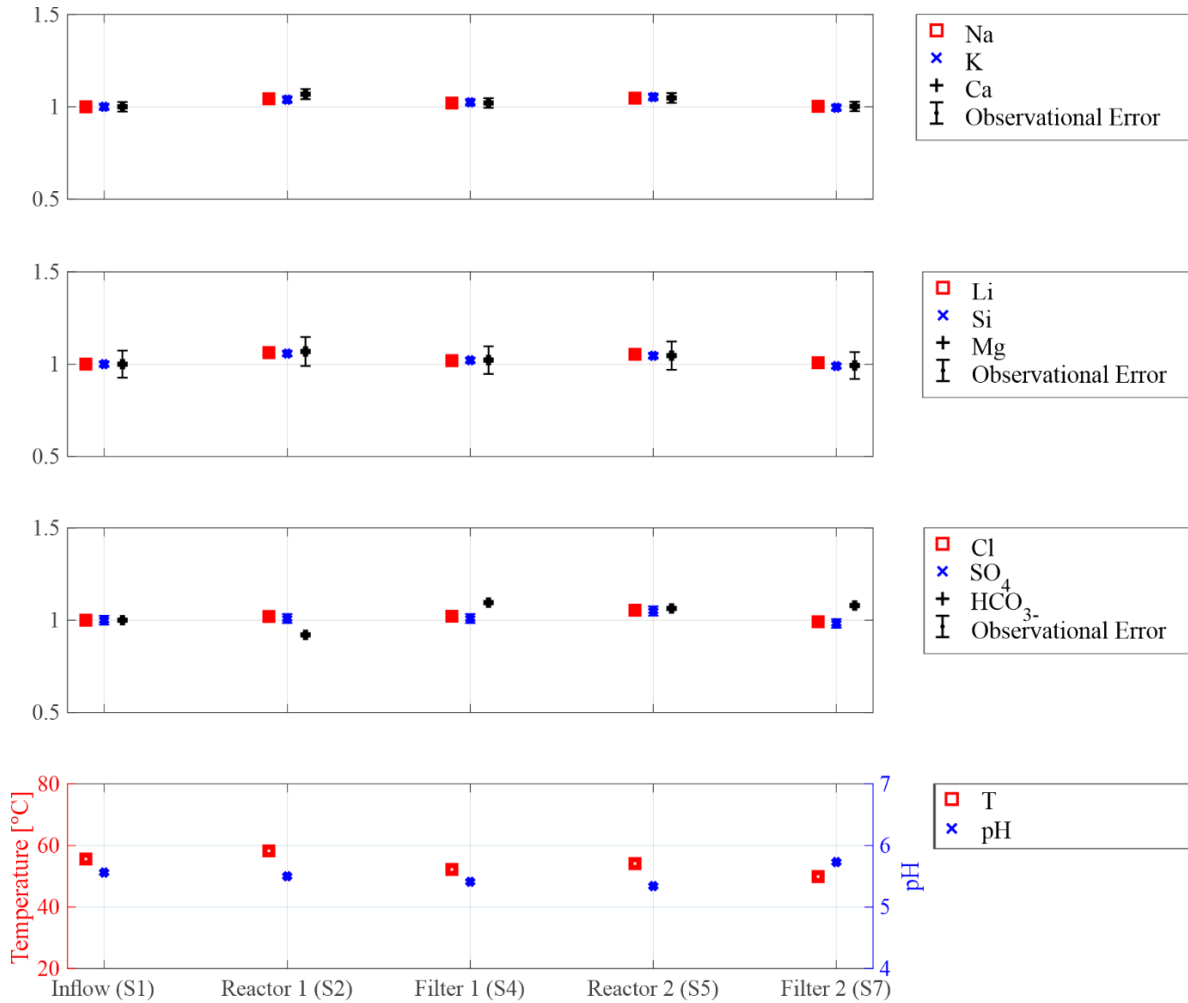


Figure 39: Influence of the prototype on the chemistry and temperature of the water. The graph shows the relative change of the geothermal fluid during the continuous operation at 20 l/h with the jacket of CSTR2 heated to 55°C. The results were referred to the initial brine composition sampled at point S1 (see Figure 30).

7.9.2 Chloride measurements

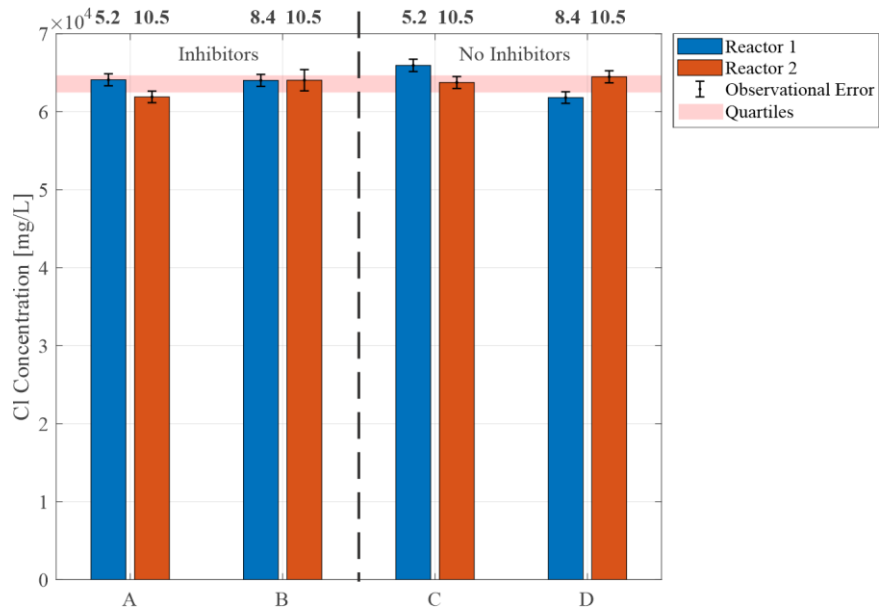


Figure 40: The development of Cl concentration during the silica treatment. Chloride as a conservative element is not included in the precipitation reactions and serves as a reference for the quality of the measurement. Generally, the values fluctuate very little and variations are in the range of naturally occurring changes and observational errors.

8 The potential of raw material extraction from thermal fluids in Chile

This manuscript has been published in *OIL GAS*. 26–33 (2021) under the title:

The potential of raw material extraction from thermal brines – Successful milestones of the BrineMine Project

Valentin Goldberg^a, Daniel Winter^b, Fabian Nitschke^a, Moritz Rath^a, Sebastian Held^a, Laura Spitzmüller^a, Ingmar Budach^d, Maximilliano Pavez^{a,e}, Diego Morata^c, Joachim Koschikowski^b, Thomas Kohl^a

^a Institute of Applied Geosciences, Division Geothermal Energy and Reservoir Technology, Karlsruhe Institute of Technology, Adenauerring 20b, 76131 Karlsruhe, Germany

^b Fraunhofer Institute for Solar Energy Systems ISE, Heidenhofstraße 2, 79110 Freiburg, Germany

^c Department of Geology and Andean Geothermal Center of Excellence (CEGA). Facultad de Ciencias Físicas y Matemáticas, Universidad de Chile, Plaza Ercilla 803, Santiago, Chile

^d Geothermie Neubrandenburg GmbH, Seestraße 7a, 17033 Neubrandenburg, Germany

^e Institute of Nuclear Waste Disposal, Karlsruhe Institute of Technology, Hermann-von-Helmholtz-Platz 1, 76344 Eggenstein-Leopoldshafen, Germany

8.1 Abstract

The BrineMine Project is a German-Chilean multidisciplinary research project realized by research and industry partners. The focus is developing strategies for raw material and water extraction from geothermal springs (Brine Mining) in Chile. The topics can be separated into a geological/geochemical part and a mechanical engineering part, which are processed in close cooperation by the project consortium. In the first part, the economic potential of the dissolved raw materials in thermal spring waters in Chile is assessed by analyzing existing geochemical data of different sites. This is complemented by hydrogeochemical and geophysical exploration campaigns. The second part focuses on the development, construction and implementation of a prototype for pre-treatment and concentration of geothermal brines. With the comprehensive expertise of the team, a treatment strategy was developed and tested in a geothermal power plant, enabling controlled silica precipitation in order to overcome this limiting factor for geothermal energy production and associated raw material extraction.

In this study, successful milestones of the BrineMine project are presented. The economic potential of elements in Chilean thermal waters is demonstrated. Additionally, the global potential of Brine Mining is outlined. The development of the silica treatment strategy is further described, as well as a possible integration of a prototype into an operating geothermal power plant. Finally, the construction and implementation of a large-scale first-generation prototype are presented with promising field results.

8.2 Introduction

The energy transition and the associated demand for non-energy, mineral raw materials have prompted the German government to expand research and development activities along the entire value chain. The focus is on economically strategic raw materials, of which the availability for future technologies and the high-tech industry must be secured to reduce dependence on the world market. The development of new resources offers the potential to complement conventional raw material extraction and thus to achieve the strategic goals set by the German government.

It is known that the highly mineralized thermal waters, which are circulated during the production of geothermal energy, sometimes have significant enrichments of economically strategic elements such as lithium, rubidium, antimony, tungsten, etc. (Neupane and Wendt 2017; Sanjuan et al. 2016a). The BrineMine project aims to describe, qualitatively and quantitatively, the occurrence of these chemical elements in geothermal waters in Chile against the background of raw material extraction. The extraction of mineral raw materials from thermal waters is still challenging in terms of the process technology but new sustainable methods are preparing the path to an economical production as an alternative to conventional extractive mining. An important milestone is the development of a large-scale prototype enabling effective precipitation and enrichment of selected raw materials from geothermal brines. The process used in the BrineMine project for the enrichment of the target substance is based on reverse osmosis and membrane distillation. It is driven by geothermal heat securing energy-neutrality and reduced greenhouse gas emissions. To ensure the longevity of the plant, an effective configuration of fluid pre-treatment and membrane modules is crucial. Due to overall high salt concentrations, selective separation of scaling-forming minerals is required in a pre-treatment stage to avoid scalings or membrane fouling in the latter process steps. The focus is on controlling silicate precipitation, which can be expected due to the change in temperature and pressure conditions. In laboratory and pilot plant tests, effective methods have been identified that allow instantaneous precipitation of up to 98% of the initial silica concentration.

The application of the developed prototype takes place in two steps, first in an operating geothermal power plant in the Upper Rhine Valley in Germany and afterward in Chile. The test location in Chile is selected according to the results of hydrogeochemical exploration campaigns supported by geophysical methods to determine the size of the subsurface reservoir and thus the economic viability.

The BrineMine project is a 3-year research project funded by the German Federal Ministry of Education and Research. The project is realized as a bi-national research project between German and Chilean research and industrial partners. The project structure features two focal points: 1) Determination of the economic potential of thermal waters as a raw material resource and 2) Pre-treatment of thermal waters prior to raw material extraction. The Fraunhofer Institute ISE (Institute for Solar Energy Systems) leads the international consortium in close cooperation with the Karlsruhe Institute of Technology (KIT) and the Andean Geothermal Centre of Excellence (CEGA) at the Universidad de Chile. Further collaborators are the

companies SolarSpring membrane solutions and Geothermie Neubrandenburg (GTN). Further Chilean partners are CSET, GTN Latin America and Transmark Renewables.

The comprehensive expertise of the consortium is required to deal with the multiple targets of the BrineMine Project. From a geological perspective, the purpose is to gain a better understanding of the resource potential from geothermal wells in Chile, as well as to carry out a large-scale exploration campaign to find appropriate locations for a prototype implementation. The project's engineering part focuses on the design, production and installation of the prototype.

8.3 Potential of geothermal Brine Mining in Chile

In geothermal waters, a large potential of raw materials is stored, already dissolved in water. This provides several benefits in comparison to traditional mining methods as a lower environmental impact, smaller land use and a minimized water consumption. While hydrothermal mineral deposits such as iron-oxide copper gold deposits are well known, thermal fluids as a deposit themselves are playing yet a minor role. The high temperatures and pressures that typically prevail in geothermal reservoirs are catalysts for water-rock interaction. In combination with the interaction time, this leads to an increase in mineralization of brines with increasing depth (Stober et al. 2014). The salinity of geothermal brines can reach values up to 400 g/L (Neupane and Wendt 2017). The chemical composition itself is highly variable and depending on the reservoir rock, the fluid genesis history and the regional flow system (Stober and Bucher 2015).

For a long time, production-induced uncontrolled mineral precipitation known as scaling or fouling was seen as a challenge for the geothermal industry (Stober and Bucher 2012). However, it is also an opportunity, as large-scale studies (as in reference (Neupane and Wendt 2017) or (Hauser 1997)) indicate significant amounts of valuable raw materials dissolved in these waters. Nevertheless, accessible data are often limited to the main ions. More detailed hydrochemical analyses can therefore reveal further raw material potentials especially in areas with high geothermal potentials.

Chile has one of the highest geothermal potentials worldwide (see Figure 41), recently affirmed by commissioning the first geothermal power plant in Chile - Cerro Pabellón with an installed capacity of 48 MW_e which will be expanded to 81 MW_e during 2021. The high potential arises from Chile's unique geological framework within the Andean volcanic arc, which yields more than 200 active volcanoes (Siebert et al. 2010). By now, approximately 70 geothermal areas are considered to potentially host high-enthalpy geothermal systems and even more are yet to be explored (Aravena et al. 2016).

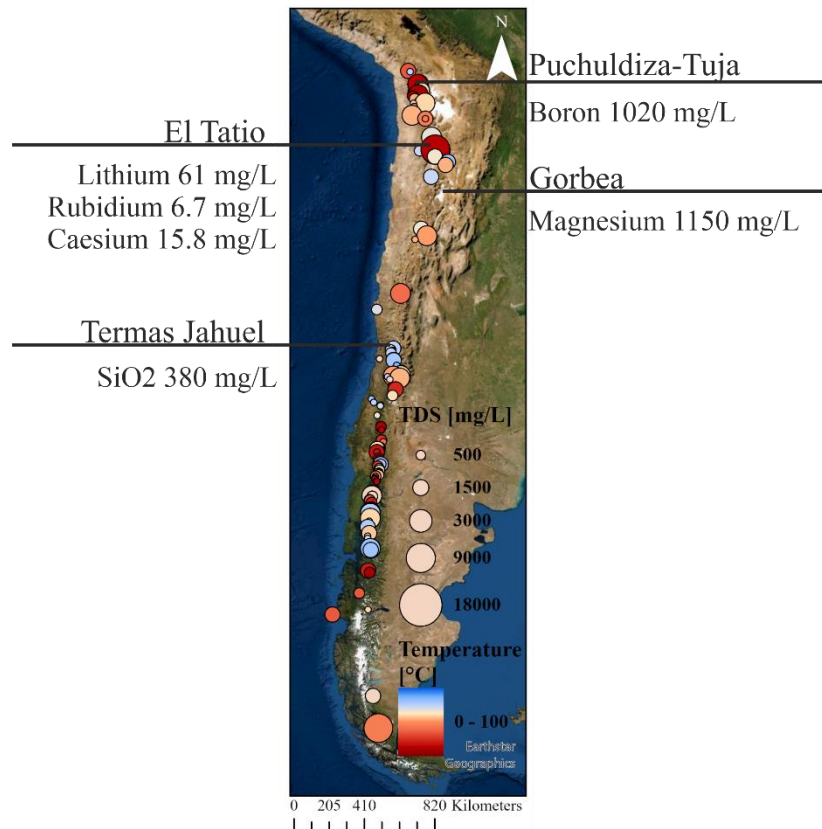


Figure 41: Distribution of thermal springs in Chile. Marker size indicates the amount of total dissolved solids. The color represents the reservoir temperature. The highlighted springs were selected due to their high values of elements, which are of economic interest in Chile.

In terms of raw material extraction in the past years, the salt lakes in the Atacama Desert in Chile have received high interest as an important source for lithium. The mining in this area is accompanied by serious environmental impact as well as high water consumption since 95 % of the Li-bearing salt lake brine has to be evaporated for the Li-enrichment (Flexer et al. 2018). This bears obvious conflict potential in one of the world's driest deserts. Furthermore, Chile has the largest copper reserves on Earth (Peña and Huijbregts 2014) which is produced by hard-rock mining. This extraction method as well as for other elements is also accompanied by high water consumption (Mudd 2008; Peña and Huijbregts 2014). Yet, the Chilean economy is dependent on these resources. Both elements, lithium and copper, are enriched in different thermal brines worldwide (Regenspurg et al. 2015b; Sanjuan et al. 2016a; Tassi et al. 2016). If springs with sufficient contents of these elements are identified and viable extraction methods are developed, Brine Mining has the potential to serve as a water-saving alternative.

Part of the BrineMine Project is the geochemical exploration in Northern Chile to identify potential springs and associated target minerals. In the course of the project, a geothermal fluid sampling campaign will be conducted to analyze the associated raw material potential of Northern Chile and create a brought and consistent data set of the thermal springs within this area. Beyond standard measurements, a holistic and standardized dataset shall be created. It focuses on springs with high temperatures and a high content of total dissolved solids (TDS). Its overall goal is an appraisal of the economic resource potential in this area. Beyond the composition, the chemical analysis allows an estimation of the geothermal resource via geothermometers which have been adapted for Chilean systems in previous studies (Nitschke

et al. 2018). Furthermore, fluid age determinations, which have been approved in Chile (Held et al. 2018), will be conducted to assess the dilution with shallow cold waters and the recharge of the system. Using these geochemical exploration tools, which are continuously developed (Ystroem et al. 2020), a sustainable exploitation scenario can be designed. Complementary geophysical surveys using magnetotelluric methods allow the determination of hydrothermal fluid circulation within faults and the visualization of alteration zones. An associated reservoir characterization provides additional information on the potential storage capacity (Pavez et al. 2020).

Due to the global COVID-19 pandemic, the geochemical sampling campaign was postponed. In order to develop different extraction scenarios, already collected literature data (see Figure 41) were used.

8.3.1 Scenario calculation for the economics of raw material extraction from geothermal brines

To exhibit the economic potential of thermal springs in terms of raw material content six simplified scenario calculations were conducted. The basis for the calculation are assumptions based on typical geothermal power plant operation parameters as e.g. at Cerro Pabellon (Cappetti 2019), hydrochemical literature data of different thermal springs in Chile and market prices for different commodities.

Figure 41 shows the distribution of thermal springs in Chile and presents maximum values for selected, potentially relevant chemical elements. To quantify the potential of different raw materials, trace elements such as lithium (scenario El Tatio 3), rubidium (scenario El Tatio 2) and cesium (scenario El Tatio 1) were chosen as well as more enriched elements like boron (scenario Puchuldiza-Tuja), magnesium (Scenario Gorbea) or silica (scenario Termas Jahuel). The economic potential of trace elements results from their high market prices, while the more enriched elements benefit from their higher concentrations in combination with average prices (see Figure 42). A location-specific economic factor (third column in Table 18) results from the stated element contents and the price per unit.

The extremely high prices of cesium and rubidium result from small trading units and the lack of public trading (Butterman et al. 2005). The units are traded in grams and thus exceed the price per tons of the other mass raw materials by far. Furthermore, the achievable price is highly dependent on the purity and the produced compound of the raw material.

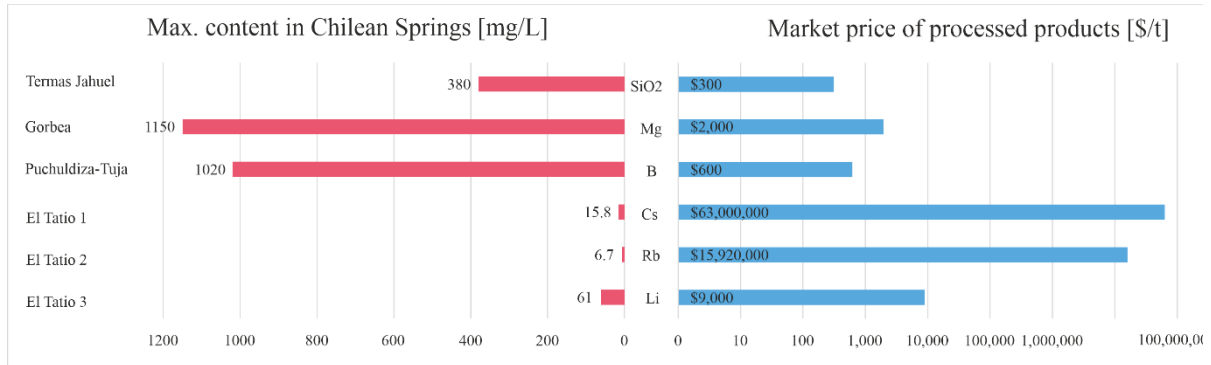


Figure 42: Economic potential of selected sites. Different raw materials can be produced from elements in thermal brines in Chile. The left side shows the occurrence of potential target elements. The right side displays the market value of processed products from these elements. Note the logarithmic scale of the market prices. The comparison displays that even elements with minor contents in brines can be lucrative exploration targets. (Bastian 2020; Brioché 2017; Dolley 2017; Tuck 2020b; Tuck 2020a).

For quantifying the circulated mass of raw materials, a representative volume stream was calculated (see Table 17). A typical flow rate for geothermal power plants is assumed (Cappetti 2019). An availability of 90 % was selected, corresponding to 36 days per year when the power plant is not running due to maintenance work. As a sum of these two parameters, the total volume of circulated brine per year is calculated. The extraction rate of 80 % for the raw material is based on literature data for lithium using ion sieves (Xu et al. 2016). Note that lithium recovery from thermal brines recently received increased research and industry interest resulting in an improvement of recovery technologies. For each element, an individual extraction methodology must be developed resulting in different extraction rates.

Table 17: Typical geothermal production scenario. The scenario assumes a flow rate of 80 L/s and an availability of 90 % of the year (329 days). The extraction rate is a conservative assessment based on the research in lithium extraction.

Flowrate	80 [L/s]
Availability (runtime/year)	90 %
Σ Annually circulated brine	2,270,592 m ³
Extraction rate for raw materials	80 %

8.3.1.1 Resulting economic potential

To assess the economic potential for each scenario, the circulated mass for each element was calculated using the volume of the circulated brine, the extraction rate and the concentration of the elements in the springs (Table 18). For boron and lithium, the mass for compounds is calculated, based on the circulated amount of substance of the pure elements. If different prices were available depending on the grade, the lower price is chosen to keep the model as conservative as possible.

Table 18: Economic potential of the production scenarios. The circulated amount results from the element content multiplied with the volume of circulated brine and the extraction rate. For boron and lithium, the amount was calculated as resulting compounds that can be produced from the pure element content.

Scenario	Compound	Economic factor spring [\$/l]	Circulated mass per year [t]	Specific price [\$/t]	Resulting economic potential [\$/yr]
Termas-Jahuel	SiO ₂	\$ 0.0001	690	\$ 300 (Dolley 2017)	\$ 207,078
Gorbea	Mg	\$ 0.0023	2,089	\$ 2,000 (Bastian 2020)	\$ 4,177,889
Puchuldiza-Tuja	H ₃ BO ₃	\$ 0.0034	10,414	\$ 600 (Brioche 2017)	\$ 6,248,663
El Tatio 1	Cs	\$ 0.9954	29	\$ 63,000,000 (Tuck 2020b)	\$ 1,808,117,821
El Tatio 2	Rb	\$ 0.1067	12	\$ 15,920,000 (Tuck 2020a)	\$ 193,752,340
El Tatio 3	LiCO ₃	\$ 0.0029	585	\$ 9,000 (Bastian 2020)	\$ 5,263,383

The resulting economic potential displays the theoretical value of the raw materials circulated in a virtual power plant, considering the chemistry of the different springs. Extraction costs, infrastructure, processing, or any further investments are not taken into account in this simplified model.

The results show that the elements with the lowest occurrence, cesium (Scenario El Tatio 1) and rubidium (El Tatio 2), possess the highest economic potentials due to their extremely high market prices. They exceed the maximum achievable value for lithium (El Tatio 3) by far, although the latter is currently the most discussed within the geothermal community for Brine Mining. Yet, there is no concept to selectively extract cesium from thermal brines at the moment. However, the model shows, that even at an extraction rate of 1% (-22.6 Mio. \$/yr) the potential still widely exceeds each of the minerals which are present in higher concentrations. Likewise, also compounds as boric acid (H₃BO₃) with the second-lowest price per ton have an economic potential in the range of lithium carbonate due to their higher occurrence (scenario Puchuldiza-Tuja). A similarly high potential is obtained for magnesium (scenario Gorbea). It is shown, that additionally to materials for the high-tech industry, bulk raw materials can be a lucrative target for geothermal Brine Mining. The market value for SiO₂ (scenario Termas-Jahuel) is by far the lowest. However, even though it is not lucrative to sell SiO₂ as raw material, SiO₂-extraction might be of economic interest as a mean for silica scaling mitigation which could increase power plant efficiency. Furthermore, the specific price for the precipitates can be increased by purifying or optimizing the produced silicon compound.

The overall potential further increases when the processes are coupled in a cascade approach, where different elements from one brine are produced in one process chain. This is demonstrated by the high potential of the three scenarios El Tatio 1-3 which all analyze the same spring. Here it is to be said that the element contents represent a minimum value since the data are from surface springs that could be diluted by meteoric waters. In a geothermal project where the reservoir is accessed via boreholes, higher values are consequently expected.

Still, as in all mining projects, the potential is site-specific, requiring an extensive exploration and exploitation strategy. To extract raw materials from liquids, various extraction methods

are developed such as adsorption, liquid-liquid extraction, ion sieves, electrochemical precipitation, co-precipitation, or membrane distillation. The choice of a particular technique depends on the composition of the fluid, the initial concentration as well as the desired compound to be processed (Ryu et al. 2016). Furthermore, it must be compatible with the challenges imposed by the chemistry of thermal waters.

8.4 Pretreatment of thermal waters

8.4.1 Methodology

In high-enthalpy geothermal fields, precipitation of amorphous silica is the limiting factor for the possible amount of extractable energy (Gunnarsson and Arnórsson 2005). With 16 GWe installed worldwide capacity in high-enthalpy geothermal power plants in 2020 (Huttrer et al. 2020) this challenge concerns major parts of the geothermal industry worldwide. Furthermore, the efficiency of raw material extraction from brines can be improved by pre-concentration of the target minerals (Ryu et al. 2016). Both processes, cooling for energy production and concentration for enhancing the extraction process, potentially increase silica precipitation. To avoid damage to the power plant or the extraction facility, silica precipitation must be controlled.

The solubility of silica phases is strongly driven by temperature as displayed in Figure 43. Geothermal brines are assumed to be in equilibrium with the surrounding lithology under reservoir conditions (Fournier and Rowe 1966). This typically results in saturation with respect to quartz under the given reservoir conditions. During production, this equilibrium is perturbed and the fluid tends to oversaturate which leads to a risk of unwanted precipitation. Likewise, oversaturation can also result from increasing the general SiO_2 content (Figure 43) during the pre-concentration step.

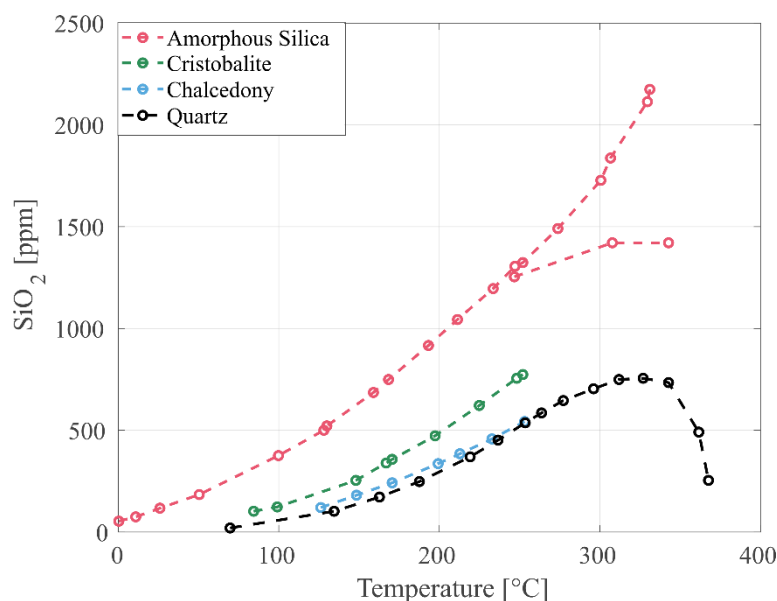


Figure 43: Solubility behavior of silica. The plot shows the solubility of different silica polymorphs/phases in dependency of the temperature (Data Source reference (Fournier and Rowe 1966)).

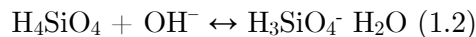
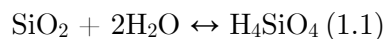
In order not to limit the potential concentration rate, the method of selective precipitation was preferred over precipitation inhibition. The challenge was to find a compound and an associated precipitation process that is cost-efficient, integrable into the power plant process, and selective for silica to not affect the content of valuable elements. With the comprehensive expertise of the research consortium in a multi-stage and interdisciplinary process (Figure 44), a treatment strategy was developed and implemented in a large-scale prototype in less than 12 months.



Figure 44: Flow chart summarizing the problem-solving approach in the BrineMine project. Based on the challenge of silica fouling, a treatment strategy was developed in the laboratory. This approach was upscaled first using a numerical design calculation. The simulation results were subsequently reproduced in a technical center leading to the construction of a 1st generation prototype.

Various precipitation methods were compared in small-scale lab experiments using artificial brines which have been designed according to the chemistry of Chilean thermal waters. The successful method results from changing the species distribution of the silica. SiO_2 dissolves in water under the formation of silicic acid (H_4SiO_4) as shown in equation 1.1 (Iler 1976). An increase in pH leads to ionization of the silicic acid (Equation 1.2 and 1.3) (Iler 1976). At a pH value of 10.5 H_3SiO_4^- is the dominant species. This negatively charged species react in the presence of double or higher valent cations (e.g. $\text{Ca}^{2+}/\text{Mg}^{2+}$) under the formation of Calcium/Magnesium-silicate-hydrate (C/MSH) phases. The associated precipitation is almost instantaneous. This enables controlled silica precipitation as a pre-treatment before concentrating.

Silica species reaction (Iler 1976):



After the small-scale testing in the laboratory was successful, the process was transferred to a larger scale at the technical center in the Fraunhofer Institute (ISE) in Freiburg. The precipitation experiment was reproduced successfully. Based on this intermediate step a large-scale prototype was developed. A numerical geochemical model was set up for extrapolating the results for the application with complex natural brines and to quantify the mass flows. Based on these results, the prototype was designed and dimensioned.

8.4.2 Prototype Design

The prototype plant is developed, built, and operated in a real-life environment to demonstrate the suitability and flexibility of the full pre-treatment process chain. The process scheme and integration strategy for the demonstrator are visualized in Figure 45. The demonstration plant

is designed to be hooked-up either to the pressurized thermal brine flow of a geothermal power plant or a non-pressurized thermal brine well. A bypass stream of the geothermal brine is extracted from the main flow path and fed into the demonstrator. The design flow rate here was a continuous stream of 20-50l/h. In the first process stage, the problematic typical high load of silica is selectively precipitated following the developed strategy. The system continuously adjusts the condition within the reactor to an optimal set of molar Ca/Si ratio as well as pH, also taking into account the natural content of calcium in the currently processed geothermal brine. The precipitates are extracted from the water stream by filtration. In the second stage, the brine is pre-concentrated with the efficient pressure-driven reverse osmosis (RO) process, which extracts fresh water through a semi-permeable membrane through which the dissolved solids cannot pass. The pre-concentration potential of this process stage depends on the natural salinity of the given brine and will reach a salinity level of about 70,000 mg/L at a typical operation with a pressure of 60 bar. Consequently, for low saline thermal brines (e.g. El Tatio, Chile, ~10,000 mg/L (Giggenbach 1978)) a significant pre-concentration is possible, for super saline brines (e.g. Upper Rhine Valley ~110,000 mg/L (Sanjuan et al. 2016a)) the pre-concentration stage is bypassed and the brine is directly forwarded to the post-concentration stage. The post-concentration relies on the thermally driven membrane distillation (MD) process, in which water is extracted from the brine by evaporation through a vapor-permeable membrane. Since MD basically relies on the phenomenon of an evaporative separation, it is not fundamentally limited to a certain final concentration. The limitation is indirectly given by energy efficiency considerations or supersaturation of specific species that induce crystal nucleation and consequently membrane scaling or flow channel clogging. The MD process stage is considered energetically highly attractive since it is driven by low-grade heat (60-90 °C) that was previously extracted from the geothermal brine. The MD permeate is considered high-quality freshwater due to the super-selective nature of evaporative separation. The concentrate outflow offers a brine with a high content of valuable resources, ready to be used in arbitrary extraction processes.

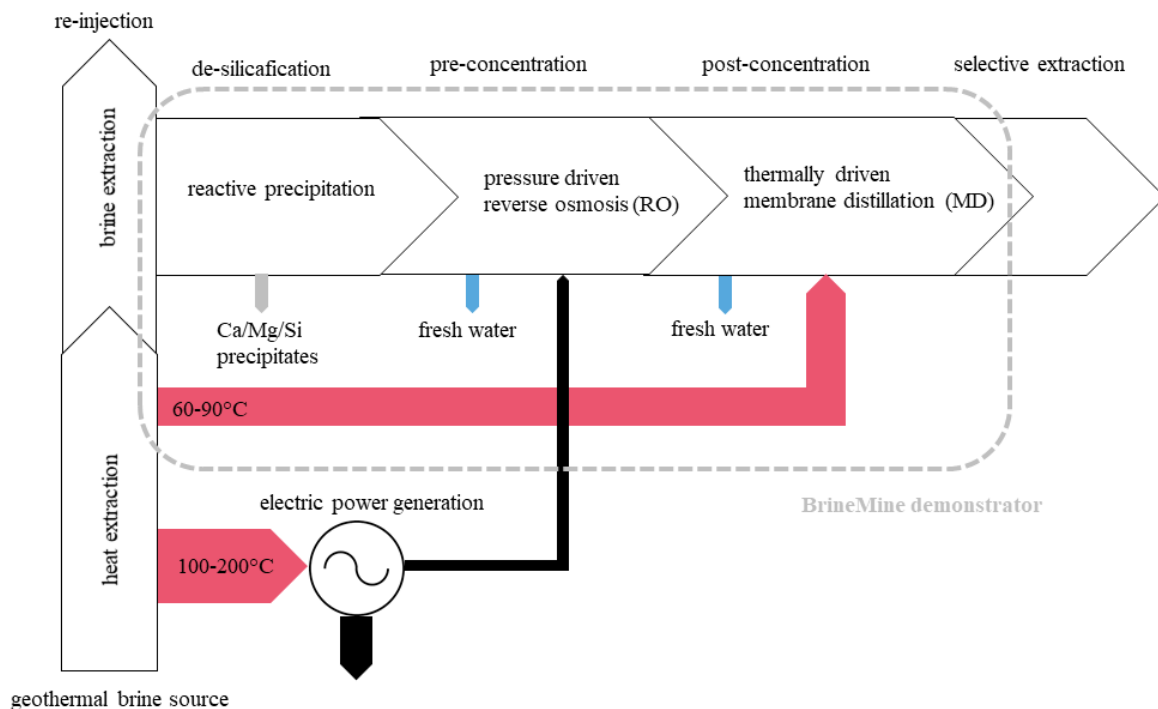


Figure 45: Process scheme and hydraulic/energetic integration strategy for the BrineMine continuous flow demonstrator.

With this design, the first step of the prototype application was conducted by installing it in an actively operating geothermal power plant located in the Upper Rhine Valley in Germany.

8.4.3 Prototype Testing

Due to the COVID-19 pandemic, the prototype could not be tested in Chile yet. An alternative was found at the geothermal power plant Insheim in the Upper Rhine Valley (Germany) operated by Pflanzwerke geofuture GmbH (Figure 46). Consequently, the prototype was calibrated for geothermal waters with higher salt load and lithium concentration, and a lower silica concentration. It was successfully implemented in a running power plant cycle operating in a continuous flow system (flow rate 20-50l/h) while handling total dissolved solids of up to 120,000 mg/L of highly corrosive brines (Figure 47).



Figure 46: Geothermal power plant Insheim (Source: Pflanzwerke geofuture GmbH).



Figure 47: Prototype installed at the geothermal power plant Insheim. The left picture shows the prototype. Precipitates are shown in the two pictures on the right. (Source: Valentin Goldberg / Sebastian Held).

Figure 48 shows the results of the successful treatment. Silicon and magnesium immediately (< 5 minutes) underwent a reduction of 98 % while calcium showed a delayed reaction. Importantly, the concentration of lithium, a potential target mineral, is not affected during the entire process time. Furthermore, preliminary results indicate no incorporation of other trace

elements such as cesium or rubidium. This proves that the developed silica controlling process is replicable for complex brines without affecting target elements. The results indicate that the risk of silica scaling is greatly reduced even in terms of further cooling and concentrating. Subsequently, the brine was concentrated by constricting the water through membrane distillation. This step facilitated the concentration of lithium up to 500 mg/L (and a total salt load of 300,000 mg/L), which corresponds to a concentration factor of ~ 3 and puts it into the realm of Chilean salt lake brines. If once applied to fluids with lower initial salt loads a higher relative raw material concentration is possible. If the El Tatio fluid with approx. 10,000 mg/L TDS and 61 mg/L of Lithium, is concentrated to the same total salt load, a lithium content of 1,830 mg/L can be achieved. Also, note that the silica and magnesium concentrations did not reach critical levels in terms of oversaturation during the application of the membrane distillation. The measurements of the permeate of the MD showed the integrity of the membrane and thus the production of pure water.

The promising results of the large-scale prototype application represent an important milestone for future mineral extraction from geothermal loops. It provides important information for a potential full-scale and long-term implementation. The kinetics were much faster than in the laboratory experiments using artificial brine. This can be explained by the higher salt load resulting in an increased salting-out effect and activity coefficient of the water (Marshall and Warakowski 1980b). In a flow-through system, the reaction time is a function of vessel size and flowrate. Fast kinetics thus enable the processing of high flow rates without requiring large reaction tanks. This improves a possible implementation in a running geothermal loop without extensive changes to the geothermal plant design and facilitates an application in geothermal power plants worldwide.

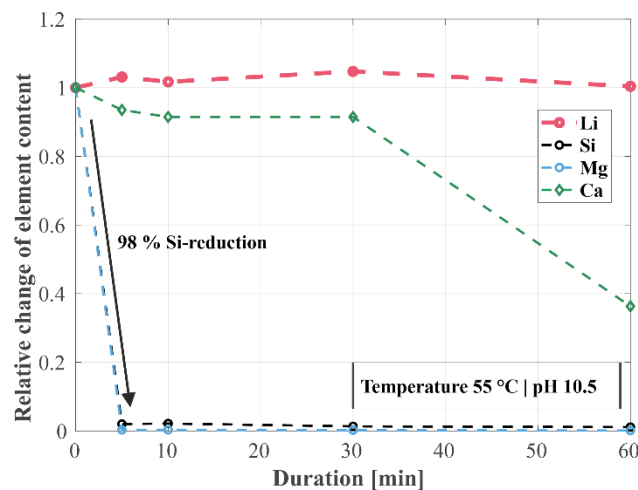


Figure 48: Effectiveness of silica treatment. The graph shows the relative change of chosen elements during the prototype testing. Within 5 minutes, the total content of Si is reduced by 98 %. Li as raw material reference stays unaffected and varies within the scope of measurement inaccuracy.

8.5 Outlook and global potential

The scenario analysis of Chilean hot springs showed the promising economic potential of thermal waters. Furthermore, the implementation of the 1st generation prototype in the Upper Rhine Valley (Germany) illustrated a successful installation of a mineral extraction facility in

an operating geothermal power plant. To extrapolate these two locally demonstrated potentials, a preliminary worldwide database was compiled (Figure 49). The aim is to collect international geothermal chemistry data to assess the global potential of Brine Mining. Beyond the economic aspect, the database can serve as a tool for upcoming exploration projects in terms of geochemical exploration or scaling risk assessment.

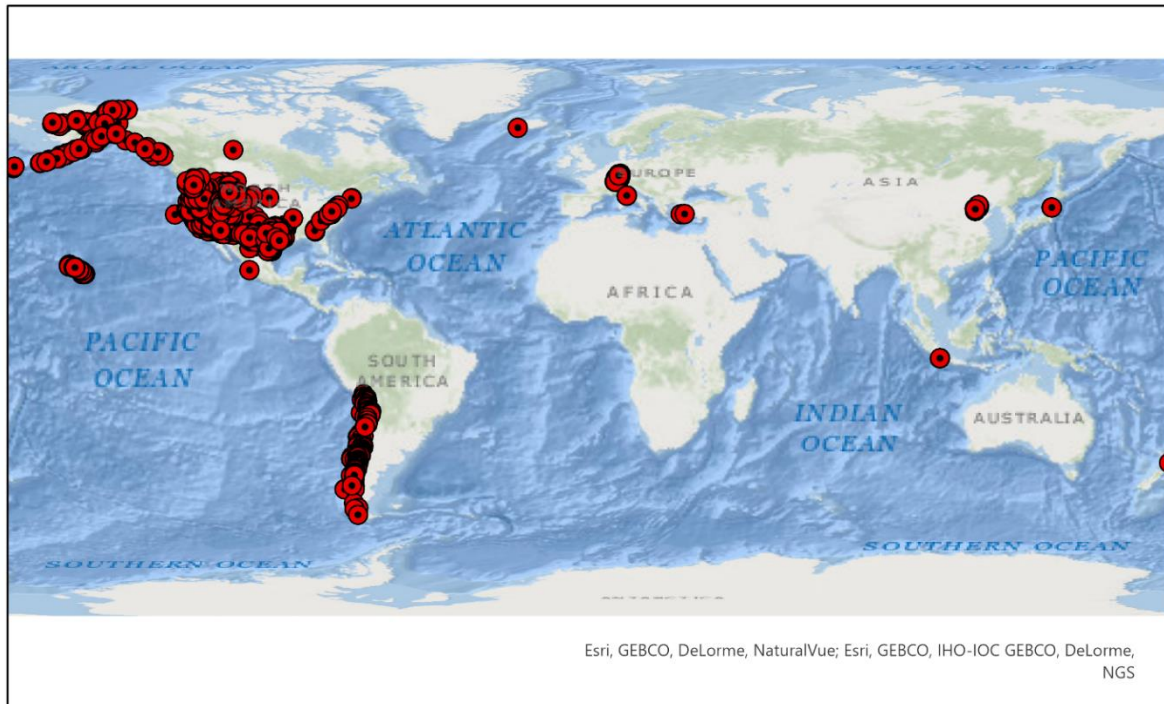


Figure 49: Preliminary worldwide database of geothermal brines. The database currently contains data of ~10,000 springs and provides the basis for the evaluation of the global economic potential of Brine Mining (Data sources: (Allen et al. 2006; Aquilina et al. 2002; Arnórsson et al. 1983; Cortecci et al. 2005; Giggenbach et al. 1994; Giggenbach 1992; Giggenbach 1978; Gokgoz et al. 2010; González-Partida et al. 2005; Grasby et al. 2000; Karamanderesi and Ölçeno 2005; Karingithi et al. 2010; Kato et al. 2003; Kaya and Kindap 2009; Lowstern et al. 1999; Neupane and Wendt 2017; Nicolau et al. 2014; Özkaya 2007; Ozler 2000; Pauwels et al. 1993; Risacher et al. 2002; Sanjuan et al. 2016a; Sanjuan et al. 2010; Serpen and Aksoy 2010; Simsek 2003a; Simsek 2003b; Tarcan et al. 2000; Tassi et al. 2011; Tekin 2010; Wrage et al. 2017; Yeltekin and Akin 2006; Yildirim et al. 2010)).

The preliminary database contains about 10,000 data points, summarizes global chemical data from hot springs and thermal wells and complements the US database collected by Neupane and Wendt (Neupane and Wendt 2017). The economic potential of raw materials demonstrated in particular thermal brines can thus be transferred to other geothermal areas. A first preliminary analysis of the collected data indicates a high worldwide potential. As displayed in Figure 50, 12 of 30 elements defined by the European Commission as critical raw materials can be enriched in geothermal brines (Europäische Kommission 2020). Further elements of high economic value are also frequently found to be enriched.

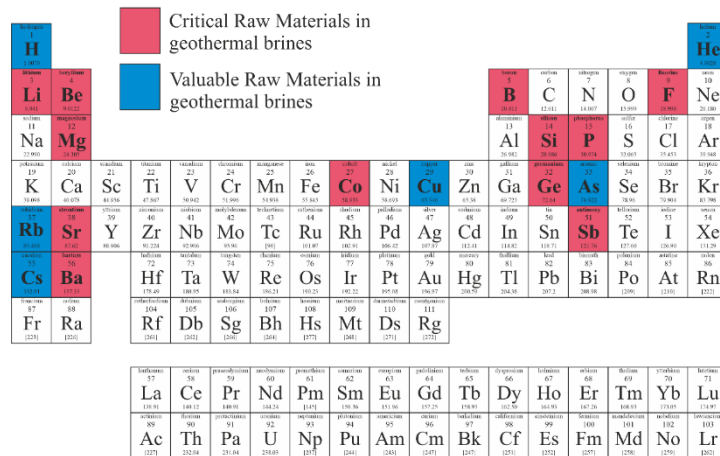


Figure 50: Economic valuable elements in thermal waters. In red: elements that are classified as critical elements by the European Commission (Europäische Kommission 2020). In blue: other elements that are of high economic value and were found to be enriched in the global brine database.

8.6 Conclusion

During the first phase of the BrineMine project, the potential of raw material extraction from geothermal waters in Chile was analyzed. Not only elements used in the high-tech industry (e.g. lithium) should be in the focus for extraction but also bulk raw materials that occur in higher quantities (e.g. boric acid). Our investigations indicate an enormous worldwide economic potential for the extractions of raw material from thermal waters. To unleash this economic potential of thermal waters with their complex chemistry an effective method to control silica precipitation was developed. Tests in an operating geothermal power plant demonstrated the possibility to treat brines for specific components like silica and simultaneously concentrate valuable raw materials like lithium. The precipitated silica-calcium-hydrate phases can also be seen as a resource themselves. The almost total reduction of silica is a potential mean for silica scaling mitigation which could increase the efficiency of conventional geothermal power plants independent of raw material extraction. The large-scale prototype demonstrated the feasibility of the developed treatment strategy during continuous operation. Furthermore, important parameters for the optimization of the prototype were identified. Based on these experiments the prototype will be adjusted to Chilean brines and implemented at its original destination.

The first real-life application of mineral extraction at an operating geothermal power plant is a huge milestone for the realization of Brine Mining’s global potential. Compared to conventional mining methods the raw materials are already dissolved in thermal waters and do not have to be leached out of a hard rock deposit. Since the fluid serves as the media of transport bringing the target minerals to the surface, efforts in terms of mining and infrastructure as well as land use are greatly reduced compared to conventional open-pit mining. Consequently, Brine Mining has a great potential for a more sustainable and environmentally friendly raw material production.

The potential has been proven. Now, economical extraction technologies for each element have to be developed, adapted to the individual brines and implemented in geothermal power plants. For entering the large economic and ecologic potentials of Brine Mining, a site-specific raw material and extraction concept will be mandatory. A buried treasure lies beneath our feet, considering the high volumes of thermal water circulated in geothermal power plants and the contents of valuable elements dissolved in these waters. Lifting this treasure will be beneficial for the geothermal industry and beyond.

8.7 Acknowledgment

The authors gratefully acknowledge research funding by BMBF Client II for the BrineMine Project (Federal Ministry of Education and Research, FKZ: 033R190B). We thank Prof. Dr. J. Kolb and Dr. E. Eiche of the department of Geochemistry & Economic Geology (Karlsruhe Institute of Technology, Division of Applied Geosciences) for the support in developing the measurement strategy and the access to laboratories and equipment as well as for fruitful discussions. The team of Pfalzwerke geofuture GmbH is thanked for the possibility of conducting the prototype implementation at the powerplant Insheim and the pleasant cooperation during sampling. Further, we thank Transmark Renewables for the productive discussions and for enabling a joint sampling campaign. Finally, we appreciate the support of the Chilean ANID-Fondap program (projects 15090013 and 15200001).

9 Prototype tests for the treatment of geothermal waters for raw material extraction and freshwater production

This manuscript has been published in *Mining Report. Glückauf*. 159, 601–610 (2023).

Valentin Goldberg^{a,b}; Daniel Winter^c, Elisabeth Eiche^{d,e}; Joachim Koschikowski^c, Thomas Kohl^a, Diego Morata^b, Rebecca Schwantes^f; Peter Seibt^g, Julian Heboldt^g, Fabian Nitschke^a

^a Chair for Geothermal Energy and Reservoir Technology, Institute of Applied Geosciences, Karlsruhe Institute of Technology, Adenauerring 20b, 76131 Karlsruhe,

^b Andean Geothermal Center of Excellence (CEGA) and Department of Geology, Facultad de Ciencias Físicas y Matemáticas, Universidad de Chile, Santiago, Chile.

^c Fraunhofer Institute for Solar Energy Systems ISE, Heidenhofstraße 2, 79110 Freiburg, Germany

^d Chair for Geochemistry and Economic Geology, Institute of Applied Geosciences, Karlsruhe Institute of Technology, Adenauerring 20b, 76131 Karlsruhe,

^e Laboratory for Environmental and Raw Materials Analysis (LERA), Institute of Applied Geosciences, Karlsruhe Institute of Technology, Adenauerring 20b, 76131 Karlsruhe,

^f SolarSpring GmbH, 79114 Freiburg, Germany

^g Geothermie Neubrandenburg GmbH, Germany

9.1 Abstract

Geothermal fluids are a proven resource for sustainable baseload energy worldwide. Recently the fluids circulated in large volume streams in geothermal power plants have also come into focus for the potential of raw material extraction, such as Lithium. Geothermal fluids are the product of high-temperature and high-pressure water-rock interaction. This results in varying degrees of enrichment of different elements. Among them are elements of economic or strategic interest (as Li, Mg, Cs) but also elements typically causing unwanted mineral precipitations (scaling) within geothermal power plants such as Si. The extraction of specific target elements is still challenging in terms of integrating the process technology in a geothermal cycle. Especially in volcanic geothermal systems target elements are lower concentrated than in conventional brine resources and further the fluids tend to silica scaling. To enable the efficient extraction of the target elements, a treatment strategy was developed, consisting of an effective precipitation unit for silica reduction and two combined concentration steps for the enrichment of the target elements. The method uses the controlled precipitation of Si as Calcium-Silica-Hydrate phases and the concentration is conducted by reverse osmosis (RO) and membrane distillation (MD) using geothermal heat. The treatment approach was incorporated in a field demonstrator and tested in a geothermal system in the Southern Volcanic Zone in Chile. The results showed an effective silica reduction, enabling concentration rates up to a concentration factor of 16 under continuous flow-through conditions. The concentration of the dissolved solids on one side of the membranes enabled further the production of freshwater from geothermal fluids on the other site. Moreover, the MD process shows high energy efficiency in comparison to conventional evaporation processes, and by geothermal sourcing also has direct potential for fossil fuel saving. Since volcanic resources are the most used in the global geothermal sector in terms of installed capacity, the effective handling of the fluids has the potential for unleashing a global geothermal raw material potential.

9.2 Introduction

The energy transition and associated electrification shifts the demand for raw materials from hydrocarbons to various metal resources. Several of these, partly rare, metals have poorly diversified value chains (e.g. Li or Co) as well as high associated environmental impacts during their production. Geothermal fluids as circulated in geothermal power plants can globally have considerable enrichments of valuable and even critical raw materials such as Li, Sb, Mg, or Cs (Goldberg et al. 2021; Neupane and Wendt 2017). The economic potential unfolds by combining the element concentration with the high flow rates (> 60 L/s) prevailing in geothermal energy production (Goldberg et al. 2022b). Chile, with more than 200 active volcanoes, shows a large abundance of hydrothermal systems. This abundance leads to one of the largest geothermal potentials worldwide (Aravena et al. 2016). The large potential for the Chilean energy sector is proofed by the first geothermal power plant Cerro Pabellón with an installed capacity of 81 MW_e (Morata et al. 2020). Its raw material potential can be outlined by combining the flowrates of the 8 production wells (up to 560 L/s) (Cappetti et al. 2020) with the measured Li concentrations (60 mg/L) (Giudetti et al. 2020) resulting in 1060 t of pure Li circulated every year. This amount equals roughly 3 % of the whole Chilean Li production in 2022 (U.S. Geological Survey 2023) and would be sufficient for about 100,000 electric vehicle batteries. A multi-use of geothermal resources could be of several benefits. The additional revenue would strongly improve the economics of geothermal projects. The approach of direct Li extraction (DLE) from geothermal fluids would be moreover less consuming in terms of water and land use compared to conventional mining and additionally be self-supplying in terms of energy. Moreover, the accumulated amounts are in an order of magnitude that would enlarge Chile's global market share in Li production significantly.

A key challenge for geothermal energy production and even more for DLE application on geothermal fluids is the uncontrolled precipitation of minerals supersaturated in the solution. Especially silica scaling poses high demands during processing (Goldberg et al. 2022a; Gunnarsson and Arnórsson 2005). For this purpose, a controlled precipitation and treatment strategy was developed in the laboratory (Spitzmüller et al. 2021) and transferred into the design and construction of a demonstrator, which was already tested in an operating geothermal power plant in Germany (Goldberg et al. 2023b). The herewith presented study shows the application of an updated version of the tested demonstrator customized for fluids from volcanic geothermal systems. Since volcanic fluids are the most frequently used source to provide geothermal power globally, successful raw material extraction would unleash an enormous potential. Therefore, the demonstrator was tested in continuous operation processing fluids from a hot spring in the Chilean Southern Volcanic Zone.

The research work presented was conducted in the framework of the BrineMine project funded by the German Federal Ministry of Education and Research (BMBF). The project was realized between 01.03.2019 and 31.03.2023 as a bi-national research project between German and Chilean research and industrial partners. The project structure features two focal points: 1) Determination of the economic potential of thermal waters as a raw material resource and 2) Pre-treatment of thermal waters prior to raw material extraction. Project partners on the German site are the Fraunhofer Institute ISE (Institute for Solar Energy Systems) the

Karlsruhe Institute of Technology (KIT), SolarSpring Membrane Solutions GmbH, and Geothermie Neubrandenburg (GTN). Associated partners in Chile are the Andean Geothermal Centre of Excellence (CEGA) at the Universidad de Chile, Fraunhofer CSET, GTN Latin America, and Transmark Renewables.

9.3 Fundamentals

9.3.1 Geothermal Setting

Geothermal resources in Chile are strongly related to the active Andean volcanism. This volcanism is the result of the ongoing subduction of the Nazca Plate under the South American Plate that has taken place since Jurassic times (Morata et al. 2020) and hosts over 300 geothermal areas (Aravena et al. 2016). The developed treatment system was tested in the field using geothermal volcanic fluids from the Termas de Puyehue, which are located in the region Los Lagos, about 100 km northeast of Puerto Montt. They were chosen because of the good accessibility via an installed well, sufficiently high temperatures (50-60 °C), and the availability of infrastructure for transporting and installing the demonstrator. The fluid has a low mineralization (~500 mg/L) yet is still enriched concerning various valuable elements such as Li, V, Mo, and Cs (Table 19). Thus, the effect of the treatment process on different elements can be determined. The chemical signature shows an intermediate water type with volcanic and meteoric influences as indicated by the ratios of the main anions and cations (Dorsch 2003). Elevated SO₄ concentrations indicate volcanic origin respectively heating by volcanic sulfuric gases or sulfate weathering. High Si concentrations (50 mg/L) are the result of the elevated temperatures and enhanced water-rock interactions, indicating subsurface temperatures of about 80 °C using conventional geothermometers (Powell and Cumming 2010). The geothermal fluids are currently used for different thermal baths, sanitary hot water, and water supply of the various kitchens and laundries.

9.3.2 Treatment strategy

For extracting raw materials from geothermal fluids, various approaches are currently being investigated (Reich et al. 2022; Stringfellow and Dobson 2021a). In terms of extraction efficiency, higher raw material concentrations are favorable (Ryu et al. 2016). Thus, concentrating the dissolved element content before the extraction process is advisable. For enabling an efficient treatment in geothermal power plants, membrane processes open up great possibilities. Especially reverse osmosis (RO) powered by high pressures and membrane distillation (MD) powered by thermal energy could efficiently be incorporated into geothermal power plants. Moreover, these processes offer the additional possibility of fresh-water production. However, membrane technologies are susceptible to silicate precipitation in volcanic areas (Salvador Cob et al. 2014; Zhang et al. 2018).

For removing silica and thus, implementing membrane processes in geothermal settings, lime precipitation was evaluated (Spitzmüller et al. 2021). The approach aims at transferring the aqueous silica into the negatively charged H₃SiO₄⁻ species by increasing the pH value > 10

(Eikenberg 1990; Iler 1976). In the presence of positively charged, divalent cations such as Ca^{2+} , Calcium-Silicate-Hydrate (CSH) phases can form (Gaboriaud et al. 1999; Maraghechi et al. 2016) and precipitate, thus reducing the Si and Ca content in solution. The described approach reached a silica removal of 98 % in previous studies (Goldberg et al. 2023b; Spitzmüller et al. 2021). In the demonstrator field tests in the geothermal power plant in Germany, a membrane distillation module downstream enabled concentrating of the already saline brine (~105 g/L TDS) by a concentration factor (CF) of 3 (Goldberg et al. 2023b). The successfully tested demonstrator was then optimized for less saline, volcanic fluids.

9.3.3 Technical Set-up

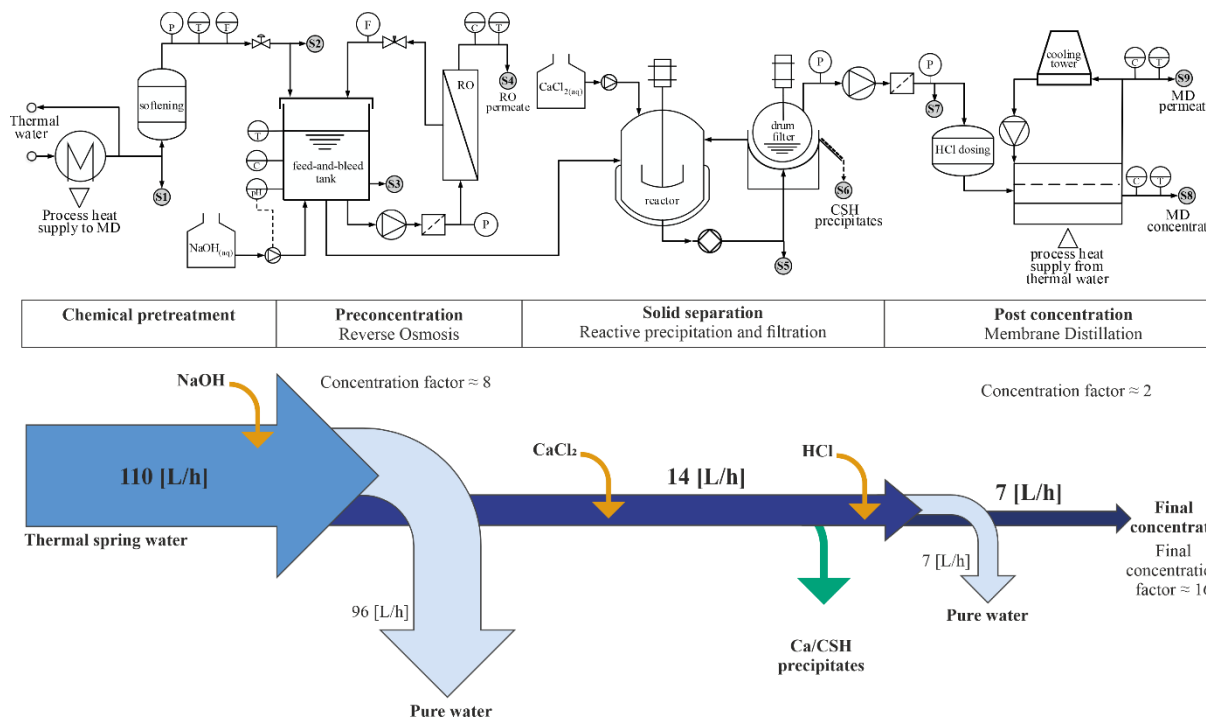


Figure 51: Technical scheme of the demonstrator setup, separated into 4 major sections. The flow diagram displays the associated mass flows in terms of solids and liquids.

The demonstration plant (Figure 52a) for continuous operation was developed and built by Fraunhofer ISE in collaboration with SolarSpring GmbH. The hydraulic scheme (Figure 51) displays the major process steps: Process heat extraction, initial softening, RO pre-concentration, Si-reduction, liquid/solid separation, and MD post-concentration. The demonstrator is connected to the thermal water directly at the thermal spring with temperatures of about 60 °C and a defined flow rate of 110 L/h. After the MD heat extraction, the fluid enters the chemical pretreatment unit (Figure 52b) at about 55 °C. To avoid spontaneous reaction with Si in the following steps the water is first passing through an initial softening step for removing bivalent ions such as Ca and Mg. Afterward, the fluid enters the 40 L recirculation buffer tank. Here the fluid is introduced by an open inflow and the pressure is relieved to atmospheric level. Furthermore, in the buffer tank, the pH is adjusted to pH 10.5 by a controlled NaOH dosing system, to increase the solubility of Si for the RO step and at the same time transferring Si into the negative aquatic species for later precipitation. This allows a significant pre-concentration of the Si-rich solution by a RO system operating at 25 bar in a feed-and-bleed operation mode and concentrates the brine by a factor of 6-10. While

the main part of the water (96 L/h) is collected as high-quality permeate, the small fraction (14 L/h) of high pH concentrate leaves the recirculation tank through an overflow and gets introduced into a continuously stirred tank reactor (CSTR) with a working volume of 14 L corresponding to a residence time of about 60 min. The reactor includes a flow-controlled dosing system that doses Ca ions in the form of an aqueous CaCl₂ solution to generate a super saturation with regard to amorphous CSH phases and thus initiates their precipitation. Along with the CSH phases, Ca carbonates form. The suspension is then passed through a custom-made miniature vacuum drum cake filter system (Figure 52c), which separates and dewateres the CSH precipitates from the suspension (Figure 52d). The pH of the filtrate is then re-adjusted using HCl before being led into the next module. The last step in the process chain is a MD post-concentration that is thermally driven by the heat extracted from the inlet section of the demonstrator. Here, a spiral-wound membrane module with an active membrane area of 9 m² is applied. The module is built in a feed-gap configuration (FGMD) (Schwantes et al. 2019). The small feed stream is passed through a narrow gap and receives heat through a thin polymeric film from a heating solution. Pure water is extracted in vapor form that passes through a hydrophobic, microporous membrane and condenses in a cold permeate stream. The permeate is recirculated through a cooling tower that acts as a heat sink and allows the control of its temperature. The integrity of the membrane is monitored by conductivity measurement of the produced water. The quantification of the water extraction is done utilizing an electronic scale. The demonstrator includes 9 sampling points, indicated with S1 to S9, that allow a chemical characterization of the water and solids in all relevant process steps.



Figure 52: a) BrineMine field demonstrator in operation with natural thermal brine in Puyehue, Chile. b) Overview precipitation section. c) Drum filter for separation of CSH precipitates d) Difference CSH Suspension in tank reactor and collected Filtrate.

9.3.4 Sampling and Analysis

During the field operation, fluid temperature and pH values were measured using a compact precision handheld meter (WTW Multi 340i). To remove particles, all fluid samples were filtered with a syringe filter using a cellulose acetate filter (0.45 μm). To avoid precipitation or further reactions after the sampling process, samples for silica measurements were directly diluted by a factor of 1:10 using distilled water. For major and trace element analysis, separate samples were acidified using suprapure (37 %) hydrochloric acid. Major cations were measured

with inductively coupled plasma optical emission spectrometry (ICP-OES, ICap 7000, ThermoFisher), anions were measured via ion chromatography (IC, Compact 930, Methrom), and trace elements with inductively coupled plasma mass spectrometry (ICP-MS, ICap RQ, ThermoFisher). Precipitates were dried in the oven overnight at 105 C. The mineralogy was analyzed with X-ray diffraction (XRD, D8 Discover, Bruker) and the major element chemistry using wavelength-dispersive X-ray spectroscopy (WDX, S4 Explorer, Bruker AXS) on fused beads. The analyses were conducted at the Laboratory for Environmental and Raw Materials Analysis (LERA), Institute of Applied Geosciences, Karlsruhe Institute of Technology.

9.4 Results

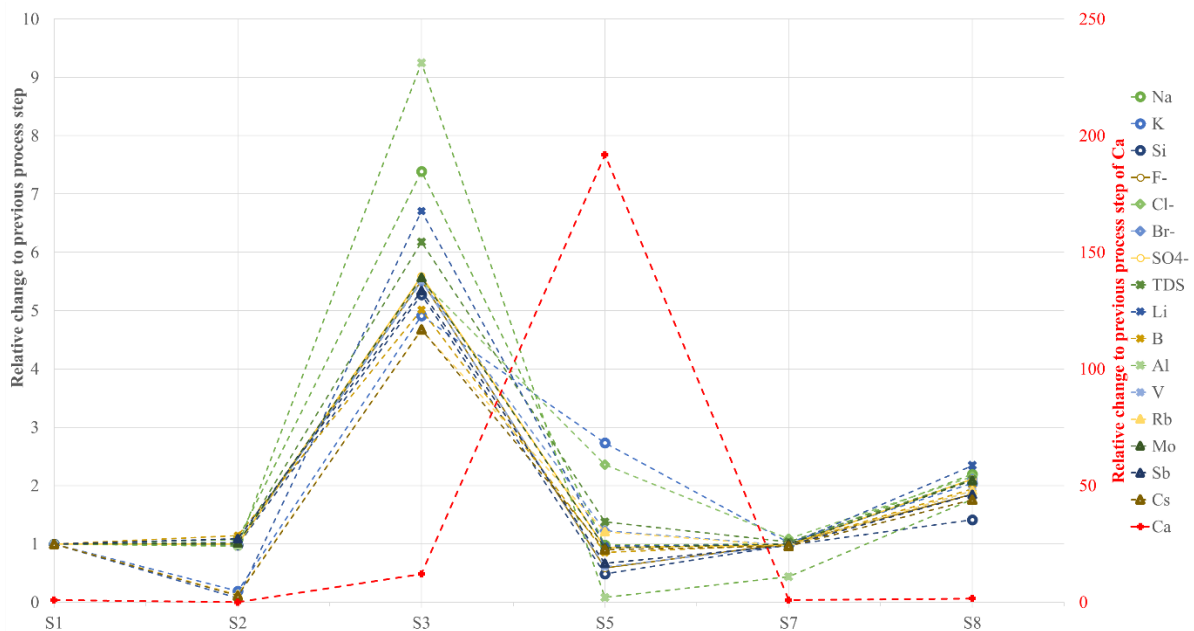


Figure 53: Influence of the different process steps on the individual element concentration. The figure shows the relative change in element concentrations (Table 19) between all sampling points. This enables to evaluate every single step in its influence on its own. Ca refers to the secondary y-axis (red).

The results of the multi-element analysis are displayed in Table 19 and the relative changes between the individual process steps, induced by the treatment can be seen in Figure 53. Si, as the major scaling forming element, passes through the first chemical treatment step. It becomes enriched by a CF of 5-6 during the RO and is reduced in its concentration through precipitation by about 50% due to the addition of CaCl_2 . During the MD step, it becomes concentrated concurrently with other elements. Na concentration increases strongly at S3 because of the NaOH addition to reach a pH value >10 and increases further along with the water extraction of the membrane processes. Ca is initially totally removed by the softener (between S1 and S2) but its concentration increases again between S3 and S5 due to the CaCl_2 addition. Cl concentration enriches conservatively during the membrane processes and shows a strong increase at S5 due to the CaCl_2 addition. The comparison with the solid chemistry (Figure 54) shows, that the formation of CSH-phases and associated co-precipitation of Ca carbonates was successful. In contrast to the previous studies (Goldberg et al. 2023b; Spitzmüller et al. 2021), the silica reduction was only 50 % instead of 98%.

The alkali metals Li, Cs, Rb, and K are negatively influenced by the primary water-softening step (between S1 and S2) and become strongly reduced by 80 – 90 %. After this step, the alkalis do not show an influence by the chemical treatment as in the previous studies (Goldberg et al. 2023b; Spitzmüller et al. 2021) and become concentrated in the order of magnitude expected from the membrane flowrates (CF 5-7 for RO and ~2 MD). Elements such as F, Al, V, and Sb pass through the softening step but partly co-precipitate during the CSH-precipitation step (between S3 and S5). SO₄, B, and Mo do not interact with the chemical processes and just become concentrated linearly with the water extraction. The analysis of the final permeate (S9) shows, that the membrane integrity could be maintained during the production, and the production of pure water (25 mg/L TDS) was successful during continuous operation. In further experiments, the MD was operated with the treated fluid in a batch feed-and-bleed mode to reach higher enrichment rates. The experiments enabled further concentration to a CF of about 5 reaching a final CF of up to 100 and a final TDS of about 40.000 mg/L.

Table 19: Chemical analysis of selected elements over the whole treatment cycle. The referred sampling points (S1-S9) can be located in Figure 51. The last row displays the results of the batch concentration experiment using pre-treated brine.

Samplin g Point	T	pH	Na	K	Ca	Si	F ⁻	Cl ⁻	Br ⁻	SO ₄	TDS	Li	B	Al	V	Rb	Mo	Sb	Cs	
	[°C]						[mg/L]									[µg/L]				
S1	50.9	8.35	160	4.69	7.77	50.9	1.83	142	0.47	118	486	344	2520	20.8	4.11	32.4	12.4	4.88	31.9	
S2	49.0	8.39	172	0.90	0.11	49.9	1.83	142	0.47	117	485	23.8	2874	20.0	4.22	4.18	12.6	5.30	3.51	
S3	41.7	11.0	1270	4.40	1.38	263	10.1	784	2.60	656	2992	160	14416	185	23.2	19.5	70.2	28.3	16.4	
S5	34.5	10.5	1247	12.0	265	128	5.91	1850	3.20	618	4129	154	12340	15.6	14.0	23.6	65.4	18.8	14.8	
S7	30.7	8.10	1248	12.3	261	126	5.92	2018	3.12	607	4281	153	12143	6.82	13.7	22.9	65.4	18.3	14.2	
S8	36.7	7.57	2739	25.1	422	178	11.0	4345	6.60	1280	9008	357	23627	12.0	26.1	43.8	137	33.8	25.0	
S9	42.5	10.4	15.6	0.05	0.24	5.3	0.01	1.55	0.01	2.40	25.1	2.06	113	6.63	0.09	0.22	<0.073	<0.346	0.17	
MD _{max}	56.0	7.93	12601	115	1733	187	7.69	21064	32.0	4417	40163	4934	79414	16.2	85.9	209	617	108	115	

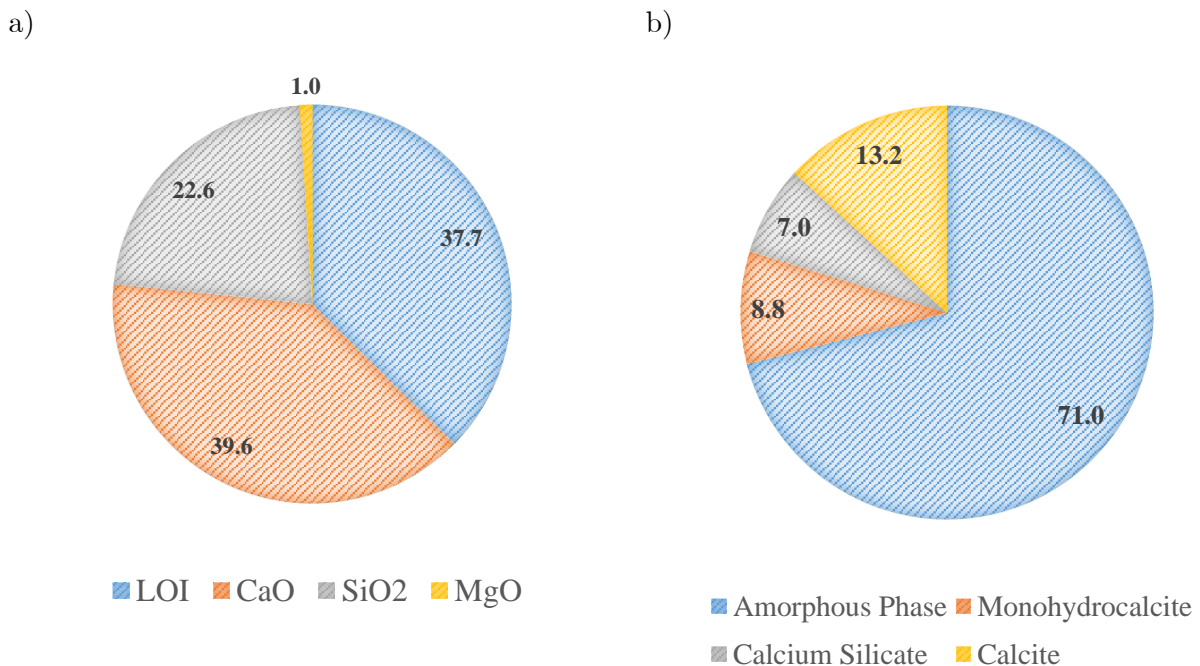


Figure 54: Chemistry and Mineralogy of the precipitates, taken at S6. a) WDX analysis (LOI stands for loss on ignition). b) XRD analysis.

The MD manufactured on average a flowrate of 14 L/h creating 7 L/h of permeate as well as 7 L/h of concentrate. The heat demand of the process was derived by cooling 300 L/h (-0,08 L/s) of spring water from -60 °C to -55°C before entering the chemical treatment unit. The thermal springs show at the central well a joint seasonal flow rate between 4.5 and 9.0 L/s. With a density of 983.55 Kg/m³ and a specific heat capacity of 4.18 kJ/kgK, different energy production scenarios were determined depending on the flow rate and potential heat extraction (Table 20). The thermal heating demand of the MD, derived by the geothermal spring was in the range of about 1.6 kW leading to an average specific heat consumption of 225 kWh/t for one ton of permeate respectively concentrate. In comparison to an ideal evaporation of one tone of water consuming about 655 kWh/t, the MD process needs even under prototype conditions, just around one-third for evaporating the same amount of water. The used energy demand equals in the tested configuration 0.9 – 1.7 % of the energy of the whole accessible volume stream. Extrapolating these values on one production week of the demonstrator, leads to a production of 1,176 L permeate using 260 kWh. This energy amount is comparable to the energy of approx. 24 L oil (assuming a calorific value of 11 kWh/L).

In an upscaling scenario using one-third of the total volume stream (1.5 – 3 L/s) for process heat, 5,180 – 10,360 kWh thermal energy could be produced per week for processing 23 – 46 t of fresh water and an equal amount of concentrated brine using geothermal energy. The geothermal energy could substitute on this scale 471 – 942 L of oil per week. Without using the heat recovery of the MD process, the energy demand and consequently the fossil fuel demand would even be higher by a factor of 3. Also, it can be highlighted, that this just represents the extraction of 5 K heat from the brine. Depending on the overall cooling of the fluid this displays just a fractional part of the overall producible energy at the given site (Table 20).

Table 20: Energetic consideration of the Puyehue spring. The assumptions are based on the site-specific parameters of the source temperature (-60°C), the density (983.55 Kg/m³), specific heat capacity (4.18 kJ/kgK), and different cooling scenarios.

	0.08 [L/s]	4.5 [L/s]	9 [L/s]
T _{inj} = 55 °C (ΔT = 5 K)	1.71 [kW]	92,5 [kW]	185 [kW]
T _{inj} = 50 °C (ΔT = 10 K)	3.43 [kW]	185 [kW]	370 [kW]
T _{inj} = 40 °C (ΔT = 20 K)	6.85 [kW]	370 [kW]	740 [kW]
T _{inj} = 30 °C (ΔT = 30 K)	10.28 [kW]	555 [kW]	1110 [kW]

9.5 Concluding remarks

The field study investigated the application of the field demonstrator for controlled silica precipitation and concentration using RO and MD in low-mineralized volcanic fluids. The treatment enabled successfully the production of fresh water. Elements were concentrated by a factor of 20 in continuous operation and up to 100 in batch operation using sustainable geothermal heat. The direct heating use of the MD technology was shown to be energy efficient for water treatment in geothermal systems demonstrating enormous fossil fuel saving potential even when using just a fraction of the overall water flow.

It was demonstrated that the silica reduction under controlled formation of CSH phases was proofed in this environment, but less efficient than in the high-salinity waters in earlier studies. This could be due to the lack of a "salting out" effect in the low mineralization fluids. A further reduction of the silica concentration could still be achieved by longer reaction times or a higher pre-concentration. The results showed that potentially valuable elements such as Li, Cs, Rb, and K are not negatively influenced by the chemical silica treatment and can be enriched using the membrane processes. However, the fluid analysis revealed that for the alkali metals, the water softener was a sink, already reducing their concentrations before entering the demonstrator. Depending on the target elements for a potential extraction, another configuration should be applied. Elements like B and Mo were not influenced by the chemical treatment and concentrated along with the water extraction.

Overall, the field study has demonstrated that even low-mineralized volcanic fluids can be successfully processed using membrane technologies in combination with the developed chemical treatment approach. The processing of these water types for raw material extraction increases the applicability of combinatorial geothermal use enormously, since these high-enthalpy reservoirs supply most of the world's installed geothermal power plants and thus represent a tremendous source of raw materials.

9.6 Acknowledgments

The authors would like to thank the Helmholtz Association for research funding within the Geoenergy subtopic in the MTET (Materials and Technologies for the Energy Transition) program of the Energy research field. Further, the BMBF (Federal Ministry of Education and Research) is thanked for funding the BrineMine project (Grant Number 033R190B) in the Client II framework. In addition, we appreciate the support of the Chilean ANID Fondap program (projects 15090013, 15200001, and ACE210005).

We thank Chantal Kotschenreuther, Maya Denker, and Claudia Mößner of the Laboratory of Environmental and Raw Materials Analysis (LERA), Chair for Geochemistry & Economic Geology (Karlsruhe Institute of Technology, Division of Applied Geosciences) for the conduction of the analysis and the access to laboratories and equipment, as well as for fruitful discussions. Finally, we want to thank the company Tánica for facilitating the implementation of the demonstrator at their Termas de Puyehue and especially Pablo Sánchez and Ronny Oyarzo for their great effort and support before, during, and after the testing phase.

10 Comparison of lime/caustic precipitation mechanisms as pre-treatment in different geothermal fluids

10.1 Abstract

For combined energy, raw material, and freshwater production from geothermal springs, uncontrolled silica precipitation poses one major challenge in terms of efficiency of production as well as longevity of the system. For evaluating a controlled silica precipitation as pre-treatment lime/caustic precipitation was tested in different natural geothermal fluids in Germany and Chile. The key-mechanism is a pH increase > 10 and the presence of divalent cations for reducing aqueous Si under the formation of calcium-silicate-hydrate (CSH) phases.

In high-saline geothermal brines in Germany the approach showed an efficient Si decrease by 98 % in less than 5 minutes, while in low-saline fluids in Chile, only 50 % of Si removal was reached. The experiments underlined that the most decisive factor in terms of Si reduction is the pH value. This relation of the solubility to the pH value enables a targeted adjustment of the residual Si concentration for possible downstream processes.

The resulting precipitates are overall dominated by calcite and in the high saline brines, by portlandite. Further, a large x-ray amorphous phase is typically found as well as amorphous silica and CSH phases. Beyond the elements targeted by the reaction (Si, Ca, Mg), the precipitation influences further metals and metalloids, such as Fe, Pb, Mn, or Zn. If (partly) removal of these elements is desired, depends on the overall setup. The removal of these elements causes an accumulation of potentially toxic elements on the surface, despite they only occur as trace elements in the precipitates. For drinking water use of geothermal fluids, this removal could be desired. Moreover showed different extraction technologies for Li extraction an incorporation of some of these elements. Therefore, could a prior reduction improve the latter raw material extraction.

10.2 Introduction

Scaling is a major challenge in geothermal energy production and during water treatment processes (Badruzzaman et al. 2011; Gunnarsson and Arnórsson 2005; Hörbrand et al. 2018; Mi and Elimelech 2013). Similar processes such as mineral precipitation, membrane fouling, incorporation of competing ions or corrosion are expected to be major barriers to the integration of combined raw material, energy and freshwater production into a geothermal fluid cycle (Kölbl et al. 2023; Reich et al. 2022). Typically scaling inhibition is a widespread treatment for the avoidance of mineral precipitation in surface facilities. In the studied approach, the method of a controlled pre-precipitation targeting silica was chosen to avoid membrane fouling by organic scaling inhibitors and to enable high mineral concentration rates for more effective down-stream mineral extraction, as well as fresh water production. The methodology developed in the laboratory (Spitzmüller et al. 2021) and described in Chapter 7 and Chapter 9 was tested in three different settings.

The fundamental principle relies on the equilibrium between solid SiO_2 and aqueous H_4SiO_4 . An increase of the pH value leads in the aqueous phase to ionization towards $\text{H}_3\text{SiO}_4^{1-}$ and further $\text{H}_2\text{SiO}_4^{2-}$ (Dove et al. 2008; Eikenberg 1990; Milne et al. 2014). The monomeric silica acid, also described as reactive silica, can copolymerize with and incorporate cations, such as divalent Mg or Ca (Lunevich et al. 2016; Ning 2003). One possible reaction is the formation and precipitation of CSH phases while removing Si and Ca from the fluid (Gallup et al. 2003; Richardson 2008). The following paragraph compares the effectiveness of the approach in the context of three different fluids from different geological settings and quantifies the resulting influences on the precipitates and trace element chemistry.

10.3 Material and Methods

Precipitation experiments revealed as key parameters for a successful Si reduction a $\text{pH} > 10$ and the presence of divalent cations in the fluid with ratios of Ca/Si or Mg/Si ratios > 1.25 (Spitzmüller et al. 2021). Depending on the fluid, these conditions can be reached by addition of $\text{Ca}(\text{OH})_2$ for increasing the pH and providing divalent cations simultaneously, by addition of NaOH if divalent cations are present in sufficient quantity, or in separated steps by firstly increasing the pH value using NaOH followed by addition of divalent cations as CaCl_2 (Table 21).

The influences of the treatment during prototype tests in Insheim (Germany) and Puyehue (Chile) (Chapter 7 and Chapter 9) are in the following paragraph compared to the data from the “Baden-Baden” (BB) experimental series from Spitzmüller et al. (2021). For evaluating the precipitation efficiency in a realistic scenario regarding the complexity of trace elements, natural thermal spring water was adapted for the BB experiments. To approach the properties of deep fluids in terms of salinity, the natural fluid was concentrated by evaporating 50 % of the water thus doubling the TDS concentration. This resulted in Si concentrations of about 135 mg/L. Furthermore, LiCl was added to reach Li concentrations of 100 mg/L and CsCl to

reach Cs concentrations of 10 mg/L. The precipitation was conducted by raising the pH value and Ca concentration in the fluid by adding $\text{Ca}(\text{OH})_2$ (Spitzmüller et al. 2021).

Table 21: Summary of the different precipitation experimental setups.

Fluids	Experimental setup	Reference
Baden-Baden (BB): - Spring: Fettquelle	<ul style="list-style-type: none"> - Laboratory experiment - Increase of TDS and silica by evaporating 50 % of the mass - Addition of 100 mg/L Li and 10 mg/L Cs - Precipitation by adding $\text{Ca}(\text{OH})_2$ for simultaneous pH increase and divalent cations 	(Spitzmüller et al. 2021)
Insheim 1 (Jul. – Aug. 2020): - Access: Geothermal power plant, after heat exchanger	<ul style="list-style-type: none"> - Demonstrator scale - Due to overall high salinity only the pH value was raised using NaOH for initiating precipitation 	(Goldberg et al. 2023b)
Insheim 2 (Feb. – Mar. 2021): - Access: Geothermal power plant, after heat exchanger	<ul style="list-style-type: none"> - Demonstrator scale - Due to overall high salinity only the pH value was raised using NaOH for initiating precipitation 	-
Puyehue: (Jan. 2023) Spring: Termas de Puyehue	<ul style="list-style-type: none"> - Demonstrator scale - Initial softening of the water for enabling pre-concentration - pH increase to 10 – 11 under NaOH addition for avoiding membrane fouling during concentration of factor 7-10 - Precipitation by adding divalent cations using CaCl_2 	(Goldberg et al. 2023a)

At the geothermal power plant Insheim, only NaOH was added to reach the precipitation conditions since the overall salinity and concentration of divalent cations were already sufficient. The experiments were conducted on-site using a field demonstrator (Chapter 7 (Goldberg et al. 2023a)). Beyond the published data (Goldberg et al. 2023b; Goldberg et al. 2023a), this chapter includes furthermore unpublished data from the different testing runs in Puyehue and Insheim. In addition to the demonstrators described in the previous chapters, an intermediate one (further referred to Insheim 2) was tested in a 2nd testing phase at the power plant Insheim (February/March 2021). The chemical treatment unit on Insheim 2 is equal to the one used in the testing phase in Puyehue (Chapter 9) without the RO pre-concentration step. The relevant sampling points for determining the influence on the chemistry are the inlet point (equal to S1 Chapter 9) and the outlet of the treatment reactor (equal to S5 Chapter 9). As described in Chapter 7 this demonstrator was also operated in a continuous operation mode and a kinetic mode. The kinetic mode was conducted using a heated beaker since the reactor itself did not include a heating jacket as in the testing phase Insheim 1.

The third data set compared results from the field demonstrator tests at the geothermal spring Puyehue, Chile (Chapter 9 (Goldberg et al. 2023a)). In the low saline fluids, the demonstrator

included a softening step, followed by NaOH addition for increasing the pH value > 10 . The TDS concentration of this pre-treated fluid was then concentrated up to a factor of 10 before the Si reduction was initiated in a tank reactor by the addition of CaCl_2 .

The influences on the fluid chemistry are determined by using the data analyzed by inductively coupled plasma optical emission spectrometry (ICP-OES, ICap 7000, ThermoFisher) for major cations, anions were measured via ion chromatography (IC, Compact 930, Methrom), and trace elements with inductively coupled plasma mass spectrometry (ICP-MS, ICap RQ, ThermoFisher). The precipitation products were pre-dried in the field using a Büchner Funnel and dried in the oven overnight at $105\text{ }^\circ\text{C}$. Phase analysis of the solids is performed with X-ray diffraction (XRD, D8 Discover, Bruker) and the mineralogical composition is qualitatively determined with the EVA software of Bruker. Major element chemistry of the precipitates is determined using wavelength-dispersive X-ray spectroscopy (WDX, S4 Explorer, Bruker AXS). Additionally, precipitates were sputter coated with gold for examination using SEM (Tescan Vega) coupled with EDS (Inca X Act). Due to the assumed incorporation of H and O in the precipitates the EDS analyses are just considered as qualitative values. Selected precipitates were dissolved using a $\text{HNO}_3\text{-HF-HClO}_4$ acid mixture for analysis using ICP-MS.

10.4 Results

10.4.1 Effectivity of the silica reduction

The results in terms of silica concentration reduction are displayed in Figure 55 and Figure 56. To ensure comparability between the precipitation mechanisms of the different sites and testing phases only the sampling points directly before and after the precipitation are considered. For analyzing the impact of the pH value, different flow-through and batch experiments were conducted, varying the pH between the initial values (pH 5.3 in Insheim, pH 8 in BB waters) and pH 11. In Puyehue, pH is already raised to about pH 11 for the pre-concentration. For initiating the Si removal, only CaCl_2 is added for deriving the divalent cations for the precipitation step.

In Insheim and the BB waters, an increase of the pH value leads in all cases to precipitation of Si independently from the overall Si concentration or salinity of the fluid. The comparison to Puyehue demonstrates that the pH on its own is not sufficient for the control of precipitation (Figure 55). While in Insheim divalent cations are already present in the natural fluid and in BB fluids are added by Ca(OH)_2 along with the pH increase, the pre-softened and concentrated fluid from the Puyehue has already a high pH value but only starts precipitation by adding CaCl_2 . The precipitation in Puyehue is accompanied by a decrease of the pH value. In this setting (Figure 55), higher pH values (prior to the precipitation) are thus correlated with higher Si concentrations, in comparison to the other experimental data showing the opposite tendency.

The data from Insheim and BB reveal that with an increase in pH value, Si does not precipitate abruptly but its solubility gradually decreases with increasing pH values. The initial Si concentrations of 90 mg/L Si at pH 5.3 in Insheim decrease continuously, showing Si concentrations of about 80 mg/L at flow-through experiments at pH 6.4, about 60 mg/L at

pH 7, and about 20 mg/L at pH 8.4. In BB, the data indicates a similar stepwise reduction, and both sites show in nearly all cases an almost complete removal of Si at pH > 10.5.

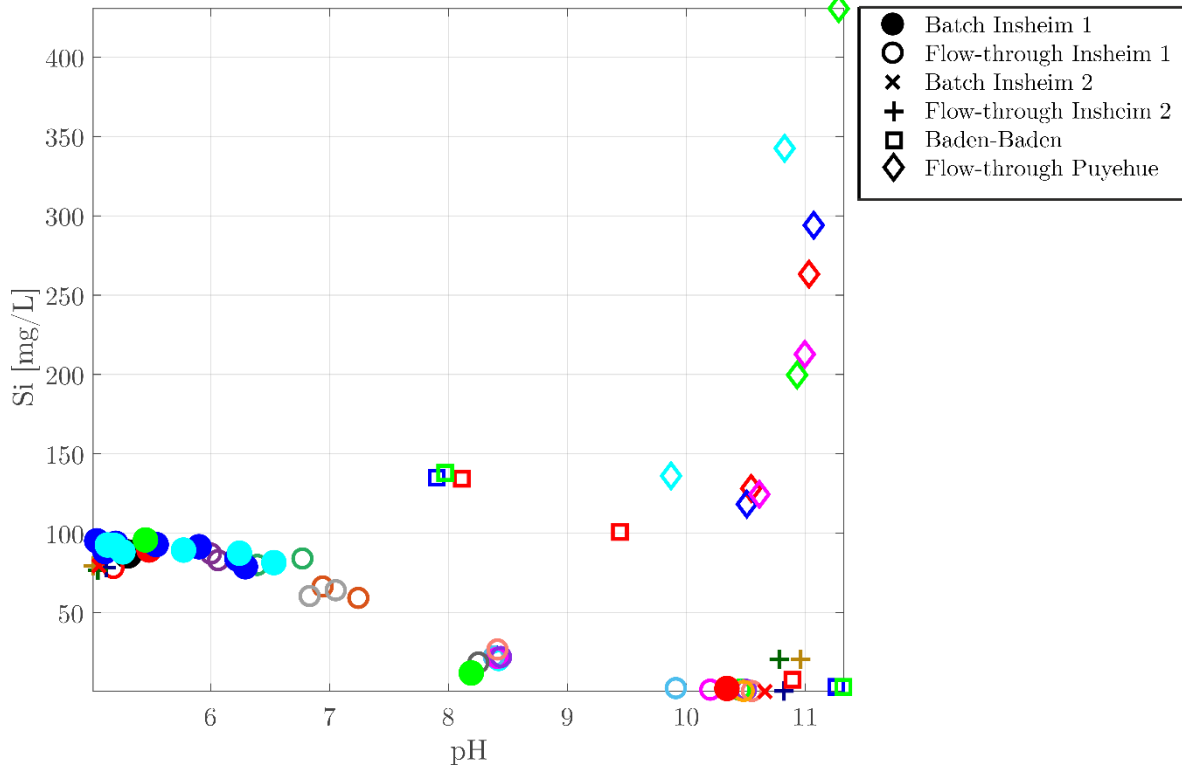


Figure 55: Comparison of the Si concentration and pH value in different flow-through and batch experiments in the two testing phases in Insheim, the pre-study with fluids from BB (Spitzmüller et al. 2021) and from the testing phase in Puyehue, Chile. Markers with the same shape and color result from the same batch or flow-through experiment. The data are displayed in Table 22.

For discussing the influence of reaction kinetics the measured time for the batch experiments (Insheim 1 KIN, Insheim 2 KIN, BB) is compared with the hydraulic retention time of the flow-through experiments (Insheim 1,2 and Puyehue) determined by the flow rate and used reaction vessel volume (Figure 56). Comparing the efficiency of the reduction with the chemical retention time shows fast kinetics, especially at the high pH values in Insheim. The kinetic experiments show in all Insheim scenarios Si removal of 98 % in less than 5 minutes at pH values of 10.5. At a pH value of 8.4, the final Si concentration is just reached at about 60 minutes. The adapted fluids from BB show a slightly slower precipitation behavior, requiring 15 – 20 minutes to remove > 90 % of Si. The flow-through experiments in Insheim 1 also show reduction rates of 98 % during the given retention time (30 – 60 min.) whereas in the Insheim 2 test phase, only 75 % Si removal is reached in hydraulic retention times between 16 and 25 minutes.

During the first testing trial at Insheim, additional kinetic experiments were conducted without adding chemical reaction agents. The fluids were only heated, stirred, and continuously sampled with and without inhibitors. The results (Figure 56) show a slow pH value increase over time in both experiments accompanied by a Si reduction.

Due to the multi-stage process in Puyehue, the governing processes are not that clear to distinguish, also no kinetic experiments using the concentrated brine could be conducted. Therefore, the kinetic behavior can only be described using the hydraulic retention times of the

precipitation tank. Here the flow-through experiments reveal that after a hydraulic time of about 40 minutes, a quasi-equilibrium state is reached where a longer retention time does not lead to further Si removal.

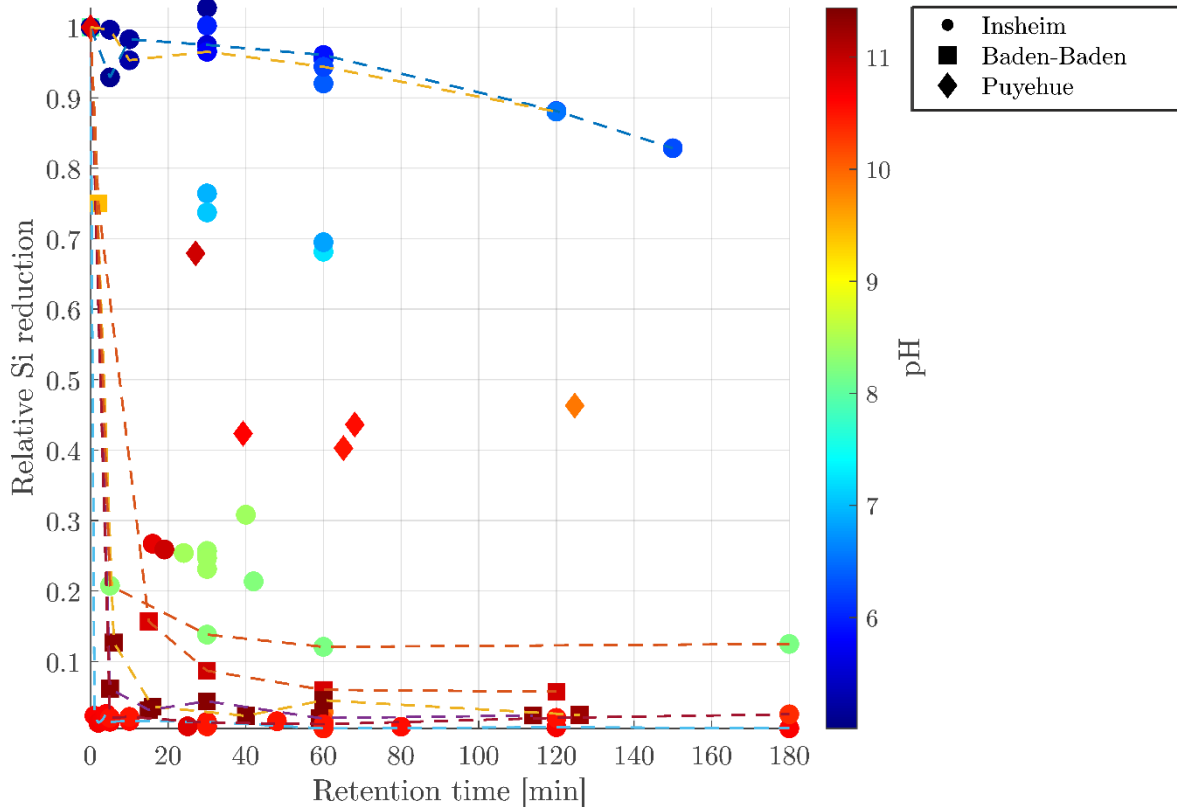


Figure 56: Comparison of the relation between the relative Si reduction, retention time, and the pH value of the different fluids from Insheim, BB (Spitzmüller et al. 2021) and Puyehue. The dashed lines connect markers from the same kinetic experiment. The data are displayed in Table 22.

10.4.2 Influences of the chemical treatment on the fluid composition

The Si removal was evaluated as a pre-treatment for the extraction of raw materials from geothermal fluids. Therefore, the influence of the treatment on trace elements was analyzed in more detail. Already the laboratory study on the BB fluids showed, that the concentration of monovalent ions such as Li, Rb, and Cs are not decreased by the lime treatment. The comparison of the trace element concentrations of the fluids and the precipitates revealed that metals, metalloids, and transition metals such as Al, Mn, Fe, Cu, and As are removed from the fluids and accumulate in the precipitates (Spitzmüller et al. 2021). The precipitation step at Puyehue (Chapter 9) indicates a similar behavior. During the Si removal step concentrations of Li, Rb, Cs, and Mo stay unaffected while those of V and Sb are lowered by 30 – 50 % and Al by 90 %.

Figure 57 illustrates the influence of the Si precipitation approach on major and trace element concentrations of different experimental series of the Insheim 1 and 2 sampling campaigns. The

percentage values of the flow through experiments refer to a “Standard Water” and its standard deviation to evaluate the influence of the treatment besides the natural fluctuation. These reference values are the average of 8 untreated water samples, collected over one month during the sampling campaign (see also Table 12 within the manuscript). The kinetic experiments as batch experiments refer to their initial composition, directly sampled during the filling of the reaction vessel. In terms of measured on-site parameters, the pH value is the most influenced by the treatment, while temperature shows mostly variations in order of magnitude of the standard deviation of the standard water. The addition of NaOH for the pH increase causes a positive correlation of the pH value and Na but due to the overall high Na concentration, the Na increase is within or slightly above the standard deviation. The experimental results indicate a negative correlation between the Si concentration and the pH, demonstrating from pH 6.9 on (from initially pH 5.3), a removal of Si lying outside the standard deviation of the standard water. Along with the Si precipitation, Mg, F, and SO₄ show also a concentration decrease at these pH values. Si is removed by about 25 % at pH 7 (Insheim 1 R and O) while Mg, F, and SO₄²⁻ concentrations decrease by 10 to 20 %. Metals or metalloids such as Fe, Mn, Pb, As, and Zn are by far more pH sensitive, and precipitate beyond the standard deviation already at pH 6. The sheer relaxation of the fluids and a retention time of 30 min without any treatment (Insheim AR1) reveals no clear precipitation tendencies if scaling inhibitors are added. The same experimental setup without the standardly used inhibitors (Insheim JR1) already indicates a minor decrease of Pb and As in the fluid. The same behavior is further demonstrated by the kinetic experiments without inhibitors (KIN o.I.) where in the time step between 30 and 60 minutes a reduction of Pb and Fe is observable. In the comparative experiments including inhibitors, this reduction starts between 60 and 120 minutes of retention time. In both experimental runs Fe and Pb are removed by 70 to 85 % at the end. Batch experiments using pH values ≥ 7 (Insheim 1 O & R) lower Pb concentration by 95 %, Fe and Zn by 65 – 75 %, and Mn and Sb by 50 – 60 %.

The pH ranges for the targeted (pre-)precipitation (pH 8.4 and 10.5) have a stronger influence on the concentration changes. Si concentration is decreased by about 75 % at pH 8.4 (BR1, KR1, KIN 8.4 T5). Due to the overall high Ca concentration, Ca removal can hardly be seen. In the KIN 8.4 experiment the Ca decrease is clearly outside the standard deviation. Mg with overall lower concentrations than Ca, becomes removed by 40 % already at this stage. Metals and metalloids such as Fe, Mn, Sb, and Pb are almost removed by 100 %. As and Zn are decreased by 50 – 70 %. In this pH range also SO₄²⁻ and F decrease by 15 – 25 %. These tendencies become stronger at the final pH of 10.5. Concentrations of Mg, Si, Fe, and Mn are removed by > 95 % in all of the scenarios (Figure 57). The Pb concentration shows a similar reduction rate in the flow-through experiments with a pre-precipitation step at pH 8.4 (Experiments B and K) while in the experiments where R1 is only used for relaxation without any chemical additives, the removal reaches only about 75 % (A & J). A similar behavior is observed for Sb. F decreases by about 20 % at the high pH for all Insheim 1 experiments. For the whole second Insheim testing phase F was mostly below the detection limit, as well as in the initial untreated samples. The general TDS concentration does not change beyond the standard deviation of the water. The addition of NaOH seems to fully compensate for the element loss due to precipitation in terms of the overall salt load.

	pH	T [°C]	Ca	Na	Si	K	Mg	F	Cl	Br	SO4	Li	Rb	Cs	B	V	Fe	Mn	Mo	Sb	Pb	As	Zn	Ba	Sr	TDS
Standard water	5.29	56.7	7566	28937	86.9	4290	119	16.2	63692	179	143	164	29.2	17.6	45.4	0.0013	33.1	30.9	0.0045	0.20	0.89	13.8	10.2	35.3	458	105867
SD [%]	4%	5%	5%	5%	9%	5%	6%	1%	2%	2%	4%	6%	4%	3%	4%	8%	4%	3%	12%	7%	7%	3%	13%	4%	3%	5%
Trace elements precipitates M			399288	41050		4760	10730						33.7			2687	2797	0.0817		89.1	1221	611	147	2195		
Deviation from standard water			5277%	142%		111%	8984%						115%			8110%	9045%	1803%		10049%	8833%	6013%	416%	479%		
Insheim 1 PR1	6.00	102%	109%	112%	100%	109%	100%	100%	104%	102%	102%	109%	100%	102%	98%	112%	95%	96%	94%	103%	78%	99%	89%	99%	99%	107%
Insheim 1 PR2	6.06	96%	107%	109%	95%	106%	98%	100%	101%	102%	99%	107%	96%	101%	94%	136%	80%	91%	118%	94%	73%	92%	88%	97%	96%	104%
Insheim 1 QR1	6.77	112%	109%	111%	97%	109%	99%	99%	102%	103%	100%	109%	102%	101%	100%	94%	95%	99%	95%	103%	71%	103%	87%	101%	102%	106%
Insheim 1 QR2	6.39	97%	111%	114%	92%	110%	101%	100%	105%	107%	103%	112%	104%	102%	100%	89%	35%	95%	96%	92%	25%	86%	76%	103%	103%	108%
Insheim 1 RR1	7.05	117%	93%	102%	74%	98%	88%	88%	102%	104%	85%	96%	98%	103%	97%	115%	26%	53%	96%	37%	8%	87%	38%	96%	95%	101%
Insheim 1 RR2	6.83	96%	90%	97%	70%	94%	88%	85%	100%	101%	89%	93%	101%	103%	101%	91%	6%	58%	105%	62%	4%	84%	35%	101%	101%	98%
Insheim 1 OR1	6.94	109%	98%	107%	76%	103%	91%	86%	97%	98%	82%	104%	99%	102%	96%	107%	33%	57%	94%	47%	6%	89%	35%	95%	96%	100%
Insheim 1 OR2	7.24	95%	96%	106%	68%	102%	91%	85%	97%	98%	80%	100%	103%	99%	100%	93%	1%	56%	103%	45%	2%	80%	31%	97%	101%	100%
Insheim 1 AR1	5.18	105%	101%	98%	90%	97%	96%	100%	101%	99%	98%	107%	105%	106%	102%	98%	107%	105%	126%	105%	110%	104%	117%	107%	106%	100%
Insheim 1 AR2	10.45	97%	40%	114%	2%	91%	0%	76%	97%	96%	89%	101%	99%	101%	87%	101%	0%	0%	129%	11%	24%	7%	42%	101%	97%	97%
Insheim 1 BR1	8.39	123%	94%	100%	26%	97%	60%	82%	101%	99%	76%	107%	104%	107%	89%	95%	0%	5%	102%	8%	1%	48%	43%	101%	101%	100%
Insheim 1 BR2	10.49	105%	39%	120%	2%	96%	0%	74%	101%	99%	75%	105%	97%	100%	82%	80%	0%	0%	87%	4%	1%	10%	43%	93%	92%	101%
Insheim 1 JR1	5.16	107%	110%	111%	103%	109%	101%	100%	104%	105%	108%	110%	98%	101%	96%	101%	96%	98%	108%	96%	92%	99%	90%	99%	98%	106%
Insheim 1 JR2	10.45	107%	92%	111%	2%	104%	1%	80%	100%	101%	96%	104%	99%	102%	87%	100%	0%	0%	88%	10%	23%	6%	30%	98%	96%	102%
Insheim 1 KR1	8.42	108%	94%	106%	23%	101%	56%	82%	97%	98%	77%	101%	94%	97%	83%	123%	0%	3%	87%	8%	1%	46%	26%	90%	91%	99%
Insheim 1 KR2	10.49	94%	66%	127%	1%	108%	3%	78%	101%	103%	86%	107%	100%	100%	85%	97%	0%	0%	90%	4%	6%	9%	22%	98%	98%	106%
Insheim 1 MR1	10.48	109%	42%	122%	1%	100%	0%	77%	98%	99%	89%	100%	100%	99%	84%	85%	0%	0%	88%	8%	19%	6%	32%	96%	95%	100%
Insheim 1 KIN 0 T0	5.04	56.0	7795	28919	95.3	4536	129	16.1	62627	178	140	165	29.2	18.2	44.6	0.0014	32.7	31.1	0.0044	0.21	0.86	13.8	11.8	35.7	456	106246
Insheim 1 KIN 0 T5	5.11	99%	94%	94%	93%	92%	92%	99%	98%	97%	97%	95%	104%	100%	104%	102%	102%	101%	101%	103%	109%	102%	92%	103%	103%	96%
Insheim 1 KIN 0 T10	5.20	98%	98%	98%	98%	97%	97%	100%	102%	104%	105%	97%	104%	95%	107%	94%	103%	102%	105%	103%	105%	103%	98%	99%	102%	100%
Insheim 1 KIN 0 T30	5.54	99%	99%	99%	97%	99%	97%	100%	104%	106%	108%	100%	107%	101%	106%	106%	101%	101%	102%	110%	115%	103%	96%	103%	106%	102%
Insheim 1 KIN 0 T60	5.90	101%	96%	98%	96%	96%	95%	100%	100%	102%	104%	98%	102%	99%	103%	98%	93%	99%	103%	106%	102%	99%	95%	101%	104%	99%
Insheim 1 KIN 0 T120	6.22	100%	95%	95%	88%	94%	94%	100%	103%	105%	107%	96%	100%	98%	101%	93%	41%	97%	102%	100%	43%	83%	93%	100%	102%	100%
Insheim 1 KIN 0 T150	6.29	100%	96%	97%	83%	95%	93%	100%	101%	100%	100%	97%	98%	97%	99%	103%	16%	96%	102%	94%	23%	76%	89%	97%	97%	99%
Insheim 1 KIN o.I. T0	5.13	53.4	7368	28451	92.6	4280	124.2	16.1	61659	178	144	155	29.2	16.8	45.9	0.0013	32.5	30.7	0.0042	0.18	0.81	13.8	9.36	34.0	457	103139
Insheim 1 KIN o.I. T5	5.19	100%	98%	99%	100%	99%	100%	99%	102%	97%	97%	98%	101%	109%	96%	102%	101%	101%	101%	102%	99%	101%	98%	104%	101%	101%
Insheim 1 KIN o.I. T10	5.26	99%	96%	96%	95%	96%	95%	100%	100%	98%	95%	96%	99%	100%	101%	94%	100%	99%	101%	102%	97%	99%	95%	100%	99%	99%
Insheim 1 KIN o.I. T30	5.77	97%	98%	99%	97%	99%	97%	101%	103%	103%	102%	100%	101%	105%	97%	88%	100%	99%	101%	104%	102%	101%	98%	105%	102%	101%
Insheim 1 KIN o.I. T60	6.24	98%	94%	93%	94%	94%	95%	102%	100%	98%	99%	94%	99%	107%	96%	104%	89%	100%	102%	95%	83%	95%	95%	102%	98%	98%
Insheim 1 KIN o.I. T120	6.53	101%	94%	94%	88%	96%	98%	101%	96%	100%	98%	93%	98%	104%	97%	103%	32%	100%	101%	93%	24%	81%	93%	100%	97%	97%
Insheim 1 KIN 8.4 T0	5.45	52.8	7495	28590	95.8	4345	127.8	16.1	65349	180	143	156	27.3	17.2	42.8	0.0013	31.5	29.8	0.0041	0.18	0.86	13.4	10.5	34.1	432	107138
Insheim 1 KIN 8.4 T5	8.30	104%	91%	98%	21%	97%	63%	84%	96%	99%	86%	96%	108%	102%	95%	94%	2%	5%	104%	55%	2%	57%	43%	100%	106%	96%
Insheim 1 KIN 8.4 T30	8.27	110%	91%	99%	14%	96%	51%	83%	96%	101%	89%	97%	108%	102%	95%	83%	2%	2%	108%	54%	2%	47%	48%	99%	106%	96%
Insheim 1 KIN 8.4 T60	8.19	105%	92%	101%	12%	97%	50%	82%	94%	98%	86%	99%	105%	95%	95%	89%	2%	1%	98%	52%	2%	39%	43%	94%	100%	96%
Insheim 1 KIN 8.4 T180	8.19	106%	94%	102%	12%	100%	50%	82%	96%	96%	85%	100%	106%	101%	93%	83%	5%	4%	99%	58%	24%	36%	48%	98%	105%	98%
Insheim 1 KIN 10.5 T0	5.48	57.1	7447	29175	89.4	4302	119	16.1	63505	176	141	161	29.7	17.2	47.1	0.00115	32.7	30.7	0.0043	0.21	0.89	13.8	8.93	35.0	461	105810
Insheim 1 KIN 10.5 T5	10.53	97%	94%	106%	2%	101%	0%	80%	100%	101%	93%	103%	102%	101%	88%	114%	1%	0%	105%	8%	15%	10%	27%	98%	101%	101%
Insheim 1 KIN 10.5 T10	10.49	94%	91%	105%	2%	99%	0%	80%	97%	99%	88%	102%	100%	102%	89%	111%	2%	0%	102%	7%	13%	9%	26%	100%	100%	99%
Insheim 1 KIN 10.5 T30	10.49	94%	91%	112%	1%	105%	0%	79%	100%	103%	94%	105%	103%	100%	89%	99%	1%	0%	103%	6%	23%	8%	47%	98%	100%	103%
Insheim 1 KIN 10.5 T60	10.50	100%	36%	123%	1%	101%	0%	0%	98%	100%	88%	100%	96%	95%	84%	91%	2%	0%	100%	7%	16%	4%	57%	93%	93%	100%
Insheim 1 KIN 10.5 T120	10.52	96%	5%	135%	2%	97%	0%	73%	97%	99%	89%	98%	100%	100%	88%	101%	2%	0%	107%	18%	17%	4%	52%	96%	95%	100%
Insheim 1 KIN 10.5 T180	10.34	97%	3%	137%	3%	97%	0%	76%	95%	94%	86%	100%	93%	93%	84%	101%	2%	0%	108%	29%	23%	5%	53%	89%	86%	100%
Insheim 2 KIN 10.5 T0	5.06	49.6	8250	30134	79.4	4332	115	0.79	63760	179	142	181	29.7	17.8	47.9	0.0013	8.08	31.6	0.0041	0.20	0.11	8.08	8.65	35.3	463	107824
Insheim 2 KIN 10.5 T1	10.65	101%	85%	101%	2%	95%	0%	0%	102%	103%	102%	95%	105%	105%	88%	81%	0%	0%	104%	11%	1%	21%	1%	99%	101%	100%
Insheim 2 KIN 10.5 T2	10.70	101%	90%	105%	1%	100%	0%	0%	101%	101%	100%	99%	99%	84%	91%	0%	0%	111%	11%	16%	17%	5%	94%	96%	101%	
Insheim 2 KIN 10.5 T3	10.68	101%	91%	104%	2%	99%	0%	0%	102%	102%	100%	100%	101%	101%												

38 wt.%, thus fitting to a combination of calcite and CSH phases. Qualitative XRD analysis indicates a large quantity of x-ray amorphous phase (71 %), and moderate quantities of calcite (13 %), monohydrocalcite (9 %) and calcium silicate (7 %).

Figure 57 and Figure 58 illustrate the chemical and mineralogical composition of a representative precipitate of a standard experiment in Insheim (Insheim 1 M, Table 22), raising the pH value to 10.5 in a continuous flow-through experiment using only one precipitation reactor. The LOI of 39 % is in a similar range like that of the precipitates at Puyehue whereas the CaO content is significantly higher (55 wt.% CaO WDX; 40 % Ca using ICP-MS, Figure 57) and SiO₂ is only detected in low quantities of 1.6 wt.% (analyzed by WDX). Considering the fluid composition and the precipitation conditions, could the LOI be composed of water, decomposition of carbonates and associated CO₂ release, or S-phases. The WDX analyzed composition matches the mineralogical composition of the precipitates detected by XRD, where no silica phases are detected. The amount of x-ray amorphous material derived from the diffractograms (qualitative approach) is significantly lower than in the Puyehue experiments. The main phase is portlandite. Calcium carbonate and halite are accessory phases. Like in the BB fluids (Spitzmüller et al. 2021), the precipitates show a porous structure under the SEM (Figure 60) and the chemical composition of the main phases measured with the coupled EDS (Table 23) match with portlandite, calcite, and halite compositions. The composition of other precipitates from experiments performed at the same pH value (Table 24) are similar regarding the main phases. According to the XRD data, the amount of x-ray amorphous phase is moderate and the main phase is portlandite followed by Ca-carbonate and minor halite. In experiment K, additionally copper sulfide is observed accessory, and in the kinetic experiment after 180 min accessories of Na-borate and Ca-Sr-Al-oxide are detected. Precipitates of experiments A and G also contain accessory Zn-sulfide. According to SEM-EDS analysis, these accessory phases could not be identified but the removal of elements like B, S, Sr, Al, and Zn in the fluid phase is evident in the fluid analysis (Figure 57). Solids from experiment J (pH 10.5, no Inhibitors, 60 min. retention times) have overall the same general composition like those from experiment M (Table 22). In one spot the qualitative SEM-EDS analysis indicates 6 wt.% Mn and 7 wt.% Fe in the solid, two elements that are absent in the corresponding fluid phase (Figure 57). Clear tendencies in terms of mineral formation concerning the reaction kinetic are not observable.

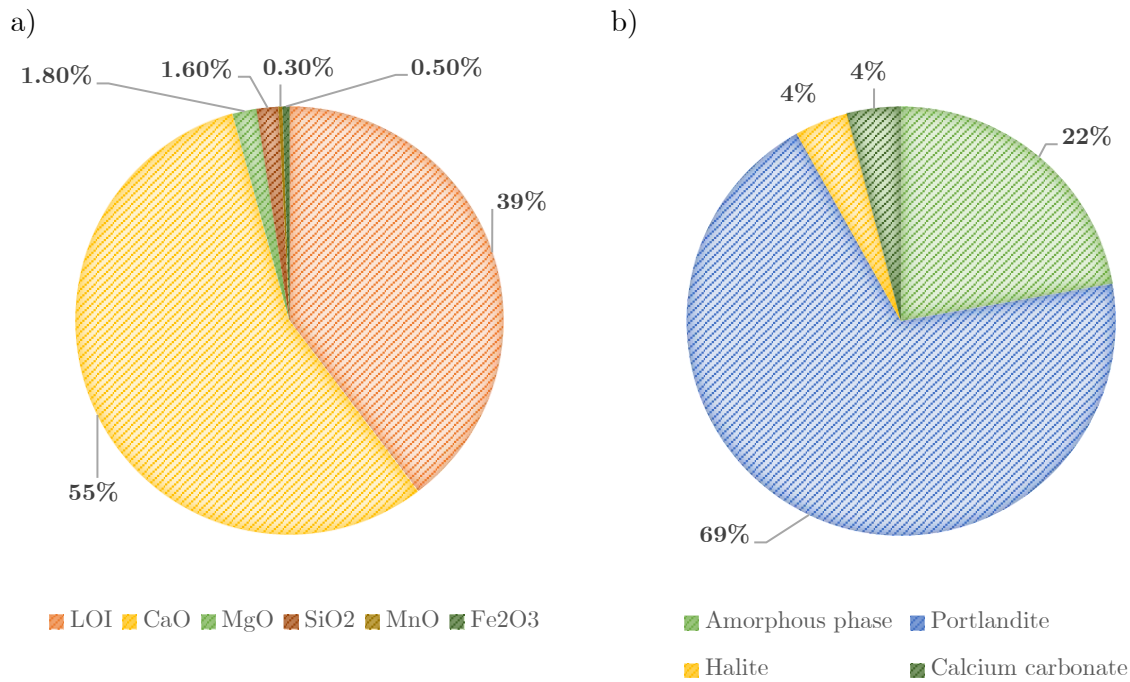


Figure 58: Mineralogical and chemical composition of the precipitates from Insheim after precipitation at pH 10.5 (Experiment M) a) WDX data. LOI = loss on ignition. Analytical error: 1% relative for major and 10% relative for minor elements. b) XRD data (Qualitative determination of the mineralogical composition done with the EVA software of Bruker).

The composition of the precipitates is different at pH 8.4. Mineralogical analysis (XRD) of the precipitates of the flow-through experiments G, Reactor 1 (pH 8.4, retention time 40 min.) indicate that calcite is the main phase associated with minor halite and sylvine. The amount of x-ray amorphous material is moderate (Figure 59b). With SEM rhombohedral calcite crystals can be observed and SEM-EDS reveals the presence of halite and of Si in some of the phases (Figure 59a). Further experiments performed under similar conditions (D R1, B R1, C R1, F R1, K R1, the Kinetic 8.4 t 180) show comparable results. The XRD analysis of precipitates from the kinetic experiment suggests a similar main composition with additional minor Mn sulfide. SEM-EDS analysis detected traces of Mn and Fe in some spots. These observations fit to the observed compositional changes of the associated fluid phase of the kinetic experiment, with Fe and Mn being removed by 95 % and SO₄ by 15 % (Figure 57).

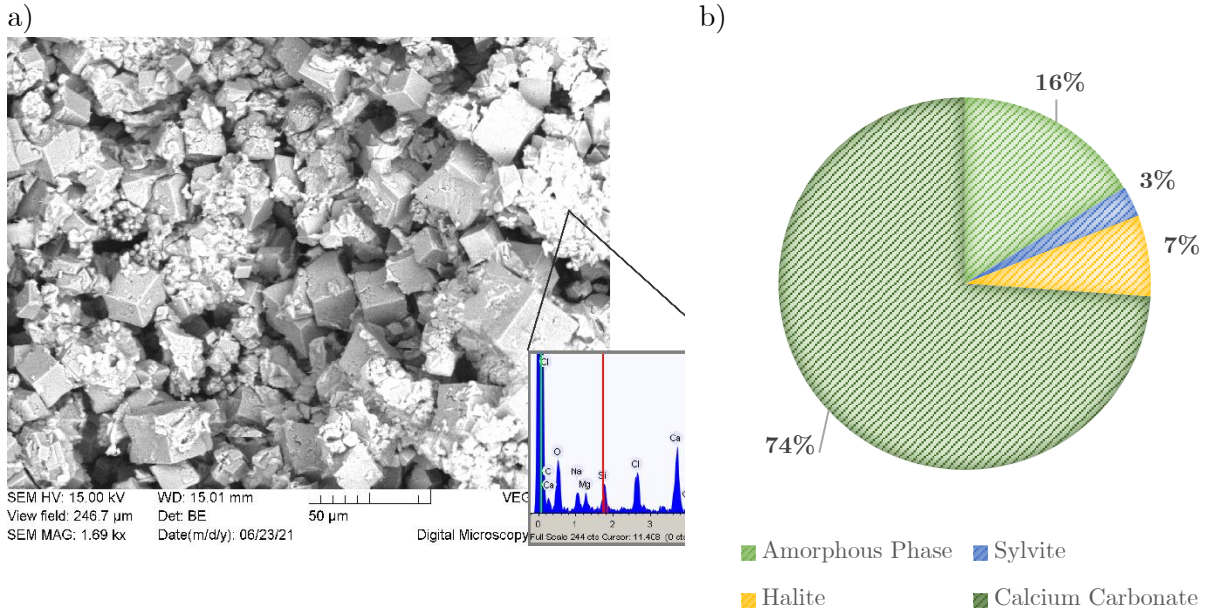


Figure 59: a) BSE image (SEM) of precipitates from experiment G, Reactor 1 at pH 8.4. Euhedral calcite crystals are covered by very tiny grains with anhedral shape. The EDS spectrum illustrates the elevated contents of Si, Ca, Mg, and Na in the grain aggregate. (b) According XRD data (Qualitative determination of the mineralogical composition done with the EVA software of Bruker).

10.5 Discussion

The comparison of the precipitation experiments shows in all cases Si removal during precipitation. In Insheim and in the BB fluids the precipitation at pH 10.5 removed up to 98 % of Si, while in Puyehue only 50 % are removed. The study on the BB fluids reveals pH values >10 and a molar Ca/Si ratio of >1.25 as ideal conditions for precipitation (Spitzmüller et al. 2021). In the fluids from the Puyehue field tests, Ca/Si ratios between 1.4 (Puyehue A) and 3.8 (Puyehue D) were measured. Thus, the previously determined “ideal conditions” were reached in all experiments. The lower performance in the Chilean fluids and on the other hand the high effectivity in Insheim could have been caused by the so-called “salting-out” effect. The salting out-effect describes a decreasing solubility of a specific phase at increasing fluid salinities. For amorphous silica, the solubility decreases by about 50 % in a solution containing 2 mol/L NaCl at 25 °C (Marshall and Warakomski 1980a), which is in the range of the salinity of the Insheim fluids. The decreasing effect on the silica solubility is even stronger if Mg cations are present in the fluid (as in Insheim) (Chen and Marshall 1982; Marshall and Warakomski 1980a). Remarkably, Mg is almost absent during the treatment at Puyehue. In comparison to the Puyehue experiments, have the BB fluids a much higher Si reduction rate with up to twice the salinity and 8 mg/L Mg (Spitzmüller et al. 2021). Following this, a stronger pre-concentration or addition of Mg could improve the latter Si reduction in the Puyehue fluids.

On the other hand, it depends on the downstream process if a higher Si reduction is required or if a lower reduction (with lower efforts/costs) and thus a minor modification of the fluid chemistry would be also satisfying. In this regard, the reproducible, gradually decreasing Si

concentration with the pH value (Figure 55, Figure 57), allows a targeted adjustment of the residual Si concentration for the specific requirements of a downstream process. Lower pH values lower the operational costs in terms of NaOH consumption. Si removal by 98 % (pH 10.5) in continuous operation (Insheim A R2, B R2, K R2, J R2, M) is associated with a strong Na increase by about 20 %. For removing just 22 % less Si (75 % in total, at pH 8.4), the NaOH addition is hardly detectable in the fluids, indicating a disproportional lower effort. This minor modification of the fluid composition also results in lower co-precipitation, for instance for Ca.

The composition of Ca-bearing minerals significantly varies in the given pH ranges. At a lower pH value of 8.4 calcite is the most abundant mineral precipitating (Figure 59) while at a pH of 10.5 portlandite is dominant (Figure 58) in Insheim. At high pH values in the BB fluids calcite and CSH-phases are found (Spitzmüller et al. 2021) while the precipitates from Puyehue contain calcite, monohydrocalcite, and calcium silicate, and a high amount of x-ray amorphous material. Beyond the parameters fixed in the experiment (temperature and pressure) high concentrations of carbonic acid and associated low pH values favor calcite solubility, while CO₂ degassing and pH rise typically result in a lowering of the calcite solubility (Miller 1952; Nicholson 1993). Considering the CO₂ measured in the fluids in Insheim (Sanjuan et al. 2016a) the degassing of CO₂ is assumed to cause the pH rise to 6.3/6.5 during the untreated kinetic experiments with and without inhibitors (Figure 57). The same experiments also indicate a Ca decrease of 5 % possibly derived by calcite precipitation. Since the measured Ca decrease is in the range of the standard deviation for Ca of the brines, this interpretation cannot be clearly confirmed. Increasing the pH value from 5.5 to 8.5 in Ca-saturated solutions under a CO₂-containing atmosphere, results in a strong Ca reduction in the aqueous phases and increasing calcite growth rates (Korchef and Touaibi 2020; Ruiz-Agudo et al. 2011). Ruiz-Agudo et al. (2011) state that by increasing the pH ≤ 8.5 , the present OH⁻ possibly increases the frequency of water exchange around Ca ions and thus facilitates Ca incorporation into the calcite structure and crystal growth. This behavior could be an explanation for the dominating calcite formation during the precipitation at a pH of 8.4 when compared to experiments performed at higher pH values. At higher pH values (>9) decreasing calcite growth rates are observed (Ruiz-Agudo et al. 2011). The size and morphology of rhombohedral calcite crystals observed in our samples (Figure 59) are similar to those of calcite of other precipitation experiments performed at pH 8-9 (Korchef and Touaibi 2020; Ruiz-Agudo et al. 2011) and show strong similarities with the calcite features described for hardened lime binders formed under CO₂ atmosphere (Cizer et al. 2008). A remaining uncertainty in the precise description of the carbonate precipitation process is the lack of data on the aquatic carbon species in the presented study.

The monohydrocalcite (MHC) found in the Puyehue precipitates, is metastable regarding calcite and aragonite and typically forms from an amorphous phase and transforms to calcite and/or aragonite with time (Nishiyama et al. 2013). Formation typically requires highly specific formation conditions such as pH 9.5 – 11 and > 0.1 mol/L Mg in the original solutions, making it a rather rare mineral in geological settings (Nishiyama et al. 2013). Since the Mg concentrations in Puyehue are by far lower a formation during carbonation of calcium hydroxide (Kimura and Koga 2011) could be a possible formation mechanism.

At high salinities and high Ca and Si concentrations, precipitation occurs in the CaO–SiO₂–H₂O system with amorphous silica and portlandite as endmembers (Blanc et al. 2010a; Jennings 1986). These conditions are characteristic for cement pore waters where high Ca and Si concentrations with low Ca/Si ratios in combination with short reaction times, lead to the formation of metastable CSH phases (Blanc et al. 2010a; Duchesene and Reardon 1995). While the CSH phases could be determined in the precipitates from the lower saline BB fluids, they were not found in the Insheim precipitates. However, the Si reduction in the fluid is obvious, and due to the overall conditions a formation of a CSH phase in the x-ray amorphous phase is likely.

In addition to Si, Ca, and Mg as the driving elements for the precipitation mechanism, also several trace elements are affected by the treatment. In all settings, the Si removal is associated with a removal of metals, metalloids, and transition metals. In the experiments with the BB fluids, the summed-up incorporation of trace elements in the precipitates is < 0.25 wt.% (Spitzmüller et al. 2021) while in the precipitates of experiment M (Insheim 1) approx. 1 % trace elements (Rb, Fe, Mn, Mo, Pb, As, Zn, Ba, Sr) are incorporated (Figure 57). The removal of metals, arsenates, or other toxic elements using portlandite carbonation or calcite-interaction is also used in groundwater or wastewater treatment processes (Bordoloi et al. 2013; Hamdouni et al. 2016; Mettler et al. 2009; Montes-Hernandez et al. 2009; Santomartino and Webb 2007). The treatment, typically using calcite, catalyzes oxidation in oxidative conditions and leads to precipitation at high pH values. For Fe for example, the high concentrations of OH⁻ at high pH, and the presence of oxygen leads to a reaction from soluble Fe²⁺ to insoluble Fe³⁺ in the form of goethite (FeOOH) or ferrihydrite (Fe(OH)₃) (Bordoloi et al. 2013; Hamdouni et al. 2016). A further removal mechanism under these conditions is also surface adsorption on calcite (Mettler et al. 2009). Apart from Fe behavior, these precipitation mechanisms are also observed for other elements such as Al, Pb, Cr, Cu, and Zn forming hydroxyl-complexes at high pH values. Like in the here presented experiments using different geothermal fluids the removal of different metals in waste waters also strongly increases by increasing the pH value from 7 to 11 with an almost total reduction at pH > 8 requiring 10 min. of reaction time (Chen et al. 2009). For geothermal systems from the NGB Regenspurg et al. (2015) also describes Pb reduction by the formation of laurionite (PbOHCl) in high Cl brines at high pH values, possibly due to the dissolution of minerals of the cementing, creating similar conditions like in the precipitation experiments in Insheim.

The observed precipitation of the metal and metalloid elements described above should be considered ambivalent. The precipitation can lead to an accumulation of potentially toxic elements at the surface. Especially critical considered should be the potential incorporation of radionuclides which are present in the URG reservoir fluids (Eggeling et al. 2018; Nitschke et al. 2014; Scheiber et al. 2019a). Regarding the radiation, however, no increased local dose rate above background radiation (0.05 µS/h) was measured in either the precipitates nor the concentrated waters (Chapter 6) (measured using RadEye PRD-ER, Personal Radiation Detector Extended Range). However, DLE experiments using Li-Ti-oxides and Li-Mn-oxides in brines of the Upper Rhine Graben with similar element compositions like those from Insheim revealed radioactive nuclide uptake (Kölbel et al. 2024a; Kölbel et al. 2024b). In both approaches the reduction of the radionuclides increased with the pH, explained by a highly negative surface charge of the sorbents due to a coverage by hydroxyl groups (Kölbel et al.

2024a). Also, both materials show an increase of the radionuclides on the sorbent surface with each Li extraction cycle due to their only partial removal during desorption cycles (Kölbel et al. 2024a; Kölbel et al. 2024b). Although these radionuclides or associated radiation were not measured during the experiments in Insheim, it is highly likely that they precipitated since the pH values in the experiments were by far higher than those of the DLE studies. Therefore, if the precipitation approach would be implemented, this incorporation must be monitored. On the other hand, could the controlled pre-precipitation also improve downstream DLE by avoiding the accumulation of radionuclides within a Li extraction facility, beyond the reduction of Si.

Nevertheless, precipitation would require an utilization or deposition strategy. A possible re-use on-site could be the recirculation of the portlandite-dominated precipitates in Insheim for the pH rise of the following fluid cycle or in other waste water treatment applications (Almendros-Ginestà et al. 2023; Hamdouni et al. 2016; Montes-Hernandez et al. 2009). Another option would be a different set-up in the first place, for example, a flow-through solution such as a limestone drain used for pH increase and removal of dissolved metals from acid mine drainage (Cravotta and Trahan 1999; Santomartino and Webb 2007). Also, the minerals precipitated are typically observed in lime binders and cement (Blanc et al. 2010a; Cizer et al. 2008; Duchesene and Reardon 1995). The trace elements concentrations in the precipitates from Insheim and the BB fluids show for most elements (Pb, Mn, Mo, Co, Cr, Cu, Ni) lower or similar (Zn) concentrations like industrial cements (Achterbosch et al. 2003). Only the As content is higher by a factor of 10 to 20 requiring a further As treatment or a dilution with As-free input materials for their usage in the cement industry.

Despite the accumulation of potentially toxic elements, their reduction also can be seen as a benefit. Especially in fluids with inflows from volcanic waters, metals or other toxic elements can be present. A reduction of these elements could exploit additional freshwater sources in remote volcanic areas, for instance in Chile. In fact, elevated concentrations of As were even detected in bottled waters from Puyehue, surpassing drinking water permits (Daniele et al. 2019). Therefore, a reduction of these components could be of local interest at the Puyehue test site.

Monovalent Cations such as Li, Cs, or Rb as potential target elements for a combined raw material and energy extraction show no strong influence by the precipitation in all settings and configurations.

10.6 Conclusion

The removal of Si was tested in different geochemical settings and operational modes. In all settings, it showed an effective Si removal, mainly depending on the adjusted pH value but also on the overall salinity. In continuous operation in Insheim, 98 % of Si was removed in less than 5 minutes. Slightly slower kinetics but the same effectivity are observed in the low-salinity fluids from Baden-Baden. The fast kinetics could make optimization in terms of hydraulic retention time possible because this implies the requirement of smaller reaction vessels in a

flow-through system. For the even lower salinity fluids from Puyehue, Chile only a 50 % reduction was reached that could be potentially increased by a further pre-concentration step.

Another lever for a more (cost-) efficient treatment is the NaOH amount used for the pH increase. Depending on the downstream requirements, a lower intervention could be sufficient such as lower reactant addition at pH values of 8.4 lowering Si concentration by already 75 %. Beyond the targeted Si and Ca also several metals or metalloids are removed during the pH value increase. Also, their removal could be minimized by using lower pH values for the treatment. Whether precipitation of these element groups is desired depends highly on the context and use of the fluid and precipitates. An initial reduction of toxic elements within the fluid phase could prepare drinking water usage for instance for the waters in volcanic areas in Chile and could hinder the adsorption of radionuclides on the surface of inorganic sorbents used for DLE. However, a deposition strategy or an after-use of the precipitates must be implemented.

Overall, the precipitation mechanism already used in waste or drinking water treatment, proofed its applicability also in different geothermal fluids. This approach has the potential to improve future geothermal metal extraction. Its versatility also allows for the preparation of associated drinking water production, while the frequently observed precipitation of cement-like phases can be seen as raw material production on its own.

10.7 Appendix

10.7.1 Comparison of silica, pH and retention time

Table 22: Parameters for characterizing the Si reduction effectivity from the different studies in Germany in Chile.

Title	pH	Final Si concentration [mg/L]	Residence Time [min]	T [°C]	TDS [mg/L]	Si reduction	Source
Insheim Inflow	5.3	87.00	0	57.0	105255	1.000	(Goldberg et al. 2023b)
Insheim 1 AR1	5.18	78.10	30	59.7	104896	0.898	(Goldberg et al. 2023b)
Insheim 1 AR2	10.45	1.36	60	55.2	102275	0.016	(Goldberg et al. 2023b)
Insheim 1 BR1	8.39	22.35	30	69.6	104806	0.257	(Goldberg et al. 2023b)
Insheim 1 BR2	10.49	1.35	60	59.4	106237	0.016	(Goldberg et al. 2023b)
Insheim 1 CR1	8.38	22.33	30	60.6	107473	0.257	(Goldberg et al. 2023b)
Insheim 1 CR2	9.91	2.46	60	55.8	112498	0.028	(Goldberg et al. 2023b)
Insheim 1 DR1	8.41	21.48	30	55.4	106152	0.247	(Goldberg et al. 2023b)
Insheim 1 DR2	10.2	1.46	60	55.6	110892	0.017	(Goldberg et al. 2023b)
Insheim 1 FR1	8.44	22.09	24	60.4	99798	0.254	(Goldberg et al. 2023b)
Insheim 1 FR2	10.5	1.33	48	53.7	103295	0.015	(Goldberg et al. 2023b)
Insheim 1 GR1	8.41	26.81	40	57.1	108857	0.308	(Goldberg et al. 2023b)
Insheim 1 GR2	10.55	0.66	80	51.8	102641	0.008	(Goldberg et al. 2023b)
Insheim 1 JR1 (C in Chapter 7)	5.16	89.40	30	60.7	111779	1.028	(Goldberg et al. 2023b)
Insheim 1 JR2 (C in Chapter 7)	10.45	1.51	60	60.5	107886	0.017	(Goldberg et al. 2023b)
Insheim 1 KR1 (D in Chapter 7)	8.42	20.12	30	61.2	104598	0.231	(Goldberg et al. 2023b)
Insheim 1 KR2 (D in Chapter 7)	10.49	1.22	60	53.5	111258	0.014	(Goldberg et al. 2023b)
Insheim 1 MR1	10.48	0.69	30	61.7	105692	0.008	(Goldberg et al. 2023b)
Insheim 1 OR1	6.94	66.48	30	61.8	105249	0.764	(Goldberg et al. 2023b)
Insheim 1 OR2	7.24	59.29	60	53.9	104961	0.681	(Goldberg et al. 2023b)
Insheim 1 PR1	6	87.20	30	57.7	112395	1.002	(Goldberg et al. 2023b)
Insheim 1 PR2	6.06	83.03	60	54.4	109401	0.954	(Goldberg et al. 2023b)
Insheim 1 QR1	6.77	84.12	30	63.5	111085	0.967	(Goldberg et al. 2023b)
Insheim 1 QR2	6.39	80.06	60	55.1	113765	0.920	(Goldberg et al. 2023b)
Insheim 1 RR1	7.05	64.14	30	66.1	106392	0.737	(Goldberg et al. 2023b)
Insheim 1 RR2	6.83	60.46	60	54.3	103282	0.695	(Goldberg et al. 2023b)
Insheim 1 KIN 0 T0	5.04	95.28	0	56.0	105572	1.000	(Goldberg et al. 2023b)
Insheim 1 KIN 0 T5	5.11	88.51	5	55.5	101493	0.929	(Goldberg et al. 2023b)
Insheim 1 KIN 0 T10	5.2	93.66	10	55.2	105993	0.983	(Goldberg et al. 2023b)
Insheim 1 KIN 0 T30	5.54	92.90	30	55.7	107454	0.975	(Goldberg et al. 2023b)
Insheim 1 KIN 0 T60	5.9	91.53	60	56.9	104386	0.961	(Goldberg et al. 2023b)
Insheim 1 KIN 0 T120	6.22	83.96	120	55.9	105536	0.881	(Goldberg et al. 2023b)
Insheim 1 KIN 0 T150	6.29	78.93	150	55.9	104679	0.828	(Goldberg et al. 2023b)

Insheim 1 KIN o.I. T0	5.13	92.62	0	53.4	102469	1.000	
Insheim 1 KIN o.I. T5	5.19	92.30	5	53.5	103439	0.997	
Insheim 1 KIN o.I. T10	5.26	88.29	10	52.9	100993	0.953	
Insheim 1 KIN o.I. T30	5.77	89.40	30	51.8	103798	0.965	
Insheim 1 KIN o.I. T60	6.24	87.43	60	52.4	99948	0.944	
Insheim 1 KIN o.I. T120	6.53	81.53	120	54.1	99647	0.880	
Insheim 1 KIN 8.4 T0	5.45	95.80	0	52.8	106498	1.000	
Insheim 1 KIN 8.4 T5	8.3	19.89	5	54.8	102677	0.208	
Insheim 1 KIN 8.4 T30	8.27	13.23	30	58.1	102642	0.138	
Insheim 1 KIN 8.4 T60	8.19	11.57	60	55.3	101842	0.121	
Insheim 1 KIN 8.4 T180	8.19	11.96	180	55.7	103928	0.125	
Insheim 1 KIN 10.5 T0	5.48	89.45	0	57.1	105132	1.000	
Insheim 1 KIN 10.5 T5	10.53	1.80	5	55.1	106300	0.020	
Insheim 1 KIN 10.5 T10	10.49	1.92	10	53.9	104182	0.021	
Insheim 1 KIN 10.5 T30	10.49	1.19	30	53.8	108060	0.013	
Insheim 1 KIN 10.5 T60	10.5	0.99	60	57.0	105780	0.011	
Insheim 1 KIN 10.5 T120	10.52	1.79	120	55.0	105620	0.020	
Insheim 1 KIN 10.5 T180	10.34	2.24	180	55.4	105120	0.025	
Insheim 2 B Einlass	5.12	78.29	0	66.6	106383	1.000	
Insheim 2 B Reaktor	10.82	0.62	25	52.0	111839	0.008	
Insheim 2 C Einlass	5.05	76.70	0	50.0	104820	1.000	
Insheim 2 C Reaktor	10.78	20.49	16	50.0	103004	0.267	
Insheim 2 D Einlass	5.01	79.52	0	49.4	107798	1.000	
Insheim 2 D Reaktor	10.96	20.59	19	49.2	109900	0.259	
Insheim 2 KIN 10.5 T0	5.06	79.45	0	49.6	100858	1.000	
Insheim 2 KIN 10.5 T1	10.65	1.83	1	50.1	98720	0.023	
Insheim 2 KIN 10.5 T2	10.7	1.03	2	50.2	101873	0.013	
Insheim 2 KIN 10.5 T3	10.68	1.33	3	50.2	100830	0.017	
Insheim 2 KIN 10.5 T4	10.66	2.03	4	50.3	101709	0.026	
Insheim 2 KIN 10.5 T5	10.64	1.15	5	50.4	97693	0.014	
Insheim 2 KIN 10.5 T10	10.57	1.23	10	51.0	100187	0.015	
Insheim 2 KIN 10.5 T30	10.83	1.14	30	50.0	103114	0.014	
Insheim 2 KIN 10.5 T60	10.47	0.39	60	50.5	98445	0.005	
Insheim 2 KIN 10.5 T120	10.68	0.53	120	50.4	105385	0.007	
Insheim 2 KIN 10.5 T180	10.66	0.41	180	50.2	98947	0.005	
Puyehue A S3	11.03	263.23	0	41.7	2993	1.000	(Goldberg et al. 2023a)
Puyehue A S5	10.544	128.26	68	34.5	4130	0.436	
Puyehue B S3	11.07	294.06	0	40.1	3316	1.000	
Puyehue B S5	10.507	118.40	65	32.1	5021	0.403	
Puyehue C S3	11.28	430.50	0	37.9	2634	1.000	
Puyehue C S5	10.93	199.71	27	34.9	4241	0.679	
Puyehue D (RO) S3	10.995	212.78	0	40.4	2331	1.000	
Puyehue D S5	10.613	124.51	39	35.8	3496	0.423	
Puyehue E (RO) S3	10.825	342.50	0	39.0	3921	1.000	
Puyehue E S5	9.87	136.16	125	32.8	6331	0.463	
BAD1	8.11	134.29	0	69.8	6000	1.000	(Spitzmüller et al. 2021)
BAD1	9.44	100.76	2	71.4	6000	0.750	

BAD1	10.85	21.05	15	72.1	6000	0.157	
BAD1	10.93	11.66	30	69.4	6000	0.087	
BAD1	10.87	8.02	60	70.2	6000	0.060	
BAD1	10.89	7.68	120	69.9	6000	0.057	
BAD2	7.9	134.95	0	70.0	6000	1.000	(Spitzmüller et al. 2021)
BAD2	11.34	17.10	6	70.1	6000	0.127	
BAD2	11.44	4.86	16	70.2	6000	0.036	
BAD2	11.39	3.09	40	70.2	6000	0.023	
BAD2	11.4	6.06	60	69.6	6000	0.045	
BAD2	11.26	3.23	126	69.4	6000	0.024	
BAD3	7.97	138.02	0	70.9	6000	1.000	(Spitzmüller et al. 2021)
BAD3	11.36	8.48	5	71.2	6000	0.061	
BAD3	11.41	4.30	15	69.5	6000	0.031	
BAD3	11.38	6.02	30	68.8	6000	0.044	
BAD3	11.37	2.72	59	67.9	6000	0.020	
BAD3	11.32	3.22	114	73.2	6000	0.023	

10.7.2 SEM and EDS spectra analysis

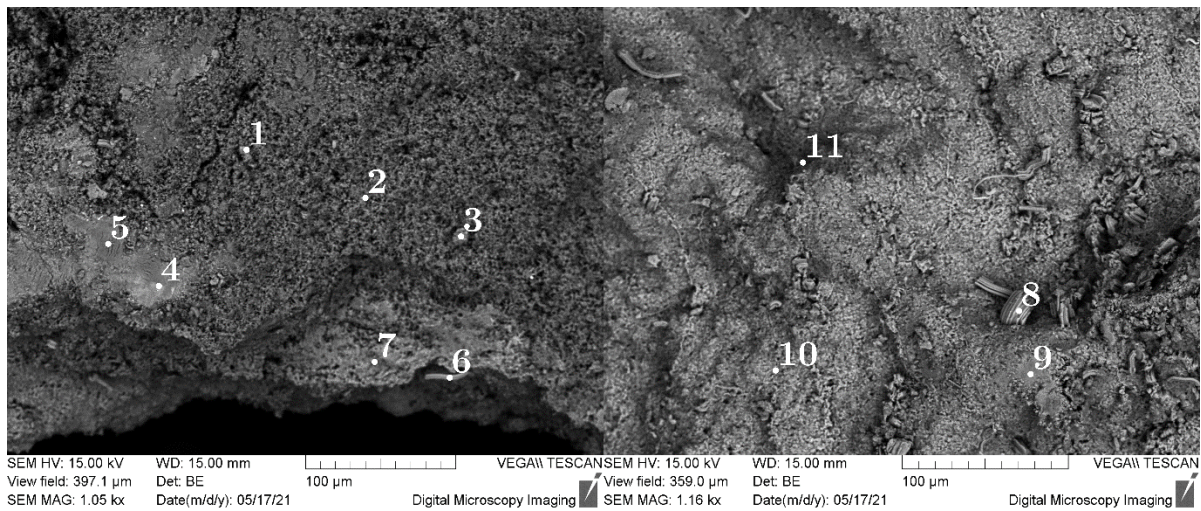


Figure 60: BSE-SEM images of the precipitates at pH 10.5 of experiment M. The precipitates mainly form aggregates of tiny grains, partly displaying a leafy shape (point 8). Locally, amorphous material covers the precipitates (points 4 and 5). Due to the small grain size of the phases, mixture analyses can't be avoided using SEM-EDS. Numbers (1-11) are explained in Table 23.

Table 23: EDS analyses of the measurement spots illustrated in Figure 60 (Experiment M). The data are given in wt.%

Name	C	O	Na	Mg	Si	Cl	K	Ca
Spectrum 1	27	36	5	1	1	11		19
Spectrum 2	0	36				2		61
Spectrum 3	23	4	31			42		1
Spectrum 4	32	28		1	1	10	8	20
Spectrum 5	10	44	2	1	1	4		38
Spectrum 6	26		27			47		1
Spectrum 7						49		51
Spectrum 8	25		29			47		
Spectrum 9	25	9	20			36		9
Spectrum 10			7			76		17
Spectrum 11	30	7	27			34		3

10.7.3 XRD results of precipitates at pH 10.5

Table 24: XRD analysis of precipitates of different precipitation experiments performed at pH 10.5. Qualitative approach using the Bruker EVA software.

	M	A R2	B R2	F R2	G R2	K R2	Insheim 1 KIN 10.5 T180
Portlandite	69%	66%	77%	82%	73%	64%	52%
Halite	acc.	acc.	acc.	acc.	acc.	5%	6%
Calcium cabonate	acc.	6%	acc.	acc.	acc.	acc.	19%
Magnesium zinc	acc.						
Magnesite		acc.					
Zinc sulfide		acc.			6%	acc.	
Potassium magnesium silicate				acc.	acc.		
Sylvite				acc.		acc.	
Copper sulfide						5%	
Brucite						acc.	
Sodium borate							8%
Calcium strontium aluminium oxid							acc.

11 Conclusion and Outlook

Geothermal energy can and should play a pivotal role in the future mix of our energy landscape and shows especially for heating purposes high efficiencies and low transformation losses (Stober and Bucher 2012). Baseload-capable, fossil energy carriers such as oil, gas, or coal become currently replaced, mainly by more volatile solar and wind power (International Energy Agency 2022). Being fully baseload capable itself, geothermal energy offers sustainable power and heat production and could thus support a reliable substitution of fossil energy. Beyond the energy transported in the fluids, they can also contain various elements needed for the energy transition.

For buffering the volatile energy production as well as for transporting the energy to the end consumer, the demand for storage facilities and batteries for mobile devices will increase continuously (DERA 2021a; Fraunhofer ISI 2022; Schmidt 2023). For state-of-the-art batteries (lithium-ion), the extraction and processing of raw materials, as well as the manufacturing of battery cells, exhibit only poorly diversified supply chains (Bridge and Faigen 2022; Wellmer et al. 2019). Geothermal fluids offer in this regard large potential for reducing geopolitical risks by providing a local raw material resource. The extraction of elements prevalent in geothermal fluids, already nowadays circulating at high flow rates for geothermal energy production, could support diversifying supply chains and serve as a more environmentally friendly addition or substitution to conventional mining.

This study analyzed the raw material potentials of geothermal fluids in Germany and Chile, evaluated extraction technologies, unveiled associated challenges, and developed solution approaches for overcoming technical hurdles.

11.1 Major findings

The extraction of Li, as one of the key elements for battery technologies, from fluid resources is proven to be feasible and has already been implemented on an industrial scale for fluids from salt flats in China and Latin America. Yet there is no full-scale application of DLE for geothermal fluids globally. The analysis and comparison of different technologies revealed key challenges for the implementation of DLE in geothermal (Chapter 4). The reaction time for loading a sorbent, solvent, or other extraction approaches is one of them. In a flow-through system, such as a geothermal power plant, reaction/equilibrium time is controlled by the hydraulic retention time, which is given by the ratio of reactor volume and flowrate. Long retention time at high geothermal flow rates thus requires large volumes (144 m³ for 30 Min. retention time at 80 L/s) which can be critical in terms of space availability as well as material requirements. Since geothermal power plants are often operated at plant pressures of up to 20 bar, large reactor volumes would cause large pressure content products requiring elaborate

processing and monitoring. A depressurization of the fluids at a long reaction time on the other hand was proven to cause mineral precipitation or require additional chemical treatment of the brine (Chapter 10). Uncontrolled mineral precipitation (scaling) during DLE is overall another major hurdle to overcome and can be caused by associated degassing, pH value changes, or cooling. These identified hurdles require targeted and site-specific solutions in terms of material research and process engineering.

Scaling, especially silica scaling, is already known as one of the major challenges in hydrothermal energy production regardless of the geothermal setting (Gallup et al. 2003; Gunnarsson and Arnórsson 2005; Rothbaum et al. 1979; Setiawan et al. 2019). Moreover, in water treatment processes, scaling or membrane fouling is one of the most prominent obstacles (Mi and Elimelech 2013; Neofotistou and Demadis 2004; Ning 2003; Zhang et al. 2018). To avoid that specifically during raw material extraction from geothermal fluids, an approach was developed in the laboratory and brought into the intended environment on a demonstrator scale in Germany and Chile (Chapter 7, Chapter 9, Chapter 10).

Silica scaling can be avoided by a controlled initial Si reduction using lime/caustic precipitation. The approach is already applied in geothermal power plants of high-enthalpy fields but its influence on potential raw materials in geothermal brines has yet to be studied. In a first laboratory study effective Si precipitation was demonstrated while not removing target elements such as Li or Cs (Spitzmüller et al. 2021). In order to conduct design calculations of an upscaled process, a new numerical data set was compiled for implementing mineral phases well known from cement mineralogy and stable at the highly alkaline environments, into the conditions of highly saline geothermal brines of the URG. Based on the numerical design calculation a field demonstrator was developed and successfully tested in different testing series in a geothermal power plant in Germany as well as at a thermal spring in Chile. The developed approach enabled a fast and efficient Si reduction of 98 % during continuous operation at the power plant in Germany and a 50 % Si reduction in the thermal system in Chile. As key parameters for the efficiency, pH value, and salinity were identified. The experiments revealed further that monovalent cations and potential target raw materials such as Li, Cs, and Rb are not removed by the treatment while metals and metalloids such as Pb, Mn, Fe, or Zn concentrations decrease strongly with increasing pH values. The removal of the latter would avoid an accumulation of this element group on oxide sorbents for DLE and thus could increase their efficiency but on the other hand requires their accumulation at surface facilities an after-use or a disposal strategy. In the low saline thermal fluids in Chile, the chemical treatment was combined with different membrane technologies, enabling a concentration of the mineral concentration up to a factor of 20 in continuous operation, by extracting freshwater. Besides energy and mineral extraction, enables this approach water production in remote areas in Chile, and by the use of the tested membrane distillation approach, can the energy demand for the process also be covered by the water's inherent heat.

DLE is despite the challenges, feasible from a technological point of view, and will most likely be up scaled for geothermal systems in the future, as it was done in the past for salt flat brines. However, beyond the technological uncertainties, there were also no reliable numbers for the real potential especially regarding the Li potential in German geothermal power plants. To give an outlook on this potential production capacities the extraction efficiencies for Li from the

analyzed studies (50 – 90 %) were used to develop production scenarios for the geothermal sector in Germany and Chile (Chapter 5, Chapter 8, Chapter 9). For Germany, entirely dependent on Li imports, the currently operating geothermal power plants could supply 2 – 13 % of the upcoming demand for the planned battery cell production without considering Li depletion in the reservoir. The large variations are due to variability in extraction efficiencies and large uncertainties of the market development on the consumer site regarding cell production. In Chile, currently 2nd largest Li-producing country worldwide, the only operating geothermal power plant could increase the country's Li production by up to 3 %. Also in Chile, with a large abundance of natural thermal springs, associated with the active Andean volcanism, chemical analysis shows additionally high concentrations of other potentially critical or valuable elements, such as Cs, Rb, Mg, or Si.

Additionally to market and technological insecurities, uncertainties remained regarding the geothermal reservoir behavior. For the state-of-the-art geothermal power plant, the focus of the planning is the avoidance of an early thermal breakthrough of the cold temperature front of the injection well at the production well. For this new approach of combined energy and raw material production, the transport of solutes and potential chemical breakthrough receives new relevance in terms of geothermal reservoir management. For different scenarios, this behavior was analyzed for the first time in a synthetic model based on a geothermal setting of the Upper Rhine Graben (Chapter 6). The modeling results revealed the lower diffusion rates of the solute in comparison to the temperature causing chemical breakthrough already in 5-10 years. Depending on the extraction and flow rate, a decrease in Li concentration between 30 and 50 % can occur, causing a 24 % lower productivity over 30 years than the static combination of flowrate and extraction efficiency. Despite the decrease, a continuous extraction over 30 years is still possible considering the model assumptions with a mean output of 234 t Li equal to 0.5 – 3 % of the future German Li demand. The study further demonstrates that the reduction rate and the resulting raw material extraction lifetime are comparable to conventional mining or raw material extraction projects. Consequently, a meaningful project life cycle could be developed as a more sustainable alternative to established approaches for mineral and energy extraction.

11.2 Outlook

The presented work studied the potential of geothermal raw material extraction with a focus on Li. The potential for Li from the geothermal sectors in Germany and Chile was demonstrated, a first model for long-time behavior was developed and different challenges were identified. These challenges were in terms of mineral scaling also approached by laboratory, numerical, and field studies. Yet there are still several remaining challenges in this promising field for the geothermal and raw material industry. The Li origin and its enrichment mechanisms are yet not fully understood, especially for the reservoirs in Germany. Therefore, genesis models for the fluids need to be improved for a concluding potential analysis and to determine further a potential Li recharge during continuous production. In this regard, it is especially for fault-dominated reservoirs not sufficient to quantify the Li in place in the reservoir's porosity but moreover, a determination of the hydraulic connectivity in terms of a

geothermal reservoir development is required. Due to the hydraulics of these reservoirs, the impact of structural uncertainties on the Li breakthrough behavior must be studied in more detail. Likewise, the breakthrough and recharge behavior should be researched in detail for volcanic settings as they host the most geothermal power plants worldwide.

Apart from modeling and predictions, large-scale and long-term production by the industry is required with fine-meshed geochemical monitoring for determining the in-situ parameters and reservoir effects. Moreover, the established materials for DLE must be customized to the special in-situ conditions in geothermal power plants. The knowledge of the different raw material incorporation processes needs further investigation to optimize extraction rates and improve cycle stabilities.

Beyond the established Br production from deep fluids, most of the industrial and academic research projects focus currently on the production of Li. Due to the conditions of geothermal reservoirs, various elements can be enriched in geothermal fluids. Therefore, also their potential needs to be examined in more detail as well as extraction technologies suitable for the prevailing concentrations developed.

By extraction of multiple elements, can a cascade extraction of different elements be pursued, analogously to a geothermal cascade use of different temperature levels. This new minimal-invasive form of mining using geothermal fluids opens up several perspectives due to its better agreement with environmental protection than most of the conventional extraction methods. Typically consume these processes large amounts of energy and/or water. A combination with the production of renewable energy and/or fresh water would provide in comparison several benefits for the local communities and could thus support the social acceptance of new projects. Only with the acceptance and support of the local community can and should these projects be realized to support our transition to renewable energies.

-
- ## References
- Achternbosch, M., Bräutigam, K.-R., Gleis, M., Hartlieb, N., Kupsch, C., Richers, U., Stemmermann, P.: Heavy metals in cement and concrete resulting from the co-incineration of wastes in cement kilns with regard to the legitimacy of waste utilisation. Forschungszentrum Karlsruhe. Umweltforschungsplan des Bundesministeriums für Umwelt, Naturschutz und Reaktorsicherheit. Förderkennzeichen (FZKA 6923). Karlsruhe (2003)
- Adams, W.: Why there's still time to avoid a lithium supply crunch, <https://insights.fastmarkets.com/why-there-is-still-time-to-avoid-a-lithium-supply-crunch-final/>. (Accessed on 31st January 2022)
- Adionics: Adionics. <http://www.adionics.com/en/homepage/markets/Lithium>. (Accessed on 31st January 2022)
- Agemar, T., Alten, J., Ganz, B., Kuder, J., Kühne, K., Schuhmacher, S., Schulz, R.: The Geothermal Information System for Germany - GeotIS. ZDGG Band. 165, 129–144 (2014)(a)
- Agemar, T., Weber, J., Schulz, R.: Deep Geothermal Energy Production in Germany. *Energies*. 7, 4397–4416 (2014)(b)
- Aguilera, F., Layana, S., Rodríguez-Díaz, A., González, C., Cortés, J., Inostroza, M.: Hydrothermal alteration, fumarolic deposits and fluids from Lastarria Volcanic Complex: A multidisciplinary study. *Andean Geol.* 43, 166 (2016). <https://doi.org/10.5027/andgeoV43n2-a02>
- Aires-Barros, L., Marques, J., Graça, R.C., Matias, M.J., Van Der Weijden, C.H., Kreulen, R., Eggenkamp, H.G.M.: Hot and cold CO₂-rich mineral waters in Chaves geothermal area (Northern Portugal). *Geothermics*. 27, 89–107 (1998). [https://doi.org/10.1016/S0375-6505\(97\)84483-5](https://doi.org/10.1016/S0375-6505(97)84483-5)
- Alexander, G.B.: The Polymerization of Monosilicic Acid. *J. Am. Chem. Soc.* 76, 2094–2096 (1954). <https://doi.org/10.1021/ja01637a017>
- Alibaba.com: Soda Liquid, <https://german.alibaba.com/p-detail/Soda-1600211390433.html?spm=a2700.themePage.107101001079000053.15.74392769B39Js6>. (Accessed on 15th January 2023)
- Allen, D.M., Grasby, S.E., Voormeij, D.A.: Determining the circulation depth of thermal springs in the southern Rocky Mountain Trench, south-eastern British Columbia, Canada using geothermometry and borehole temperature logs. *Hydrogeol. J.* 14, 159–172 (2006). <https://doi.org/10.1007/s10040-004-0428-z>

- Almendros-Ginestà, O., Missana, T., García-Gutiérrez, M., Alonso, U.: Analysis of radionuclide retention by the cement hydrate phase portlandite: A novel modelling approach. *Prog. Nucl. Energy.* 159, 104636 (2023). <https://doi.org/10.1016/j.pnucene.2023.104636>
- Appelo, C.A.J.: Principles, caveats and improvements in databases for calculating hydrogeochemical reactions in saline waters from 0 to 200°C and 1 to 1000atm. *Appl. Geochemistry.* 55, 62–71 (2015). <https://doi.org/10.1016/j.apgeochem.2014.11.007>
- Aquilina, L., Ladouche, B., Doerfliger, N., Seidel, J.L., Bakalowicz, M., Dupuy, C., Le Strat, P.: Origin, evolution and residence time of saline thermal fluids (Balaruc springs, southern France): Implications for fluid transfer across the continental shelf. *Chem. Geol.* 192, 1–21 (2002). [https://doi.org/10.1016/S0009-2541\(02\)00160-2](https://doi.org/10.1016/S0009-2541(02)00160-2)
- Aravena, D., Muñoz, M., Morata, D., Lahsen, A., Parada, M.Á., Dobson, P.: Assessment of high enthalpy geothermal resources and promising areas of Chile. *Geothermics.* 59, 1–13 (2016). <https://doi.org/10.1016/j.geothermics.2015.09.001>
- Arnórsson, S., Gunnlaugsson, E., Svavarsson, H.: The chemistry of geothermal waters in Iceland. II. Mineral equilibria and independent variables controlling water compositions. *Geochim. Cosmochim. Acta.* 47, 547–566 (1983). [https://doi.org/10.1016/0016-7037\(83\)90277-6](https://doi.org/10.1016/0016-7037(83)90277-6)
- Arnórsson, S., Stefansson, A., Bjarnason, J.O.: Fluid-Fluid Interactions in Geothermal Systems. *Rev. Mineral. Geochemistry.* 65, 259–312 (2007). <https://doi.org/10.2138/rmg.2007.65.9>
- Arulrajan, A.C., Dykstra, J.E., van der Wal, A., Porada, S.: Unravelling pH Changes in Electrochemical Desalination with Capacitive Deionization. *Environ. Sci. Technol.* 55, 14165–14172 (2021). <https://doi.org/10.1021/acs.est.1c04479>
- Babel, M., Schreiber, B.C.: Geochemistry of Evaporites and Evolution of Seawater. In: *Treatise on Geochemistry.* pp. 483–560. Elsevier (2014)
- Baccarin, F., Büsing, H., Buske, S., Dini, A., Manzella, A., Rabbel, W.: Understanding supercritical resources in continental crust. In: *European Geothermal Congress 2019.* Den Haag, The Netherlands (2019)
- Bächler, D., Kohl, T., Rybach, L.: Impact of graben-parallel faults on hydrothermal convection—Rhine Graben case study. *Phys. Chem. Earth, Parts A/B/C.* 28, 431–441 (2003). [https://doi.org/10.1016/S1474-7065\(03\)00063-9](https://doi.org/10.1016/S1474-7065(03)00063-9)
- Bachmann, G.H., Müller, M., Weggen, K.: Evolution of the Molasse Basin (Germany, Switzerland). *Tectonophysics.* 137, 77–92 (1987). [https://doi.org/10.1016/0040-1951\(87\)90315-5](https://doi.org/10.1016/0040-1951(87)90315-5)

- Badruzzaman, M., Subramani, A., DeCarolis, J., Pearce, W., Jacangelo, J.G.: Impacts of silica on the sustainable productivity of reverse osmosis membranes treating low-salinity brackish groundwater. *Desalination*. 279, 210–218 (2011).
<https://doi.org/10.1016/j.desal.2011.06.013>
- Ball, J., Nordstrom, D., Cunningham, K., Schoonen, M., Xu, Y., Demonge, J.: *Water-Chemistry and On-Site Sulfur- Speciation Data for Selected Springs in Yellowstone National Park, Wyoming*. (1995)
- Bastian, D.: *DERA Preismonitor Oktober 2020*. Deutsche Rohstoffagentur (DERA) in der Bundesanstalt für Geowissenschaften und Rohstoffe (BGR) (2020)
- Battistel, A., Palagonia, M.S., Brogioli, D., La Mantia, F., Trócoli, R.: Electrochemical Methods for Lithium Recovery: A Comprehensive and Critical Review. *Adv. Mater.* 32, 1905440 (2020)(a). <https://doi.org/10.1002/adma.201905440>
- Battistel, A., Palagonia, M.S., Brogioli, D., La Mantia, F., Trócoli, R.: Electrochemical Methods for Lithium Recovery: A Comprehensive and Critical Review. *Adv. Mater.* 32, (2020)(b). <https://doi.org/10.1002/adma.201905440>
- Bauer, J.F., Meier, S., Philipp, S.L.: Architecture, fracture system, mechanical properties and permeability structure of a fault zone in Lower Triassic sandstone, Upper Rhine Graben. *Tectonophysics*. 647, 132–145 (2015).
<https://doi.org/10.1016/j.tecto.2015.02.014>
- Bauer, M., Freeden, W., Jacobi, H., Neu, T.: *Handbuch Tiefe Geothermie*. Springer Spektrum, Berlin, Heidelberg (2014)
- Baujard, C., Genter, A., Dalmais, E., Maurer, V., Hehn, R., Rosillette, R., Vidal, J., Schmittbuhl, J.: Hydrothermal characterization of wells GRT-1 and GRT-2 in Rittershoffen, France: Implications on the understanding of natural flow systems in the rhine graben. *Geothermics*. 65, 255–268 (2017).
<https://doi.org/10.1016/j.geothermics.2016.11.001>
- Bayerisches Staatsministerium für Wirtschaft Landesentwicklung und Energie: *Bayerischer Geothermieatlas*. 1–138 (2022)
- Bear, J.: *Dynamics of fluids in porous media*. American Elsevier (Environmental science series), New York (1972)
- Benek, R., Kramer, W., McCann, T., Scheck, M., Negendank, J.F.W., Korich, D., Huebscher, H.D., Bayer, U.: Permo-Carboniferous magmatism of the Northeast German Basin. *Tectonophysics*. 266, 379–404 (1996). [https://doi.org/10.1016/S0040-1951\(96\)00199-0](https://doi.org/10.1016/S0040-1951(96)00199-0)
- Benson, T.R., Coble, M.A., Rytuba, J.J., Mahood, G.A.: Lithium enrichment in intracontinental rhyolite magmas leads to Li deposits in caldera basins. *Nat. Commun.* 8, 270 (2017). <https://doi.org/10.1038/s41467-017-00234-y>
- Bertold, C.E., Baker, D.H.: Lithium recovery from geothermal fluids, in: *Lithium resources and requirements by the year 2000*. *Geol. Surv. Prof. Pap.* 1005, 61–66 (1976)

- Bethke, C.M.: *Geochemical and Biogeochemical Reaction Modeling*. Cambridge (2008)
- Biesheuvel, P.M., Porada, S., Elimelech, M., Dykstra, J.E.: Tutorial review of reverse osmosis and electrodialysis. *J. Memb. Sci.* 647, 120221 (2022). <https://doi.org/10.1016/j.memsci.2021.120221>
- Blanc, P.: *Thermoddem: Update for the 2017 version. Final Report*. BRGM/RP-66811-FR. (2017)
- Blanc, P., Bourbon, X., Lassin, A., Gaucher, E.C.: Chemical model for cement-based materials: Temperature dependence of thermodynamic functions for nanocrystalline and crystalline C-S-H phases. *Cem. Concr. Res.* 40, 851–866 (2010)(a). <https://doi.org/10.1016/j.cemconres.2009.12.004>
- Blanc, P., Bourbon, X., Lassin, A., Gaucher, E.C.: Chemical model for cement-based materials: Thermodynamic data assessment for phases other than C-S-H. *Cem. Concr. Res.* 40, 1360–1374 (2010)(b). <https://doi.org/10.1016/j.cemconres.2010.04.003>
- Blanc, P., Lassin, A., Piantone, P., Azaroual, M., Jacquemet, N., Fabbri, A., Gaucher, E.C.: *Thermoddem: A geochemical database focused on low temperature water/rock interactions and waste materials*. *Appl. Geochemistry*. 27, 2107–2116 (2012). <https://doi.org/10.1016/j.apgeochem.2012.06.002>
- Bordoloi, S., Nath, M., Dutta, R.K.: pH-conditioning for simultaneous removal of arsenic and iron ions from groundwater. *Process Saf. Environ. Prot.* 91, 405–414 (2013). <https://doi.org/10.1016/j.psep.2012.10.002>
- Boulatov, R., Du, B., Meyers, E.A., Shore, S.G.: Two novel lithium-15-crown-5 complexes: An extended LiCl chain stabilized by crown ether and a dimeric complex stabilized by hydrogen bonding with water. *Inorg. Chem.* 38, 4554–4558 (1999). <https://doi.org/10.1021/ic9904790>
- Bourcier, W., Lin, M., Nix, G.: *Recovery of Minerals and Metals from Geothermal Fluids*. In: 2003 SME Annual Meeting. p. 18 (2005)
- Brasser, T., Feige, S., Frieling, G., Herbert, H.-J., Heinen, C., Strack, C., Vieten, C.: *Geosys Systemanalyse der geothermalen Energieerzeugung Teil B Ausführliche Ergebnisdokumentation*. GRS - 316 (Teil B). ISBN 978-3-939355-95-3. (2014)
- Bridge, G., Faigen, E.: Towards the lithium-ion battery production network: Thinking beyond mineral supply chains. *Energy Res. Soc. Sci.* 89, 102659 (2022). <https://doi.org/10.1016/j.erss.2022.102659>
- Brioche, A.: *2017 USGS Minerals Yearbook - Boron*. (2017)
- Browne, P.R.L.: Hydrothermal Alteration in Active Geothermal Fields. *Annu. Rev. Earth Planet. Sci.* 6, 229–248 (1978). <https://doi.org/10.1146/annurev.ea.06.050178.001305>
- Bucher, K., Stober, I.: Fluids in the upper continental crust. *Geofluids*. 10, 241–253 (2010). <https://doi.org/10.1111/j.1468-8123.2010.00279.x>

- Bundesverband Geothermie: Geothermie in Zahlen. Stand 2023. <https://www.geothermie.de/aktuelles/geothermie-in-zahlen> (Accessed on 1st December 2023)
- Burisch, M., Walter, B.F., Gerdes, A., Lanz, M., Markl, G.: Late-stage anhydrite-gypsum-siderite-dolomite-calcite assemblages record the transition from a deep to a shallow hydrothermal system in the Schwarzwald mining district, SW Germany. *Geochim. Cosmochim. Acta.* **223**, 259–278 (2018). <https://doi.org/10.1016/j.gca.2017.12.002>
- Butterman, W.C., Brooks, W.E., Reese, R.G.J.: Mineral Commodity Profiles: Cesium. U.S. Geol. Surv. 1–10 (2005)
- Calvo, E.J.: Electrochemical methods for sustainable recovery of lithium from natural brines and battery recycling. *Curr. Opin. Electrochem.* **15**, 102–108 (2019). <https://doi.org/10.1016/j.coelec.2019.04.010>
- Calvo, G., Mudd, G., Valero, A., Valero, A.: Decreasing Ore Grades in Global Metallic Mining: A Theoretical Issue or a Global Reality? *Resources.* **5**, 36 (2016). <https://doi.org/10.3390/resources5040036>
- Cappetti, G.: Cerro Pabellón geothermal plant: a success story. 2019. <https://newenergyevents.com/geolac/wp-content/uploads/sites/7/2019/07/Guido-Cappetti-Cerro-Pabellon.pdf>, (Accessed on 2nd February 2024)
- Cappetti, G., Giorgi, N., Arias, A., Volpi, G., Rivera, G., Cei, M., Fedeli, M., Marzio, G. Di, Pasti, M., Massei, S., Baccarin, F.: The Cerro Pabellón Geothermal Project (Chile): from Surface Exploration to Energy Production. In: *Proceedings World Geothermal Congress 2020*. pp. 1–9. Reykjavik (2020)
- Charrier, R., Pinto, L., Rodríguez, M.P.: Tectonostratigraphic evolution of the Andean Orogen in Chile. In: *The Geology of Chile*. pp. 21–114. Geological Society Special Publication (2007)
- Chen, C.T.A., Marshall, W.L.: Amorphous silica solubilities IV. Behavior in pure water and aqueous sodium chloride, sodium sulfate, magnesium chloride, and magnesium sulfate solutions up to 350°C. *Geochim. Cosmochim. Acta.* **46**, 279–287 (1982)
- Chen, J.J., Thomas, J.J., Taylor, H.F.W., Jennings, H.M.: Solubility and structure of calcium silicate hydrate. *Cem. Concr. Res.* **34**, 1499–1519 (2004). <https://doi.org/10.1016/j.cemconres.2004.04.034>
- Chen, Q., Luo, Z., Hills, C., Xue, G., Tyrer, M.: Precipitation of heavy metals from wastewater using simulated flue gas: Sequent additions of fly ash, lime and carbon dioxide. *Water Res.* **43**, 2605–2614 (2009). <https://doi.org/10.1016/j.watres.2009.03.007>
- Chian, E.S.K., Chen, J.P., Sheng, P.-X., Ting, Y.-P., Wang, L.K.: Reverse Osmosis Technology for Desalination. In: Wang, L.K., Hung, Y.-T., and Shammass, N.K. (eds.) *Advanced Physicochemical Treatment Technologies*. pp. 329–366. Humana Press, Totowa, NJ (2007)

- Choi, J.H., Edwards, P., Ko, K., Kim, Y.S.: Definition and classification of fault damage zones: A review and a new methodological approach. *Earth-Science Rev.* 152, 70–87 (2016). <https://doi.org/10.1016/j.earscirev.2015.11.006>
- Cizer, O., Van Balen, K., Elsen, J., Gemert, D. Van: Crystal Morphology of Precipitated Calcite Crystals From Accelerated Carbonation of Lime Binders. 2nd Int. Conf. Accel. Carbonation Environ. Mater. Eng. Rome, Italy, 1-3 Oct. 2008. 1–3 (2008)
- Coffey, D.M., Munk, L.A., Ibarra, D.E., Butler, K.L., Boutt, D.F., Jenckes, J.: Lithium Storage and Release From Lacustrine Sediments: Implications for Lithium Enrichment and Sustainability in Continental Brines. *Geochemistry, Geophys. Geosystems.* 22, 1–22 (2021). <https://doi.org/10.1029/2021GC009916>
- Colàs, E., Riba, O., Campos, I., Duro, L., Grivé, M.: ThermoChimie Technical report Introduction to the ThermoChimie guidelines. (2019)
- Controlled Thermal Ressources: The power of California’s Lithium Valley, <https://www.cthermal.com/projects>. (Accessed on 15th July 2022)
- Cortecci, G., Boschetti, T., Mussi, M., Lameli, C.H., Mucchino, C., Barbieri, M.: New chemical and original isotopic data on waters from El Tatio geothermal field, northern Chile. *Geochem. J.* 39, 547–571 (2005). <https://doi.org/10.2343/geochemj.39.547>
- Cravotta, C.A., Trahan, M.K.: Limestone drains to increase pH and remove dissolved metals from acidic mine drainage. *Appl. Geochemistry.* 14, 581–606 (1999). [https://doi.org/10.1016/S0883-2927\(98\)00066-3](https://doi.org/10.1016/S0883-2927(98)00066-3)
- Daniele, L., Cannatelli, C., Buscher, J.T., Bonatici, G.: Chemical composition of Chilean bottled waters: Anomalous values and possible effects on human health. *Sci. Total Environ.* 689, 526–533 (2019). <https://doi.org/10.1016/j.scitotenv.2019.06.165>
- Dashti, A., Gholami Korzani, M., Geuzaine, C., Egert, R., Kohl, T.: Impact of structural uncertainty on tracer test design in faulted geothermal reservoirs. *Geothermics.* 107, 102607 (2023). <https://doi.org/10.1016/j.geothermics.2022.102607>
- DERA: Batterierohstoffe für die Elektromobilität. – DERA Themenheft: 26 S.; Berlin. (2021)(a)
- DERA: DERA-Rohstoffliste 2021 - DERA Rohstoffinformationen 49. DERA-Deutsche Rohstoffagentur in der Bundesanstalt für Geowissenschaften und Rohstoffe, Berlin. ISBN: 978-3-948532-45-1. (2021)(b)
- Destatis: Energiepreisentwicklung. 2023. <https://www.destatis.de/DE/Themen/Wirtschaft/Preise/Publicationen/Energiepreise/energiepreisentwicklung-pdf-5619001.html>. (Accessed on 15th March 2023)
- Dezayes, C., Sanjuan, B., Gal, F., Lerouge, C., Brach, M.: Forage d’exploration géothermique GRT-1. Suivi géochimique des fluides et caractérisation des zones fracturées. Rapport final BRGM. RP-62546-FR (2013)

-
- Dibble, W., Dickson, J., Dickson, F.: The Behavior of lithium in experimental rock-water interaction studies. U.S. Geol. Surv. (1976)
- Dilger, G., Deinhardt, A., Reimer, D., Link, K., Zwicklhuber, K., Götzl, G.: Tiefe Geothermie-Projekte in Deutschland 2021/2022. Geotherm. Energie, Fachzeitschrift für Geotherm. Forsch. und Anwendung Deutschland, Österreich und der Schweiz, 30. Jahrgang, H. Nr. 100. (2021)
- DiPippo, R.: The Geysers Dry-Steam Power Plants, Sonoma and Lake Counties, California, USA. In: DiPippo, R. (ed.) Geothermal Power Plants. pp. 345–367 (2015)
- Dolley, T.: 2017 USGS Minerals Yearbook - Silica. (2017)
- Dorsch, K.: Hydrogeologische Untersuchungen der Geothermalfelder von Puyehue und Cordón Caulle, Chile. Dissertation der Fakultät für Geowissenschaften, Ludwig-Maximilians-Universität München. (2003)
- Dove, P.M., Han, N., Wallace, A.F., De Yoreo, J.J.: Kinetics of amorphous silica dissolution and the paradox of the silica polymorphs. Proc. Natl. Acad. Sci. U. S. A. 105, 9903–9908 (2008). <https://doi.org/10.1073/pnas.0803798105>
- Drüppel, K., Stober, I., Grimmer, J.C., Mertz-Kraus, R.: Experimental alteration of granitic rocks: Implications for the evolution of geothermal brines in the Upper Rhine Graben, Germany. Geothermics. 88, 101903 (2020). <https://doi.org/10.1016/j.geothermics.2020.101903>
- Duan, Z., Sun, R.: An improved model calculating CO₂ solubility in pure water and aqueous NaCl solutions from 273 to 533 K and from 0 to 2000 bar. 193, 257–271 (2003)
- Duan, Z., Sun, R., Zhu, C., Chou, I.M.: An improved model for the calculation of CO₂ solubility in aqueous solutions containing Na⁺, K⁺, Ca²⁺, Mg²⁺, Cl⁻, and SO₄²⁻. Mar. Chem. 98, 131–139 (2006). <https://doi.org/10.1016/j.marchem.2005.09.001>
- Duchesene, J., Reardon, E.J.: Measurement and prediction of Portlandite solubility in alkali solutions. Cem. Concr. Res. 25, 1043–1053 (1995)
- Dugamin, E.J.M., Cathelineau, M., Boiron, M.C., Richard, A., Despinois, F.: Lithium enrichment processes in sedimentary formation waters. Chem. Geol. 635, 121626 (2023). <https://doi.org/10.1016/j.chemgeo.2023.121626>
- Dussel, M., Lüschen, E., Thomas, R., Agemar, T., Fritzer, T., Sieblitz, S., Huber, B., Birner, J., Schulz, R.: Forecast for thermal water use from Upper Jurassic carbonates in the Munich region (South German Molasse Basin). Geothermics. 60, 13–30 (2016). <https://doi.org/10.1016/j.geothermics.2015.10.010>
- Dykstra, J.E., Keesman, K.J., Biesheuvel, P.M., van der Wal, A.: Theory of pH changes in water desalination by capacitive deionization. Water Res. 119, 178–186 (2017). <https://doi.org/10.1016/j.watres.2017.04.039>
- Egert, R., Gholami Korzani, M., Held, S., Kohl, T.: Implications on large-scale flow of the fractured EGS reservoir Soultz inferred from hydraulic data and tracer

- experiments. *Geothermics*. 84, (2020).
<https://doi.org/10.1016/j.geothermics.2019.101749>
- Egert, R., Gholami Korzani, M., Held, S., Kohl, T.: Thermo-hydraulic Modeling of an Enhanced Geothermal System in the Upper Rhine Graben Using MOOSE/TIGER. In: World Geothermal Congress (WGC 2021), Reykjavík, Island, 21.05.2021 – 26.05.2021. Reykjavík (2021)
- Eggeling, L., Herr, K., Goldberg, V., Siefert, D., Köhler, J., Kölbl, T., Reith, S.: Schlussbericht zum Verbundprojekt ANEMONA. Anlagenmonitoring als Schlüsseltechnologie für den erfolgreichen Betrieb von Geothermiekraftwerken in Deutschland, (2018)
- Eikenberg, J.: On the Problem of Silica Solubility at High pH. Paul Scherrer Institut. PSI-Bericht Nr. 74. Würenlingen und Villigen (1990)
- Eisbacher, G.H., Fielitz, W.: Karlsruhe und seine Region. In: Sammlung geologischer Führer Band 103. Gebrüder Borntraeger Verlagsbuchhandlung, Stuttgart (2010)
- Ellis, A.J.: Chemical and isotopic techniques in geothermal investigations. *Geothermics*. 5, 3–12 (1977). [https://doi.org/10.1016/0375-6505\(77\)90003-7](https://doi.org/10.1016/0375-6505(77)90003-7)
- Energy Source Minerals: Energy Source Minerals, <https://www.esminerals.com/project>. (Accessed on 31st January 2022)
- Eramet: EuGeLi 31.01.2022, <https://www.eramet.com/en/activities/innovate-design/eugeli-project>. (Accessed on 31st January 2022)
- Eramet: Eramet, <https://www.eramet.com/en/eramet-and-electricite-de-strasbourg-announce-success-first-pilot-test-extract-lithium-geothermal>. (Accessed on 31st January 2022)
- Europäische Kommission: Widerstandsfähigkeit der EU bei kritischen Rohstoffen: Einen Pfad hin zu größerer Sicherheit und Nachhaltigkeit abstecken. Mitteilung der Kommission an das Eur. Parlam. den Rat, den Eur. Wirtschafts- und Sozialausschuss und den Ausschuss der Reg. 27 (2020)
- Europäisches Parlament: Fit für 55: Abgeordnete unterstützen Ziel der Emissionsneutralität für neue Autos und Lieferwagen ab 2035, <https://www.europarl.europa.eu/news/de/press-room/20220603IPR32129/fit-fur-55-emissionsneutralitat-fur-neue-pkw-und-lieferwagen-ab-2035>. (Accessed on 1st March 2023)
- EVA-M: Verbundvorhaben EvA-M: Einsatz von Ausfällungsinhibitoren im Molassebecken ' Begleitendes Monitoring und Experimente in unterschiedlichen Skalen, Teilvorhaben A: Inhibitorevaluierung unter Anlagen- und Reservoir-Bedingungen, Anlagenmonitoring und Modellie. (2021)
- Evans, J.P., Forster, C.B., Goddard, J. V.: Permeability of fault-related rocks, and implications for hydraulic structure of fault zones. *J. Struct. Geol.* 19, 1393–1404 (1997). [https://doi.org/10.1016/S0191-8141\(97\)00057-6](https://doi.org/10.1016/S0191-8141(97)00057-6)

- Faltlhauser, M.: Zahlen und Fakten zur Stromversorgung in Deutschland 2016. Wirtschaftsbeirat Bayern. 1–24 (2016)
- Feldrappe, H., Obst, K., Wolfgramm, M.: Die mesozoischen Sandsteinaquifere des Norddeutschen Beckens und ihr Potential für die geothermische Nutzung. *Zeitschrift für Geol. Wissenschaften*. 36 (4–5), 199–222 (2008)
- Feng, Q., Miyai, Y., Kanoh, H., Ooi, K.: Li + Extraction / insertion with Spinel-Type Lithium Manganese Oxides . Characterization of Redox-Type and Ion-Exchange-Type Sites. *Langmuir*. 1861–1867 (1992)
- Finster, M., Clark, C., Schroeder, J., Martino, L.: Geothermal produced fluids: Characteristics, treatment technologies, and management options. *Renew. Sustain. Energy Rev.* 50, 952–966 (2015). <https://doi.org/10.1016/j.rser.2015.05.059>
- Flexer, V., Baspineiro, C.F., Galli, C.I.: Lithium recovery from brines: A vital raw material for green energies with a potential environmental impact in its mining and processing. *Sci. Total Environ.* 639, 1188–1204 (2018). <https://doi.org/10.1016/j.scitotenv.2018.05.223>
- Fournier, R.O., Rowe, J.J.: Estimation of underground temperatures from the silica content of water from hot springs and wet-steam wells. *Am. J. Sci.* 264, 685–697 (1966). <https://doi.org/10.2475/ajs.264.9.685>
- Francke, H., Thorade, M.: Density and viscosity of brine: An overview from a process engineers perspective. *Geochemistry*. 70, 23–32 (2010). <https://doi.org/10.1016/j.chemer.2010.05.015>
- Franz, M., Barth, G., Zimmermann, J., Budach, I., Nowak, K., Wolfgramm, M.: Geothermal resources of the North German Basin: Exploration strategy, development examples and remaining opportunities in Mesozoic hydrothermal reservoirs. *Geol. Soc. Spec. Publ.* 469, 193–222 (2018). <https://doi.org/10.1144/SP469.11>
- Frape, S.K., Blyth, A., Stotler, R.L., Ruskeeniemi, T., Blomqvist, R., McNutt, R.H., Gascoyne, M.: Deep Fluids in the Continents. In: *Treatise on Geochemistry*. pp. 517–562. Elsevier (2014)
- Fraunhofer ISI: Geplante gesamte Batteriezellproduktionskapazität [GWh], <https://www.isi.fraunhofer.de/de/presse/2022/presseinfo-17-Batteriezellfertigung-Verzehnfachung-2030.html>. (Accessed on 15th March 2023)
- Gaboriaud, F., Nonat, A., Chaumont, D., Craievich, A.: Aggregation and gel formation in basic silico-calco-alkaline solutions studied: A SAXS, SANS, and ELS study. *J. Phys. Chem. B.* 103, 5775–5781 (1999). <https://doi.org/10.1021/jp990151s>
- Gallup, D.L., Sugiaman, F., Capuno, V., Manceau, A.: Laboratory investigation of silica removal from geothermal brines to control silica scaling and produce usable silicates. *Appl. Geochemistry*. 18, 1597–1612 (2003). [https://doi.org/10.1016/S0883-2927\(03\)00077-5](https://doi.org/10.1016/S0883-2927(03)00077-5)

- Garcés, I., Alvarez, G.: Water mining and extractivism of the Salar de Atacama, Chile. *WIT Trans. Ecol. Environ.* 245, 189–199 (2020). <https://doi.org/10.2495/EID200181>
- Garrett, D.E.: Lithium. In: *Handbook of Lithium and Natural Calcium Chloride*. pp. 1–235. Elsevier (2004)
- Geolith: Geolith, <https://en.geolith.fr/copie-de-technologies>. (Accessed on 31st January 2022)
- Geothermie Unterhaching: Meilensteine: Geothermie Unterhaching, https://www.geothermie-unterhaching.de/cms/geothermie/web.nsf/id/pa_historie.html. (Accessed on 15th July 2022)
- German Lithium Participation: Reale Preisentwicklung und prognostizierter Preistrend für battery grade Lithiumcarbonat, <https://germanlithium.com/preisentwicklung-lithium/>. (Accessed on 31st January 2022)
- Geuzaine, C., Remacle, J.-F.: Gmsh: A 3-D finite element mesh generator with built-in pre- and post-processing facilities. *Int. J. Numer. Methods Eng.* 79, 1309–1331 (2009). <https://doi.org/10.1002/nme.2579>
- Geyer, O.F., Gwinner, M., Simon, T.: *Geologie von Baden-Württemberg*, 5, Völlig neu Bearbeitete Auflage. Schweizerbart, Stuttgart (2011)
- Ghergut, J., Wiegand, B., Behrens, H., Sauter, M.: Model-Independent, and Model- Dependent Aspects of ‘Geothermal Solute’ Co-Production Forecast for Hydrothermal vs . Petrothermal Reservoirs. *Proceedings, 48th Workshop on Geothermal Reservoir Engineering*. 1–9, California (2023)
- Gholami Korzani, M., Held, S., Kohl, T.: Numerical based filtering concept for feasibility evaluation and reservoir performance enhancement of hydrothermal doublet systems. *J. Pet. Sci. Eng.* 190, 106803 (2020). <https://doi.org/10.1016/j.petrol.2019.106803>
- Giffaut, E., Grivé, M., Blanc, P., Vieillard, P., Colàs, E., Gailhanou, H., Gaboreau, S., Marty, N., Madé, B., Duro, L.: Andra thermodynamic database for performance assessment: ThermoChimie. *Appl. Geochemistry*. 49, 225–236 (2014). <https://doi.org/10.1016/j.apgeochem.2014.05.007>
- Giggenbach, W., Sheppard, D., Robinson, B., Stewart, M., Lyon, G.: Geochemical structure and position of the Waiotapu geothermal field, New Zealand. *Geothermics*. 23, 599–644 (1994). [https://doi.org/10.1016/0375-6505\(94\)90022-1](https://doi.org/10.1016/0375-6505(94)90022-1)
- Giggenbach, W.F.: The isotopic composition of waters from the El Tatio geothermal field, Northern Chile. *Geochim. Cosmochim. Acta.* 42, 979–988 (1978). [https://doi.org/10.1016/0016-7037\(78\)90287-9](https://doi.org/10.1016/0016-7037(78)90287-9)
- Giggenbach, W.F.: Geothermal mineral equilibria. *Geochim. Cosmochim. Acta.* 45, 393–410 (1981). [https://doi.org/10.1016/0016-7037\(81\)90248-9](https://doi.org/10.1016/0016-7037(81)90248-9)

- Giggenbach, W.F.: Isotopic shifts in waters from geothermal and volcanic systems along convergent plate boundaries and their origin. *Earth Planet. Sci. Lett.* 113, 495–510 (1992)
- Giudetti, G., Tempesti, L., Power, E.G., Pisano, V.A.: First Geochemical Data from Cerro Pabellón Geothermal Project (Apacheta Region, Chile). In: *Proceedings World Geothermal Congress 2020*. pp. 1–10 (2020)
- Gokgoz, A., Yilmazli, I.E., Gungor, I., Yavuzer, I.: Hydrogeology and Environmental Study at the Karahayit Geothermal Field (Western Turkey). 25–29 (2010)
- Goldberg, V., Kluge, T., Nitschke, F.: Herausforderungen und Chancen für die Lithiumgewinnung aus geothermalen Systemen in Deutschland – Teil 1: Literaturvergleich bestehender Extraktionstechnologien. *Grundwasser*. 27, 239–259 (2022)(a). <https://doi.org/10.1007/s00767-022-00522-5>
- Goldberg, V., Nitschke, F., Kluge, T.: Herausforderungen und Chancen für die Lithiumgewinnung aus geothermalen Systemen in Deutschland – Teil 2: Potenziale und Produktionsszenarien in Deutschland. *Grundwasser*. 27, 261–275 (2022)(b). <https://doi.org/10.1007/s00767-022-00523-4>
- Goldberg, V., Winter, D., Eiche, E., Koschikowski, J., Kohl, T., Morata, D., Schwantes, R., Seibt, P., Heboldt, J., Nitschke, F.: Prototype Tests for the Treatment of Geothermal Waters for Raw Material Extraction and Freshwater Production. *Min. Rep. Glückauf*. 159, 601–610 (2023)(a)
- Goldberg, V., Winter, D., Nitschke, F., Held, S., Groß, F., Pfeiffle, D., Uhde, J., Morata, D., Koschikowski, J., Kohl, T.: Development of a continuous silica treatment strategy for metal extraction processes in operating geothermal plants. *Desalination*. 564, 116775 (2023)(b). <https://doi.org/10.1016/j.desal.2023.116775>
- Goldberg, V., Winter, D., Nitschke, F., Rath, M., Held, S., Spitzmüller, L., Budach, I., Pavez, M., Morata, D., Koschikowski, J., Kohl, T.: The potential of raw material extraction from thermal brines – Successful milestones of the BrineMine project. *OIL GAS*. 26–33 (2021). <https://doi.org/10.19225/210306>
- González-Partida, E., Carrillo-Chávez, A., Levresse, G., Tello-Hinojosa, E., Venegas-Salgado, S., Ramirez-Silva, G., Pal-Verma, M., Tritlla, J., Camprubi, A.: Hydro-geochemical and isotopic fluid evolution of the Los Azufres geothermal field, Central Mexico. *Appl. Geochemistry*. 20, 23–39 (2005). <https://doi.org/10.1016/j.apgeochem.2004.07.006>
- Grant, A.: From Catamarca to Qinghai: The Commercial Scale Direct Lithium Extraction Operations. *Jade Cove Partners*. 1–10 (2020)
- Grasby, S.E., Hutcheon, I., Krouse, H.R.: Erratum: The influence of water-rock interaction on the chemistry of thermal springs in western Canada (*Applied Geochemistry* (2000) 15 (439-454) PII: S0883292799000669). *Appl. Geochemistry*. 15, 1069 (2000). [https://doi.org/10.1016/S0883-2927\(00\)00020-2](https://doi.org/10.1016/S0883-2927(00)00020-2)

- Greenberg, S.A.: The nature of the silicate species in sodium silicate solutions. *J. Am. Chem. Soc.* 6508–6511 (1958)
- Greenberg, S.A., Chang, T.N.: Investigation of the colloidal hydrated calcium silicates. II. Solubility relationships in the calcium oxide-silica-water system at 25°. *J. Phys. Chem.* 69, 182–188 (1965). <https://doi.org/10.1021/j100885a027>
- Greenberg, S.A., Price, E.W.: The Solubility of Silica in Solutions of Electrolytes. *J. Phys. Chem.* 61, 1539–1541 (1957)
- Greim, P., Solomon, A.A., Breyer, C.: Assessment of lithium criticality in the global energy transition and addressing policy gaps in transportation. *Nat. Commun.* 11, 4570 (2020). <https://doi.org/10.1038/s41467-020-18402-y>
- Grew, E.S.: The Minerals of Lithium. *Elements.* 16, 235–240 (2020). <https://doi.org/10.2138/gselements.16.4.235>
- Grimmer, J.C., Ritter, J.R.R., Eisbacher, G.H., Fielitz, W.: The Late Variscan control on the location and asymmetry of the Upper Rhine Graben. *Int. J. Earth Sci.* 106, 827–853 (2017). <https://doi.org/10.1007/s00531-016-1336-x>
- Guillou-Frottier, L., Carré, C., Bourguin, B., Bouchot, V., Genter, A.: Structure of hydrothermal convection in the Upper Rhine Graben as inferred from corrected temperature data and basin-scale numerical models. *J. Volcanol. Geotherm. Res.* 256, 29–49 (2013). <https://doi.org/10.1016/j.jvolgeores.2013.02.008>
- Gunn, G.: *Critical Metals Handbook*. Wiley (2014)
- Gunnarsson, I., Arnórsson, S.: Impact of silica scaling on the efficiency of heat extraction from high-temperature geothermal fluids. *Geothermics.* 34, 320–329 (2005)
- Hamdouni, A., Montes-Hernandez, G., Tlili, M., Findling, N., Renard, F., Putnis, C. V.: Removal of Fe(II) from groundwater via aqueous portlandite carbonation and calcite-solution interactions. *Chem. Eng. J.* 283, 404–411 (2016). <https://doi.org/10.1016/j.cej.2015.07.077>
- Hans Wedepohl, K.: The composition of the continental crust. *Geochim. Cosmochim. Acta.* 59, 1217–1232 (1995). [https://doi.org/10.1016/0016-7037\(95\)00038-2](https://doi.org/10.1016/0016-7037(95)00038-2)
- Hauser, A.: *Catastro y caracterización de las fuentes de aguas minerales y termales de Chile*. Servicio Nacional de Geología y Minería (1997)
- Hawkins, A.J., Tester, J.W.: Geothermal Systems. In: *Encyclopedia of Geochemistry*. *Encyclopedia of Earth Sciences Series*. pp. 592–597. Springer (2018)
- He, K., Stober, I., Bucher, K.: Chemical evolution of thermal waters from limestone aquifers of the Southern Upper Rhine Valley. *Appl. Geochemistry.* 14, 223–235 (1999). [https://doi.org/10.1016/S0883-2927\(98\)00046-8](https://doi.org/10.1016/S0883-2927(98)00046-8)
- Hedenquist, J.W., Lowenstern, J.B.: The role of magmas in the formation of hydrothermal ore deposits. *Nature.* 370, 519–527 (1994). <https://doi.org/10.1038/370519a0>

-
- Held, S., Genter, A., Kohl, T., Kölbl, T., Sausse, J., Schoenball, M.: Economic evaluation of geothermal reservoir performance through modeling the complexity of the operating EGS in Soultz-sous-Forêts. *Geothermics*. 51, 270–280 (2014). <https://doi.org/10.1016/j.geothermics.2014.01.016>
- Held, S., Schill, E., Schneider, J., Nitschke, F., Morata, D., Neumann, T., Kohl, T.: Geochemical characterization of the geothermal system at Villarrica volcano, Southern Chile; Part 1: Impacts of lithology on the geothermal reservoir. *Geothermics*. 74, 226–239 (2018). <https://doi.org/10.1016/j.geothermics.2018.03.004>
- Henley, R.W.: pH and silica scaling control in geothermal field development. *Geothermics*. 12, 307–321 (1983). [https://doi.org/10.1016/0375-6505\(83\)90004-4](https://doi.org/10.1016/0375-6505(83)90004-4)
- Henley, R.W., Ellis, A.J.: Geothermal systems ancient and modern: a geochemical review. *Earth Sci. Rev.* 19, 1–50 (1983)(a). [https://doi.org/10.1016/0012-8252\(83\)90075-2](https://doi.org/10.1016/0012-8252(83)90075-2)
- Henley, R.W., Ellis, A.J.: Geothermal systems ancient and modern: a geochemical review. *Earth-Science Rev.* 19, 1–50 (1983)(b). [https://doi.org/10.1016/0012-8252\(83\)90075-2](https://doi.org/10.1016/0012-8252(83)90075-2)
- Hervé, F., Faundez, V., Calderón, M., Massonne, H.-J., Willner, A.: Metamorphic and plutonic basement complexes. In: *Geology of Chile*. pp. 5–19. Geological Society London (2007)
- Hochstein, M.P.: Assessment and modelling of geothermal reservoirs (small utilization schemes). *Geothermics*. 17, 15–49 (1988). [https://doi.org/10.1016/0375-6505\(88\)90004-1](https://doi.org/10.1016/0375-6505(88)90004-1)
- Hohmann, M.: Durchschnittlicher Preis von Lithiumcarbonat weltweit in den Jahren von 2002 bis 2018 (in US-Dollar je Tonne), <https://de.statista.com/statistik/daten/studie/979746/umfrage/durchschnittliche-r-preis-von-lithium-weltweit/>. (Accessed on 31st January 2022)
- Höök, M., Davidsson, S., Johansson, S., Tang, X.: Decline and depletion rates of oil production: A comprehensive investigation. *Philos. Trans. R. Soc. A Math. Phys. Eng. Sci.* 372, (2014)(a). <https://doi.org/10.1098/rsta.2012.0448>
- Höök, M., Davidsson, S., Johansson, S., Tang, X.: Decline and depletion rates of oil production: a comprehensive investigation. *Philos. Trans. R. Soc. A Math. Phys. Eng. Sci.* 372, 20120448 (2014)(b). <https://doi.org/10.1098/rsta.2012.0448>
- Hörbrand, T., Baumann, T., Moog, H.C.: Validation of hydrogeochemical databases for problems in deep geothermal energy. *Geotherm. Energy*. 6, (2018). <https://doi.org/10.1186/s40517-018-0106-3>
- Horstman, E.L.: The distribution of lithium, rubidium and caesium in igneous and sedimentary rocks. *Geochim. Cosmochim. Acta*. 12, 1–28 (1957). [https://doi.org/10.1016/0016-7037\(57\)90014-5](https://doi.org/10.1016/0016-7037(57)90014-5)
-

- Hoyer, M., Kummer, N.-A., Merkel, B.: Sorption of Lithium on Bentonite, Kaolin and Zeolite. *Geosciences*. 5, 127–140 (2015). <https://doi.org/10.3390/geosciences5020127>
- Huttrer, G.W., Rica, C., Salvador, E.: Geothermal Power Generation in the World 2015-2020 Update Report. 1–17 (2020)
- Iler, R.K.: *The Chemistry of Silica*. Wiley Interscience, New York (1976)
- International Energy Agency: *World Energy Outlook 2022*. IEA Publications. Paris (2022)
- Isupov, V.P., Kotsupalo, N.P., Nemudry, A.P., Menzeres, L.T.: Aluminium hydroxide as selective sorbent of lithium salts from brines and technical solutions. *Stud. Surf. Sci. Catal.* 120 A, 621–652 (1999). [https://doi.org/10.1016/s0167-2991\(99\)80567-9](https://doi.org/10.1016/s0167-2991(99)80567-9)
- Itoh, T., Billah, M., Honjo, T., Terada, K.: Separation and determination of a trace amount of lithium using its thenoyltrifluoroacetone complex with 12-crown-4 through synergic extraction and flame photometry. *Anal. Sci.* 7, 47–50 (1991). https://doi.org/10.2116/analsci.7.Supple_47
- Jennings, H.M.: Aqueous Solubility Relationships for Two Types of Calcium Silicate Hydrate. *J. Am. Ceram. Soc.* 69, 614–618 (1986). <https://doi.org/10.1111/j.1151-2916.1986.tb04818.x>
- Jiang, H., Yang, Y., Sun, S., Yu, J.: Adsorption of lithium ions on lithium-aluminum hydroxides: Equilibrium and kinetics. *Can. J. Chem. Eng.* 98, 544–555 (2020). <https://doi.org/10.1002/cjce.23640>
- Jones, D., Blanchard, C., Templeman, L., Fitzpatrick, L.: Is lithium a ‘green’ alternative?, https://www.dbresearch.com/PROD/RPS_EN-PROD/PROD0000000000518496/Q%26A_series%3A_Is_lithium_a_‘green’_alternative%3F.pdf?undefined&reload=NfunTjMdzVdyuNFxqpz3sEw9wumftGRGj5ktGV2dFcWO~6dsE0AWj62WZeRSLfc8. (Accessed on 31st January 2022)
- Kanoh, H., Ooi, K., Miyai, Y., Katoh, S.: Electrochemical recovery of lithium ions in the aqueous phase. *Sep. Sci. Technol.* 28, 643–651 (1993). <https://doi.org/10.1080/01496399308019512>
- Karamanderesi, İ.H., Ölçeno, K.: Geology of the Denizli Sarayköy (Gerali) Geothermal Field, Western Anatolia, Turkey. *World Geotherm. Congr.* 2005. 24–29 (2005)
- Karingithi, C.W., Arnórsson, S., Gródienvold, K.: Processes controlling aquifer fluid compositions in the Olkaria geothermal system, Kenya. *J. Volcanol. Geotherm. Res.* 196, 57–76 (2010). <https://doi.org/10.1016/j.jvolgeores.2010.07.008>
- Kato, K., Ueda, A., Mogi, K., Nakazawaka, H., Shimizu, K.: Silica recovery from Sumikawa and Ohnuma geothermal brines (Japan) by addition of CaO and cationic precipitants in a newly developed seed circulation device. *Geothermics*. 32, 239–273 (2003)

- Kavanagh, L., Keohane, J., Garcia Cabellos, G., Lloyd, A., Cleary, J.: Global Lithium Sources—Industrial Use and Future in the Electric Vehicle Industry: A Review. *Resources*. 7, 57 (2018). <https://doi.org/10.3390/resources7030057>
- Kaya, T., Kindap, A.: Kizildere – New Geothermal Power Plant In Turkey. *Int. Geotherm. Days Conf. Summer Sch.* (2009)
- Kharaka, Y.K., Hanor, J.S.: Deep Fluids in the Continents: I. Sedimentary Basins. In: *Treatise on Geochemistry*. pp. 1–48. Elsevier (2003)
- Kimura, T., Koga, N.: Monohydrocalcite in Comparison with Hydrated Amorphous Calcium Carbonate: Precipitation Condition and Thermal Behavior. *Cryst. Growth Des.* 11, 3877–3884 (2011). <https://doi.org/10.1021/cg200412h>
- Kirnbauer, T.: Hydrothermale Bildungen des Thermalwassersystems von Bad Nauheim (Wetterau) und dessen Alter. *Jahrbücher des Nassau. Vereins für Naturkd.* 158, 39–96 (2008)
- Kölbel, L., Herrmann, L., Kölbel, T., Schneider, J.: Lithium extraction from geothermal brines: Adsorption-desorption studies on ^{226}Ra (^{228}Ra) and ^{210}Pb on lithium-titanium-oxides (LTO). *Appl. Geochemistry*. 162, 105913 (2024)(a). <https://doi.org/10.1016/j.apgeochem.2024.105913>
- Kölbel, L., Kölbel, T., Herrmann, L., Kaymakci, E., Ghergut, I., Poirel, A., Schneider, J.: Lithium extraction from geothermal brines in the Upper Rhine Graben: A case study of potential and current state of the art. *Hydrometallurgy*. 221, 106131 (2023). <https://doi.org/10.1016/j.hydromet.2023.106131>
- Kölbel, L., Slunitschek, K., Kaymakci, E., Kölbel, T., Reich, R., Schneider, J.: Lithium recovery from geothermal brines: An investigation into radioactive nuclide uptake on lithium-manganese-oxide (LMO) granules. *Hydrometallurgy*. 224, 106266 (2024)(b). <https://doi.org/10.1016/j.hydromet.2024.106266>
- Korchef, A., Touaibi, M.: Effect of pH and temperature on calcium carbonate precipitation by CO_2 removal from iron-rich water. *Water Environ. J.* 34, 331–341 (2020). <https://doi.org/10.1111/wej.12467>
- Kutus, B., Gácsi, A., Pallagi, A., Pálinkó, I., Peintler, G., Sipos, P.: A comprehensive study on the dominant formation of the dissolved $\text{Ca}(\text{OH})_2(\text{aq})$ in strongly alkaline solutions saturated by $\text{Ca}(\text{II})$. *RSC Adv.* 6, 45231–45240 (2016). <https://doi.org/10.1039/c6ra05337h>
- Lahsen, A.: Chilean geothermal resources and their possible utilization. *Geothermics*. 17, 401–410 (1988). [https://doi.org/10.1016/0375-6505\(88\)90068-5](https://doi.org/10.1016/0375-6505(88)90068-5)
- Lee, J.-S., Tai Kim, S., Cao, R., Choi, N.-S., Liu, M., Lee, K.T., Cho, J.: Metal-Air Batteries with High Energy Density: Li-Air versus Zn-Air. *Adv. Energy Mater.* 1, 34–50 (2011). <https://doi.org/10.1002/aenm.201000010>
- Leiter, C., Elsner, M.: Geologische Vorausprofile der Bohrungen GN-Th-1 & GN-Th-2, Graben-Neudorf. *Hauptbetriebsplan - Geotherm. Graben-neud.* (2020)

- Li, X., Mo, Y., Qing, W., Shao, S., Tang, C.Y., Li, J.: Membrane-based technologies for lithium recovery from water lithium resources: A review. *J. Memb. Sci.* 591, 117317 (2019)(a). <https://doi.org/10.1016/j.memsci.2019.117317>
- Li, Y., Zhao, Y., Wang, H., Wang, M.: The application of nanofiltration membrane for recovering lithium from salt lake brine. *Desalination.* 468, 114081 (2019)(b). <https://doi.org/10.1016/j.desal.2019.114081>
- Li, Z., Mercken, J., Li, X., Riaño, S., Binnemans, K.: Efficient and Sustainable Removal of Magnesium from Brines for Lithium/Magnesium Separation Using Binary Extractants. *ACS Sustain. Chem. Eng.* 7, 19225–19234 (2019)(c). <https://doi.org/10.1021/acssuschemeng.9b05436>
- Lide, D.R.: *CRC Handbook of Chemistry and Physics*. CRC Press, Boca Raton, FL (2005)
- Lithium Valley: Lithium Valley, <https://www.energy.ca.gov/data-reports/california-power-generation-and-power-sources/geothermal-energy/lithium-valley>. (Accessed on 31st January 2022)
- Liu, G., Zhao, Z., Ghahreman, A.: Novel approaches for lithium extraction from salt-lake brines: A review. *Hydrometallurgy.* 187, 81–100 (2019). <https://doi.org/10.1016/j.hydromet.2019.05.005>
- Livent: Report on Resources and Reserves, Pre-Feasibility Study Salar del Hombre Muerto. Philadelphia (2023)
- Loges, A., Wagner, T., Kirnbauer, T., Göb, S., Bau, M., Berner, Z., Markl, G.: Source and origin of active and fossil thermal spring systems, northern Upper Rhine Graben, Germany. *Appl. Geochemistry.* 27, 1153–1169 (2012). <https://doi.org/10.1016/j.apgeochem.2012.02.024>
- Lowstern, J., Janik, C., Fournier, R.O., Tesfai, T., Duffield, W., Clynne, M.A., Smith, J.G., Woldegiorgis, L., Weldemariam, K., Kahsai, G.: A geochemical reconnaissance of the Alid volcanic center and geothermal system \ Danakil depression \ Eritrea. *Geothermics.* 28, 161–187 (1999)
- Lüders, V., Plessen, B., Romer, R.L., Weise, S.M., Banks, D.A., Hoth, P., Dulski, P., Schettler, G.: Chemistry and isotopic composition of Rotliegend and Upper Carboniferous formation waters from the North German Basin. *Chem. Geol.* 276, 198–208 (2010). <https://doi.org/10.1016/j.chemgeo.2010.06.006>
- Lund, J.W., Toth, A.N.: Direct utilization of geothermal energy 2020 worldwide review. *Geothermics.* 90, 101915 (2021). <https://doi.org/10.1016/j.geothermics.2020.101915>
- Lunevich, L., Sanciolo, P., Dumée, L.F., Gray, S.R.: Silica fouling in high salinity waters in reverse osmosis desalination (sodium-silica system). *Environ. Sci. Water Res. Technol.* 2, 539–548 (2016). <https://doi.org/10.1039/c6ew00065g>

-
- Ma, P., Chen, X.D., Hossain, M.M.: Lithium Extraction from a Multicomponent Mixture Using Supported Liquid Membranes. *Sep. Sci. Technol.* 35, 2513–2533 (2000). <https://doi.org/10.1081/SS-100102353>
- Macedonio, F.: Membrane Distillation (MD). In: Macdonio, F. (ed.) *Encyclopedia of Membranes*. pp. 1–9. Springer Berlin Heidelberg, Berlin, Heidelberg (2015)
- Mankins, J.C.: Technology Readiness Levels: A White Paper. From: <http://www.hq.nasa.gov/office/codeq/trl/trl>. (1995). (Accessed on 31st January 2022)
- Mankins, J.C.: Technology readiness assessments: A retrospective. *Acta Astronaut.* 65, 1216–1223 (2009). <https://doi.org/10.1016/j.actaastro.2009.03.058>
- Maraghechi, H., Rajabipour, F., Pantano, C.G., Burgos, W.D.: Effect of calcium on dissolution and precipitation reactions of amorphous silica at high alkalinity. *Cem. Concr. Res.* 87, 1–13 (2016). <https://doi.org/10.1016/j.cemconres.2016.05.004>
- Marsh, A.R., Klein, G., Vermeulen, T.: Polymerisation kinetics and equilibria of silicic acid in aqueous systems. Lawrence Berkly Lab. Rep. (1975)
- Marshall, W.L., Warakomski, J.M.: Amorphous silica solubilities-II. Effect of aqueous salt solutions at 25°C. *Geochim. Cosmochim. Acta.* 44, (1980)(a). [https://doi.org/10.1016/0016-7037\(80\)90281-1](https://doi.org/10.1016/0016-7037(80)90281-1)
- Marshall, W.L., Warakomski, J.M.: Amorphous silica solubilities-II. Effect of aqueous salt solutions at 25°C. *Geochemica Cosmochem.* 44, 915–924 (1980)(b)
- Martin, G., Rentsch, L., Höck, M., Bertau, M.: Lithium market research -- global supply, future demand and price development. *Energy Storage Mater.* 6, 171–179 (2017). <https://doi.org/10.1016/j.ensm.2016.11.004>
- Maurer, H.: Rekonstruktion der Ablagerungsverhältnisse im Nordalpinen Vorlandbecken Südwest-Deutschlands. Dissertation Institut für Geologie und Paläontologie der Universität Stuttgart (2006)
- Maurer, V., Gaucher, E., Grunberg, M., Koepke, R., Pestourie, R., Cuenot, N.: Seismicity induced during the development of the Rittershoffen geothermal field, France. *Geotherm. Energy.* 8, (2020). <https://doi.org/10.1186/s40517-020-0155-2>
- Mayrhofer, C., Niessner, R., Baumann, T.: Hydrochemistry and hydrogen sulfide generating processes in the Malm aquifer, Bavarian Molasse Basin, Germany. *Hydrogeol. J.* 22, 151–162 (2014). <https://doi.org/10.1007/s10040-013-1064-2>
- Mazur, S., Scheck-Wenderoth, M.: Constraints on the tectonic evolution of the Central European Basin System revealed by seismic reflection profiles from Northern Germany. *Netherlands J. Geosci. - Geol. en Mijnb.* 84, 389–401 (2005). <https://doi.org/10.1017/S001677460002120X>
- Melin, T., Rautenbach, R.: *Membranverfahren*. Springer Berlin Heidelberg, Berlin, Heidelberg (2007)
-

- Meng, F., McNeice, J., Zadeh, S.S., Ghahreman, A.: Review of Lithium Production and Recovery from Minerals, Brines, and Lithium-Ion Batteries. *Miner. Process. Extr. Metall. Rev.* 42, 123–141 (2021). <https://doi.org/10.1080/08827508.2019.1668387>
- Mettler, S., Wolthers, M., Charlet, L., Gunten, U. von: Sorption and catalytic oxidation of Fe(II) at the surface of calcite. *Geochim. Cosmochim. Acta.* 73, 1826–1840 (2009). <https://doi.org/10.1016/j.gca.2009.01.003>
- Mi, B., Elimelech, M.: Silica scaling and scaling reversibility in forward osmosis. *Desalination.* 312, 75–81 (2013). <https://doi.org/10.1016/j.desal.2012.08.034>
- Miller, J.P.: A Portion of the system calcium carbonate-carbon dioxide-water, with geological implications. *Am. J. Sci.* 250, 161–203 (1952)
- Milne, N.A., O'Reilly, T., Sancio, P., Ostarcevic, E., Beighton, M., Taylor, K., Mullett, M., Tarquin, A.J., Gray, S.R.: Chemistry of silica scale mitigation for RO desalination with particular reference to remote operations. *Water Res.* 65, 107–133 (2014). <https://doi.org/10.1016/j.watres.2014.07.010>
- Moeck, I.S.: Catalog of geothermal play types based on geologic controls. *Renew. Sustain. Energy Rev.* 37, 867–882 (2014). <https://doi.org/10.1016/j.rser.2014.05.032>
- Monnin, C.: A thermodynamic model for the solubility of barite and celestite in electrolyte solutions and seawater to 200 °C and to 1 kbar. *Chem. Geol.* 153, 187–209 (1999)
- Montes-Hernandez, G., Concha-Lozano, N., Renard, F., Quirico, E.: Removal of oxyanions from synthetic wastewater via carbonation process of calcium hydroxide: Applied and fundamental aspects. *J. Hazard. Mater.* 166, 788–795 (2009). <https://doi.org/10.1016/j.jhazmat.2008.11.120>
- Morata, D., Aravena, D., Lahsen, A., Muñoz, M., Valdenegro, P.: Chile Up-Date: The First South American Geothermal Power Plant After One Century Of Exploration. In: *Proceedings World Geothermal Congress 2020* (2020)
- Mpelwa, M., Tang, S.-F.: State of the art of synthetic threshold scale inhibitors for mineral scaling in the petroleum industry: a review. *Pet. Sci.* 16, 830–849 (2019). <https://doi.org/10.1007/s12182-019-0299-5>
- Mroczek, E., Dedual, G., Graham, D., Bacon, L.: Lithium Extraction from Wairakei Geothermal Fluid using Electrodialysis. *Proc. World Geotherm. Congr.* 2015. 6 (2015)
- Mudd, G.M.: Sustainability Reporting and Water Resources: a Preliminary Assessment of Embodied Water and Sustainable Mining. *Mine Water Environ.* 27, 136–144 (2008). <https://doi.org/10.1007/s10230-008-0037-5>
- Naumann, D.: Salinare Tiefenwässer in Norddeutschland - Salinare Tiefenwässer in Norddeutschland Gas- und isotopengeochemische Untersuchungen. *Sci. Tech. Rep. STR00 / 21.* (2000)

- Neofotistou, E., Demadis, K.D.: Use of antiscalants for mitigation of silica (SiO₂) fouling and deposition: fundamentals and applications in desalination systems. *Desalination*. 167, 257–272 (2004). <https://doi.org/10.1016/j.desal.2004.06.135>
- Neupane, G., Wendt, S.: Assessment of Mineral Resources in Geothermal Brines in the US. Proceedings, 42nd Workshop on Geothermal Reservoir Engineering, Stanford, California, (2017)
- Nguyen, T.H., Lee, M.S.: A review on the separation of lithium ion from leach liquors of primary and secondary resources by solvent extraction with commercial extractants. *Processes*. 6, 1–15 (2018). <https://doi.org/10.3390/pr6050055>
- Nicholson, K.: *Geothermal Fluids Chemistry and Exploration Techniques*. Springer-Verlag Berlin Heidelberg (1993)
- Nicolau, C., Reich, M., Lynne, B.: Physico-chemical and environmental controls on siliceous sinter formation at the high-altitude El Tatio geothermal field, Chile. *J. Volcanol. Geotherm. Res.* 282, 60–76 (2014). <https://doi.org/10.1016/j.jvolgeores.2014.06.012>
- Ning, R.Y.: Discussion of silica speciation, fouling, control and maximum reduction. *Desalination*. 151, 67–73 (2003). [https://doi.org/10.1016/S0011-9164\(02\)00973-6](https://doi.org/10.1016/S0011-9164(02)00973-6)
- Nishiyama, R., Munemoto, T., Fukushi, K.: Formation condition of monohydrocalcite from CaCl₂–MgCl₂–Na₂CO₃ solutions. *Geochim. Cosmochim. Acta.* 100, 217–231 (2013). <https://doi.org/10.1016/j.gca.2012.09.002>
- Nitschke, F., Held, S., Neumann, T., Kohl, T.: Geochemical characterization of the Villarrica geothermal system, Southern Chile, part II: Site-specific re-evaluation of SiO₂ and Na-K solute geothermometers. *Geothermics*. 74, 217–225 (2018). <https://doi.org/10.1016/j.geothermics.2018.03.006>
- Nitschke, F., Scheiber, J., Kramar, U., Neumann, T.: Formation of alternating layered Ba-Sr-sulfate and Pb-sulfide scaling in the geothermal plant of Soultz-sous-Forêts. *J. Mineral. Geochemistry*. 191, 145–156 (2014). <https://doi.org/10.1127/0077-7757/2014/0253>
- Obata, K., Van De Krol, R., Schwarze, M., Schomäcker, R., Abdi, F.F.: In situ observation of pH change during water splitting in neutral pH conditions: Impact of natural convection driven by buoyancy effects. *Energy Environ. Sci.* 13, 5104–5116 (2020). <https://doi.org/10.1039/d0ee01760d>
- Özkaya, M.: Numerical Modeling of the Kizildere Geothermal Field, Master Thesis at the Graduate School of Natural and Applied Sciences of Middle East Technical University. (2007)
- Ozler, H.M.: Hydrogeology and geochemistry in the Curuksu (Denizli) hydrothermal field, western Turkey. *Environ. Geol.* 39, 1169–1180 (2000). <https://doi.org/10.1007/s002540000139>

- Palagonia, M.S., Brogioli, D., Mantia, F.L.: Influence of Hydrodynamics on the Lithium Recovery Efficiency in an Electrochemical Ion Pumping Separation Process. *J. Electrochem. Soc.* 164, E586–E595 (2017). <https://doi.org/10.1149/2.1531714jes>
- Palmer, T.D., Howard, J.H., Lande, D.P.: Geothermal Development of the Salton Trough, California and Mexico, UCRL-51775. Livermore, CA, USA (1975)
- Parada, M.A., López-Escobar, L., Oliveros, V., Fuentes, F., Morata, D., Calderón, M., Aguirre, L., Féraud, G., Espinoza, F., Moreno, H., Figueroa, O., Muñoz, J., Rosa, B., Vásquez, T., Stern, C.R.: Andean magmatism. In: *The Geology of Chile*. pp. 115–146. The Geological Society of London (2007)
- Paranthaman, M.P., Li, L., Luo, J., Hoke, T., Ucar, H., Moyer, B.A., Harrison, S.: Recovery of Lithium from Geothermal Brine with Lithium-Aluminum Layered Double Hydroxide Chloride Sorbents. *Environ. Sci. Technol.* 51, 13481–13486 (2017). <https://doi.org/10.1021/acs.est.7b03464>
- Park, J., Jung, Y., Kusumah, P., Lee, J., Kwon, K., Lee, C.K.: Application of ionic liquids in hydrometallurgy. *Int. J. Mol. Sci.* 15, 15320–15343 (2014). <https://doi.org/10.3390/ijms150915320>
- Parkhurst, D.L., Appelo, C. a. .: Description of Input and Examples for PHREEQC Version 3—A Computer Program for Speciation, Batch-Reaction, One-Dimensional Transport, and Inverse Geochemical Calculations. *U.S. Geol. Surv. Tech. Methods*. 497 (2013)
- Pauwels, H., Fouillac, C., Fouillac, A.M.: Chemistry and isotopes of deep geothermal saline fluids in the Upper Rhine Graben: Origin of compounds and water-rock interactions. *Geochim. Cosmochim. Acta.* 57, 2737–2749 (1993). [https://doi.org/10.1016/0016-7037\(93\)90387-C](https://doi.org/10.1016/0016-7037(93)90387-C)
- Pavez, M., Schill, E., Held, S., Díaz, D., Kohl, T.: Visualizing preferential magmatic and geothermal fluid pathways via electric conductivity at Villarrica Volcano, S-Chile. *J. Volcanol. Geotherm. Res.* 400, 106913 (2020). <https://doi.org/10.1016/j.jvolgeores.2020.106913>
- Pearson, R.G.: Hard and Soft Acids and Bases. *J. Am. Ceram. Soc.* 85, 7 (1963)
- Peña, C.A., Huijbregts, M.A.J.: The Blue Water Footprint of Primary Copper Production in Northern Chile. *J. Ind. Ecol.* 18, 49–58 (2014). <https://doi.org/10.1111/jiec.12036>
- Peng, D.-Y., Robinson, D.B.: A New Two-Constant Equation of State. *Ind. Eng. Chem. Fundam.* 15, 59–64 (1976). <https://doi.org/10.1021/i160057a011>
- Pérez-Moreno, R., Reich, M., Daniele, L., Morata, D., Held, S., Kleinsasser, J.: Stable isotope and anthropogenic tracer signature of waters in an Andean geothermal system. *Appl. Geochemistry*. 128, (2021). <https://doi.org/10.1016/j.apgeochem.2021.104953>
- Permann, C.J., Gaston, D.R., Andrš, D., Carlsen, R.W., Kong, F., Lindsay, A.D., Miller, J.M., Peterson, J.W., Slaughter, A.E., Stogner, R.H., Martineau, R.C.: MOOSE:

- Enabling massively parallel multiphysics simulation. *SoftwareX*. 11, 100430 (2020).
<https://doi.org/10.1016/j.softx.2020.100430>
- Powell, T., Cumming, W.: Spreadsheets for Geothermal Water and Gas Geochemistry. Thirty-Fifth Work. *Geotherm. Reserv. Eng.* 408–417 (2010)
- Q-con GmbH, Deutsche Erdwärme GmbH: Seismische Gefährdungsstudie für das Geothermieprojekt Graben-Neudorf. (2020)
- Quist-Jensen, C.A., Ali, A., Mondal, S., Macedonio, F., Drioli, E.: A study of membrane distillation and crystallization for lithium recovery from high-concentrated aqueous solutions. *J. Memb. Sci.* 505, 167–173 (2016)(a).
<https://doi.org/10.1016/j.memsci.2016.01.033>
- Quist-Jensen, C.A., Macedonio, F., Drioli, E.: Membrane crystallization for salts recovery from brine---an experimental and theoretical analysis. *Desalin. Water Treat.* 57, 7593–7603 (2016)(b). <https://doi.org/10.1080/19443994.2015.1030110>
- Rahardianto, A., Gao, J., Gabelich, C.J., Williams, M.D., Cohen, Y.: High recovery membrane desalting of low-salinity brackish water: Integration of accelerated precipitation softening with membrane RO. *J. Memb. Sci.* 289, 123–137 (2007).
<https://doi.org/10.1016/j.memsci.2006.11.043>
- Ramalingam, A., Arumugam, S.: Experimental study on specific heat of hot brine for salt gradient solar pond application. *Int. J. ChemTech Res.* 4, 956–961 (2012)
- Ramos, V.A.: Anatomy and global context of the Andes: Main geologic features and the Andean orogenic cycle. In: *Backbone of the Americas: Shallow Subduction, Plateau Uplift, and Ridge and Terrane Collision*. Geological Society of America (2009)
- Regenspurg, S., Dilling, J., Mielcarek, J., Korte, F., Schkade, U.K.: Naturally occurring radionuclides and their geochemical interactions at a geothermal site in the North German Basin. *Environ. Earth Sci.* 72, 4131–4140 (2014).
<https://doi.org/10.1007/s12665-014-3306-6>
- Regenspurg, S., Feldbusch, E., Byrne, J., Deon, F., Driba, D.L., Henniges, J., Kappler, A., Naumann, R., Reinsch, T., Schubert, C.: Mineral precipitation during production of geothermal fluid from a Permian Rotliegend reservoir. *Geothermics*. 54, 122–135 (2015)(a). <https://doi.org/10.1016/j.geothermics.2015.01.003>
- Regenspurg, S., Feldbusch, E., Norden, B., Tichomirowa, M.: Fluid-rock interactions in a geothermal Rotliegend/Permo-Carboniferous reservoir (North German Basin). *Appl. Geochemistry*. 69, 12–27 (2016).
<https://doi.org/10.1016/j.apgeochem.2016.03.010>
- Regenspurg, S., Milsch, H., Schaper, J.: Copper in Geothermal Brine: Origin, Reactions, Risks, and Chances. *World Geotherm. Congr. 2015*. 5 (2015)(b)
- Regenspurg, S., Wiersberg, T., Brandt, W., Huenges, E., Saadat, A., Schmidt, K., Zimmermann, G.: Supplement 3. *Chemie der Erde*. 70, 3–12 (2010).
<https://doi.org/10.1016/j.chemer.2010.05.002>

- Reich, R., Danisi, R.M., Kluge, T., Eiche, E., Kolb, J.: Structural and compositional variation of zeolite 13X in lithium sorption experiments using synthetic solutions and geothermal brine. *Microporous Mesoporous Mater.* 359, 112623 (2023). <https://doi.org/10.1016/j.micromeso.2023.112623>
- Reich, R., Slunitschek, K., Danisi, R.M., Eiche, E., Kolb, J.: Lithium Extraction Techniques and the Application Potential of Different Sorbents for Lithium Recovery from Brines. *Miner. Process. Extr. Metall. Rev.* 00, 1–20 (2022). <https://doi.org/10.1080/08827508.2022.2047041>
- Reinecker, J., Tingay, M., Müller, B., Heidbach, O.: Present-day stress orientation in the Molasse Basin. *Tectonophysics.* 482, 129–138 (2010). <https://doi.org/10.1016/j.tecto.2009.07.021>
- Rettenmaier, D., Millot, R., Blandine, G., Sanjuan, B., Elodie, J., Sophie, L., Clement, B., Zorn, R.: Rohstoff Lithium aus Geothermie – und aus Europa (EuGeLi - European Geothermal Lithium). In: *Der Geothermie Kongress 2021. Essen* (2021)
- Richardson, I.G.: The calcium silicate hydrates. *Cem. Concr. Res.* 38, 137–158 (2008). <https://doi.org/10.1016/j.cemconres.2007.11.005>
- Risacher, F., Alonso, H., Salazar, C.: Hydrochemistry of two adjacent acid saline lakes in the Andes of northern Chile. *Chem. Geol.* 187, 39–57 (2002). [https://doi.org/10.1016/S0009-2541\(02\)00021-9](https://doi.org/10.1016/S0009-2541(02)00021-9)
- Rojas, A., Sruoga, P., Lamberti, M.C., Agosto, M., Tondreau, J., Mendoza, N., Daniele, L., Morata, D.: Unravelling the hydrothermal system of Laguna del Maule restless volcanic field, in the Andean Southern Volcanic Zone (36° 10'S). *J. Volcanol. Geotherm. Res.* 424, 107498 (2022). <https://doi.org/10.1016/j.jvolgeores.2022.107498>
- Romero, V.C.E., Llano, K., Calvo, E.J.: Electrochemical extraction of lithium by ion insertion from natural brine using a flow-by reactor: Possibilities and limitations. *Electrochem. commun.* 125, 106980 (2021). <https://doi.org/10.1016/j.elecom.2021.106980>
- De Rose, A., Buna, M., Strazza, C., Olivieri, N., Stevens, T., Peeters, L., Tawil-Jarnault, D.: *Technology Readiness Level: Guidance Principles for Renewable Energy technologies.* European Union, Luxembourg (2017)
- Rothbaum, H.P., Anderton, B.H.: Removal of Silica and Arsenic from Geothermal Discharge Waters by Precipitation of Useful Calcium Silicates. In: *Second united nations symposium on the development and use of geothermal resources.* pp. 1417–1425 (1975)
- Rothbaum, H.P., Anderton, B.H., Harrison, R.F., Rohde, A.G., Slatter, A.: Effect of silica polymerisation and pH on geothermal scaling. *Geothermics.* 8, 1–20 (1979). [https://doi.org/10.1016/0375-6505\(79\)90062-2](https://doi.org/10.1016/0375-6505(79)90062-2)

- Rotstein, Y., Edel, J.-B., Gabriel, G., Boulanger, D., Schaming, M., Munsch, M.: Insight into the structure of the Upper Rhine Graben and its basement from a new compilation of Bouguer Gravity. *Tectonophysics*. 425, 55–70 (2006). <https://doi.org/10.1016/j.tecto.2006.07.002>
- Ruiz-Agudo, E., Putnis, C.V., Rodriguez-Navarro, C., Putnis, A.: Effect of pH on calcite growth at constant ratio and supersaturation. *Geochim. Cosmochim. Acta*. 75, 284–296 (2011). <https://doi.org/10.1016/j.gca.2010.09.034>
- Ryu, T., Haldorai, Y., Rengaraj, A., Shin, J., Hong, H.J., Lee, G.W., Han, Y.K., Huh, Y.S., Chung, K.S.: Recovery of Lithium Ions from Seawater Using a Continuous Flow Adsorption Column Packed with Granulated Chitosan-Lithium Manganese Oxide. *Ind. Eng. Chem. Res.* 55, 7218–7225 (2016). <https://doi.org/10.1021/acs.iecr.6b01632>
- Ryu, T., Shin, J., Ghoreishian, S.M., Chung, K.S., Huh, Y.S.: Recovery of lithium in seawater using a titanium intercalated lithium manganese oxide composite. *Hydrometallurgy*. 184, 22–28 (2019). <https://doi.org/10.1016/j.hydromet.2018.12.012>
- Salvador Cob, S., Hofs, B., Maffezzoni, C., Adamus, J., Siegers, W.G., Cornelissen, E.R., Genceli Güner, F.E., Witkamp, G.J.: Silica removal to prevent silica scaling in reverse osmosis membranes. *Desalination*. 344, 137–143 (2014). <https://doi.org/10.1016/j.desal.2014.03.020>
- Sanchez-Alfaro, P., Reich, M., Arancibia, G., Pérez-Flores, P., Cembrano, J., Driesner, T., Lizama, M., Rowland, J., Morata, D., Heinrich, C.A., Tardani, D., Campos, E.: Physical, chemical and mineralogical evolution of the Tolhuaca geothermal system, southern Andes, Chile: Insights into the interplay between hydrothermal alteration and brittle deformation. *J. Volcanol. Geotherm. Res.* 324, 88–104 (2016). <https://doi.org/10.1016/j.jvolgeores.2016.05.009>
- Sandrock, M., Maaß, C., Weiselder, S., Westholm, H., Schulz, W., Löschan, G., Bausch, C., Kreuter, H., Reyer, D., Mangold, D., Riegger, M., Köhler, C.: Kommunaler Klimaschutz durch Verbesserung der Effizienz in der Fernwärmeversorgung mittels Nutzung von Niedertemperaturwärmequellen am Beispiel tiefegeothermischer Ressourcen - Abschlussbericht 31/2020. Umweltbundesamt. *Climate Ch*, 357 (2020)
- Sanjuan, B., Gourcerol, B., Millot, R., Rettenmaier, D., Jeandel, E., Rombaut, A.: Lithium-rich geothermal brines in Europe: An up-date about geochemical characteristics and implications for potential Li resources. *Geothermics*. 101, (2022). <https://doi.org/10.1016/j.geothermics.2022.102385>
- Sanjuan, B., Millot, R., Dezayes, C., Brach, M.: Main characteristics of the deep geothermal brine (5 km) at Soultz-sous-Forêts (France) determined using geochemical and tracer test data. *Comptes Rendus - Geosci.* 342, 546–559 (2010). <https://doi.org/10.1016/j.crte.2009.10.009>

- Sanjuan, B., Millot, R., Innocent, C., Dezayes, C., Scheiber, J., Brach, M.: Major geochemical characteristics of geothermal brines from the Upper Rhine Graben granitic basement with constraints on temperature and circulation. *Chem. Geol.* 428, 27–47 (2016)(a). <https://doi.org/10.1016/j.chemgeo.2016.02.021>
- Sanjuan, B., Scheiber, J., Gal, F., Touzelet, S., Genter, A., Villadangos, G.: Inter-well chemical tracer testing at the Rittershoffen geothermal site (Alsace, France). *Eur. Geotherm. Congr.* 19–24 (2016)(b)
- Santomartino, S., Webb, J.A.: Estimating the longevity of limestone drains in treating acid mine drainage containing high concentrations of iron. *Appl. Geochemistry.* 22, 2344–2361 (2007). <https://doi.org/10.1016/j.apgeochem.2007.04.020>
- Schallenberg, K.: Das Geothermische Heizwerk in Neustadt-Glewe im Betriebsjahr 1996. GFZ Potsdam, STR99/206 04, Geothermie Report 99-1, (1999)
- Scheck-Wenderoth, M., Lamarche, J.: Crustal memory and basin evolution in the Central European Basin System—new insights from a 3D structural model. *Tectonophysics.* 397, 143–165 (2005). <https://doi.org/10.1016/j.tecto.2004.10.007>
- Scheiber, J., Hettkamp, T., Schindler, M., Wahl, G., Baumgärtner, J.: Schlussbericht Verbundvorhaben Sulfidinhibition und Deponierbarkeit (SUBITO): Verbesserung der Wirtschaftlichkeit von Geothermieranlagen durch Inhibition natürlich belasteter Ablagerungen. (2019)(a)
- Scheiber, J., Seibt, A., Jähnichen, S., Degering, D., Mouchot, J.: Combined Application of Inhibitors for Scale and Corrosion Mitigation: Lessons Learned. *Eur. Geotherm. Congr.* 11–14 (2019)(b)
- Schilling, F., Stober, I., Müller, B., Kiefer, E.: Fragen und Antworten zur Tiefen Geothermie. Landesforschungszentrum Geothermie, KIT Campus Süd. Karlsruhe (2022)
- Schmidt, M.: Rohstoffrisikobewertung - Lithium: Rohstoffinformationen 33. DERA-Deutsche Rohstoffagentur in der Bundesanstalt für Geowissenschaften und Rohstoffe, Berlin (2017)
- Schmidt, M.: Raw material requirements for lithium-ion batteries and hydrogen electrolysis - Supply risks for Europe as an industrial location? In: *Ulm Electrochemical Talks.* Ulm (2021)
- Schmidt, M.: Rohstoffrisikobewertung – Lithium – Rohstoffinformationen 54. DERA-Deutsche Rohstoffagentur in der Bundesanstalt für Geowissenschaften und Rohstoffe, Berlin (2023)
- Schneider, M.: Geothermie macht Unterhaching unabhängig: Ein Dorf braucht keinen Gaspreisdeckel, <https://www.merkur.de/wirtschaft/unterhaching-geothermie-germering-kosten-waerme-heizen-heizung-bayern-energiekrise-gaspreisdeckel-92017391.html>
- Schwantes, R., Seger, J., Bauer, L., Winter, D., Hogen, T., Koschikowski, J., Geißen, S.-U.: Characterization and Assessment of a Novel Plate and Frame MD Module for

- Single Pass Wastewater Concentration–FEED Gap Air Gap Membrane Distillation. Membranes (Basel). (2019).
<https://doi.org/10.3390/membranes9090118>
- Segnit, E.R., Holland, H.D., Biscardi, C.J.: The solubility of calcite in aqueous solutions—I The solubility of calcite in water between 75° and 200° at CO₂ pressures up to 60 atm. *Geochim. Cosmochim. Acta.* 26, 1301–1331 (1962).
[https://doi.org/10.1016/0016-7037\(62\)90057-1](https://doi.org/10.1016/0016-7037(62)90057-1)
- Serpen, U., Aksoy, N.: Reassessment of Reinjection in Salavatli-Sultanhisar Field of Turkey. 25–29 (2010)
- Setiawan, F.A., Rahayuningsih, E., Petrus, H.T.B.M., Nurpratama, M.I., Perdana, I.: Kinetics of silica precipitation in geothermal brine with seeds addition: minimizing silica scaling in a cold re-injection system. *Geotherm. Energy.* 7, 22 (2019).
<https://doi.org/10.1186/s40517-019-0138-3>
- Sharma, A.D., Patil, N.D., Patwardhan, A.W., Moorthy, R.K., Ghosh, P.K.: Synergistic interplay between D2EHPA and TBP towards the extraction of lithium using hollow fiber supported liquid membrane. *Sep. Sci. Technol.* 51, 2242–2254 (2016).
<https://doi.org/10.1080/01496395.2016.1202280>
- Sheikholeslami, R., Bright, J.: Silica and metals removal by pretreatment to prevent fouling of reverse osmosis membranes. *Desalination.* 143, 255–267 (2002).
[https://doi.org/10.1016/S0011-9164\(02\)00264-3](https://doi.org/10.1016/S0011-9164(02)00264-3)
- Shi, C., Jing, Y., Xiao, J., Wang, X., Yao, Y., Jia, Y.: Solvent extraction of lithium from aqueous solution using non-fluorinated functionalized ionic liquids as extraction agents. *Sep. Purif. Technol.* 172, 473–479 (2017).
<https://doi.org/10.1016/j.seppur.2016.08.034>
- Shi, D., Zhang, L., Peng, X., Li, L., Song, F., Nie, F., Ji, L., Zhang, Y.: Extraction of lithium from salt lake brine containing boron using multistage centrifuge extractors. *Desalination.* 441, 44–51 (2018). <https://doi.org/10.1016/j.desal.2018.04.029>
- Siebert, L., Simkin, T., Kimberly, P.: *Volcanoes of the World: Third Edition.* (2010)
- Šiler, P., Ğ, I.K., Sehnal, T., Másilko, J.Ğ., Opravil, T.: The determination of the influence of pH value of curing conditions on Portland cement hydration. *Cem. Concr. Res.* 151, 10–17 (2016). <https://doi.org/10.1016/j.proeng.2016.07.393>
- Simsek, S.: Hydrogeological and isotopic survey of geothermal fields in the Buyuk Menderes graben, Turkey. *Geothermics.* 32, 669–678 (2003)(a).
[https://doi.org/10.1016/S0375-6505\(03\)00072-5](https://doi.org/10.1016/S0375-6505(03)00072-5)
- Simsek, S.: Present status and future development possibilities of Aydın-Denizli Geothermal Province. *Production.* 11–16 (2003)(b)
- Sipos, P.: Application of the Specific Ion Interaction Theory (SIT) for the ionic products of aqueous electrolyte solutions of very high concentrations. *J. Mol. Liq.* 143, 13–16 (2008). <https://doi.org/10.1016/j.molliq.2008.04.003>

- Slunitschek, K., Kolb, J., Eiche, E.: Lithiumextraktion aus geothermischen Solen: Moderne Adsorptionsmethode zur Rohstoffgewinnung, Wiley Analytical Magazine (2021)
- Somrani, A., Hamzaoui, A.H., Pontie, M.: Study on lithium separation from salt lake brines by nanofiltration (NF) and low pressure reverse osmosis (LPRO). *Desalination*. 317, 184–192 (2013). <https://doi.org/10.1016/j.desal.2013.03.009>
- van der Spek, M., Ramirez, A., Faaij, A.: Challenges and uncertainties of ex ante techno-economic analysis of low TRL CO₂ capture technology: Lessons from a case study of an NGCC with exhaust gas recycle and electric swing adsorption. *Appl. Energy*. 208, 920–934 (2017). <https://doi.org/10.1016/j.apenergy.2017.09.058>
- Spitzmüller, L., Goldberg, V., Held, S., Grimmer, J.C., Winter, D., Genovese, M., Koschikowski, J., Kohl, T.: Selective silica removal in geothermal fluids: Implications for applications for geothermal power plant operation and mineral extraction. *Geothermics*. 95, 102141 (2021). <https://doi.org/10.1016/j.geothermics.2021.102141>
- Srinivasan, V., Hafemeister, D., Levi, B., Levine, M., Schwartz, P.: Batteries for Vehicular Applications. In: AIP Conference Proceedings. pp. 283–296. AIP (2008)
- Stechern, A.: BGR koordiniert Projekt: Forschungsverbund untersucht Lithium-Potenziale in Deutschland, https://www.bgr.bund.de/DE/Gemeinsames/Oeffentlichkeitsarbeit/Pressemitteilungen/BGR/bgr-2021-10-26_lithium-potenziale-deutschland.html;jsessionid=31A00B00135E288DDE576D5CC4D2F455.1_cid331?nn=1544712. (Accessed on 15th July 2022)
- Steiger, K., Hilgers, C., Kolb, J.: Lithiumbedarf Für Die Batteriezellen-Produktion in Deutschland und Europa Im Jahr 2030. S., Karlsruhe (2022). DOI 10.5445/IR/1000153059
- Stern, C.R.: Active Andean volcanism: its geologic and tectonic setting. *Rev. geológica Chile*. 31, (2004). <https://doi.org/10.4067/S0716-02082004000200001>
- Stern, C.R., Moreno, H., López-Escobar, L., Clavero, J., Lara, L., Naranjo, J., Parada, M.Á., Skewes, A.: Chilean volcanoes. In: Moreno, T. and Gibbons, W. (eds.) *The Geology of Chile*. pp. 147–178. The Geological Society of London (2007)
- Stober, I.: Hydrochemical properties of deep carbonate aquifers in the SW German Molasse basin. *Geotherm. Energy*. 2, (2014). <https://doi.org/10.1186/s40517-014-0013-1>
- Stober, I., Bucher, K.: *Hydrogeology of Crystalline Rocks*. Springer Netherlands, Dordrecht (2000)
- Stober, I., Bucher, K.: *Geothermie*. Springer Verlag Berlin, Heidelberg (2012)
- Stober, I., Bucher, K.: Hydraulic and hydrochemical properties of deep sedimentary reservoirs of the Upper Rhine Graben, Europe. *Geofluids*. 15, 464–482 (2015). <https://doi.org/10.1111/gfl.12122>

-
- Stober, I., Wolfgramm, M., Birner, J.: Hydrochemie der Tiefenwässer in Deutschland. *Z. geol. Wiss.* 339–380 (2014)
- Stoffyn-Egli, P., MacKenzie, F.T.: Mass balance of dissolved lithium in the oceans. *Geochemica Cosmochem.* 48, 859–872 (1984)
- Straub, J.: In search of technology readiness level (TRL) 10. *Aerosp. Sci. Technol.* 46, 312–320 (2015). <https://doi.org/10.1016/j.ast.2015.07.007>
- Stricker, K., Grimmer, J.C., Egert, R., Bremer, J., Korzani, M.G., Schill, E., Kohl, T.: The potential of depleted oil reservoirs for high-temperature storage systems. *Energies.* 13, 1–26 (2020). <https://doi.org/10.3390/en13246510>
- Stringfellow, W.T., Dobson, P.F.: Technology for the Recovery of Lithium from Geothermal Brines. *Energies.* 14, 6805 (2021)(a). <https://doi.org/10.3390/en14206805>
- Stringfellow, W.T., Dobson, P.F.: Technology for Lithium Extraction in the Context of Hybrid Geothermal Power. *PROCEEDINGS, 46th Work. Geotherm. Reserv. Eng.* 46, 1–20 (2021)(b)
- Stronach, S.A., Glasser, F.P.: Modelling the impact of abundant geochemical components on phase stability and solubility of the CaO-SiO₂-H₂O system at 25 °C: Na⁺, K⁺, .. *Adv. Cem. Res.* 167–181 (1997)
- Sun, D., Meng, M., Yin, Y., Zhu, Y., Li, H., Yan, Y.: Highly selective, regenerated ion-sieve microfiltration porous membrane for targeted separation of Li⁺. *J. Porous Mater.* 23, 1411–1419 (2016). <https://doi.org/10.1007/s10934-016-0201-4>
- Sun, S.Y., Cai, L.J., Nie, X.Y., Song, X., Yu, J.G.: Separation of magnesium and lithium from brine using a Desal nanofiltration membrane. *J. Water Process Eng.* 7, 210–217 (2015). <https://doi.org/10.1016/j.jwpe.2015.06.012>
- Sun, Y., Wang, Q., Wang, Y., Yun, R., Xiang, X.: Recent advances in magnesium/lithium separation and lithium extraction technologies from salt lake brine. *Sep. Purif. Technol.* 256, 117807 (2021). <https://doi.org/10.1016/j.seppur.2020.117807>
- Swain, B.: Separation and purification of lithium by solvent extraction and supported liquid membrane, analysis of their mechanism: a review. *J. Chem. Technol. Biotechnol.* 91, 2549–2562 (2016). <https://doi.org/10.1002/jctb.4976>
- Swain, B.: Recovery and recycling of lithium: A review. *Sep. Purif. Technol.* 172, 388–403 (2017). <https://doi.org/10.1016/j.seppur.2016.08.031>
- Talybov, M.A., Abdulagatov, I.M.: High-temperature and high-pressure PVT measurements and derived thermodynamic properties of geothermal fluids from East Turkey. *Geothermics.* 95, 102125 (2021). <https://doi.org/10.1016/j.geothermics.2021.102125>
- Taran, Y., Kalacheva, E.: Acid sulfate-chloride volcanic waters; Formation and potential for monitoring of volcanic activity. *J. Volcanol. Geotherm. Res.* 405, 107036 (2020). <https://doi.org/10.1016/j.jvolgeores.2020.107036>
-

- Tarcan, G., Filiz, S., Gemici, Ü.: Geology and Geochemistry of the Salihli Geothermal Fields, Turkey. *World Geotherm. Congr.* 2000. 1829–1834 (2000)
- Tarquin, A., Walker, W.S., Delgado, G., Bustamante, A.: UTEP–EPW university–utility partnership: Concentrate enhanced–recovery reverse osmosis process for high water recovery from silica-saturated desalination concentrates. *Water Environ. Res.* 92, 369–377 (2020). <https://doi.org/10.1002/wer.1176>
- Tassi, F., Aguilera, F., Benavente, O., Paonita, A., Chiodini, G., Caliro, S., Agosto, M., Gutierrez, F., Capaccioni, B., Vaselli, O., Caselli, A., Saltori, O.: Geochemistry of fluid discharges from Peteroa volcano (Argentina-Chile) in 2010–2015: Insights into compositional changes related to the fluid source region(s). *Chem. Geol.* 432, 41–53 (2016). <https://doi.org/10.1016/j.chemgeo.2016.04.007>
- Tassi, F., Aguilera, F., Darrah, T., Vaselli, O., Capaccioni, B., Poreda, R.J., Delgado Huertas, A.: Fluid geochemistry of hydrothermal systems in the Arica-Parinacota, Tarapacá and Antofagasta regions (northern Chile). *J. Volcanol. Geotherm. Res.* 192, 1–15 (2010). <https://doi.org/10.1016/j.jvolgeores.2010.02.006>
- Tassi, F., Aguilera, F., Vaselli, O., Darrah, T., Medina, E.: Gas discharges from four remote volcanoes in northern Chile (Putana, Olca, Irruputuncu and Alitar): A geochemical survey. *Ann. Geophys.* 54, 121–136 (2011). <https://doi.org/10.4401/ag-5173>
- Tavakkoli, S., Lokare, O.R., Vidic, R.D., Khanna, V.: A techno-economic assessment of membrane distillation for treatment of Marcellus shale produced water. *Desalination.* 416, 24–34 (2017). <https://doi.org/10.1016/j.desal.2017.04.014>
- Tekin, S.: Estimation of the formation temperature from the inlet and outlet mud temperatures while drilling geothermal formations. Master Thesis of the Graduate School of Natural and Applied Sciences of Middle East Technical University. (2010)
- Templeton, C.C.: Solubility of barium sulfate in sodium chloride solutions from 25 °C to 95 °. *Chem. Eng. Sci. Data* 5, 514–516 (1960)
- Thoenen, T., Hummel, W., Berner, U., Curti, E.: The PSI/Nagra Chemical Thermodynamic Database 12/07. (2014)
- Thomas, D.L., Bird, D.K., Arnórsson, S., Maher, K.: Geochemistry of CO₂-rich waters in Iceland. *Chem. Geol.* 444, 158–179 (2016). <https://doi.org/10.1016/j.chemgeo.2016.09.002>
- Thomas, J.J., Chen, J.J., Jennings, H.M., Neumann, D.A.: Ca-OH bonding in the C-S-H gel phase of tricalcium silicate and white portland cement pastes measured by inelastic neutron scattering. *Chem. Mater.* 15, 3813–3817 (2003). <https://doi.org/10.1021/cm034227f>
- Thorpe, R.S.: The Tectonic Setting of Active Andean Volcanism. In: *Andean Magmatism*. pp. 4–8. Birkhäuser Boston, Boston, MA (1984)

-
- Toba, A.L., Nguyen, R.T., Cole, C., Neupane, G., Paranthaman, M.P.: U.S. lithium resources from geothermal and extraction feasibility. *Resour. Conserv. Recycl.* 169, 105514 (2021). <https://doi.org/10.1016/j.resconrec.2021.105514>
- Toner, J.D., Catling, D.C.: A Low-Temperature Thermodynamic Model for the Na-K-Ca-Mg-Cl System Incorporating New Experimental Heat Capacities in KCl, MgCl₂, and CaCl₂ Solutions. *J. Chem. Eng. Data.* 62, 995–1010 (2017). <https://doi.org/10.1021/acs.jced.6b00812>
- Trading Economics: Lithium Carbonate Prices. 2022, <https://tradingeconomics.com/commodity/lithium>. (Accessed on 14th November 2022).
- Trading Economics: Lithium Carbonate Prices. 2023, <https://tradingeconomics.com/commodity/lithium>. (Accessed on 15th March 2023).
- Tuck, C.: Rubidium - USGS Report. Mineral Commodity Summaries. (2020)(a). <https://doi.org/10.3133/mcs2022>
- Tuck, C.: Cesium - USGS Report. Mineral Commodity Summaries. (2020)(b). <https://doi.org/10.3133/mcs2022>
- U.S. Geological Survey: Mineral commodity summaries 2023. (2023). <https://doi.org/10.3133/mcs2023>
- Ueda, A., Kato, K., Mogi, K., Mroczek, E., Thain, I.A.: Silica removal from Mokai, New Zealand, geothermal brine by treatment with lime and a cationic precipitant. *Geothermics.* 32, 47–61 (2003). [https://doi.org/10.1016/S0375-6505\(02\)00050-0](https://doi.org/10.1016/S0375-6505(02)00050-0)
- Uhde, J.: Welcome to the Geothermal Power Plant Insheim. In: 9th European Geothermal Workshop (2021)
- Unlimited: Unlimited 31.01.2022, <https://www.geothermal-lithium.org/>. (Accessed on 31st January 2022)
- Vera, M.L., Torres, W.R., Galli, C.I., Chagnes, A., Flexer, V.: Environmental impact of direct lithium extraction from brines. *Nat. Rev. Earth Environ.* 4, 149–165 (2023). <https://doi.org/10.1038/s43017-022-00387-5>
- Vidal, J., Genter, A.: Overview of naturally permeable fractured reservoirs in the central and southern Upper Rhine Graben: Insights from geothermal wells. *Geothermics.* 74, 57–73 (2018). <https://doi.org/10.1016/j.geothermics.2018.02.003>
- Vulcan Energy Vulcan Zero Carbon Lithium™ Project Phase One DFS Results and Resources-Reserves Update. 2023. <https://v-er.eu/vulcan-zero-carbon-lithium-project-phase-one-dfs-results-and-resources-reserves-update/>. (Accessed on 15th March 2023)
- Vulcan Energy Resources: Vulcan energy resources ASX announcement (15 January 2021), positive pre-feasibility study, highlights - Plant design. (2021)(a).
-

- <https://vul.live.irmau.com/site/PDF/6a9c79d2-5c99-40d7-ba32-72cd6ea3a6f6/PositivePreFeasibilityStudy>. (Accessed on 31st January 2022)
- Vulcan Energy Resources: Diversified mix of offtakers sharing our decarbonisation ambitions. (2021)(b). https://www.linkedin.com/posts/vulcan-energy-resources_negotiating-offtake-agreements-and-collaborating-activity-6874247684241293312-XIfh. (Accessed on 31st January 2022)
- Vulcan Energy Resources: Binding lithium offtake agreement with Volkswagen Group. (2021)(c). <https://vul.live.irmau.com/site/PDF/4a8714c5-51c8-4cd5-8ae8-2e684c200107/BindingOfftakeAgreementSignedwithVolkswagenGroup>. (Accessed on 31st January 2022)
- Vulcan Energy Resources: Binding lithium offtake agreement with Renault. (2021)(d). <https://vul.live.irmau.com/site/PDF/346fc118-1b04-4c8c-98e0-50cc3534ff14/BindingOfftakeAgreementSignedwithRenault>. (Accessed on 31st January 2022)
- Vulcan Energy Resources: Quarterly Activities Report - March 2021. (2021)(e). <https://vul.live.irmau.com/site/PDF/88d6ee23-6598-4127-b206-fac8ae8a74df/QuarterlyActivitiesReport>. (Accessed on 31st January 2022)
- Vulcan Energy Resources: Vulcan Energy signs lithium supply agreement with Stellantis. (2021)(f). <https://vul.live.irmau.com/site/PDF/99900137-8ade-467e-b794-74528c328bb7/VulcansignslithiumsupplyagreementwithStellantis>. (Accessed on 31st January 2022)
- Warren, I.: Techno-Economic Analysis of Lithium Extraction from Geothermal Brines Techno-Economic Analysis of Lithium Extraction from Geothermal Brines. Natl. Renew. Energy Lab. 48 (2021)
- Wedin, F.: Vulcan Energy Resources 2022 Corporate presentation Q1 2022. (2022) <https://www.v-er.eu>. (Accessed on 15th July 2022)
- Wedin, F., Harrison, S.: Direct Lithium Extraction (DLE) - Technical Update. Vulcan Energy Resources Ltd. (2021). <https://announcements.asx.com.au/asxpdf/20211112/pdf/452x0szzdhhc86.pdf>. (Accessed on 31st January 2022)
- Weinand, J.M., Vandenberg, G., Risch, S., Behrens, J., Pflugradt, N., Linßen, J., Stolten, D.: Low-carbon lithium extraction makes deep geothermal plants cost-competitive in future energy systems. Adv. Appl. Energy. 11, 100148 (2023). <https://doi.org/10.1016/j.adapen.2023.100148>
- Wellmer, F.-W., Buchholz, P., Gutzmer, J., Hagelüken, C., Herzig, P., Littke, R., Thauer, R.K.: Conclusions. In: Raw Materials for Future Energy Supply. pp. 169–177. Springer International Publishing, Cham (2019)

- Weng, D., Duan, H., Hou, Y., Huo, J., Chen, L., Zhang, F., Wang, J.: Introduction of manganese based lithium-ion Sieve-A review. *Prog. Nat. Sci. Mater. Int.* 30, 139–152 (2020). <https://doi.org/10.1016/j.pnsc.2020.01.017>
- Wenzel, F., Brun, J.-P.: A deep reflection seismic line across the Northern Rhine Graben. *Earth Planet. Sci. Lett.* 104, 140–150 (1991). [https://doi.org/10.1016/0012-821X\(91\)90200-2](https://doi.org/10.1016/0012-821X(91)90200-2)
- Winter, D., Koschikowski, J., Düver, D., Hertel, P., Beuscher, U.: Evaluation of MD process performance: Effect of backing structures and membrane properties under different operating conditions. *Desalination*. 323, 120–133 (2013). <https://doi.org/10.1016/j.desal.2013.04.007>
- Winter, D., Koschikowski, J., Gross, F., Maucher, D., Düver, D., Jositz, M., Mann, T., Hagedorn, A.: Comparative analysis of full-scale membrane distillation contactors - methods and modules. *J. Memb. Sci.* 524, 758–771 (2017). <https://doi.org/10.1016/j.memsci.2016.11.080>
- Winter, D., Koschikowski, J., Wieghaus, M.: Desalination using membrane distillation: Experimental studies on full scale spiral wound modules. *J. Memb. Sci.* 375, 104–112 (2011). <https://doi.org/10.1016/j.memsci.2011.03.030>
- Wisniewska, M., Fijałkowska, G., Ostolska, I., Franus, W., Nosal-Wiercinska, A., Tomaszewska, B., Goscińska, J., Wójcik, G.: Investigations of the possibility of lithium acquisition from geothermal water using natural and synthetic zeolites applying poly(acrylic acid). *J. Clean. Prod.* 195, 821–830 (2018)
- Wolf, M., Breitkopf, O., Puk, R.: Solubility of calcite in different electrolytes at temperatures between 10° and 60°C and at CO₂ partial pressures of about 1 kPa. *Chem. Geol.* 76, 291–301 (1989). [https://doi.org/10.1016/0009-2541\(89\)90097-1](https://doi.org/10.1016/0009-2541(89)90097-1)
- Wrage, J., Tardani, D., Reich, M., Daniele, L., Arancibia, G., Cembrano, J., Sánchez-Alfaro, P., Morata, D., Pérez-Moreno, R.: Geochemistry of thermal waters in the Southern Volcanic Zone, Chile – Implications for structural controls on geothermal fluid composition. *Chem. Geol.* 466, 545–561 (2017). <https://doi.org/10.1016/j.chemgeo.2017.07.004>
- Wu, L., Li, L., Evans, S.F., Eskander, T.A., Moyer, B.A., Hu, Z., Antonick, P.J., Harrison, S., Paranthaman, M.P., Riman, R., Navrotsky, A.: Lithium aluminum-layered double hydroxide chlorides (LDH): Formation enthalpies and energetics for lithium ion capture. *J. Am. Ceram. Soc.* 102, 2398–2404 (2019). <https://doi.org/10.1111/jace.16150>
- Xiang, W., Liang, S., Zhou, Z., Qin, W., Fei, W.: Extraction of lithium from salt lake brine containing borate anion and high concentration of magnesium. *Hydrometallurgy*. 166, 9–15 (2016). <https://doi.org/10.1016/j.hydromet.2016.08.005>

- Xiang, W., Liang, S., Zhou, Z., Qin, W., Fei, W.: Lithium recovery from salt lake brine by counter-current extraction using tributyl phosphate/FeCl₃ in methyl isobutyl ketone. *Hydrometallurgy*. 171, 27–32 (2017).
<https://doi.org/10.1016/j.hydromet.2017.04.007>
- Xu, C., Dai, Q., Gaines, L., Hu, M., Tukker, A., Steubing, B.: Future material demand for automotive lithium-based batteries. *Commun. Mater.* 1, 10 (2020).
<https://doi.org/10.1038/s43246-020-00095-x>
- Xu, P., Hong, J., Qian, X., Xu, Z., Xia, H., Tao, X., Xu, Z., Ni, Q.Q.: Materials for lithium recovery from salt lake brine. *J. Mater. Sci.* 56, 16–63 (2021)(a).
<https://doi.org/10.1007/s10853-020-05019-1>
- Xu, W., He, L., Zhao, Z.: Lithium extraction from high Mg/Li brine via electrochemical intercalation/de-intercalation system using LiMn₂O₄ materials. *Desalination*. 503, 114935 (2021)(b). <https://doi.org/10.1016/j.desal.2021.114935>
- Xu, X., Chen, Y., Wan, P., Gasem, K., Wang, K., He, T., Adidharma, H., Fan, M.: Extraction of lithium with functionalized lithium ion-sieves. *Prog. Mater. Sci.* 84, 276–313 (2016). <https://doi.org/10.1016/j.pmatsci.2016.09.004>
- Yan, G., Busch, B., Egert, R., Esmaeilpour, M., Stricker, K., Kohl, T.: Transport mechanisms of hydrothermal convection in faulted tight sandstones. *EGU sphere*. (2022).
<https://doi.org/https://doi.org/10.5194/egusphere-2022-1185>
- Yeltekin, K., Akin, S.: Analysis of Long Term Tracer Test. Production. Proceedings, Thirty-First Workshop on Geothermal Reservoir Engineering. Stanford University, Stanford, California 1–6. (2006)
- Yildirim, N., Önc, S., Akman, U.A.: High Enthalpy Geothermal Potential Possibility in SW of Büyük Menderes Graben, Turkey. *Proc. World Geotherm. Congr.* 25–29 (2010)
- Ystroem, L.H., Nitschke, F., Held, S., Kohl, T.: A multicomponent geothermometer for high-temperature basalt settings. *Geotherm. Energy*. 8, (2020).
<https://doi.org/10.1186/s40517-020-0158-z>
- Ystroem, L.H., Nitschke, F., Kohl, T.: MulT_predict - An optimised comprehensive multicomponent geothermometer. *Geothermics*. 105, 102548 (2022).
<https://doi.org/10.1016/j.geothermics.2022.102548>
- Yu, X., Fan, X., Guo, Y., Deng, T.: Recovery of lithium from underground brine by multistage centrifugal extraction using tri-isobutyl phosphate. *Sep. Purif. Technol.* 211, 790–798 (2019). <https://doi.org/10.1016/j.seppur.2018.10.054>
- Zandevakili, S., Ranjbar, M., Ehteshamzadeh, M.: Recovery of lithium from Urmia Lake by a nanostructure MnO₂ ion sieve. *Hydrometallurgy*. 149, 148–152 (2014).
<https://doi.org/10.1016/j.hydromet.2014.08.004>
- Zarga, Y., Elfil, H., Ben Boubaker, H.: Calcium Sulfate and Calcium Carbonate Simple and Mixed Precipitations. *J. New Sci.* 8, 7–16 (2014)

- Zhang, P., Pabstmann, A., Gray, S., Duke, M.: Silica fouling during direct contact membrane distillation of coal seam gas brine with high sodium bicarbonate and low hardness. *Desalination*. 444, 107–117 (2018). <https://doi.org/10.1016/j.desal.2018.07.015>
- Zhang, Z., Jia, Y., Liu, B., Sun, H., Jing, Y., Zhang, Q., Shao, F., Qi, M., Yao, Y.: Study on behavior of lithium ion in solvent extraction and isotope separation. *J. Mol. Liq.* 324, 114709 (2021). <https://doi.org/10.1016/j.molliq.2020.114709>
- Zhao, X., Yang, H., Wang, Y., Sha, Z.: Review on the electrochemical extraction of lithium from seawater/brine. *J. Electroanal. Chem.* 850, 113389 (2019). <https://doi.org/10.1016/j.jelechem.2019.113389>

Declaration of Authorship

Chapter 4: Technology assessment for Direct Lithium Extraction from geothermal fluids

This study was funded by the Helmholtz Association within the Geoenergy subtopic in the MTET (Materials and Technologies for the Energy Transition) program of the Energy research field. Further support was given by the BMBF (Federal Ministry of Education and Research) by funding the BrineMine project (Grant Number 033R190B) in the Client II framework.

As first author, Valentin Goldberg wrote the entire article and visualized the results with inputs from Tobias Kluge and Fabian Nitschke as co-authors. He developed the concept of the study, compiled the literature data, conducted the technological assessment of different extraction approaches, and elaborated on the challenges for the integration within geothermal cycles. The discussions with all co-authors as well as the revision contributed further to this manuscript.

Chapter 5: Potential Evaluation and Production Scenarios for Geothermal Lithium in Germany

This study was funded by the Helmholtz Association within the Geoenergy subtopic in the MTET (Materials and Technologies for the Energy Transition) program of the Energy research field. Further support was given by the BMBF (Federal Ministry of Education and Research) by funding the BrineMine project (Grant Number 033R190B) in the Client II framework.

As first author, Valentin Goldberg wrote the entire article and visualized the results with inputs from Tobias Kluge and Fabian Nitschke as co-authors. He developed the concept of the study and compiled the literature data and technical data. The scenario analysis and all associated calculations were designed and carried out independently by Valentin Goldberg. The discussions with all co-authors as well as the revision contributed further to this manuscript.

Chapter 6: Reservoir behavior of lithium-depleted brine in a geothermal reservoir

This study was funded by the Helmholtz Association within the Geoenergy subtopic in the MTET (Materials and Technologies for the Energy Transition) program of the Energy research field. Further support was given by the BMBF (Federal Ministry of Education and Research) by funding the BrineMine project (Grant Number 033R190B) in the Client II framework.

As first author, Valentin Goldberg wrote the entire article with inputs from Robert Egert and Ali Dashti as co-authors. He designed the different scenarios, conducted all simulations, and performed the analysis, interpretation, and visualization of the model results. Robert Egert and Binil Benny developed the initial geological model which was modified and extended by Valentin Goldberg. The provision of FE-Mesh by Ali Dashti is highly appreciated. The discussions with all co-authors as well as the revision contributed further to this manuscript.

Chapter 7: Development of a continuous silica treatment strategy for metal extraction processes in operating geothermal plants

This study was carried out in the framework of the German-Chilean Project BrineMine (Grant Number 033R190B) funded by the BMBF (Federal Ministry of Education and Research) in the Client II framework. Further support was given by the Helmholtz Association for research funding within the Geoenergy subtopic in the MTET (Materials and Technologies for the Energy Transition) program of the Energy research field and the Chilean ANID Fondap program (projects 15090013, 15200001, and ACE210005). Access to the geothermal brine was enabled at the powerplant Insheim by the Pfalzwerke geofuture GmbH.

As the first author, Valentin Goldberg wrote the entire article with the input of Daniel Winter as co-author. He developed the concept for the numerical design simulation, gathered all laboratory data for the validation of the results, and consequently compiled a new thermodynamic data set for facilitating the final simulation. Goldberg further conducted the simulation and analyzed and visualized the results.

Valentin Goldberg set up the concept, and organized and conducted the geochemical sampling campaign during the prototype field tests. In terms of chemical analysis, he prepared and conducted the major cation analysis using ICP-OES and the analysis of the mineralogical composition using XRD. The development, construction, and installation of the demonstrator by co-authors Daniel Winter and Florian Groß is highly appreciated. The discussions with all co-authors as well as the revision contributed further to this manuscript.

Chapter 8: The potential of raw material extraction from thermal fluids in Chile

This study was carried out in the framework of the German-Chilean Project BrineMine (Grant Number 033R190B) funded by the BMBF (Federal Ministry of Education and Research) in the Client II framework. Further support was given by the Chilean ANID Fondap program (projects 15090013, 15200001, and ACE210005). Access to the geothermal brine was enabled at the powerplant Insheim by the Pfalzwerke geofuture GmbH.

As the first author, Valentin Goldberg wrote the entire article. He developed the concept of the study and compiled the literature and technical data. The scenario analysis and all associated calculations were designed and carried out independently by Valentin Goldberg. Further, he analyzed, interpreted, and visualized the results. The discussions with all co-authors as well as the revision contributed further to this manuscript.

Chapter 9: Prototype tests for the treatment of geothermal waters for raw material extraction and freshwater production

This study was carried out in the framework of the German-Chilean Project BrineMine (Grant Number 033R190B) funded by the BMBF (Federal Ministry of Education and Research) in the Client II framework. Further support was given by the Helmholtz Association for research funding within the Geoenergy subtopic in the MTET (Materials and Technologies for the Energy Transition) program of the Energy research field and the Chilean ANID Fondap program (projects 15090013, 15200001, and ACE210005). Access to the geothermal fluid was enabled at the Termas de Puyehue by the company Tánica.

As the first author, Valentin Goldberg wrote the entire article with the input of Daniel Winter as co-author. Valentin Goldberg set up the concept, and organized and conducted the geochemical sampling campaign during the prototype field test. The development, construction, and installation of the demonstrator was conducted by the co-author Daniel Winter. The coordination of chemical analysis and conduction of the XRD measurement and interpretation by co-author Elisabeth Eiche is highly appreciated. The development of the energetic potential calculation was conducted by Valentin Goldberg with inputs from the co-author Julian Heboldt. The interpretation and visualization of the results was conducted by Valentin Goldberg. The discussions with all co-authors as well as the revision contributed further to this manuscript.

Appendix

Simulation results and experimental data related to the thesis can be found in the online archive Zenodo and cited as:

Goldberg, V. (2024). Appendices dissertation: The potential of direct mineral extraction from geothermal fluids [Zenodo]. <https://doi.org/10.5281/zenodo.10637212>

The [Archive](#) contains:

- Chapter 6: Simulation data of the different extraction scenarios
- Chapter 7: „PITZER_CSH.dat“ data set
- Chapter 7: Simulation data of the design calculation
- Chapter 10: Chemical analysis of the different precipitation experiments

Publication list

Scientific Publications

1. Spitzmüller, L., Goldberg, V., Held, S., Grimmer, J. C., Winter, D., Genovese, M., Koschikowski, J. & Kohl, T. (2021). Selective silica removal in geothermal fluids: Implications for applications for geothermal power plant operation and mineral extraction. *Geothermics*, 95(May), 102141.
<https://doi.org/10.1016/j.geothermics.2021.102141>
2. Goldberg, V., Winter, D., Nitschke, F., Rath, M., Held, S., Spitzmüller, L., Budach, I., Pavez, M., Morata, D., Koschikowski, J., Kohl, T.: The potential of raw material extraction from thermal brines – Successful milestones of the BrineMine project. *OIL GAS*. 26–33 (2021). <https://doi.org/10.19225/210306>
3. Pavez, M.; Diaz, D.; Brasse, H.; Kapinos, G.; Budach, I.; Goldberg, V.; Morata, D.; Schill, E.: Visualizing Shallow and Deep Electric Structures in the Tolhuaca Geothermal System (S. Chile) Investigated by Magnetotellurics. *Remote Sensing*, 14 (23), Art.-Nr.: 6144 (2022)
<https://doi.org/10.3390/rs14236144>
4. Goldberg, V., Kluge, T., Nitschke, F.: Herausforderungen und Chancen für die Lithiumgewinnung aus geothermalen Systemen in Deutschland – Teil 1: Literaturvergleich bestehender Extraktionstechnologien. *Grundwasser*. 27, 239–259 (2022)(a).
<https://doi.org/10.1007/s00767-022-00522-5>
5. Goldberg, V., Nitschke, F., Kluge, T.: Herausforderungen und Chancen für die Lithiumgewinnung aus geothermalen Systemen in Deutschland – Teil 2: Potenziale und Produktionsszenarien in Deutschland. *Grundwasser*. 27, 261–275 (2022)(b).
<https://doi.org/10.1007/s00767-022-00523-4>
6. Goldberg, V., Winter, D., Nitschke, F., Held, S., Groß, F., Pfeiffle, D., Uhde, J., Morata, D., Koschikowski, J., Kohl, T.: Development of a continuous silica treatment strategy for metal extraction processes in operating geothermal plants. *Desalination*. 564, 116775 (2023)(b). <https://doi.org/10.1016/j.desal.2023.116775>
7. Goldberg, V., Dashti, A., Egert, R., Benny, B., Kohl, T., Nitschke, F.: Challenges and Opportunities for Lithium Extraction from Geothermal Systems in Germany—Part 3: The Return of the Extraction Brine. *Energies*. 16, 5899 (2023).
<https://doi.org/10.3390/en16165899>

-
- Goldberg, V., Winter, D., Eiche, E., Koschikowski, J., Kohl, T., Morata, D., Schwantes, R., Seibt, P., Heboldt, J., Nitschke, F.: Prototype Tests for the Treatment of Geothermal Waters for Raw Material Extraction and Freshwater Production. Min. Rep. Glückauf. 159, 601–610 (2023)(a)

Conference presentations

- Goldberg, V.; Held, S.; Egert, R.; Kohl, T.: Numerical modeling of thermal front propagation caused by fluid injection in a fractured reservoir for forecasting thermal-induced seismicity. 2019, Oktober. 7th European Geothermal Workshop (EGW 2019), Karlsruhe, Deutschland, 9.–10. Oktober 2019
- Goldberg, V.; Held, S.; Nitschke, F.; Siefert, D.; Kölbel, T.; Kohl, T.: Calculation of CO₂ solubility in thermal waters in the context of geothermal utilization. 2018, November. Student Technical Conference (STC 2018), Freiberg, Deutschland, 8.–9. November 2018
- Spitzmüller, L.; Goldberg, V.; Held, S.; Grimmer, J. C.; Winter, D.; Koschikowski, J.; Kohl, T.: Removal of Silica from geothermal water by addition of Ca(OH)₂. 2020, November 5. Student Technical Congress - German Section (STC 2020), Online, 4.–6. November 2020
- Spitzmüller, L.; Goldberg, V.; Held, S.; Grimmer, J. C.; Winter, D.; Koschikowski, J.; Kohl, T.: Entwicklung eines elementspezifischen Fällungsprozesses zur Reduktion der Siliziumdioxidkonzentration aus geothermalen Wässern. 2020, November 11. Der digital Geothermiekongress (DGK 2020), Essen, Germany, 9.–13. November 2020
- Goldberg, V.; Held, S.; Winter, D.; Spitzmüller, L.; Nitschke, F.; Morata, D.; Kohl, T.; Budach, I.; Koschikowski, J.: Nachhaltige Rohstoffgewinnung aus Thermalwässern: das BrineMine Projekt. 2020, November 12. Der digital Geothermiekongress (DGK 2020), Essen, Germany, 9.–13. November 2020
- Goldberg, V.; Winter, D.; Nitschke, F.; Morata, D.; Koschikowski, J.; Kohl, T.: Development of a brine treatment strategy for enhancing geothermal energy production and associated raw material extraction. 2021, Juli 9. Goldschmidt (2021), Online, 4.–9. July 2021
- Goldberg, V.; Winter, D.; Nitschke, F.; Morata, D.; Koschikowski, J.; Kohl, T.: Development of a fluid treatment strategy to enable combined raw material and freshwater recovery from geothermal fluids. 2021, September 20. GeoKarlsruhe (DGGV 2021), Karlsruhe, Germany, 19.–24. September 2021
- Goldberg, V.; Winter, D.; Nitschke, F.; Morata, D.; Koschikowski, J.; Kohl, T.: Entwicklung einer Aufbereitungsstrategie zur kombinierten Rohstoff- und

- Frischwassergewinnung aus geothermalen Fluiden. 2021, December 1. Der Geothermiekongress (DGK 2021), Essen, Germany, 30. November–2. December 2021
9. Goldberg, V.: Combined raw material and fresh water production from geothermal brines. 2022: DAAD Chile: Simposios Minería 2022: Simposio 3 Mining: Circular Economy and Social Transformation.
 10. Goldberg, V.: Panel: Sustainable Utilization of Raw Resources - Transitioning from Extraction to Added Value through Science and Innovation. 2022: Red INVECA (Red de Investigadores Chilenos en Alemania): 10 años fomentando la interacción científica chileno-alemana
 11. Goldberg, V.: Challenges and Opportunities for Lithium Extraction from Geothermal Systems in Germany. 2023, Juni 13. 12th European Metallurgical Conference (EMC 2023), Düsseldorf, Deutschland, 11.–14. Juni 2023
 12. Goldberg, V.; Nitschke, F.; Kluge, T.; Egert, R.; Kohl, T.: Invited Session Keynote: Lithiumresources. 2023, September 6. GeoBerlin (2023), Berlin, Deutschland, 3.–7. September 2023
 13. Yström, L.; Trumpp, M.; Goldberg, V.; Eichinger, F.; Amtmann, J.; Winter, D.; Koschikowski, J.; Kohl, T.; Nitschke, F.: MALEG – Machine Learning for Enhancing Geothermal Energy. 2023, November 9. European Geothermal Workshop (EGW 2023), Utrecht, Netherlands, November 8–9, 2023
 14. Goldberg, V.; Nitschke, F.; Kluge, T.; Egert, R.; Kohl, T.: Invited Session Keynote: Lithium extraction from geothermal systems in Germany – challenges and opportunities for a local raw material supply. 2023, December 5. LithiumDays (2023), Halle, Germany, 4.–5. December 2023

Conference Session Chair

1. Student Technical Congress STC of the German Section of the Society of Petroleum Engineers: 2020. Session chair of the session Student Lectures Geothermal
2. GeoKarlsruhe: 2021: Session chair of the session 10.2 Material use of geothermal waters
3. Student Technical Congress STC of the German Section of the Society of Petroleum Engineers: 2021. Session chair of the session Geothermics & Brine Mining

Publications Submitted

1. Book of the Institute of Eco-Industrial Development (IECO):
Eco-Industrial Development as an industrial strategy.
Contributions from a German-Chilean Research Cooperation
 - a. Chapter D1:

Multi-Use of Hydrothermal Systems - Perspectives for renewable baseload energy and green mining

Valentin Goldberg, Fabian Nitschke, Diego Morata, Eva Schill, Thomas Kohl
 - b. Chapter D2:

Challenges and Opportunities for Lithium Extraction from Geothermal Systems in Germany

Part 1: A Literature Review of Existing Extraction Technologies

Valentin Goldberg, Tobias Kluge, Fabian Nitschke
 - c. Chapter D3:

Challenges and Opportunities for Lithium Extraction from Geothermal Systems in Germany

Part 2: Potential and Production Scenarios in Germany

Valentin Goldberg, Fabian Nitschke, Tobias Kluge
 - d. Chapter D4:

Raw Material Potential of Geothermal Systems in Chile

Ignacio Pérez, Valentin Goldberg, Fabian Nitschke, Diego Morata, Joachim, Koschikowski, Thomas Kohl

Reports and further publications

1. Eggeling, L.; Konstantin, H.; Goldberg, V.; Siefert, D.; Köhler, J.; Kölbl, T.; Reith, S.: Anlagenmonitoring als Schlüsseltechnologie für den erfolgreichen Betrieb von Geothermiekraftwerken in Deutschland: Teilprojekte: AP 10: Reservoircharakterisierung mittels Radionuklidanalytik, AP 11: Optimierung geothermischer Betriebsmonitoringsysteme am Beispiel von Bruchsal: Schlussbericht zum Verbundprojekt ANEMONA: Projektlaufzeit: 01.01.2014-31.01.2018. 2018. Technische Informationsbibliothek (TIB). doi:10.2314/GBV:1039267769
2. Goldberg, V.; Held, S.; Siefert, D.; Nitschke, F.; Kölbl, T.: Calculation of the CO₂-solubility in thermal waters in the context of geothermal utilization: CO₂-bubble point analysis in thermal waters of the Büyük Menderes Graben. 2019. @SPEgermany, 29, 18–22

3. Schwarz, K.; Hänsch, S.; Bertram, A.; Gauß, M.; Goldberg, V.; Lohse, C.; Rüter, H.; Kasper, S.: Geothermie – Erneuerbare Energie aus der Tiefe. Ein Lernheft für die Klassenstufen 5 und 6. 2021. Projekt GeoSchulB.
https://www.geothermie.de/fileadmin/user_upload/Geothermie/Einstieg_in_die_Geothermie/GEO_SCHUL_B_Lernheft_1_FD_150dpi.pdf
4. Schwarz, K.; Hänsch, S.; Bertram, A.; Gauß, M.; Goldberg, V.; Lohse, C.; Rüter, H.; Kasper, S.: Geothermie – Erneuerbare Energie aus der Tiefe. Ein Lernheft für die Klassenstufen 7 und 8. 2021. Projekt GeoSchulB.
https://www.geothermie.de/fileadmin/user_upload/Geothermie/Einstieg_in_die_Geothermie/GEO_SCHUL_B_Lernheft_2_FD_150dpi_Web.pdf
5. Schwarz, K.; Kaufmann, G.; Bertram, A.; Gauß, M.; Goldberg, V.; Lohse, C.; Rüter, H.; Kasper, S.: Geothermie – Erneuerbare Energie aus der Tiefe. Ein Lernheft für die Klassenstufe 9 und 10. 2021. Projekt GeoSchulB.
https://www.geothermie.de/fileadmin/user_upload/Geothermie/Einstieg_in_die_Geothermie/GEO_SCHUL_B_Lernheft_3_FD_150dpi_Web.pdf
6. Schwarz, K.; Kaufmann, G.; Bertram, A.; Gauß, M.; Goldberg, V.; Lohse, C.; Rüter, H.; Kasper, S.: Geothermie – Erneuerbare Energie aus der Tiefe. Ein Lernheft für die Klassenstufen 11 und 13. 2021. Projekt GeoSchulB.
https://www.geothermie.de/fileadmin/user_upload/Geothermie/Einstieg_in_die_Geothermie/GEO_SCHUL_B_Lernheft_4_FD_150dpi_Web.pdf
7. Goldberg, V.; Nitschke, F.; Winter, D.; Koschikowski, J.; Kohl, T.: Geothermale Wässer als nachhaltige Rohstoff- und Frischwasserquelle. 2022. Energiewirtschaftliche Tagesfragen. 3/2022. <https://emagazin.et-magazin.de/de/profiles/cb1a7fd451c4/editions/c454fe8531bd390ce426>
8. SWR Planet Wissen: Lithiumhype am Rhein - Chancen und Risiken. 07.09.2023. <https://www.ardmediathek.de/video/Y3JpZDovL3dkci5kZS9CZWl0cmFnLTA5NmM5YWU2LWRiODEtNGZmYS05MGFjLWNhNjU4NDc1MjRhYw>
9. Zachmann, G.; Goldberg, V.: Strom und Wärme aus Thermalquellen am Oberrhein. 2022. Podcast: Nachgefragt – wissen, wie's läuft. doi:10.5445/IR/1000160452. <https://publikationen.bibliothek.kit.edu/1000160452>
10. SWR Science Talk: Die Chancen der Geothermie in Deutschland. 16.10.2023. <https://www.swr.de/swr2/wissen/chancen-der-geothermie-in-deutschland-valentin-goldberg-swr-science-talk-100.html>

Curriculum Vitae

Working Experience

- 09.2019 – 02.2024: Karlsruhe Institute of Technology: Researcher in the Department of Geothermal Energy and Reservoir Technology. Technical Project lead of the BrineMine project.
- 05.2018 – 03.2019: EnBW Energie Baden-Württemberg AG: Intern and later student assistant at the Department of Research and Development in the field of geothermal energy production.
- 11.2012 – 07. 2016: SchulLV GmbH: Till December 2015 student trainee in the section of content development. Later content manager and partner with a focus on assembling and leading a team for the development of a digital textbook with a focus on natural sciences.

Academic Experience

- 10.2012 – 01.2016: Karlsruhe Institute of Technology: Bachelor of Science. Bachelor thesis about the iron ore deposits She-Chahun in central Iran.
- 10.2016 – 12.2019: Karlsruhe Institute of Technology: Master of Science. Focus on applied geothermics, topics of geothermal research, reservoir geology, as well as deposition systems. Master thesis: Numerical modeling of thermal front propagation caused by fluid injection in a fractured reservoir for forecasting thermal-induced seismicity.
- 09.2019 – 02.2024: Karlsruhe Institute of Technology, Department of Geothermal Energy and Reservoir Technology & Universidad de Chile, Department of Geology and Andean Geothermal Center of Excellence (CEGA):

Ph.D. Studies on the potential of direct mineral extraction from geothermal fluids.

Teaching

Karlsruhe Institute of Technology:

- Assistant: Lecture Applied Geosciences (2nd Semester Master, 2020)
- Assistant: Lecture Applied Geosciences (2nd Semester Master, 2021)
- Assistant: Lecture Applied Geosciences (2nd Semester Master, 2023)

Universidad de Chile:

- Professor Auxiliar: Principios de Geotermia (Bachelor, 2022)

Memberships

1. Society of Petroleum Engineers SPE:
 - a. 2016: Co-Founder SPE Student Group Karlsruhe
 - b. 2018 - 2020: Member of the organization team of the yearly Student Technical Congress (STC)
 - c. 2019-2023: Board member of the German Section: Student Chapter Liaison
 - d. Since 2019: Author of the „Geothermal News“ of the GSSPE Newsletter
 - e. Since 2023: Board member of the German Section: Geothermal Liaison
2. Since 2019: Member Institute of Eco-Industrial Development (IECO):
Virtual German-Chilean Institute of KIT, Universidad de Chile, Universidad Austral, Universidad de Concepción
 - a. Active Member in Topic 3: T3 - Eco-industrial use of subsoil resources
3. Since 2021: Member German Geothermal Association
 - a. 2021-2022: Scientific consultant within the project GeoSchulB for developing geothermal schoolbooks.
4. Since 2022: Member GDMB Society of Metallurgists and Miners e. V.
5. Since 2023: Member European Association of Geoscientists & Engineers EAGE

Awards

1. GSSPE Student Award 2018
German Section of the Society of Petroleum Engineers
2. 3rd Place Energie-Campus 2021, Stiftung Energie & Klimaschutz · Nov. 2021
<https://www.energie-klimaschutz.de/energie-campus-2021-nachwuchswissenschaftlerinnen-ausgezeichnet/>
3. Young Scientist Award 2022 of the GDMB Society of Metallurgists and Miners e. V.

*Ein Hoch auf alle, die da graben
nach Kohle, Salz und edlem Erz.
In rauher Schale schlägt erhaben
des Bergmanns großes, weiches Herz!*

- Aus dem Erzgebirge.